

Non-absorbable iron chelators for the treatment of colorectal cancer

By

Rama Byravan



**UNIVERSITY OF
BIRMINGHAM**

A thesis submitted to the University of Birmingham for the degree of

DOCTOR OF PHILOSOPHY

School of Chemistry

College of Engineering and Physical Sciences

University of Birmingham

March 2015

UNIVERSITY OF
BIRMINGHAM

University of Birmingham Research Archive

e-theses repository

This unpublished thesis/dissertation is copyright of the author and/or third parties. The intellectual property rights of the author or third parties in respect of this work are as defined by The Copyright Designs and Patents Act 1988 or as modified by any successor legislation.

Any use made of information contained in this thesis/dissertation must be in accordance with that legislation and must be properly acknowledged. Further distribution or reproduction in any format is prohibited without the permission of the copyright holder.

Abstract

There is growing epidemiological and experimental evidence implicating excess luminal iron in the context of colorectal cancer. High levels of dietary iron is thought to aid carcinogenesis, due to the formation of reactive oxygen species from the redox cycling of iron, which can cause oxidative tissue damage and disrupt cellular signalling pathways. Hence, it is proposed that removal of this excess iron will suppress the development of this cancer.

A clinically used iron chelator deferasirox and a modified version of this ligand, were attempted to be conjugated onto biopolymers chitosan and alginate. These non-absorbable polymers were hypothesised to be undigested in the gastrointestinal tract, thus specifically capable of targeting and removing excess iron from the colon. These chelator incorporated polymer materials, be they conjugated polymers or functional material blends, were subsequently shown to have improved iron binding properties compared to the parent polymers. Culturing RKO colorectal cancer cells with iron and alginate-ligand material did not significantly affect intracellular iron uptake, however culturing RKO cells with iron and chitosan-ligand material elicited a suppression in iron mediated ferritin expression and overall intracellular iron status. Based on these *in vitro* results, that the material obtained from reaction of chitosan with ligand elicits the desired inhibition of iron uptake, the chitosan-ligand material was administered to a mouse model of colorectal cancer. Apc Hom Pten Hom mice show reduced mitosis and increased apoptosis of intestinal crypt cells, demonstrating anti-neoplastic activity by iron chelation.

Preface

Whilst polymer characterisation was sometimes challenging, the advice of the PhD examiners proved highly informative. As such additional diffusion NMR characterisation experiments were run post *viva voce* on new batches of polymer derivative, with the aid of Dr Melanie Britton and Catherine Smith. Data generated in these additional experiments confirm conjugation of alginate-ligand material but suggest that chitosan-ligand material is not covalently conjugated. In light of this new data, alternative interpretations of the results in this thesis are provided. However, due to time passed the batches used for these suggested experiments were not the same as those that underwent the majority of experiments in this thesis. Thus caution must be exercised when interpreting the data as batch-to-batch variation means that it is unclear whether conjugation occurred in previous batches of chitosan-ligand material or if it was a polymer-ligand mixture. Despite this it still remains exciting that the chitosan-ligand material, as a conjugated polymer or a mixture, can have such profound bioactivity and this opens a whole new field of scientific research.

Acknowledgements

I'd like to thank John and Chris for their supervision and guidance without which this thesis would not have been possible, and to the School of Chemistry at the University of Birmingham for the funding and studentship support.

JSF group: I'd like to thank all the people who have shared the trials and tribulations of research with me, and everyone who proof read this thesis. The first JSF group member I met was Antonio and despite his messiness in the lab and his tendency to smell out the office by cooking pasta every lunchtime, he really liked Chemistry and was always willing to offer advice. Dan's keen eye to spot mistakes in group meetings and enthusiasm to ask questions, although sometimes annoying, were actually very helpful when he came up with some good ideas, and he is actually nice sometimes. Wenlei has such a cheerful disposition that made him very friendly to work with. Alex always has an excuse for a coffee break, but his relaxed attitude helped to keep things in perspective when I got stressed. I'm glad Will decided to join the group and that we didn't totally put him off as a Masters student. He's a smart guy and provided good company in the lab partly due to his old man views and taste in music. Mark was very good at making me cups of tea and kept me going when things got difficult. He was also good fun to work with and put up with me venting and stressing, and gave me little pep talks so thank you. I'd also like to thank the other group members who have contributed to my time here: Mat, Eric, Akina, Mariwan and all the project students.

CT group: As a Chemist in a Biology lab, most members of this group were imperative in teaching me aspects of Biology and got me through the latter half of my project. Richard showed me how to look after cells, helped me plan experiments and taught me most of the biological assays. Dan and Matt were always approachable and answered many of my questions when I was confused about new techniques. The mice experiments were carried out by Sorina and Victoria. I learnt the

basics of mice genetics and histology from Victoria, who patiently stained slides with me and was always willing to help. Sarah was a great person to work with and offered mutual solidarity through the character building moments. Although I didn't spend much time in the lab with Elisabeth and Imogen, they were friendly when I was new to the group.

The analytical staff have been tremendous. Neil knows everything about NMR and allowed me to run a sample in TFA despite his worries for his £20k probe. Chi always seemed to be busy but made time to offer advice and Doug helped me optimise MALDI experiments.

The examiners are also thanked for their suggestions which helped to bring a greater understanding of the research discussed in this thesis. Dr Melanie Britton and Catherine Smith performed the diffusion NMR experiments which permitted an alternative interpretation of the data and are thanked for their valuable contribution.

Finally, I'd like to thank my family: Amma, Appa and Swetha for all their patience and support over the years.

Abbreviations

A	Absorbance
AAS	Atomic absorption spectroscopy
Apc	Adenomatous polyposis coli
Bpy	2,2'-bipyridine
Bu	Butyl
Boc	tert-butyloxycarbonyl
c	Concentration
CDI	1,1'-carbonyldiimidazole
CHCA	α -cyano-4-hydroxycinnamic acid
CRC	Colorectal cancer
DCC	<i>N,N'</i> -Dicyclohexylcarbodiimide
DCM	Dichloromethane
DCYTB	Duodenal cytochrome B
DMEM	Dulbecco's modified eagle medium
DFO	Desferrioxamine
DMAP	4-dimethylaminopyridine
DMF	Dimethylformamide
DMT1	Divalent metal transporter 1
DMSO	Dimethyl sulfoxide
DNA	Deoxyribonucleic acid
DTPA	Diethylenetriaminepentaacetic acid

E _b	Binding energy
E _k	Kinetic energy
ECL	Enhanced chemiluminescence
ECM	Extracellular matrix
EDAC	1-Ethyl-3-(3-dimethylaminopropyl)carbodiimide
EDTA	Ethylenediaminetetraacetic acid
ELISA	Enzyme-linked immunosorbent assay
eq	Equivalent
ES	Electrospray
Et	Ethyl
FAP	Familial adenomatous polyposis
FCS	Foetal calf serum
G	α -L-gluronic
GI	Gastrointestinal
GPC	Gel permeation chromatography
h	hours
H&E	Hematoxylin and eosin
HEPES	4-(2-hydroxyethyl)-1-piperazineethanesulfonic acid
HOBt	Hydroxybenzotriazole
Hom	Homozygous
HOMO	Highest occupied molecular orbital
HP	Hepcidin

HSAB	Hard-soft-acid-base
IR	Infrared
ITC	Isothermal titration calorimetry
l	Path length
L	Ligand
LUMO	Lowest unoccupied molecular orbital
M	β -D-mannuronic
MALDI	Matrix assisted laser desorption ionisation
Me	Methyl
MES	2-(<i>N</i> -morpholino)ethanesulfonic acid
min	Minutes
Ms	Mesyl
MS	Mass spectrometry
MTT	3-(4,5-dimethylthiazol-2-yl)-2,5-diphenyltetrazolium bromide
nOe	Nuclear Overhauser Effect
NAB	Non-absorbable backbone
NHS	<i>N</i> -hydroxysuccinimide
NMR	Nuclear magnetic resonance
PAGE	Polyacrylamide gel electrophoresis
PAMAM	Polyaminoamide
PBS	Phosphate buffered saline
PEG	Polyethylene glycol

PGSTE	Pulsed gradient stimulated echo
Ph	Phenyl
PHT	Phosphohistone
PMN	Polymorphonuclear leukocyte
Pr	Propyl
PSAA	Phenol/sulphuric acid assay
Pten	Phosphatase and tensin homolog
RAFT	Reversible addition fragment chain transfer
RIPA	Radioimmunoprecipitation assay
ROS	Reactive oxygen species
rpm	Revolutions per minute
rt	Room temperature
SDS	Sodium dodecyl sulphate
SEC	Size exclusion chromatography
SEM	Standard error of the mean
TBS	Tris-buffered saline
TBST	Tris-buffered saline tween
TCA	Trichloroacetic acid
TEMED	Tetramethylethylenediamine
TF	Transferrin
TFA	Trifluoroacetic acid
TFR1	Transferrin receptor 1

THF	Tetrahydrofuran
TLC	Thin layer chromatography
Ts	Tosyl
UK	United Kingdom
UV-Vis	Ultraviolet-visible
w/v	weight/volume
w/w	weight/weight
XPS	X-Ray photoelectron spectroscopy

Contents

1	Introduction	1
1.1	Biological role of iron	1
1.2	Iron and colorectal cancer.....	2
1.2.1	Epidemiological evidence.....	2
1.2.2	Iron metabolism and regulation in cancer	3
1.2.3	<i>In vivo</i> evidence	5
1.3	The influence of iron in oxidative stress	5
1.4	Iron chelation therapy.....	6
1.5	Iron chelator design	7
1.5.1	Siderophores: Enterobactin	9
1.6	Iron chelators in clinical use.....	11
1.6.1	Desferrioxamine	11
1.6.2	Aminocarboxylates.....	12
1.6.3	Deferiprone (L1, Ferriprox®).....	13
1.6.4	Deferasirox (ICL670A, Exjade®)	14
1.7	Macromolecular iron chelators.....	16
1.7.1	Polymeric iron chelators.....	16
1.7.2	Dendritic iron chelators	19
1.8	Alginate	21
1.8.1	Egg box structure and cation binding.....	21
1.8.2	Chemical modifications of alginate.....	23
1.9	Chitosan.....	24
1.9.1	Chemical modifications of chitosan	25
1.10	Conclusion.....	26
2	Project overview and Aims	28

3	Synthesis	29
3.1	Background.....	29
3.2	Ligand synthesis and modifications	30
3.3	Polymer reactions	42
3.3.1	Polymer-deferasirox conjugates	42
3.3.2	Polymer-catechol conjugates.....	46
3.4	Dendrimer reactions	48
3.5	Summary.....	50
4	Polymer Characterisation.....	51
4.1	Background.....	51
4.2	Infrared Spectroscopy.....	51
4.3	Nuclear Magnetic Resonance Spectroscopy.....	53
4.3.1	Diffusion NMR Spectroscopy	56
4.4	Ultraviolet-visible Spectroscopy	60
4.4.1	Phenol/Sulphuric acid assay (PSAA)	62
4.5	X-Ray Photoelectron Spectroscopy.....	66
4.6	Summary.....	72
5	Iron binding studies.....	76
5.1	Background.....	76
5.2	Titrations by UV-vis spectroscopy.....	76
5.3	Dialysis methods	81
5.4	Summary.....	89
6	Cellular studies	90
6.1	Background.....	90
6.2	MTT assay	92
6.3	Ferritin western blot	94

6.4	Ferritin ELISA.....	97
6.5	Intracellular iron by ferrozine assay.....	100
6.6	Probing intracellular Exkite activity.....	102
6.7	Summary.....	104
7	Mouse model studies.....	106
7.1	Background.....	106
7.2	Exkite safety and tolerability in mice.....	109
7.3	Mouse survival.....	110
7.4	Histology.....	112
7.5	Summary.....	117
8	Conclusion and Future work.....	119
8.1	Conclusion.....	119
8.2	Future work.....	121
9	Experimental.....	126
9.1	General Chemical Experimental.....	126
9.2	Compounds synthesised.....	128
9.2.1	2-(2-hydroxyphenyl)-4H-benzo[e][1,3]oxazin-4-one.....	128
9.2.2	4-(3,5-bis(2-hydroxyphenyl)-1H-1,2,4-triazol-1-yl)benzoic acid.....	129
9.2.3	4-(3,5-bis(2-hydroxyphenyl)-1H-1,2,4-triazol-1-yl)-N-isopropylbenzamide.....	130
9.2.4	2,2'-(1-(4-nitrophenyl)-1H-1,2,4-triazole-3,5-diyl)diphenol.....	131
9.2.5	Tert-butyl (2-(2-(2-aminoethoxy)ethoxy)ethyl)carbamate.....	131
9.2.6	4-(3,5-bis(2-hydroxyphenyl)-1H-1,2,4-triazol-1-yl)benzoyl chloride.....	132
9.2.7	Tert-butyl-(2-(2-(2-(4-(3,5-bis(2-hydroxyphenyl)-1H-1,2,4-triazol-1-yl)benzamido)ethoxy)ethoxy)ethyl)carbamate.....	133
9.2.8	N-(2-(2-(2-aminoethoxy)ethoxy)ethyl)-4-(3,5-bis(2-hydroxyphenyl)-1H-1,2,4-triazol-1-yl)benzamide.....	134
9.2.9	Methyl 4-(3,5-bis(2-hydroxyphenyl)-1H-1,2,4-triazol-1-yl)benzoate.....	134

9.2.10	Ethyl 4-(3,5-bis(2-hydroxyphenyl)-1H-1,2,4-triazol-1-yl)benzoate	135
9.2.11	2,2'-(1-(2-hydroxyethyl)-1H-1,2,4-triazole-3,5-diyl)diphenol	136
9.2.12	2-(3,5-bis(2-hydroxyphenyl)-1H-1,2,4-triazol-1-yl)ethyl benzoate	136
9.2.13	2-(3,5-bis(2-hydroxyphenyl)-1H-1,2,4-triazol-1-yl)ethyl-4-methyl benzenesulfonate	137
9.2.14	2-(3-(2-hydroxyphenyl)-1-(2-(tosyloxy)ethyl)-1H-1,2,4-triazol-5-yl)phenyl-4- methylbenzenesulfonate	138
9.2.15	Alginate-deferasirox conjugate Exalg	139
9.2.16	Chitosan-deferasirox conjugate Exkite.....	141
9.2.17	Alginate-catechol conjugate	142
9.2.18	Chitosan-catechol conjugate.....	143
9.3	Phenol/Sulphuric acid assay	144
9.3.1	Ligand concentration	144
9.3.2	Polymer concentration	144
9.3.3	Percentage modification	145
9.4	UV-Vis spectroscopy iron titration experiments	145
9.5	Iron binding by polymer dialysis.....	145
9.5.1	Dialysis experiments	145
9.5.2	Ferrozine assay of polymers.....	146
9.5.3	Atomic absorption spectroscopy	146
9.6	Cell culture	147
9.7	MTT cell viability assay.....	147
9.8	Western blot.....	148
9.8.1	Sample preparation	148
9.8.2	SDS-Polyacrylamide gel electrophoresis (SDS-PAGE)	149
9.8.3	Transfer of gels.....	150
9.8.4	Blocking membranes	151

9.8.5	Primary antibody	151
9.8.6	Secondary antibody	151
9.8.7	Developing blots.....	151
9.9	Ferritin ELISA.....	152
9.10	Intracellular ferrozine assay.....	152
9.10.1	Sample preparation.....	152
9.10.2	Protein assay.....	153
9.10.3	Ferrozine assay	153
9.11	Preloading cells with iron.....	154
9.12	Murine studies	155
9.13	Exkite activity in mice.....	156
9.13.1	Exkite safety and tolerability.....	156
9.13.2	Deferasirox detection in blood plasma.....	156
9.13.3	Deferasirox detection in crypt cells.....	156
9.14	Mouse survival studies	157
9.15	Immunohistochemistry.....	158
9.15.1	De-wax and rehydrate slides.....	158
9.15.2	Antigen retrieval.....	158
9.15.3	Prevention of endogenous staining/Blocking.....	158
9.15.4	Primary antibody	159
9.15.5	Secondary antibody	159
9.15.6	Visualisation of positivity.....	159
9.15.7	Scoring of slides	159
9.16	Statistical analysis	160
10	References.....	161

1 Introduction

1.1 *Biological role of iron*

Iron, a first row transition metal of the periodic table, is not only one of the most abundant elements on the Earth¹ but is also an essential nutrient found in most living organisms.² It is vital in many mammalian cellular processes including DNA synthesis, proliferation and growth³ and is also utilised in numerous enzymes through the formation of iron-sulphur clusters.⁴ Furthermore, it plays an imperative role in the transport and storage of oxygen in the iron containing metalloproteins haemoglobin and myoglobin.⁵

Iron absorption in humans occurs in the duodenum with only 10% of dietary iron being absorbed.⁶ This is a heavily regulated process since humans do not possess a physiological mechanism for excreting excess iron, therefore deviation from this tightly regulated process can be particularly harmful.⁷ Iron deficiency anaemia occurs when there is an inadequate amount of iron in the body to meet physiological demands, and can result in fatigue and compromised immunity.⁸ Conversely, iron overload can occur in patients suffering from hemochromatosis, which is a genetic disorder resulting in excessive accumulation of iron, and also in patients receiving long term blood transfusions for various blood disorders such as β -thalassemia.⁵ Iron overload can cause iron deposits to occur around vital organs causing tissue damage, contributing to heart and liver diseases.^{9, 10} Aside from the complications arising from iron overload, it has been also been observed that patients suffering from iron overload diseases are also at increased risk of liver and colorectal cancer (CRC).¹¹

1.2 Iron and colorectal cancer

Numerous factors are associated with an increased risk of colorectal cancer (CRC) which includes genetic predisposition, age, history of inflammatory bowel disease and an unhealthy lifestyle. However, iron has been recognised in the aetiology of CRC,^{7, 12, 13} which causes approximately 16,000 deaths per year in the UK, making it the second most common cause of death from cancer in the UK.¹⁴

1.2.1 Epidemiological evidence

Many epidemiology studies have shown that there is a greater incidence of CRC in developed nations^{15, 16} with 60% of all cases occurring in Western Europe, North America and Australia (Figure 1).¹⁷ This has been specifically associated with an iron rich diet comprising of red and processed meat which are rich sources of haem containing compounds.^{7, 13} Therefore, a high dietary iron intake has been identified as CRC risk factor.¹⁸

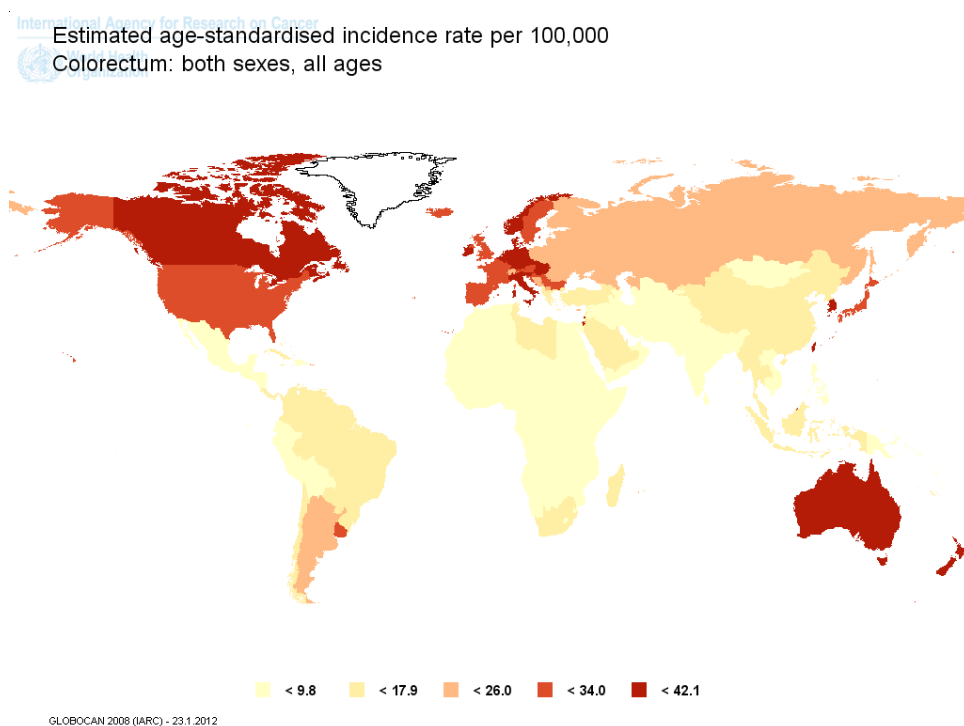


Figure 1 Map showing colorectal cancer incidence in different regions of the world. More developed regions including Australia, New Zealand, Europe and North America have significantly greater cancer incidence than less developed regions.

1.2.2 Iron metabolism and regulation in cancer

Iron absorption in humans principally happens in the duodenum (the first section of the small intestine), where dietary iron, mostly in the ferric (Fe (III)) form, is absorbed through the action of a reductase, duodenal cytochrome b (DCYTB) which reduces ferric (Fe (III)) iron to ferrous (Fe (II)) iron. Divalent metal transporter 1 (DMT1) enzyme transports ferrous iron into the enterocytes, and exits through the action of an iron efflux pump ferroportin and the oxidase hephaestin which oxidizes ferrous to ferric iron, which is then loaded onto transferrin (TF).¹⁹ This circulates in the bloodstream to deliver iron to sites of use (Figure 2). Hepcidin (HP), a peptide hormone produced by the liver is the ‘master regulator’ of systemic iron homeostasis.²⁰ Hepcidin is expressed in response to excess iron and binds to ferroportin, preventing iron from being exported from enterocytes.

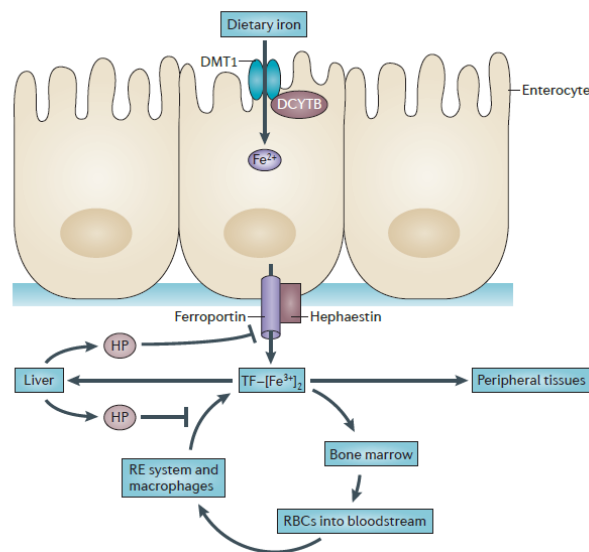


Figure 2 Iron homeostasis in humans. (Reprinted with permission from Macmillan Publishers Ltd, Copyright 2013.)

When the transferrin bound iron reaches a site of use, it binds to transferrin receptor 1 (TFR1) on the plasma membrane of cells and is endocytosed, where ferric iron is released and reduced to ferrous iron by the ferrireductase STEAP3. DMT1 transports ferrous iron out of the endosome and into the labile iron pool, and from here iron is taken to multiple destinations for various applications

including DNA synthesis and repair, energy generation by mitochondria and haem synthesis.² Excess iron is stored in the iron storage protein ferritin. Iron leaves the cell through ferroportin, under the action of an oxidase such as hephaestin or ceruloplasmin which converts ferrous to ferric iron for loading onto transferrin (Figure 3).¹⁹

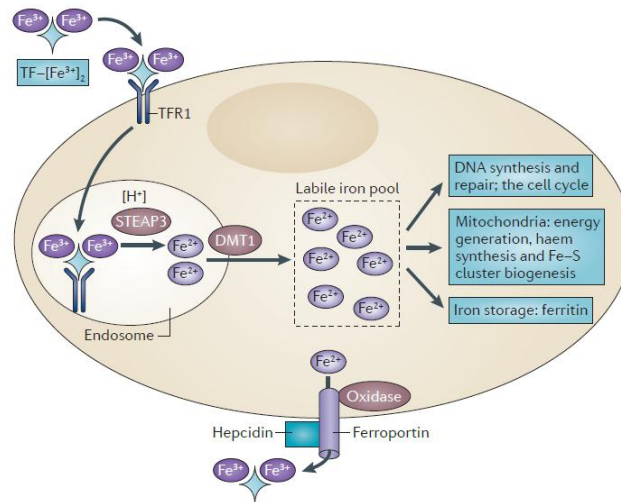


Figure 3 Iron metabolism in mammalian cells. (Reprinted with permission from Macmillan Publishers Ltd, Copyright 2013.)

Cancer cells have amplified amounts of metabolically available iron due to increasing iron uptake *via* TFR1 and decreasing iron storage in ferritin.²¹ Iron efflux *via* ferroportin is also reduced by the upregulation of hepcidin leading to ferroportin degradation.²² Increased intracellular iron levels can fuel proliferation of cancer cells.²³ Furthermore, adenomatous polyposis coli (Apc) gene is a tumour suppressor gene which is mutated or deleted in the majority of CRC cases.²⁴ This genetic aberration is known to activate oncogenic signalling pathways,²⁵ and is an early event in the adenoma to carcinoma sequence, resulting in multiple intestinal polyps which progress to cancerous tumours. It has been shown that following Apc deletion, there is a rapid induction of iron import proteins TFR1 and DMT1, which suggests an intimate relationship between iron and CRC, in the background of Apc deletion.²⁶

1.2.3 *In vivo* evidence

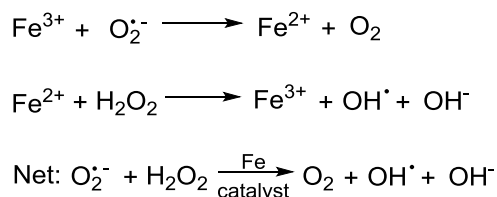
Mouse model studies were conducted by Radulescu *et al.* using $Apc^{min/+}$ mice which carry the germline *Apc* mutation and are representative of early stage CRC as they develop multiple intestinal adenomas.²⁶ When these mice were fed an iron rich diet, the tumour burden increased significantly in both tumour number and size, whereas mice fed an iron deficient diet had a greatly reduced tumour burden compared to the controls. In order to elucidate the role of luminal iron as opposed to systemic iron, mice were given intravenous iron supplementation to induce systemic iron overload whilst on an iron deficient diet. These mice still showed a decreased tumour burden which indicates that systemic iron overload does not affect CRC, whereas luminal iron levels are critical.²⁶

Patients suffering from ulcerative colitis and Crohn's disease are also at risk of anaemia due to persistent colonic blood loss and are often recommended iron rich diets as well as oral iron supplements in order to counteract the resultant loss of iron from the body.²⁷ However, recent studies have shown that an iron-enriched diet not only exaggerates ulcerative colitis symptoms, but also elevates the development of ulcerative colitis related colorectal carcinoma.⁶ It has also been shown that a reduction of luminal iron leads to a lowering of ileitis associated with Crohn's disease and offers significant alterations to gut microbiota.²⁸

1.3 *The influence of iron in oxidative stress*

The inherent ability of iron to gain and loose electrons, the very attribute that makes iron useful biologically, is also the attribute which contributes towards the toxicity of iron when present in excess. The ability to redox cycle between two stable oxidation states, ferric (Fe (III)) and ferrous iron (Fe (II)), allows it to partake in potentially deleterious reactions which generate reactive oxygen species (ROS) such as the hydroxyl radical (Scheme 1).²⁹ This can interact with most

biological molecules causing oxidative tissue damage, and can also initiate lipid peroxidation leading to the loss of cell membrane structure and function, which is thought to cause the formation of cancerous cells.³⁰ In cases such as transfusion induced iron overload, the excess iron can lead to free radical induced tissue damage which can prove to be fatal without chelation therapy.³¹



Scheme 1 The Haber-Weiss reaction generates toxic hydroxyl radical species *via* Fenton chemistry enabled by redox cycling by Fe (II) and Fe (III) in the presence of superoxide radical ($\text{O}_2^{\cdot-}$) and hydrogen peroxide (H_2O_2).

1.4 Iron chelation therapy

Metal chelation therapy was initially developed in the early 1900s to counteract the toxicity of drugs containing arsenic and antimony, which were frequently used in the treatment of parasitic diseases. The arrival of the industrial revolution resulted in a large increase in cases of accidental heavy metal exposure, in addition to chemical warfare which instigated the development of chelators for mercury and lead poisoning.³²

Iron chelators have emerged to be of importance in the treatment of iron overload disorders and blood conditions such as β -thalassemia which is a genetic defect affecting haemoglobin, in which long term blood transfusions are required leading to iron overload.³¹ Iron chelators have also been investigated as therapeutic agents for degenerative diseases such as Alzheimer's Disease, Parkinson's Disease, and Friedreich's Ataxia. It is proposed that one of the causes of such neurodegenerative diseases is the accumulation of iron in the brain leading to oxidative stress and tissue damage *via* redox cycling.³³

An emerging application of iron chelators is in the treatment of cancer, whereby depleting iron from proliferating cancer cells deprives these cells of an essential nutrient needed for cell replication, therefore can inhibit or retard tumour growth (Figure 4).²¹

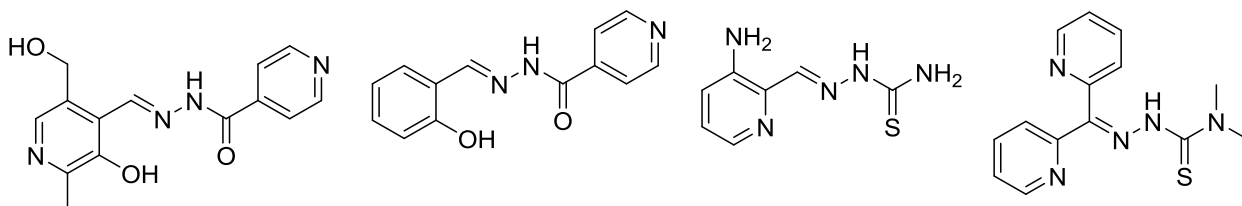


Figure 4 A series of aroylhydrazones and thiosemicarbazones that are known to have potent anti-tumour activity due to their *in vivo* iron chelation and ROS promotion properties.

In addition, kinetically labile bidentate or tridentate chelators, or those containing soft donor atoms which have lower redox potentials can be used to exploit the redox property of iron to target cancer cells.³⁴ The highly reactive nature of ROS species can be harmful, as aforementioned, however the same property of ROS can be used against cancer cells as these iron chelators can be used to promote oxidative damage and subsequent cancer cell death.³⁵ This is particularly advantageous when tumours develop resistance to standard chemotherapeutics and provides an alternate mode of treatment.

1.5 Iron chelator design

There are numerous factors that need to be considered in designing therapeutic iron chelators. Hard-soft-acid-base (HSAB) theory is of importance when considering the number and type of ligands that are appropriate for chelation. Hard acids and bases have small atomic or ionic radius and high oxidation states so that they are charge dense and have low polarizability, whereas soft acids and bases have larger atomic or ionic radius and low oxidation states with high polarizability. In terms of metal chelation, this refers to the donation of electron density from the ligand to the empty *d*-orbitals of the metal,³² with possible back donation from metal to ligand.³⁶ Fe (III) is a hard metal ion which will bind preferentially to hard donors such as oxygen in catechol and

carboxylate groups, as observed in $[\text{Fe}(\text{C}_2\text{O}_4)_3]^{3-}$ in which the hard oxygen donors of the oxalate groups stabilise ferric iron (Figure 5).³⁷ However, Fe (II) is a borderline metal ion with preferential binding to soft donor atoms such as nitrogen,³⁸ such as in $[\text{Fe}(\text{bpy})_3]^{2+}$ which is a stable ferrous iron complex with donation from soft nitrogen donor atoms and back donation to low lying π^* orbitals (Figure 5).³⁹

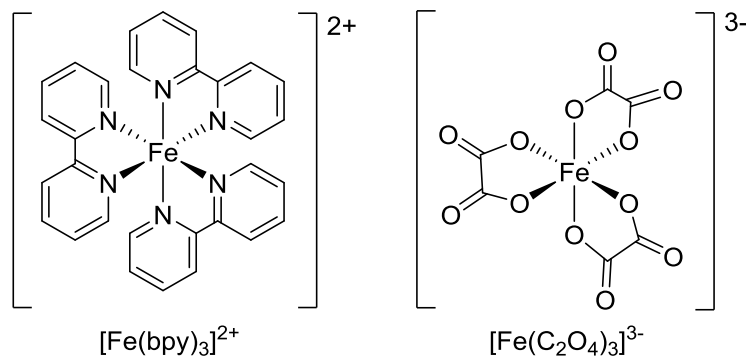


Figure 5 Ferrous bipyridine and ferric oxalate complexes.

The thermodynamic stability of the iron complex is also an important factor. The chelate effect states that as the denticity of the ligand is increased the resultant complex will be more thermodynamically stable due to a favourable entropy change upon exchange of many monodentate ligands of a solvated metal ion for fewer multidentate ligands.³² Also, the size and number of chelate rings formed is driven by thermodynamic factors as the most favourable chelate ring size is five or six membered, and the number of chelate rings formed is five for an octahedral complex (Figure 6).⁴⁰

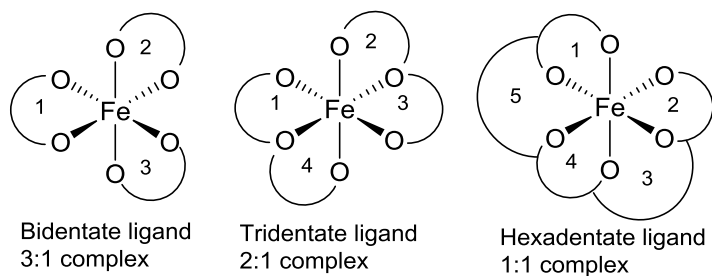


Figure 6 The formation of chelate rings with bi-, tri- and hexadentate ligands.

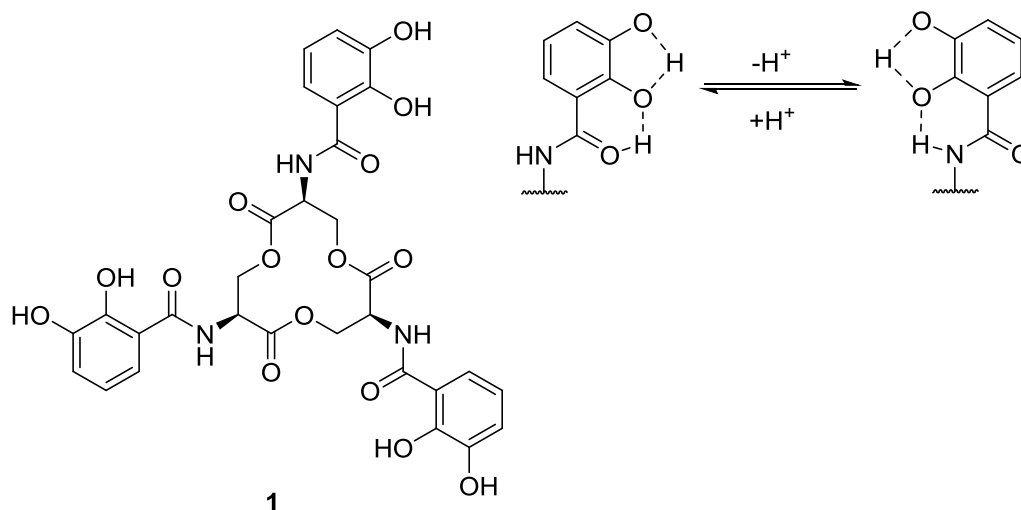
Thus, since Fe (III) is a high spin metal with octahedral coordination sphere, the thermodynamic stability of its complex can be maximised by utilising a hexadentate ligand which will form five chelate rings. Iron chelators designed for therapeutic use must be selective towards iron only so as to prevent deficiencies of other biologically important metals within the body. Whilst it is possible to design ligands for preferential Fe (II) chelation with respect to Fe (III), such ligands can bind to other divalent metals such as Cu (II) and Zn (II). Similarly, Fe (III) chelators containing oxygen donor ligands can have an affinity for other trivalent metals such as Al (III) and Ga (III).⁴⁰ Moreover, ligands with a high affinity for Fe (III) can bind Fe (II) and promote autoxidation of Fe (II) to Fe (III) in aerobic conditions, suggesting that under physiological conditions, a highly Fe (III) selective chelator can bind both Fe (II) and Fe (III).⁴¹

Iron must be tightly bound once chelated in order to minimise exposure to oxygen or hydrogen peroxide to prevent the generation of harmful ROS. Most hexadentate ligands such as desferrioxamine (DFO) (Section 1.6.1) encapsulate Fe (III) by occupying the coordination sphere of the metal ion resulting in a kinetically inert complex diminishing ROS production.⁴² However, ethylenediaminetetraacetic acid (EDTA) (Section 1.6.2) is more kinetically labile with a possible seventh coordination site occupied by water, which can exchange rapidly with oxygen and hydrogen peroxide leading to enhanced ROS production.⁴³

1.5.1 Siderophores: Enterobactin

Due to the importance of iron in many metabolic processes, molecules of low molecular weight and high Fe (III) selectivity called siderophores are produced by microbes in response to iron deficiency in order to scavenge iron from the environment for uptake as soluble Fe (III) complexes.⁴⁴ Siderophores can generally be divided into two groups depending upon the structural functionality that is used to chelate iron: catecholamides or hydroxamates.⁴⁵ Since Fe (III) is a charge dense, hard lewis acid, a hard lewis base such as oxygen is preferred for binding.

Enterobactin, **1** is a naturally occurring siderophore most commonly found in gram-negative bacteria such as *Escherichia coli* and *Salmonella typhimurium*.⁴⁴ The binding affinity for Fe (III) is $K = 10^{52}$ and so it is regarded as the strongest known siderophore.⁴⁶



Scheme 2 Structure of enterobactin **1** and changes in conformation of catechol units by rotation about C-C bond driven by hydrogen bonding.

Enterobactin consists of three catechol functionalities linked by amide bonds to a cyclic trilactone scaffold (Scheme 2). Fe (III) is bound by the catechol groups which form a stable high-spin hexacoordinate octahedral complex; the entropy difference upon binding is minimised by utilising a hexadentate ligand as opposed to bi- or tridentate ligands.

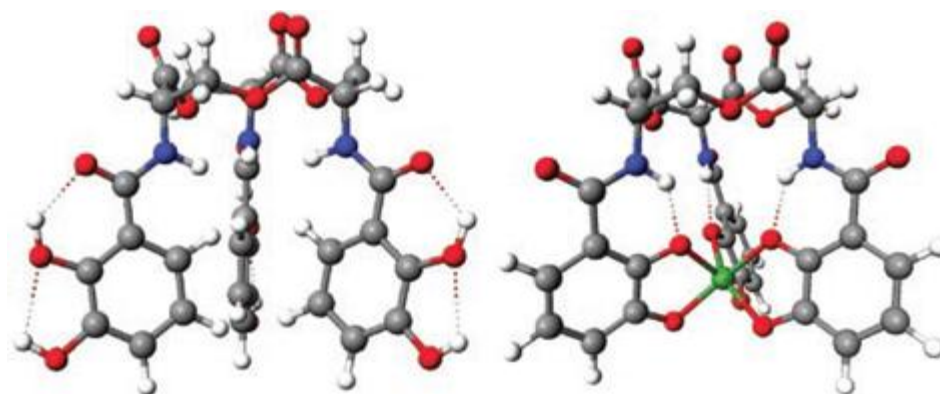


Figure 7 Model of enterobactin showing hydrogen bonding within uncomplexed structure (left) and in that of Fe (III) complex (right) in which grey is carbon, blue is nitrogen, red is oxygen, white is hydrogen and dotted lines represent hydrogen bonds (Copyright 2003 National Academy of Sciences, USA).

Hydrogen bonding is important as catechol groups are effectively locked in one of two conformations. Interconversion between conformations is achieved upon metal complexation, in which deprotonation of catechols are required (Figure 7).⁴⁷ The use of enterobactin for iron chelation therapy has been investigated but is prohibited due to high toxicity encountered in animal studies resulting in inflammation and sepsis, associated with enterobactin's ability to stimulate microbial growth.⁴⁵

1.6 Iron chelators in clinical use

1.6.1 Desferrioxamine

Desferrioxamine (DFO), **2** is a naturally occurring siderophore produced by *Streptomyces pilosus* (Figure 8) and has been the leading Fe (III) chelator in clinical use for the treatment of chronic iron overload since mid-1960s.⁴⁸

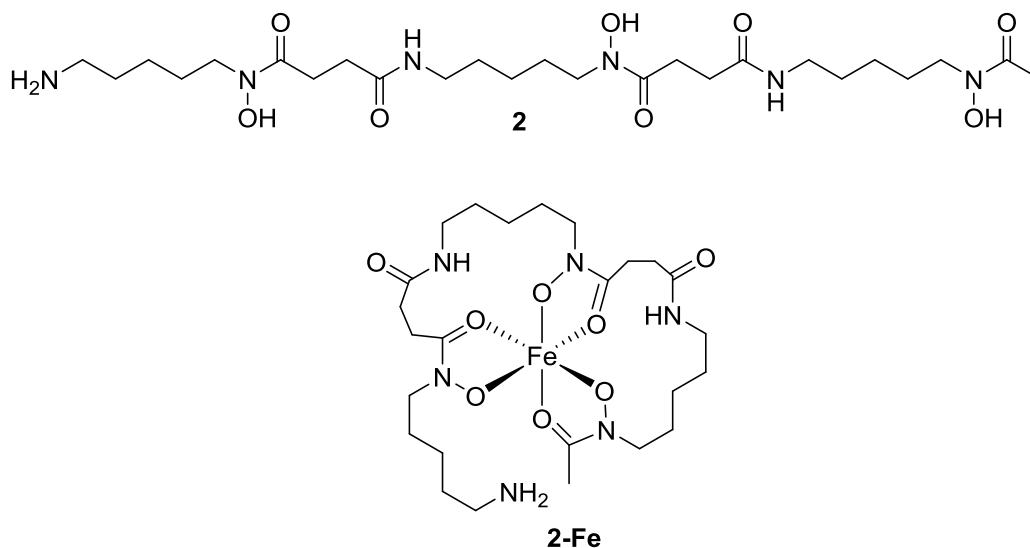


Figure 8 Structure of DFO **2** and its ferric iron complex **2-Fe**.

It is a hexadentate hydroxamate chelator with good affinity for Fe (III) over other trivalent species (Table 1), binding ferric iron in a 1:1 molar ratio. Its hydrophilic nature means that it has poor oral

bioavailability and must be administered subcutaneously or intravenously for 8-12 hours per day, 5-7 days a week. Hence, treatment by DFO is expensive and often has poor patient compliance.³⁴

1.6.2 Aminocarboxylates

Ethylenediaminetetraacetic acid (EDTA), **3** is a synthetic hexadentate chelator binding through two amine nitrogens and carboxylates, although an additional water molecule may also coordinate forming a seven coordinate complex. Diethylenetriaminepentaacetic acid (DTPA), **4** is an expanded version of EDTA and is potentially an oxadentate ligand (Figure 9).⁴⁹ Both bind with excellent affinity for Fe (III) and consequently have been extensively investigated for clinical use, being administered to patients who are intolerant to DFO. However, their lack of selectivity for Fe (III) renders them unsuitable as they also have good affinity for Zn (II) leading to zinc depletion (Table 1), as well as the formation of labile iron complexes resulting in the formation of toxic ROS.⁴⁰

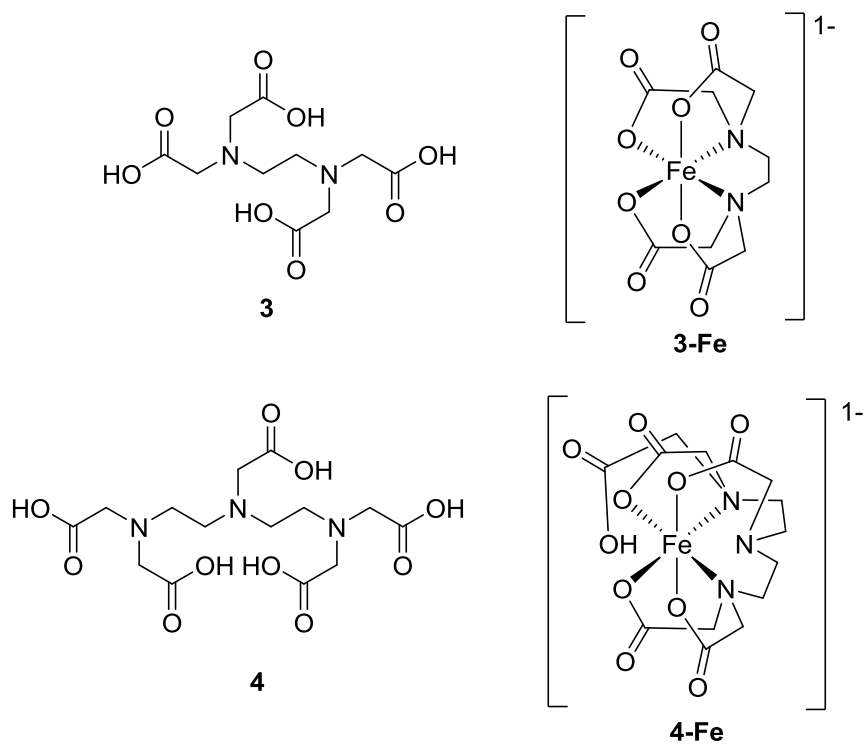


Figure 9 Structure of EDTA **3** and its iron complex **3-Fe**, and DTPA **4** and its iron complex **4-Fe**.

In addition to chelation therapy, the non-specific metal binding ability of EDTA and DTPA renders them useful for other applications such as sequestering of metals in textiles, paper and food industries.⁵⁰ Titrations with EDTA is often used to quantify metal ions in solution based on the stoichiometric formation of metal-EDTA complex.⁵¹ Furthermore, EDTA acts as an anticoagulant in blood samples,⁵² and it can also be used to deactivate metal dependant enzymes by using in excess.⁵³

Table 1 Log cumulative stability constants of various cations with ligands.

Log Cumulative Stability Constants						
Ligand	Fe (III)	Al (III)	Ga (III)	Cu (II)	Zn (II)	Fe (II)
DFO	30.6	25.0	27.6	14.1	11.1	7.2
EDTA	25.1	16.5	21.0	18.8	16.5	14.3
DTPA	28.0	18.6	25.5	21.6	18.4	16.5
Deferiprone	37.2	35.8	32.6	21.7	13.5	12.1

1.6.3 Deferiprone (L1, Ferriprox®)

Deferiprone, **5** belongs to the bidentate hydroxypyridone family extensively investigated by Hider and co-workers for their iron chelation properties.³³ Binding of Fe (III) occurs in a 3:1 molar ratio *via* the *O*-donors (Figure 10).

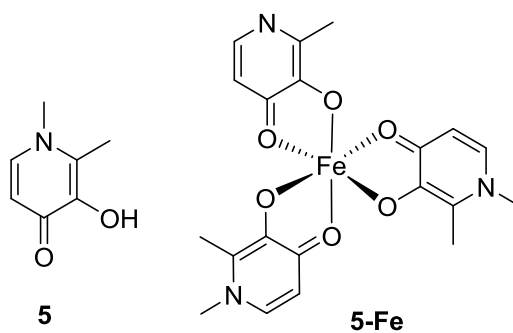


Figure 10 Structure of deferiprone **5** and the ferric iron complex **5-Fe**.

It was developed and quickly applied for therapeutic treatment of iron overload in the early 1980s with the main advantage of deferiprone being that it is available for oral administration.⁵⁴ Unfortunately, deferiprone is only effective at relatively large doses and can lead to side effects, most commonly abdominal pain and nausea. It has also been associated with more severe side effects leading to acute conditions such as agranulocytosis in which white blood cell count is extremely diminished such that the immune system is compromised, and arthropathy which causes inflammation of joints.⁵⁵

1.6.4 Deferasirox (ICL670A, Exjade®)

Deferasirox, **6** is a tridentate chelator with ligand donation arising from the triazole nitrogen and two phenolate oxygens binding in a 2:1 molar ratio with Fe (III) (Figure 11). It has great selectivity for Fe (III) over other divalent ions and is hydrophobic, lending to its oral bioavailability.⁵⁶

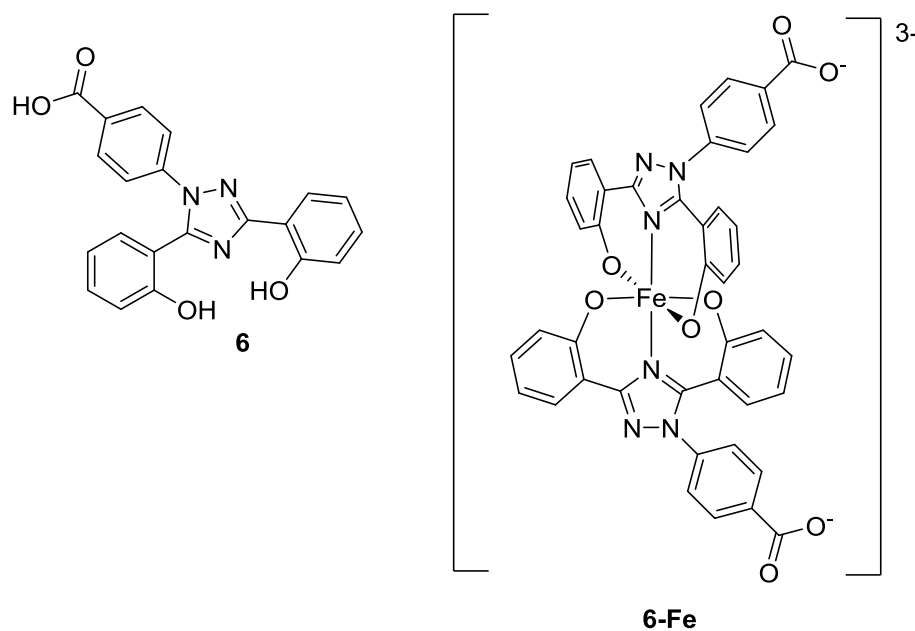


Figure 11 Deferasirox **6** and the ferric iron complex **6-Fe**.

As Fe (III) is best chelated by oxygen containing ligands (HSAB theory), it would be expected that the presence of a borderline donor such as nitrogen would diminish Fe (III) selectivity in favour of divalent metal cations. However, if steric properties of the complex are considered, the ligand-

metal unit is planar with O-M-O bond angle of 180° leading to short bond lengths for M-O and M-N to be 1.60 Å and 1.90 Å respectively.⁵⁷ Such small bond lengths can only be achieved by the binding of small metal ions such as Fe (III). Furthermore, the formation of a six membered chelate ring is also preferred by smaller metal ions. The intrinsic steric strain of the complex system increases as the size of the metal ion is increased contributing to the selectivity of the ligand for Fe (III). Deferasirox also has a relatively good affinity for Al (III) owing to its small ionic radius, but low affinity for other divalent ions (Table 2).⁵⁸ This is currently the leading therapeutic agent for chronic iron overload in favour of DFO and deferiprone due to its oral bioavailability and absence of severe side effects.⁵⁹

Table 2 Formation constants for [MH_xL_y] in H₂O/ DMSO, where M refers to the metal cation, L refers to deferasirox, and H refers to the degree of protonation of the ligand at the carboxylic acid.

	Log Formation Constant					
	Mg (II)	Ca (II)	Cu (II)	Zn (II)	Al (III)	Fe (III)
[ML]	7.6	5.5	18.8	13.3	19.8	23.3
[M(HL)]					24.1	27.5
[ML ₂]			23.9	17.5	34.0	38.6
[ML(HL)]					39.4	44.4
[M(HL) ₂]					44.7	48.7

Deferasirox has also been investigated as a therapeutic against neurodegenerative diseases. Kamalinia *et al.* conjugated deferasirox to lactoferrin in order to improve the water solubility and brain permeability of the ligand. Rat model studies using this compound confirmed the neuroprotective properties of iron chelation in the brain.⁶⁰ There has also been growing interest in the anti-neoplastic activity of deferasirox,⁶¹ as it has been shown to overcome cisplatin resistance to inhibit oesophageal cancer growth,⁶² and is also effective against human lung tumour xenografts in murine models.⁶³ Although anti-neoplastic data of deferasirox in humans is currently limited, it

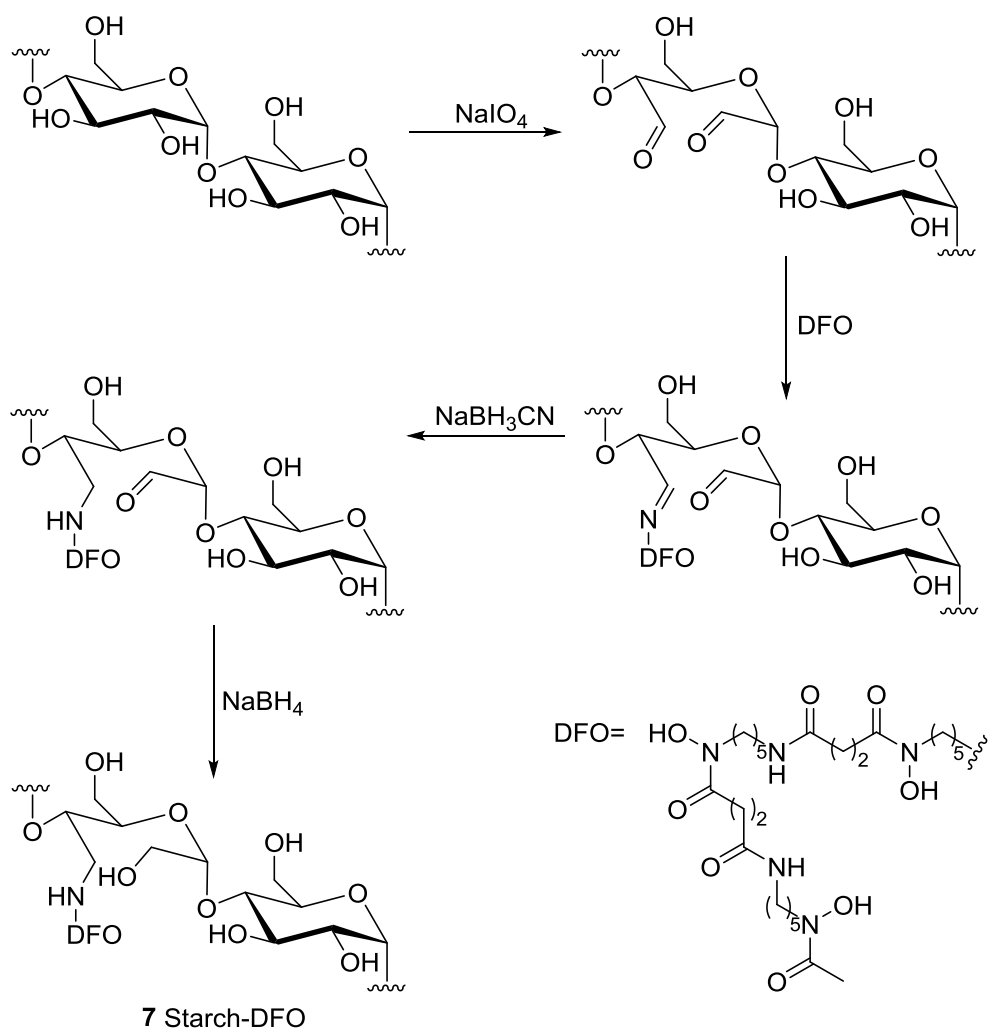
is clear that due to its oral bioavailability, safety profile, and *in vitro* anti-tumour activity, deferasirox is a potential chemotherapeutic for the treatment of cancer.

1.7 Macromolecular iron chelators

Polymeric chelators have applications in water purification,⁶⁴ metal recovery⁶⁵ and pollution regulation.⁶⁶ Macromolecular iron chelators for pharmaceutical use have also been reported, which display unique properties compared to their small molecule counterparts. The high molecular weight renders them non-absorbable in the gastrointestinal tract if taken orally, and increases their blood serum half-life if given intravenously, and they have also been demonstrated to have a lower toxicity profile compared to small molecule chelators.⁶⁷

1.7.1 Polymeric iron chelators

Current methods of iron chelation therapy for chronic iron overload often has poor patient compliance due to the frequency of administration and monitoring required.⁵ In particular, DFO can pose severe problems as the dosage is limited by its acute toxicity and adverse effects on blood pressure which can lead to hypotension. It also has a short plasma half-life so it must be administered by prolonged subcutaneous infusions, which can be uncomfortable or impractical for the patient. To circumvent these problems, a high molecular weight iron chelator was developed by covalently attaching DFO to biopolymers dextran and starch. This was achieved by oxidation of the alcohol groups of the polysaccharide by sodium metaperiodate to yield aldehydes. DFO was added to the activated polysaccharide, and the resultant imine was reduced by cyanoborohydride. Any remaining aldehyde groups were reduced by sodium borohydride, and the reaction mixture was purified by extensive diafiltration to yield compound **7** in Scheme 3.⁶⁸



Scheme 3 Synthesis of 7 starch-DFO conjugate.

The degree of incorporation was calculated to be 20-30% for dextran-DFO and 10-20% for starch-DFO. These substituted polymers showed greatly reduced toxicity in mice and increased plasma half-life of over tenfold compared to free DFO, and any adverse effects on blood pressure was negated.⁶⁹

The starch-DFO conjugate was tested in Phase 1B clinical trial with 21 β -thalassaemia patients suffering from transfusion induced iron overload. This was a single dose study where the patients were given one hour intravenous infusion of the drug at various concentrations ranging 150-900 mg/kg. The starch-DFO conjugate was well tolerated with only four of the patients exhibiting mild urticarial reactions. Plasma and urine iron content were monitored which showed prolonged urinary

iron excretion over seven days, with a linear dose response relationship.⁷⁰ Therefore, these substituted polymers have an iron binding capacity that is identical to the free drug with reduced acute toxicity and increased plasma half-life, allowing higher doses of the active drug to be administered at a lower frequency of administration.

Other examples of DFO based macromolecular chelators include addition of a DFO polymer conjugate to polyethelene glycol (PEG) methacrylate by reversible addition fragment chain transfer (RAFT) copolymerisation (Figure 12) to give **8**. This polymer also had improved vascular retention and *in vitro* cytotoxicity. The DFO moiety is attached to the polymer by an amide linkage, whereas the ester linkage to PEG can be hydrolysed, which will decrease the polymer size enabling effective renal clearance for excretion of the iron bound polymer complex in urine.⁷¹

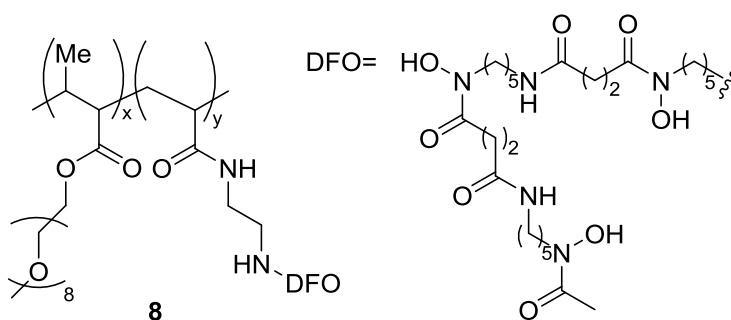


Figure 12 DFO polymer with PEG groups.

DFO immobilised nylon 6,6 chelate fibres were also synthesised which show good affinity for high valence metal ions.⁷² Furthermore, the hydroxamine acid moiety of DFO was exploited to make polymeric hydroxamine acid iron chelators such as **9**, **10** and **11** for the treatment of iron overload, which show improved iron binding compared to DFO due to cooperative binding from a polymeric structure (Figure 13).⁷³

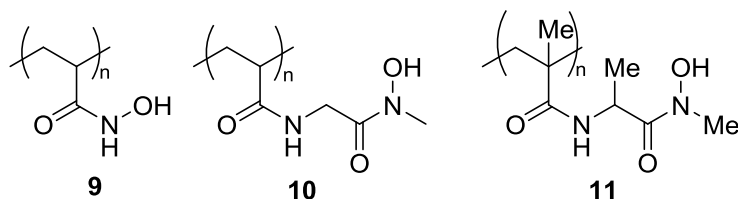
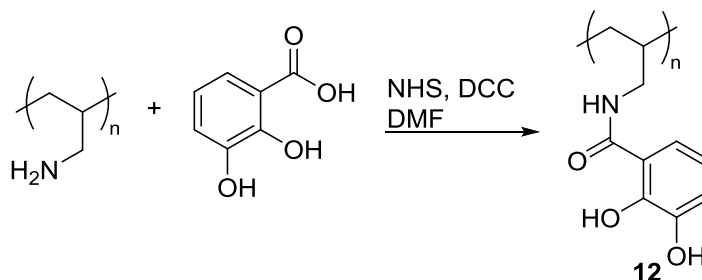


Figure 13 Hydroxamine acid based polymers.

Enterobactin inspired hydrogel was made by Berkland and co-workers in which the catechol iron binding domain was attached to polyallyamine *via* NHS/DCC peptide coupling (Scheme 4) to yield **12**. This afforded improved ferric iron chelation compared to polyallyamine alone, but it also had good affinity towards other divalent metals such as Ni (II), Mn (II) and Cu (II) which may be problematic for application in chelation therapy.⁷⁴



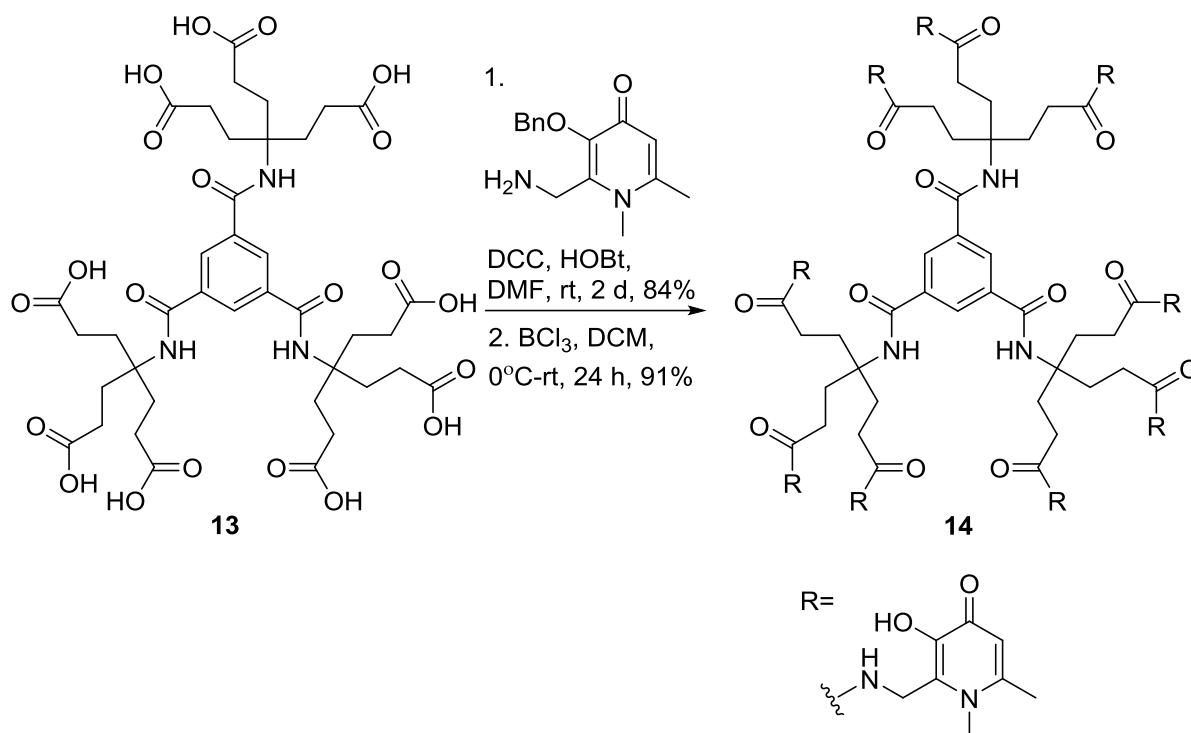
Scheme 4 Synthesis of enterobactin mimetic hydrogel.

Although bidentate chelators may be more readily available or synthesised, it is more difficult to form an ideal octahedral iron complex when in a polymeric chain. Hexadentate chelators are entropically favoured and form stable iron complexes, and this property was utilised by Zhou *et al.* by preparing 3-hydroxypyridin-4-one hexadentate ligands *via* a multistep synthesis. This was incorporated into a block copolymer to form a highly iron selective reusable polymer. *In vitro* perfusion studies using rat intestines suggest that this polymer can be used to remove intestinal iron for patients with hemochromatosis.⁷⁵

1.7.2 Dendritic iron chelators

Dendrimers are repetitively branched molecules with functional groups on the molecular surface, and are usually classified by generation which refers to the number of repeating branching units

from the core.⁷⁶ Although polymers can be easier to synthesise and purify, dendrimers offer the advantage of having a precise molecular weight. Divergent and convergent synthetic strategies were employed to decorate a first and second generation dendrimer respectively with hexadentate ligands, which are effectively three equivalent bidentate 3-hydroxypyridin-4-one moieties (Scheme 5).⁷⁷ Dendrimer-Fe complexes were observed by MALDI mass spectrometric analysis. Iron chelation was also confirmed by titration methods.⁷⁸



Scheme 5 Synthesis of first generation dendrimer containing hexadentate ligands.

DFO appended dendrimers have also been developed by Lim *et al.* which is accessed from a commercially available third generation dendrimer in seven steps, and 35% overall yield containing twelve DFO groups.⁷⁹ The concise structure of dendritic-DFO may afford more robust pharmacokinetic and pharmacodynamic data, compared to starch-DFO which has a poorly defined polymeric size.

1.8 Alginate

Alginic acids (alginates) are heteropolysaccharides distributed widely in nature, most commonly found in marine brown algae and some bacteria.⁸⁰ They consist of (1-4) linked β -D-mannuronic acid (M) and α -L-guluronic acid (G) residues (Figure 14) occurring in MM, GG or MG block copolymeric sequence.⁸¹ The physical properties of alginates can differ depending upon the average molecular weight and distribution of the polymer, as well as the sequence of M and G residues.⁸²

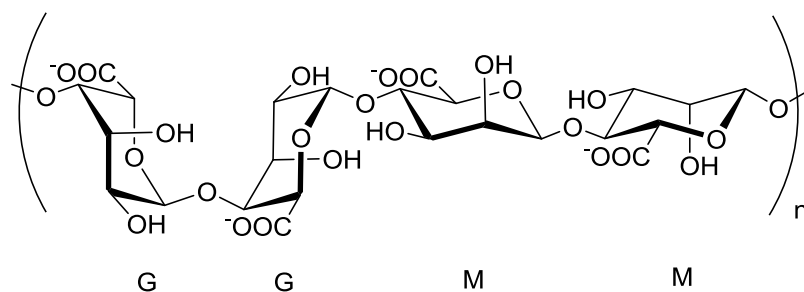


Figure 14 Alginate polymer chain containing G and M residues.

1.8.1 Egg box structure and cation binding

The most important physical property of alginates is the ability to form gels in the presence of cations.⁸³ Alginates are well known to bind Ca (II) with G blocks having a greater selectivity for Ca (II) than M block or MG heteroblock. This can be explained in terms of molecular conformation as when G blocks are packed together, cavities can form into which Ca (II) ions can insert and bind. This is known as the egg box model (Figure 15).⁸⁴ Additionally, Wang *et al.* have shown that there is strong autocoperative binding between Ca (II) and G residues in which all functional groups including hydroxyl and carboxyl groups are involved in binding, thus supporting the egg box model.⁸⁵ Ca (II) has a weaker association with the M residues as these do not pack into a regular egg box structure.⁸⁶

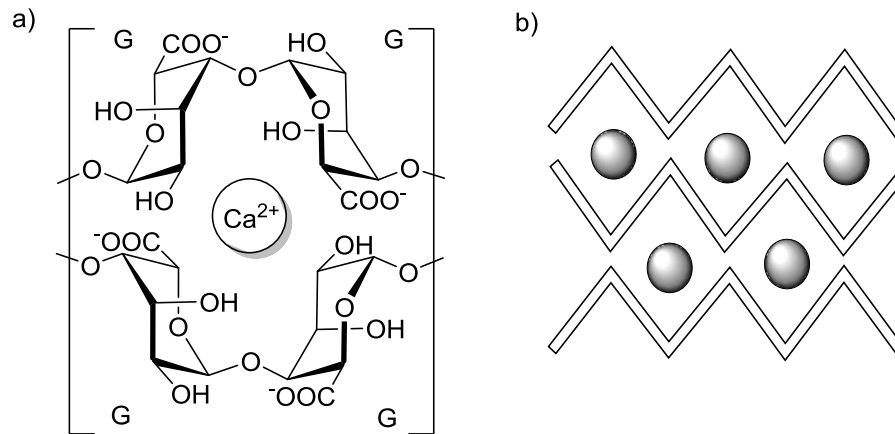


Figure 15 a) The regular packing of G blocks from two alginate strands results in cavities which Ca (II) cations can occupy by interacting with all carboxyl and hydroxyl groups, b) a schematic representation of poly-G units in which the grey spheres represent Ca (II) ions.

Alginates have many applications in which this gelling property is exploited. They are commonly used as a gelling and thickening agent in the food industry as well as in many biomedical applications such as wound dressings, dental impression materials, drug delivery and formulations preventing gastric reflux.⁸⁷ Indigestible viscous polysaccharides such as alginates are non-absorbable in the gastrointestinal tract⁸⁸ and are also known to lower serum cholesterol levels due to their ability to disperse in water.⁸⁹

Alginates have gained recent attention as potential non-absorbable iron chelators for bowel cancer therapy as they do have a propensity for binding other cations such as Fe (II). The ability to bind iron was demonstrated to be related to M:G ratio, with a high M:G ratio displaying high iron binding and reduced calcium binding. Further study using mouse models of colorectal tumorigenesis showed that alginate treatment was able to reduce tumour burden in APC^{min/+} mice.⁹⁰ However, the main limitation of this approach is that iron binding by alginate is not necessarily specific as it can also bind other physiologically relevant metals such as calcium and cause unwanted side effects from calcium deficiency.

1.8.2 Chemical modifications of alginate

Current interest in alginates include chemical modifications of the polymer, especially that of the carboxylic group for numerous applications. The ability of alginates to form hydrogels means that they have been extensively used in medicine as synthetic extracellular matrices (ECM) for cell immobilisation and transplantation in tissue engineering.⁹¹ However, the mechanical properties of hydrogels formed in the presence of divalent cations decays over time due to the loss of cations to the surrounding medium as well as exchange with other cations, which impose significant limitations to their biomedical use. This was overcome by covalently coupling cross-linkers such as polyethylene glycol diamines between alginate chains utilising the carboxylic group and aqueous carbodiimide chemistry to offer greater control over its mechanical properties.⁹² Similarly, alginates can be coupled to short peptides⁹¹ and galactose moieties⁹³ to improve cell anchorage for ECM applications. Furthermore, biotin-alginate conjugate **15** has been synthesised to probe streptavidin-biotin interaction within cells for use as biosensors (Figure 16), which was characterised by FTIR, ¹³C NMR and fluorescence spectroscopy.⁸²

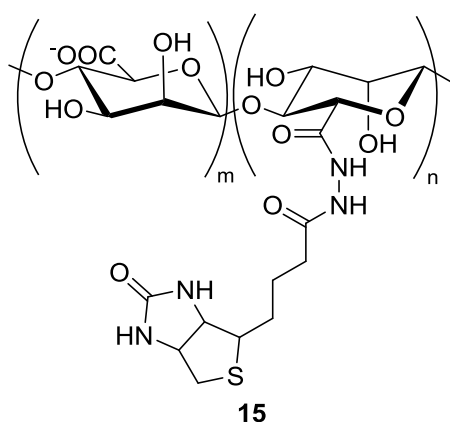


Figure 16 Alginate-biotin conjugate for use as biosensors.

Dopamine modified alginate **16** was synthesised by activation of carboxylic group of alginate by NHS/EDAC coupling chemistry, followed by addition of dopamine (Figure 17) which was characterised by UV-vis and fluorescence spectroscopy, elemental analysis and imaging methods.⁹⁴

This was then alternatively deposited onto CaCO₃ templates with titanium (IV) bis(ammoniumlactato) dihydroxide, so that alginate-titanium microcapsules can be obtained upon removal of the template. This is achieved by the coordination of the catechol moiety to Ti (IV). Similar coupling chemistry was employed to incorporate cystine onto alginate to stabilise gold nano-particles for use as imaging agents.⁹⁵

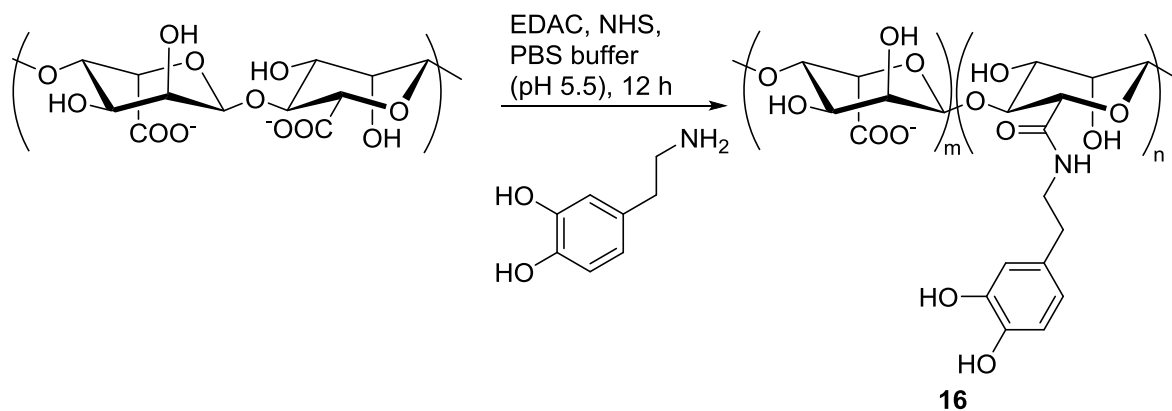


Figure 17 Dopamine modified alginate used to bind to Ti (VI).

1.9 Chitosan

Chitosan is a linear polysaccharide containing randomly distributed (1-4) linked β -D-glucosamine.⁹⁶ It is derived by the deacylation of chitin which is found in the exoskeleton of crustaceans such as crabs and shrimps, and also in the cell walls of fungi, and is second only to cellulose in terms of the most abundant biopolymer in nature.⁹⁷ Chitosan is known to be highly adsorbant of heavy metals such as Cd, Cr, Hg and Pb compared to chitin due to coordination from the free amino groups exposed during the deacylation process, however sorption properties will depend upon the degree of deacylation and amino group content.⁹⁸ The key structural difference between alginate and chitosan is the presence of a primary amine group in place of the carboxylic acid group (Figure 18); however chitosan is also known to form hydrogels in aqueous media lending to similar physical properties and applications.

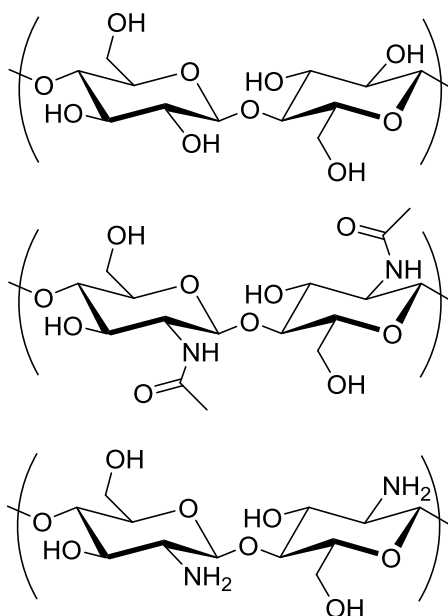


Figure 18 The structure of cellulose (top), chitin (middle) and chitosan (bottom).

The digestion of chitosan by human digestive enzymes and colonic bacteria is unclear. One study suggests that non-crosslinked chitosan is readily digested by pancreatic and colonic bacteria, whereas crosslinked chitosan is more resistant.⁹⁹ Moreover, chitosan itself may influence the concentration of certain types of colonic bacteria present, which was found to be dependent upon the molecular weight of the chitosan.¹⁰⁰

1.9.1 Chemical modifications of chitosan

Protonation of the amino group forms pH sensitive hydrogels¹⁰¹ that are biodegradable and biocompatible enabling applications in tissue engineering and biotechnology.¹⁰² Furthermore, cross linked chitosan has been extensively investigated as a drug delivery agent as it is non-toxic if orally ingested and hydrogels enable sustained and controlled drug delivery.¹⁰³ Modified forms of chitosan beads which allow selective sorption of Fe (III) is also of interest with the potential application of iron removal from contaminated and waste water.¹⁰⁴

Chemical modification of chitosan utilising the amine functionality is widely reported: *N*-carboxymethyl chitosan synthesized from chitosan and chloroacetic acid¹⁰⁵ or glyoxylic acid¹⁰⁶ is

a common ingredient in cosmetic hydrating creams due to its moisturising properties on skin.⁹⁶ Chitosan bound to sugars such as D- and L- fructose as reported by Morimoto and co-workers were investigated for biological interactions with lectins and canine polymorphonuclear leukocyte (PMN) cells.¹⁰⁷ Dendrimers, which are known to have viral inhibiting properties, containing an aldehyde moiety and spacers are also attached to chitosan by reductive *N*-alkylation.¹⁰⁸ Furthermore, chitosan linked to cyclodextrins have gained prominence due to the hydrophobic nature of the cyclodextrin core, allowing selective binding small molecules with potential applications in drug delivery and cosmetics.¹⁰⁹

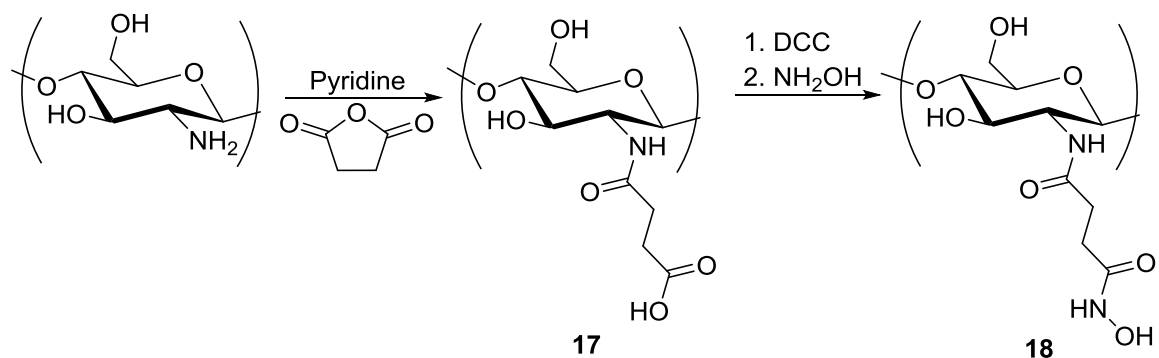


Figure 19 Chitosan succinate and hydroxymated chitosan succinate used to cross link with Fe (III).

Metal binding of modified chitosan is also used to form cross linked polymer beads for drug delivery; chitosan succinate **17** and hydroxamated chitosan succinate **18** (Figure 19) were prepared, principally characterised by IR spectroscopy, and cross linked by addition of FeCl₃ due to chelation by *O*-donor groups of succinate for prolonged drug delivery applications in which iron leeching was found to be minimal, suggesting tight coordination of ferric iron.¹¹⁰

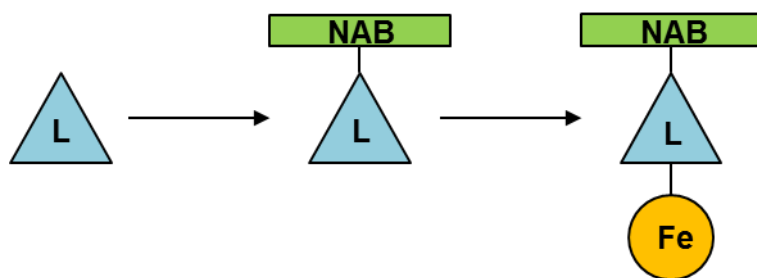
1.10 Conclusion

With the growing prevalence of colorectal cancer in developed countries, the emergence of iron chelators as a potential therapeutic and preventative agent is of great importance. The current course of treatment for colorectal cancer is invasive surgery to remove cancerous tissue and

chemotherapy which has many unpleasant side effects. The use of non-absorbable backbones such as alginate and chitosan attached to chelators will enable targeted chelation therapy and may provide an additional option for treatment. Due to the increasing cost of cancer care, the development of cancer preventative agents could also contribute towards lowering cancer incidence and mortality, and consequently is likely to enable the provision of more affordable cancer treatment.¹¹¹

2 Project overview and Aims

Due to the innate association between luminal iron and colorectal cancer, the main objective of this project is to design and synthesise an iron chelator which can be utilised to specifically target and remove excess iron from the colon. This can be used as a therapeutic agent for those already affected with the disease or as a preventative agent for those at increased risk of the disease (Scheme 6). The extent of redox cycling between ferrous (Fe (II)) and ferric states (Fe (III)) of iron is unknown under physiological conditions so both states of iron will be taken into account. The iron chelator must bind iron selectively in the presence of other physiologically relevant ions and offer good chelation to suppress and minimise redox cycling of iron.



Scheme 6 The development of ligand (L) attached to a non-absorbable backbone (NAB) for chelation of iron.

Consequently, the proposed system should deliver iron chelators to the colon and conjugation with non-absorbable polymer conjugates represent an ideal platform to achieve this. However, aggregate and salt-like systems for colonic ligand delivery may also provide an alternative approach. It is important that the chelator is not digested and absorbed into the blood stream as this may cause systemic iron deficiency and associated side effects. This will be enabled by a targeted approach in which the chelator should specifically remove iron from the bowel. Finally, iron binding studies of the polymer materials will establish the iron binding strength of the polymers which will contribute to *in vitro* and *in vivo* studies in which the toxicity and chelation properties of these compounds can be determined.

3 Synthesis

3.1 Background

The state-of-the-art evidence discussed previously (Chapter 1) led to the conclusion that excess free luminal iron is a driver of carcinogenesis in the colon. Chelators developed thus far are predominantly used for the removal of systemic, plasma circulating iron and are often orally active with limited toxicity. However, the design of an iron chelator that will sequester luminal iron should be non-absorbable and non-fermentable by the microbiota in the gastrointestinal tract so that iron removal occurs specifically in the colon, to prevent systemic iron deficiency by absorption of the iron chelator into the bloodstream. Furthermore, iron must be bound selectively by ligands ideally removing excess luminal iron *via* excretion; removal of non-target physiologically important metals may potentially be deleterious.

Clinically used iron chelators such as desferrioxamine, deferiprone and deferasirox were considered as their iron binding properties and toxicity profiles are well characterised. Additionally, such chelators have already undergone rigorous clinical trials in humans to assess safety and tolerability. Desferrioxamine and deferiprone both have low tolerability, risk of side effects, and a chemical structure that cannot be easily altered without affecting the key iron binding functionalities. Therefore, deferasirox **6** (ICL670A, Exjade®, Figure 20) was chosen as a suitable iron chelator for investigation in the role of CRC therapy due to its high affinity and selectivity of iron over other physiologically relevant metals, a facile two step synthesis from commercially available starting materials, and a chemical structure that lends itself for further chemical manipulation. Deferasirox is also known to exhibit anti-neoplastic effects against specific cancerous tumours (Section 1.6.4).

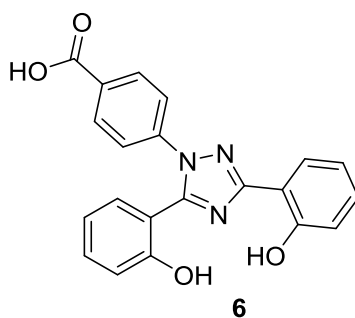
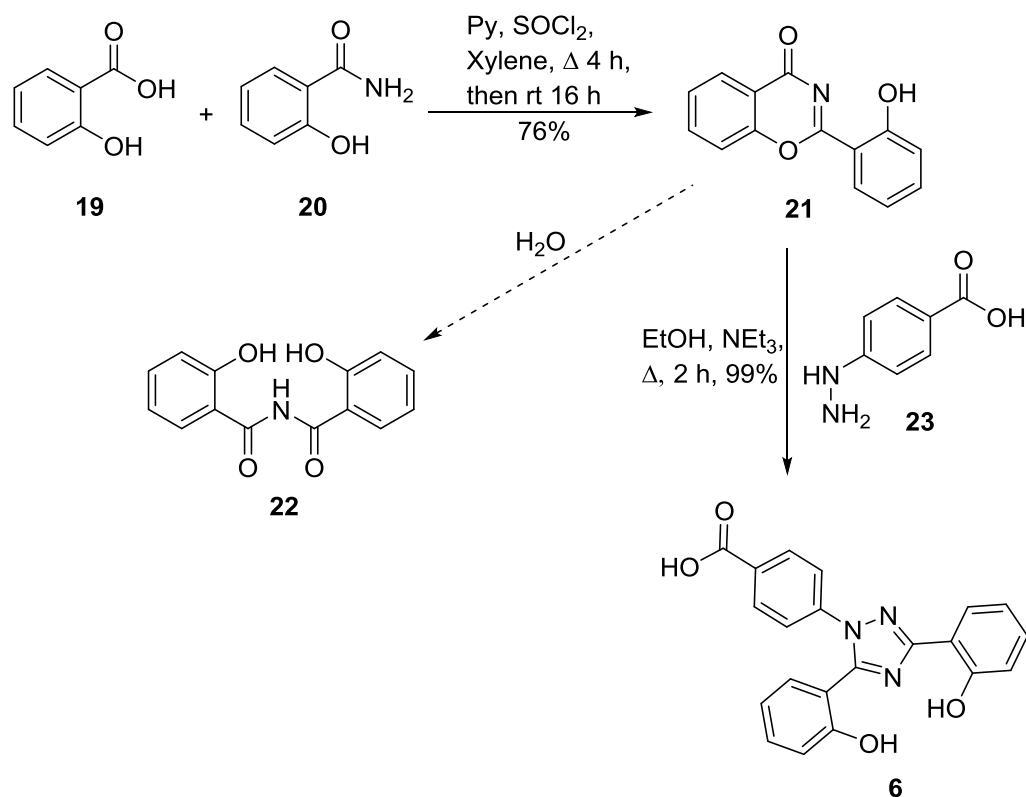


Figure 20 Structure of deferasirox **6**.

In order for this chelator to be non-absorbable in the gastrointestinal tract, the design proposed allows attachment to a polymeric backbone, which should also be non-toxic and safe to consume. Naturally occurring polymers were considered, in particular alginate and chitosan which are already used in many food products as thickening agents so are approved for human consumption. They also have chemical moieties that can be utilised to attach deferasirox to afford non-absorbable iron chelators. As such, investigations in the use of this ligand and these polymers, whether as conjugates or hybrid material presents a reasonable strategy for moving forwards towards the clinic given they have independent low toxicity.

3.2 Ligand synthesis and modifications

The synthesis of deferasirox **6** was based on work by Steinhauser *et al.*⁵⁷ and began with commercially available salicylic acid **19** and salicylic amide **20** to afford intermediate **21** via the formation of the acid chloride, which aids cyclisation. This was further reacted with 4-hydrazinobenzoic acid **23** in which the hydrazine attacks the electrophilic sites of the carbonyl and imine carbons to produce the triazole **6** in 99% yield (Scheme 7). It was discovered during synthesis that intermediate **21** readily decomposes in the presence of moisture into **22** which was very difficult to remove from the mixture by column chromatography or recrystallisation. Therefore, **21** was synthesised and immediately used in the next step of ligand formation.

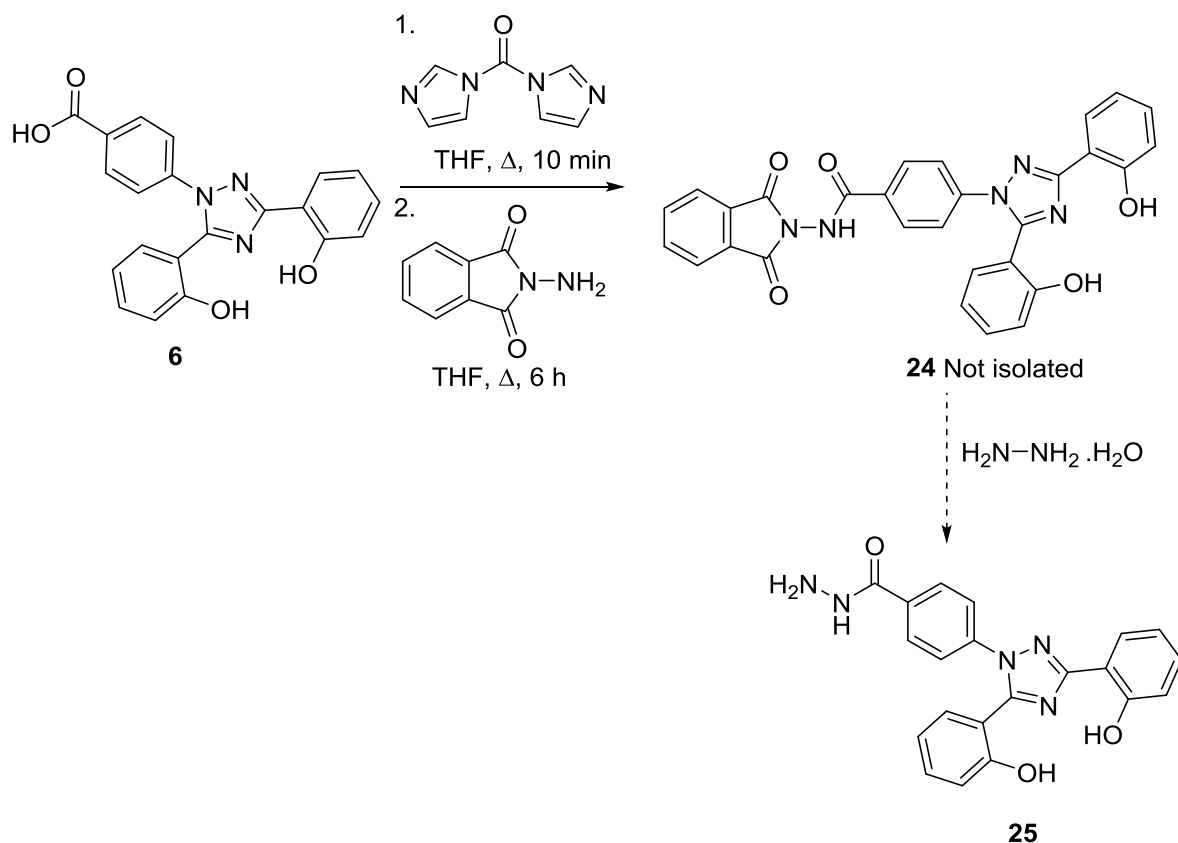


Scheme 7 Two-step synthesis leading to the formation of deferasirox **6**.

Since the iron binding capacity of deferasirox comes from the phenolic oxygens and nitrogen of the triazole, this part of the molecule must be left unmodified for it to be an effective ligand. However, attachment to a non-absorbable backbone can occur through utilisation of the carboxylic acid or by exchanging **23** with hydrazines that contain different functionalities. In the first instance, alginate which contains carboxylic acid groups was identified as a suitable non-absorbable backbone. Carbodiimide mediated cross coupling reactions utilising the free carboxylic acid groups of alginates with amines are well known and documented (Section 1.8.2). Hence, it was proposed that the carboxylic acid group of ligand **6** can be chemically modified to an amine for further coupling to alginate.

Initial attempts were based on the synthesis of *N*-protected aminophthalimides with the removal of the phthaloyl group leading to the corresponding hydrazine **25**, by Brosse *et al.*¹¹² 1,1'-carbonyldiimidazole (CDI) is a highly reactive carbonylating agent used to activate carboxylic

acids *via* the formation of the reactive *N*-acylimidazole intermediate, with the release of carbon dioxide as the entropic driving force. This can further react with *N*-amiophthalimide to afford the product **24**. The removal of the phthaloyl group using hydrazine hydrate as a nucleophilic agent to give the corresponding hydrazine **25** (Scheme 8) would have allowed direct coupling of the product to alginate in a similar method to that described by Polyak *et al.*⁸²



Scheme 8 CDI mediated amide formation of **6** followed by a proposed reaction with hydrazine hydrate.

However, **24** could not be isolated from the reaction mixture after column chromatography despite mass spectrometry (MS) evidence for product formation (Figure 21). This was repeated using benzoic acid as a model reaction but similar purification problems were encountered.

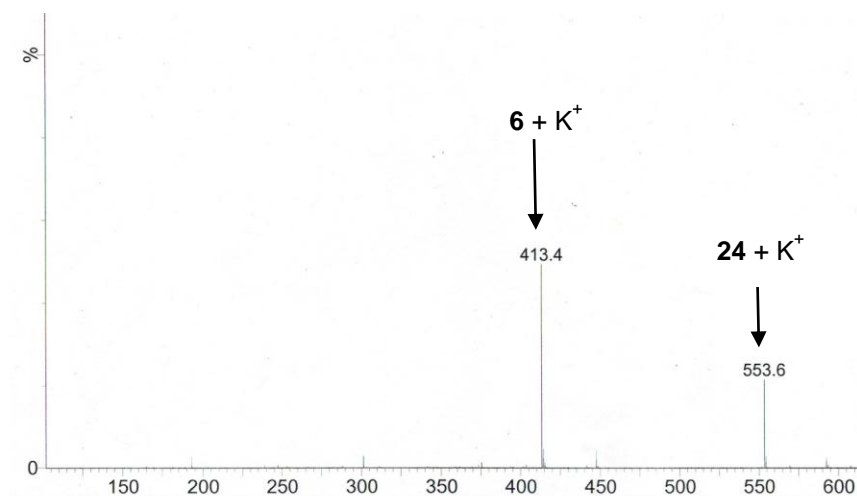
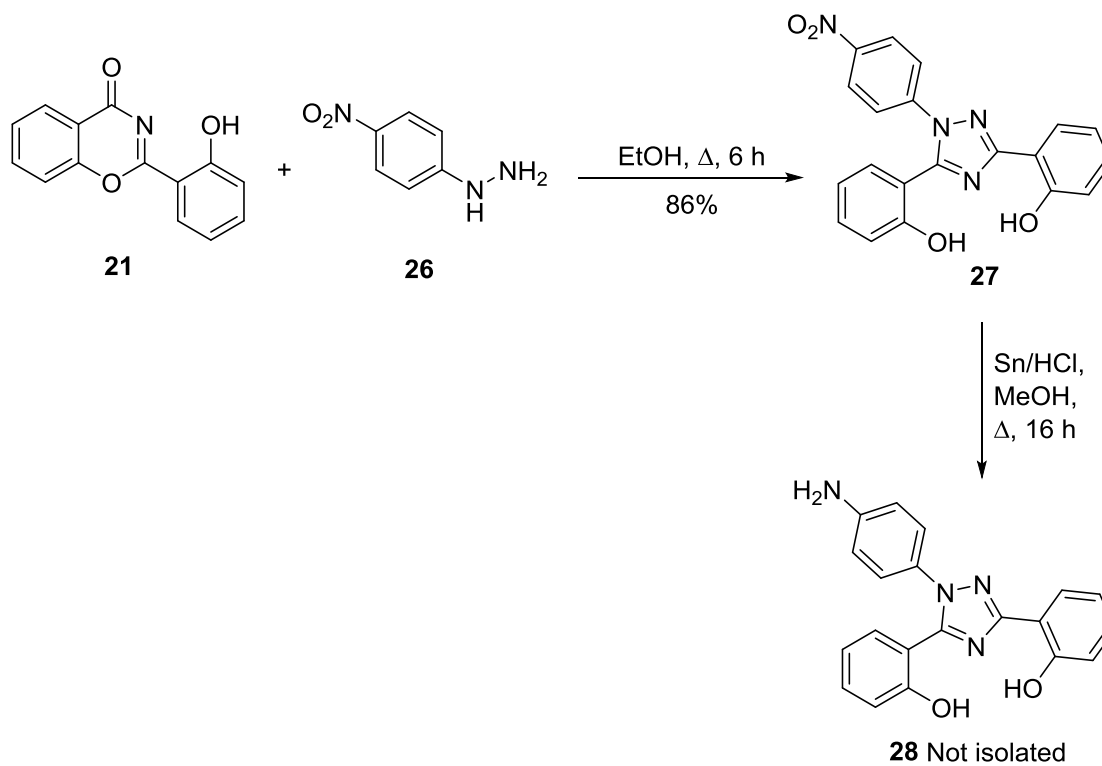


Figure 21 Mass spectra of reaction mixture showing unreacted starting material **6** + K^+ and product **24** + K^+

Alternatively, different hydrazines can be used to incorporate different functionalities and as such 4-nitrophenyl hydrazine **26** was reacted with intermediate **21** to give product **27** in 86% yield (Scheme 9).



Scheme 9 Synthesis of nitro-ligand **27** and attempted hydrogenation.

Reduction of the nitro group in **27** was attempted utilising two different methods to try and form the corresponding amine (Scheme 9). Hydrogenation was attempted with Pd/C catalyst and hydrogen gas in a sealed reaction vessel, however this gave a mixture of compounds that could not be separated by column chromatography. Therefore, the reduction was tried with Sn/HCl, and although there was evidence for product **28** formation by MS (Figure 22), it could not be isolated in good purity or yield.

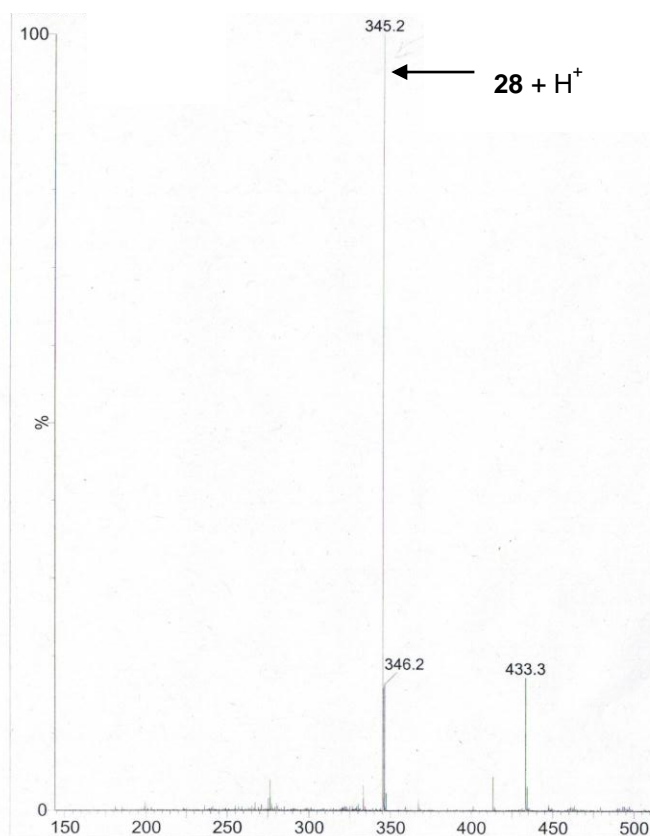
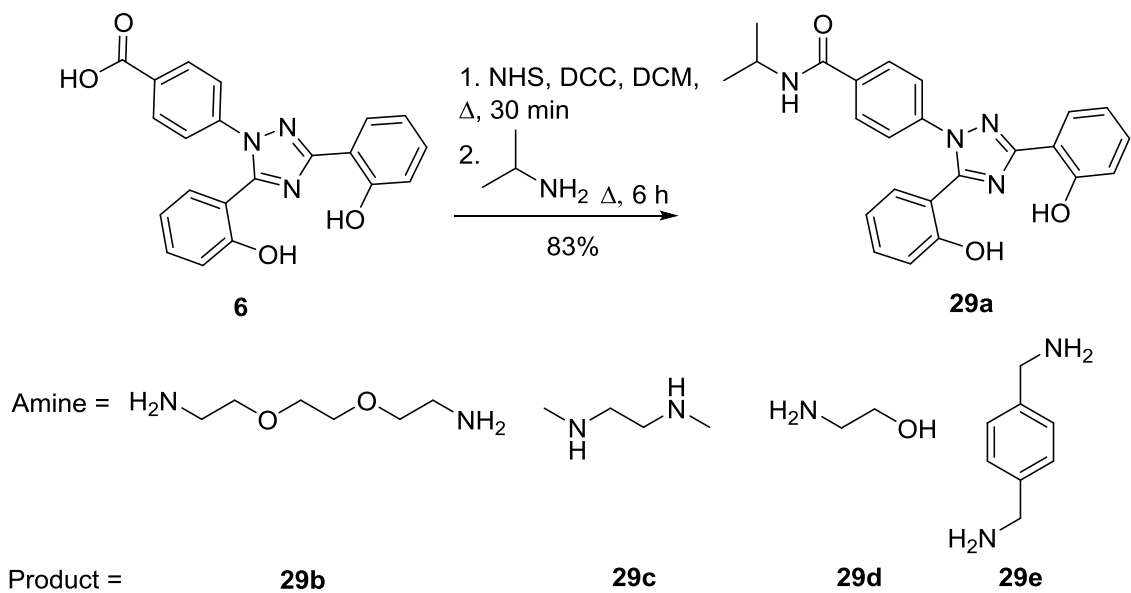


Figure 22 Mass spectra of reaction mixture after reduction of **27** to **28** by Sn/HCl showing product **28** +H⁺ as main peak.

The carboxylic acid group on ligand **6** can also be utilised in NHS/DCC mediated coupling reactions with amines to afford amides. Hence, it was proposed that reacting **6** with excess diamine would incorporate a free amine for further coupling to the carboxylic groups of alginate. Amide formation with **6** was initially tested using isopropylamine to establish the protocol which gave **29a** in 83% yield after column chromatography. Consequently, numerous diamines were used in the attempted synthesis of an amino-amide moiety (Scheme 10).



Scheme 10 Amide formation with isopropyl amine (top) to yield **29a**, and other amines tried in this reaction (bottom).

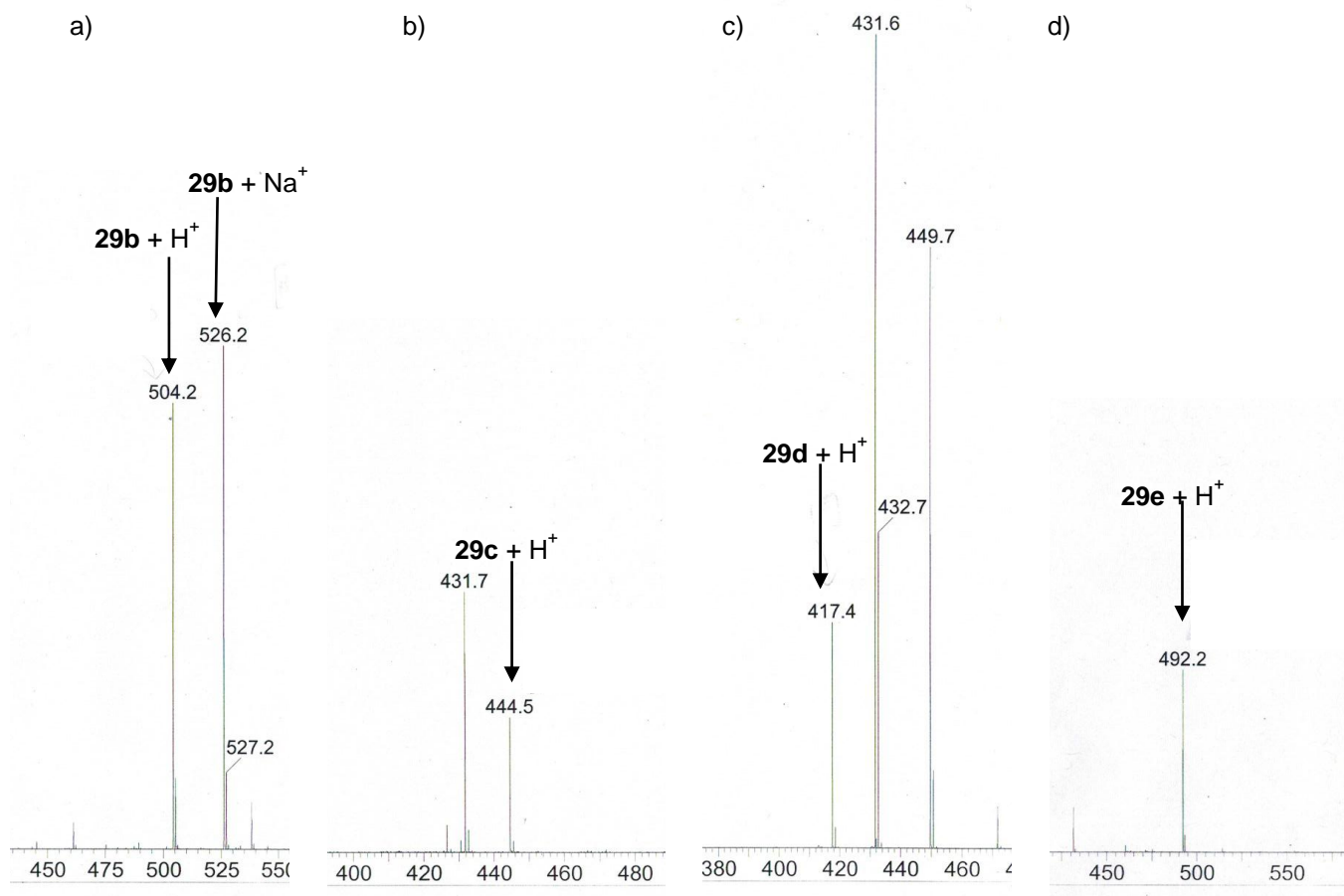
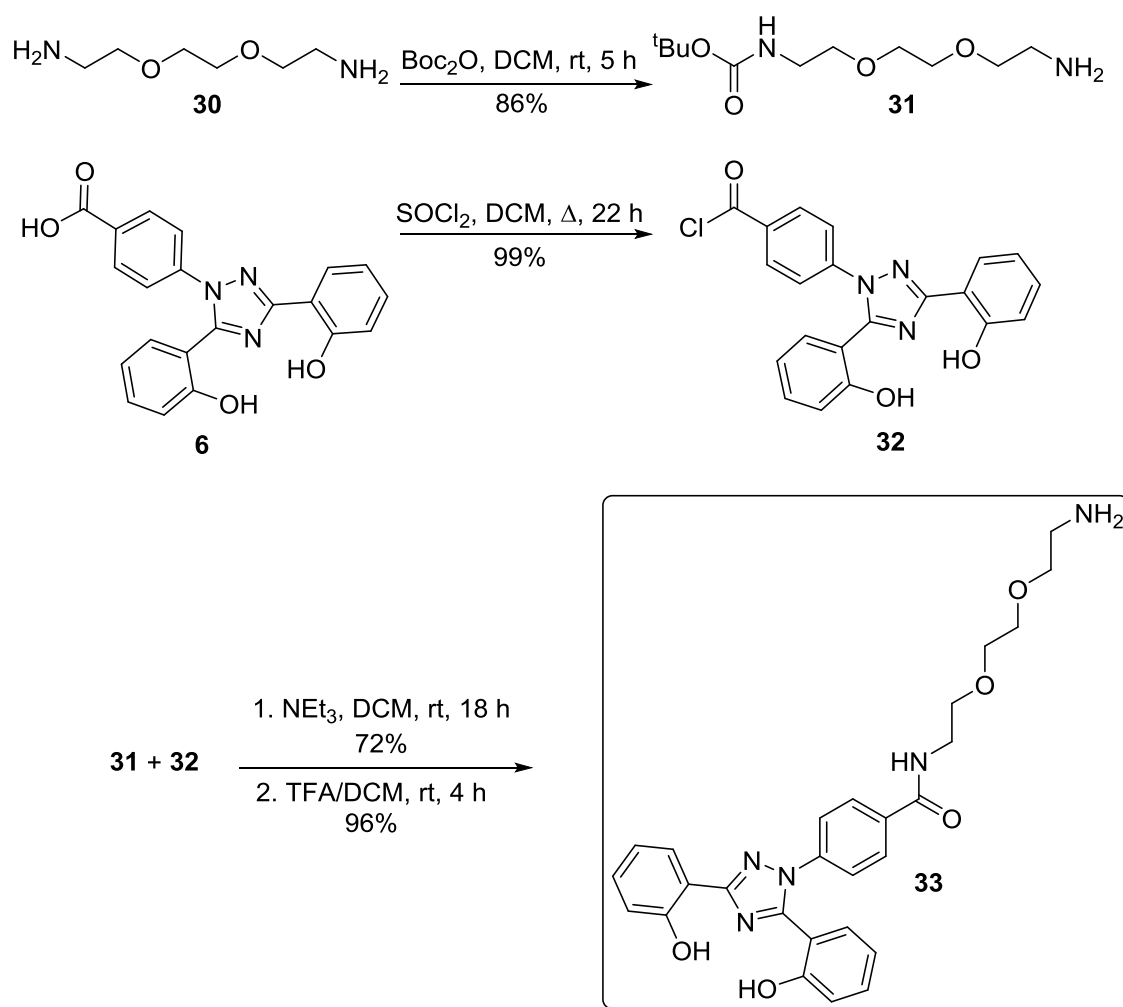
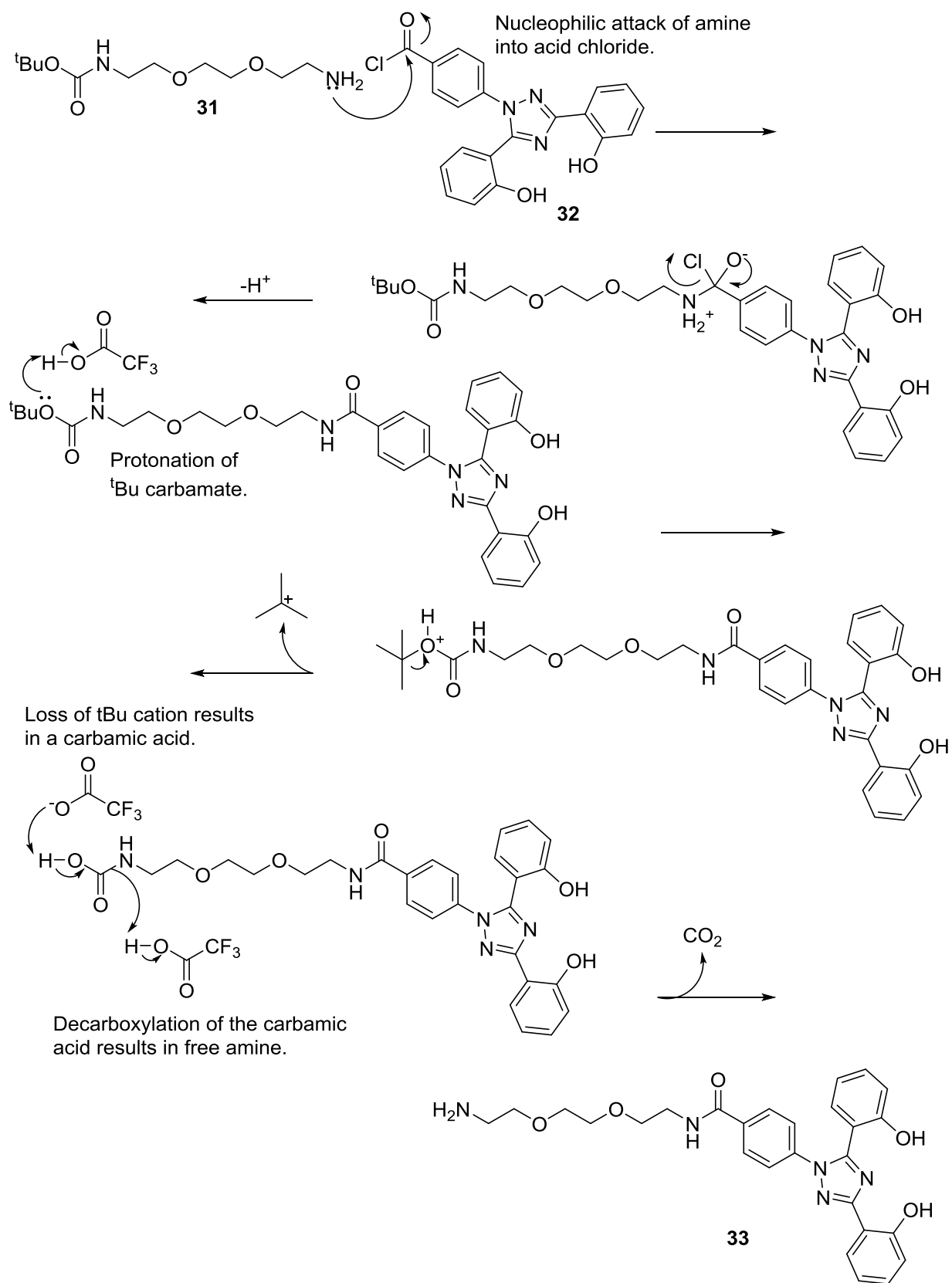


Figure 23 Relevant mass spectra showing peaks for a) product **29b** + H^+ and **29b** + Na^+ , b) **29c** + H^+ , c) **29d** + H^+ and d) **29e** + H^+ .

However, despite mass spectrometry evidence for product formation **29b-e** (Figure 23), isolation of products proved to be problematic. Column chromatography using silica was investigated with a range of eluent conditions but products seemed to stick or streak on silica, despite using very polar eluent conditions (e.g. 5% MeOH, 1% NEt₃ in CHCl₃). Precipitations and recrystallisations were attempted, however clean products were unable to be isolated due to the persistent contamination of amine or urea side product from DCC coupling. In order to overcome the isolation problems encountered, a mono-Boc protection of a diamine was proposed so that an excess of diamine would not have to be used in reaction with the ligand, as this was very difficult to remove at the end of the reaction (Scheme 11).



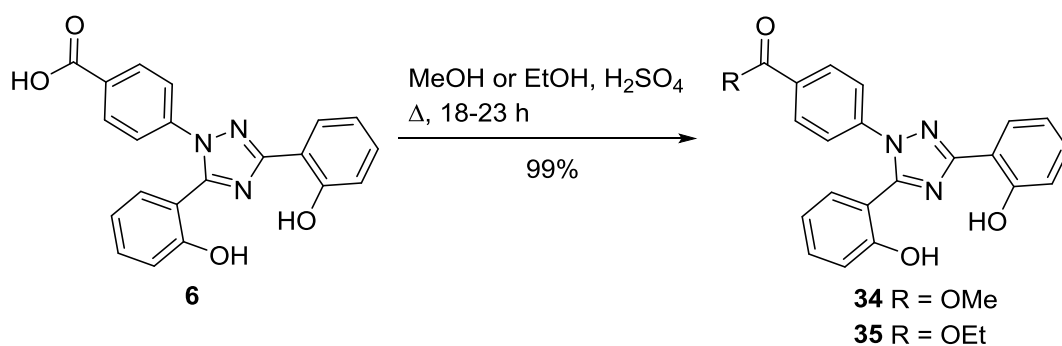
Scheme 11 Synthesis of amine appended ligand **33** from Boc protected amine **31** and acid chloride **32**.



Scheme 12 The mechanism for the formation of 33 from 31 and 32.

In addition, thionyl chloride was used to convert the carboxylic acid group of **6** into an acid chloride so that this could be reacted with the amine. This would circumvent the use of NHS/DCC coupling method, so would avoid contamination from the urea side product. Initial attempts at formation of **32** gave incomplete conversion after refluxing for 7 hours; hence a longer reaction time of 22 hours was required to obtain full conversion to the acid chloride. In order to aid the water solubility of the modified polymer, it was proposed that a glycol linker between the polymer and ligand would be beneficial. For that reason, 2,2 (ethylenedioxy)bis(ethylamine) was mono-Boc protected to give **31** and subsequently reacted with **32**. The Boc protected amine group was deprotected by stirring in TFA/DCM to give **33** in 96% yield (Scheme 11). The mechanism is shown in Scheme 12. This amine appended ligand was now suitable for reacting with carboxylic acid groups of alginate.

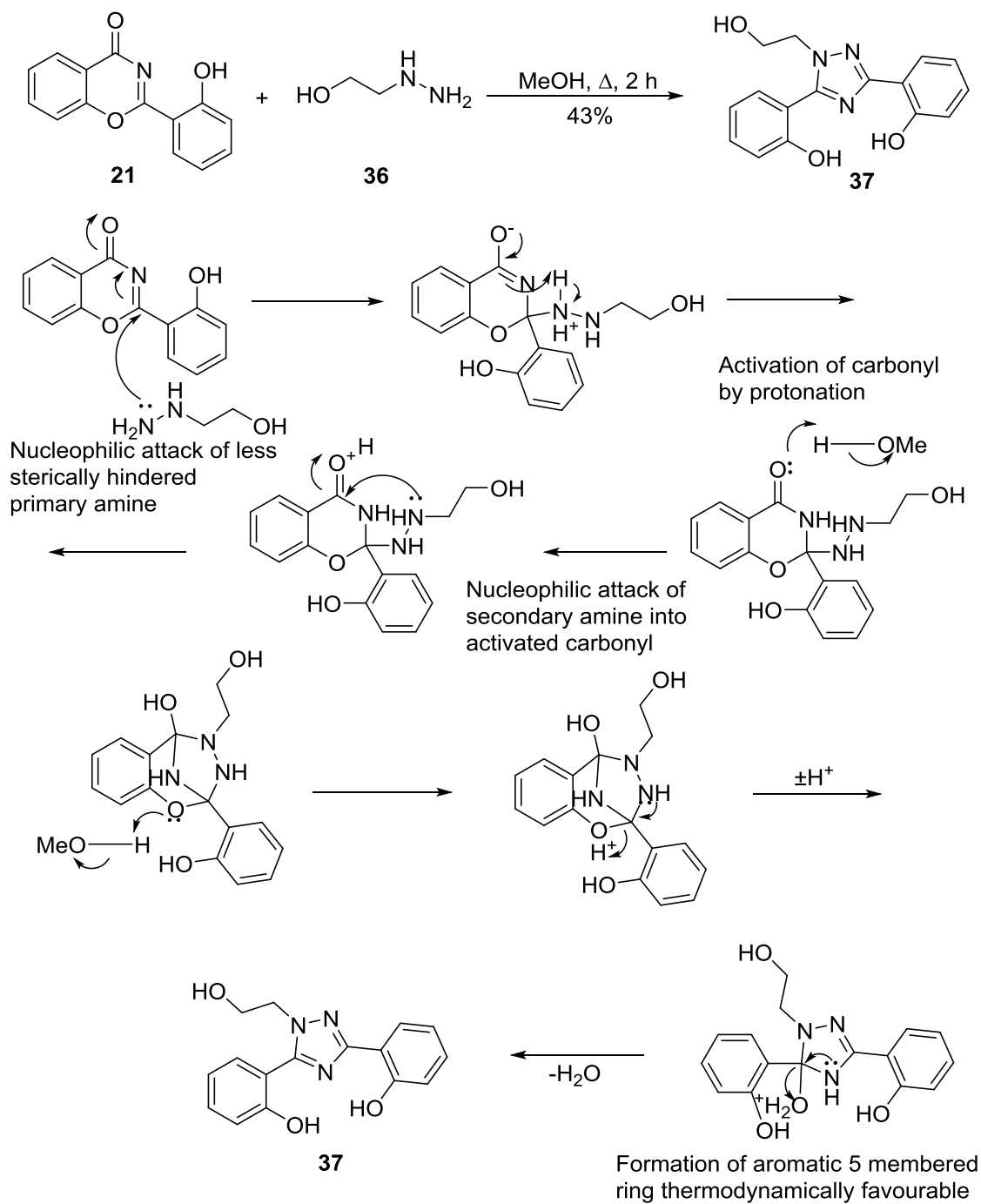
Although there is greater literature precedent for carbodiimide-mediated amide formation reactions with alginate, esterification reactions utilising the carboxylic acid moiety of the alginate also seemed chemically accessible. Esterification reactions were first tested with the ligand to check for viability. Therefore, deferasirox **6** was refluxed in methanol and ethanol with sulphuric acid to give the corresponding methyl and ethyl esters **34** and **35** in 99% yield (Scheme 13).



Scheme 13 Formation of methyl ester **34** and ethyl ester **35**.

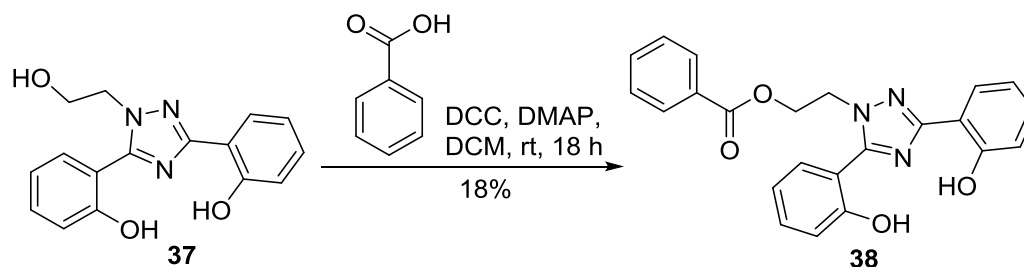
Furthermore, intermediate **21** was reacted with 2-hydroxyethyl hydrazine **36** to give an alcohol appended version of the ligand **37** in 43% yield (Scheme 14). Nucleophilic attack of the primary amine of **36** into the electrophilic imine site of **21** is followed by the activation of the carbonyl by

protonation. This undergoes a second nucleophilic attack by the secondary amine of **36** leading to cyclisation to form a five membered ring, and further loss of a water molecule leads to a thermodynamically stable aromatic triazole product **37**.



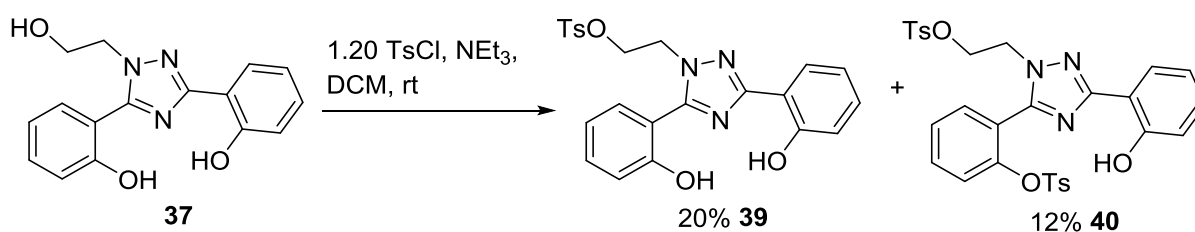
Scheme 14 Reaction conditions for the formation of alcohol appended ligand **37** (top) and the proposed mechanism for the formation of **37** from **21** and **36** (bottom).

This was used in a Steiglish esterification with benzoic acid, and after purification by column chromatography the desired ester **38** was isolated in 18% yield (Scheme 15). The poor yield may be due to the mild reaction conditions employed, as the starting material **37** was also isolated from the column. However, for the purpose of a model reaction, it was performed at room temperature so that the conditions would be transferable to alginate. Nevertheless, the formation of an ester linkage using **37** was confirmed as product **38** was isolated from the reaction mixture.



Scheme 15 Formation of ester **38** from **37**.

Additionally, with the alcohol appended ligand **37** in hand it was thought that the alcohol group could be tosylated or mesylated into a good leaving group for further reactions with nucleophiles. Therefore, tosylation of the primary alcohol of **37** was attempted initially with 1.20 equivalents of TsCl, however, after purification by column chromatography, two products **39** and **40** were isolated in 20% and 12% yield respectively (Scheme 16).



Scheme 16 Tosylation of **37** resulted in two products **39** and **40**.

The position of the second tosylation on **40** was confirmed by Nuclear Overhauser Effect (nOe) studies. Irradiation of protons α to sulphur of tosyl groups resulted in nOe to protons shown (Figure 24) confirming tosylation of primary alcohol and one of the phenolic rings.

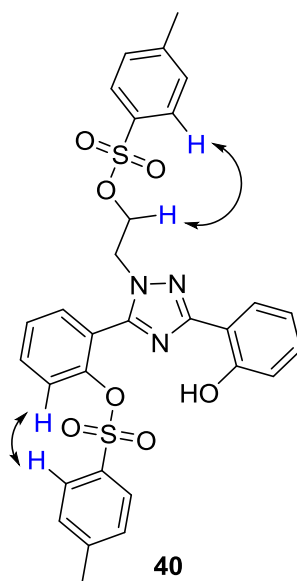


Figure 24 Observed nOe in **40** to confirm positions of tosyl groups

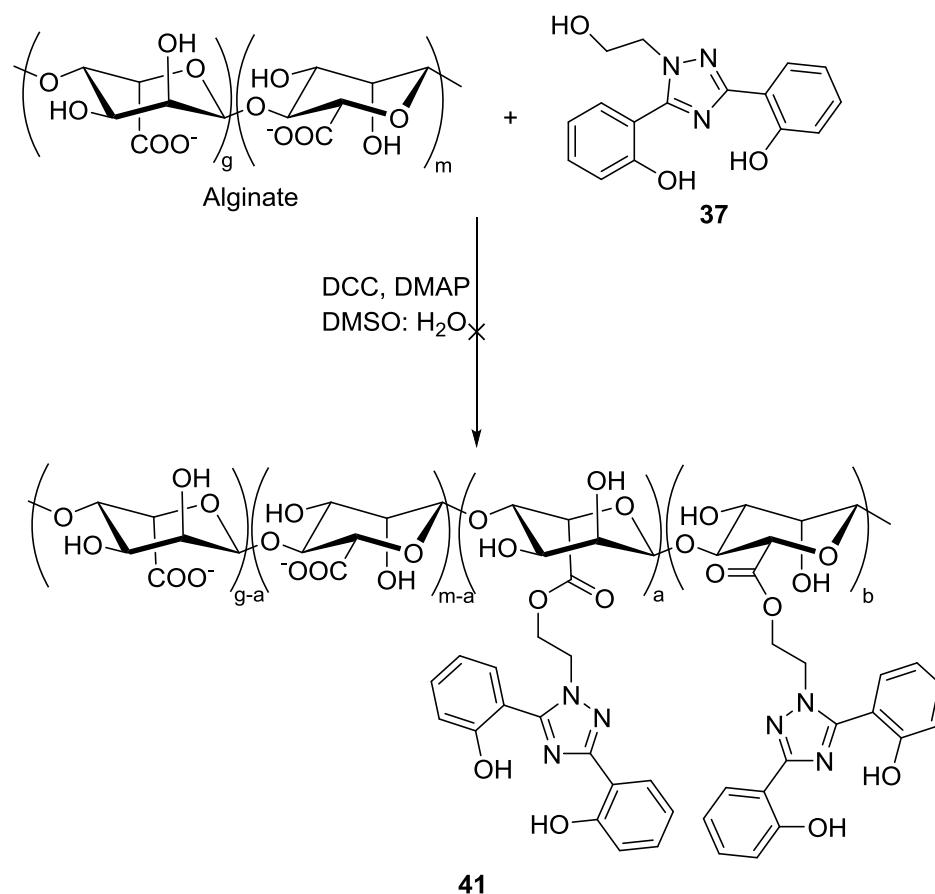
The primary alcohol should be chemically more nucleophilic and reactive than the phenolic alcohol as the O lone pair of electrons can be conjugated into the aromatic system, so the reaction was repeated using 1.00 equivalent of TsCl to minimise the formation of **40**. Although the extent of the second tosylation occurring seemed to decrease, mixtures of **39** and **40** were still isolated in 43% and 7% yield respectively. A similar reaction using 1.00 equivalent of MsCl was attempted, however mixtures of products still seemed to occur as confirmed by crude ^1H NMR spectroscopy and mass spectroscopy. In this instance, the compounds could not be separated by column chromatography.

The tosylated product **39** was further reacted with excess *p*-xylenediamine, however **37** was isolated with quantitative mass recovery in which the diamine had failed to react with the tosylate, and in addition the tosyl group had reverted back to the alcohol. Due to the poor reactivity of **39** under the conditions employed, this avenue of investigation was not pursued.

3.3 Polymer reactions

3.3.1 Polymer-deferasirox conjugates

After the successful esterification of **37** with benzoic acid to give **38**, similar conditions were employed to attempt to couple **37** to alginate. Alginate is water soluble and does not dissolve in organic solvents, whereas **37** is organo-soluble with poor water solubility. Therefore, in the first attempt **37** was dissolved in a few drops of DMSO and added to an aqueous solution containing alginate, DCC and DMAP (Scheme 17).



Scheme 17 Attempted esterification reaction with alginate and **37**.

However, upon addition the solution turned cloudy indicating precipitation of the ligand in aqueous media, and DCC is also poorly soluble in water. The reaction was repeated using 1:1 THF:H₂O

mix, however DCC was still poorly soluble. Therefore, in the final attempt EDAC.HCl was used instead in 1:5 THF:H₂O solvent mix.

In all cases, the purification protocol involved dialysis in which the reaction medium was transferred to cellulose membrane tubing. This was then suspended in deionised water for three days, with the water being changed regularly. This should ensure that polymeric alginate remains inside the tubing, whilst all other soluble small molecules can freely cross the membrane barrier into the surrounding water to only leave the desired alginate product in the tubing.

Characterisation of the alginate product proved problematic as matrix-assisted laser desorption/ionisation (MALDI) or electrospray mass spectra was not obtainable so the change in molecular weight upon desired modification could not be monitored. Proton NMR spectroscopy indicated a lack of aromatic protons suggesting that product **41** was not formed, and IR spectroscopy was used to determine the frequency of the ester band ($\sim 1735 - 1750 \text{ cm}^{-1}$) which would have been diagnostic of product formation, however this was not observed. Ultimately, UV-vis spectroscopy was used to shed light into the electronic properties in solution. A spectrum of unmodified alginate was compared to that obtained after the reaction. With modification, the spectrum should differ due to the incorporation of **37** which contains an aromatic conjugated system. However, it was found that the spectrum of the unmodified alginate were identical to those obtained after all reactions, thus conclusively indicating the absence of ligand **37** on alginate (Figure 25). This may be due to alginate itself containing secondary alcohol groups which may be of similar reactivity to the primary alcohol group of **37**, therefore this alcohol is not nucleophilic enough in the alginate environment to attack the reactive intermediate in order to form the ester.

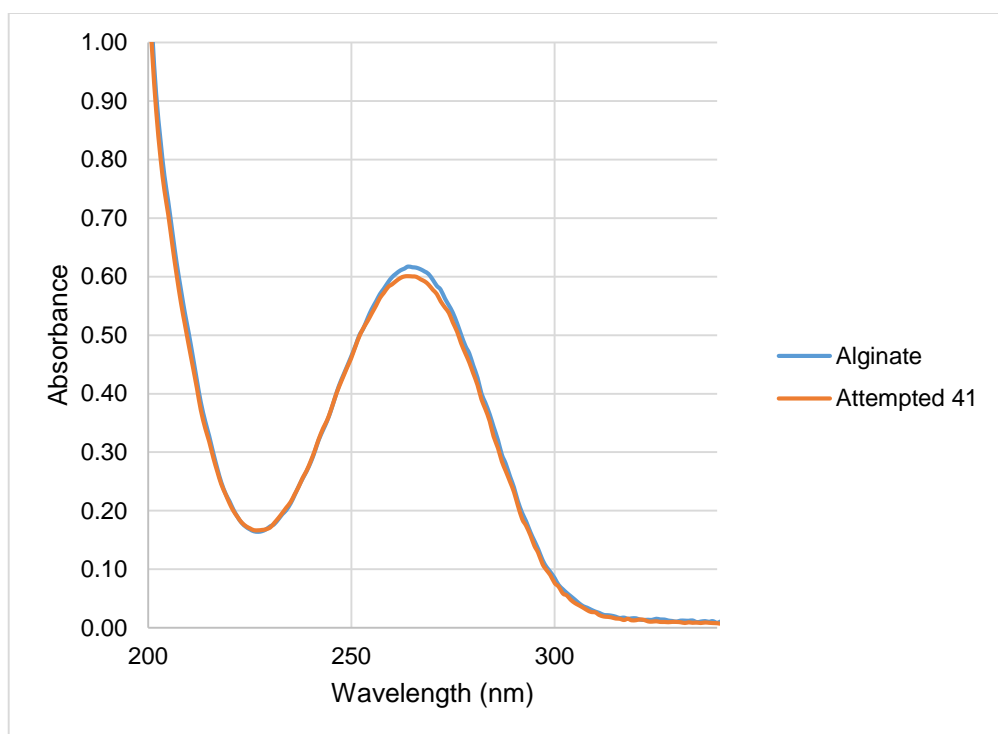
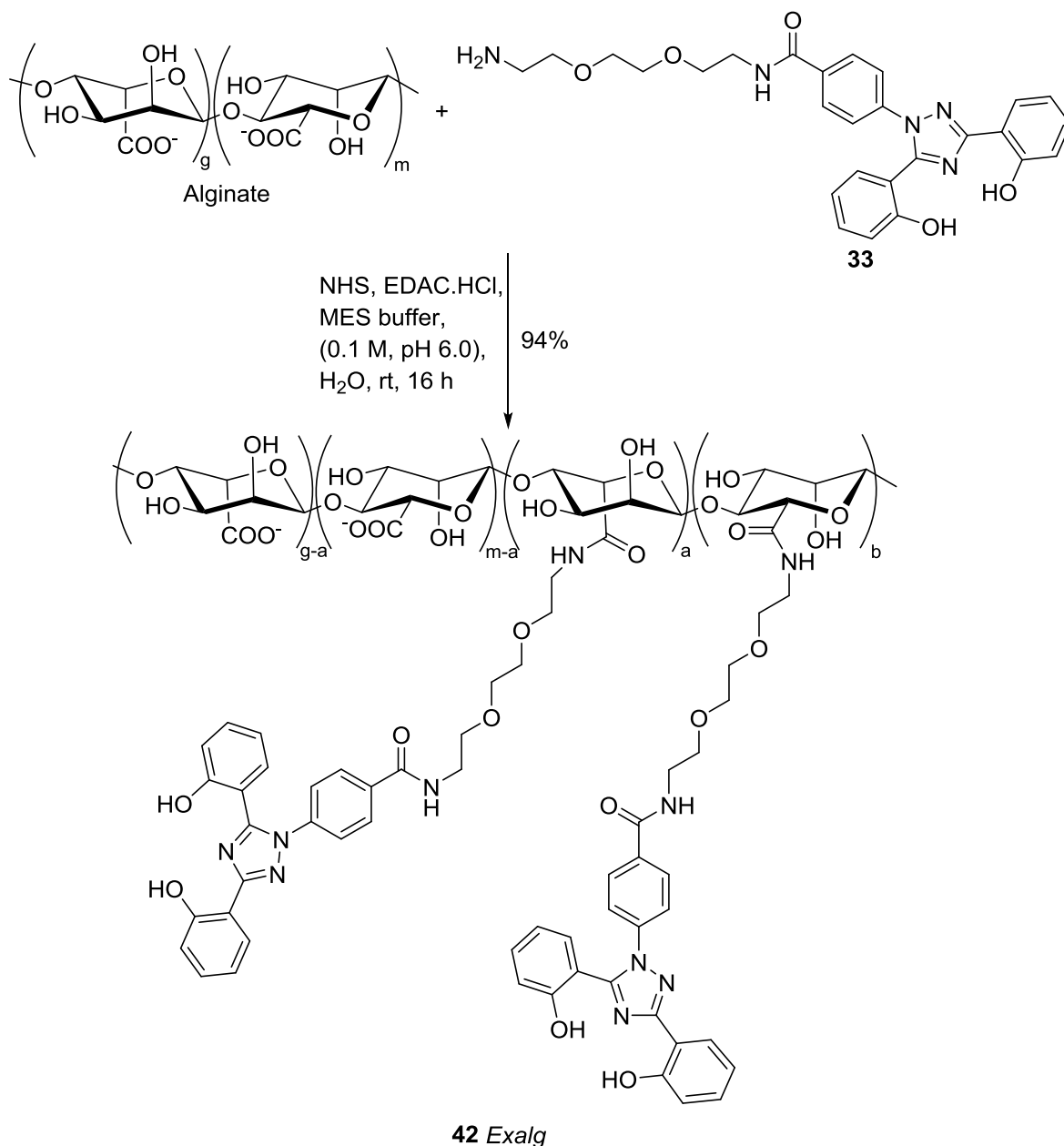


Figure 25 UV-vis spectra of alginate and attempted product **41** both showing an absorbance at 265 nm indicating that no modifications were made to alginate and compound **41** was not formed.

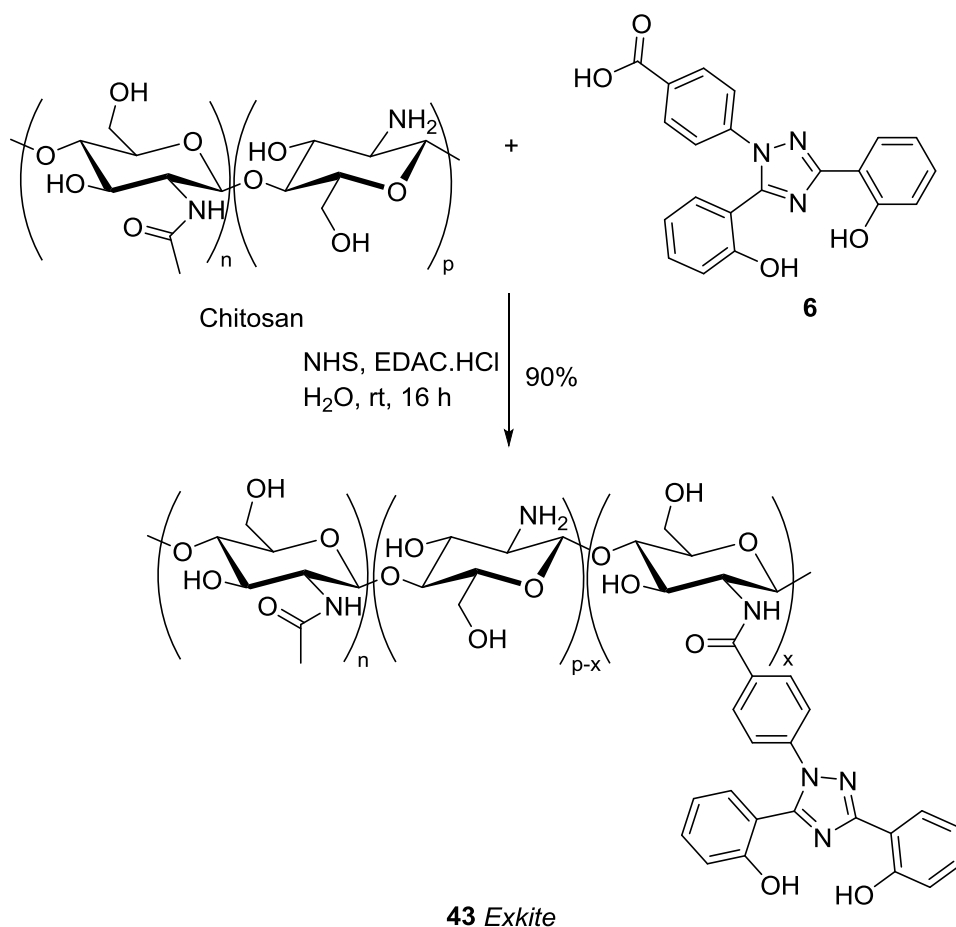
Amide formations using amines may be a more viable route as *N*-lone pair electrons are higher in energy than *O*-lone pair electrons, rendering amines more nucleophilic than alcohols. Hence, the water soluble amine appended ligand **33** was reacted with alginate using similar NHS/EDAC.HCl coupling chemistry to yield product **42**, *Exalg* (Scheme 18). After stirring at room temperature for 16 hours, the resulting precipitate was isolated by centrifuge. Characterisation by proton NMR spectroscopy showed distinctive peaks in the aromatic region of 7 – 8 ppm indicative of ligand incorporation into the material (Section 4.3, page 53). Characterisation by IR spectroscopy showed an amide band at 1634 cm^{-1} (Section 4.2, page 51), and UV-vis spectroscopy also showed distinctive peaks at 247 and 301 nm from the incorporated ligand (Section 4.4, page 60). Full characterisation is discussed in Chapter 4. Alginate (LFR5/60) has 65% G composition, however it is assumed that there is no bias towards modification of M or G units.



Scheme 18 Synthesis of alginate-ligand conjugate **42 Exalg**.

In addition to alginate, chitosan was also identified as a suitable biopolymer for application as a non-absorbable backbone. Chitosan contains primary amine groups, which could be utilised in carbodiimide mediated cross coupling with deferasirox **6**. Chitosan is soluble in weakly acidic aqueous media whereas **6** is soluble in organic solvents. Therefore, **6** was dissolved in DMSO and then added to an aqueous solution containing chitosan, EDAC.HCl and NHS which was subsequently stirred at room temperature for 16 hours (Scheme 19). This was further dialysed in

water at ambient temperature for three days, and water was removed *in vacuo* to yield a product believed to be **43**, *Exkite* as a brown film.



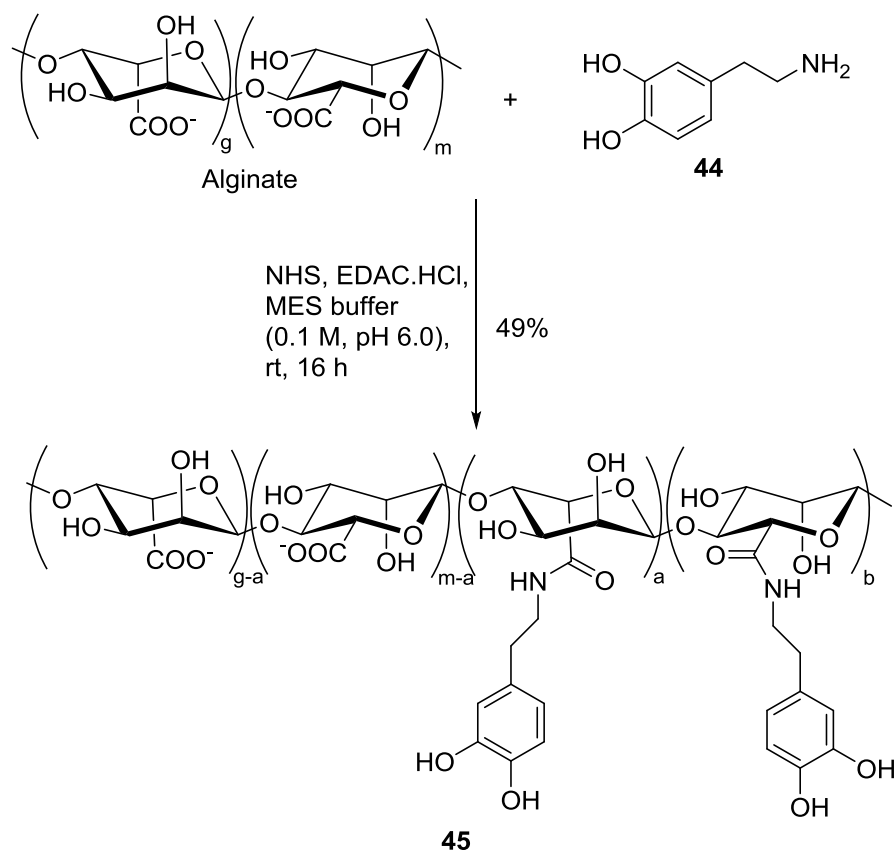
Scheme 19 Synthesis of chitosan-ligand conjugate **43 Exkite**.

As chitosan is derived from chitin which contains *N*-acylated groups, chitosan will always contain a minor component of the *N*-acylated group as the deacylation process rarely goes to completion. The proton NMR spectrum of the *Exkite* product showed distinct resonances in the aromatic region (7 - 8 ppm) compared to that of chitosan alone indicating the presence of ligand **6** (Section 4.3, page 53). Full characterisation of this polymer is discussed in Chapter 4.

3.3.2 Polymer-catechol conjugates

Catechol groups are widely found in siderophores such as enterobactin and are known to have good affinity for Fe (III) due to HSAB theory in which small charge dense cations bind well to hard

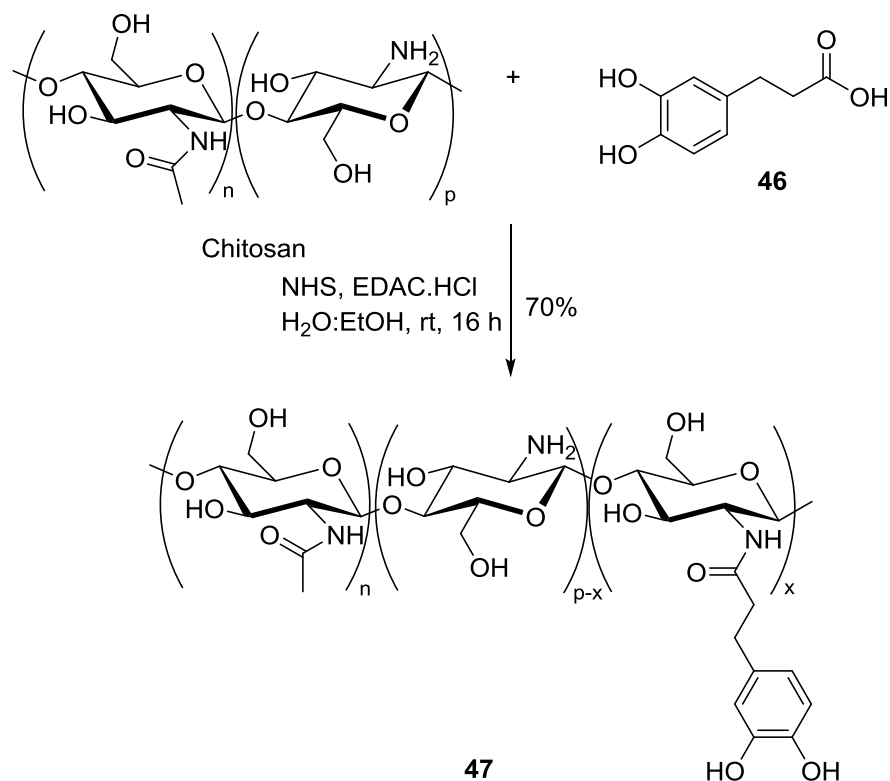
oxygen donors. Therefore, coupling catechol groups to chitosan and alginate were attempted by using similar methods. Alginate was reacted with **44** in an aqueous solution (Scheme 20), and chitosan was reacted with **46** in 1:1 H₂O:EtOH to aid the solution of **46** in the presence of NHS and EDAC.HCl coupling reagents (Scheme 21).



Scheme 20 Synthesis of alginate-catechol polymer **45**.

After purification by dialysis in water at ambient temperature over three days, the resulting products **45** and **47** were isolated by lyophilisation. However, the poor solubility of **45** and **47** made characterisation of the polymers extremely difficult. Elemental analysis suggested ligand incorporation for both polymers due to the significant difference in elemental composition between unmodified and modified polymers. In particular, alginate alone does not contain any nitrogen however, after modification there was an increase in nitrogen composition to 5.28% which could

have only come from the ligand. Despite these promising results, these polymers were not carried forward for further investigations due to their poor solubility.



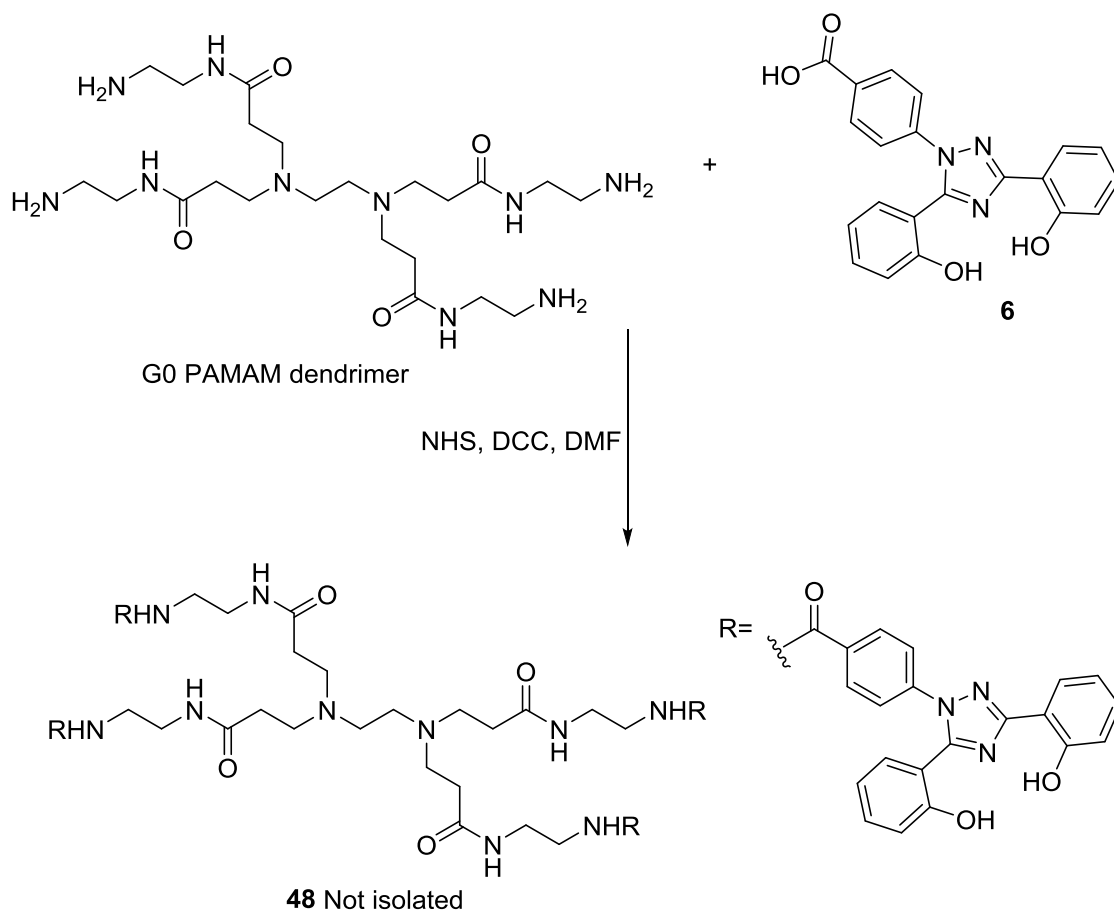
Scheme 21 Synthesis of chitosan-catechol polymer 47.

3.4 Dendrimer reactions

Poly(aminoamide) (PAMAM) dendrimer is a class of spherical dendrimer that consists of repeating branching units containing amine and amide functionalities. They have been extensively studied for many different applications including drug delivery and nanotechnology, and are known to have good biocompatibility.⁷⁶ Furthermore, the defined structure allows for structural control during synthesis and low polydispersity compared to polymers. PAMAM dendrimers are functionalised with amines on the surface, hence it was envisaged that this could be reacted with deferasirox ligand to produce iron binding dendrimers.

For proof of concept, a commercially available generation zero (G0) PAMAM dendrimer was chosen and this was initially reacted with four equivalents of acid chloride functionalised ligand

32, with triethylamine in DCM at room temperature for 16 hours. However, monitoring by TLC showed numerous spots that were very difficult to separate by column chromatography. It was thought that the acid chloride moiety may have been too reactive and may have added multiple times to the dendrimer causing numerous addition products.



Scheme 22 A synthetic route to compound **48**.

Therefore, in order to better control the addition of the ligand, carbodiimide chemistry was employed. The dendrimer was added to four equivalents deferasirox **6**, DCC and NHS in DMF, and was stirred at room temperature for two days (Scheme 22). After purification by repeated precipitation in MeOH/DCM, a product with the mono-addition of the ligand was observed by ^1H NMR spectroscopy and mass spectrometry. In order to drive the reaction to completion, the reaction was repeated with heating for 16 hours, however this also gave multiple products by TLC that were difficult to separate. In the next attempt, six equivalents of deferasirox **6**, NHS and DCC

were used and the reaction mixture in DMF was heated at reflux for five days. After purification by column chromatography, none of the compounds seen previously were observed, possibly due to the decomposition of the dendrimer when heated for a prolonged period of time in DMF. The reaction was repeated in DCM which has a lower boiling point at 40 °C, however the product could not be isolated despite conducting column chromatography of the reaction material twice. In a final attempt, HOBt with DCC was used instead of NHS, and the reaction mixture in DMF was stirred at room temperature for three days, but there was no evidence for product formation by ¹H NMR spectroscopy or mass spectroscopy.

Reactions with the dendrimer were extremely difficult to control due to incomplete additions of the ligand to give mono-, bi- and tri- addition products, which also hampered the purification process due to a mixture of compounds being produced that were very similar in size and polarity. Reaction conditions were probed to force the reaction to completion, but addition of four ligands to a dendrimer was still difficult to achieve and even more difficult to isolate.

3.5 Summary

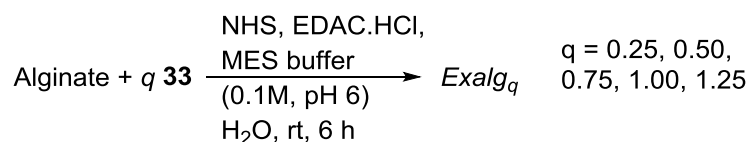
Deferasirox ligand was synthesised in two steps from commercially available starting materials. The carboxylic acid moiety of this ligand was utilised and reacted with diamines in order to produce amine appended ligands but products were difficult to isolate. Therefore, Boc-protected amine **31** was used and reacted with the acid chloride of deferasirox to yield amine appended ligand **33**. This was further utilised in NHS/EDAC.HCl mediated reaction with alginate to produce a material identified as *Exalg* **42**. Deferasirox **6** itself was reacted with chitosan to give a material named *Exkite* **43**. Catechol containing compounds were also reacted with alginate and chitosan but products were poorly soluble and difficult to characterise. Additionally, reactions of deferasirox **6** with dendrimers were challenging to control and the desired products could not be isolated with a satisfactory purity or yield.

4 Polymer Characterisation

4.1 Background

Numerous methods were employed in an attempt to characterise the modified polymers *Exkite* (Scheme 19) and *Exalg* (Scheme 18). Due to their poor solubility in aqueous media, traditional polymer characterisation methods such as gel permeation chromatography (GPC) and size exclusion chromatography (SEC) were not feasible. However, efforts were focused on qualitative and quantitative analysis of the polymers, in particular calculating the amount of ligand incorporation or ligand loading of the polymer material that was believed to be modified.

In order to further investigate the effects of ligand loading and subsequent iron binding properties, alginate was also reacted with varying amount of ligand **33** from 0.25 equiv to 1.25 equiv to give the corresponding products *Exalg*_{0.25}, *Exalg*_{0.50}, *Exalg*_{0.75}, *Exalg*_{1.00} and *Exalg*_{1.25} (Scheme 23). The ligand loading of *Exalg* in particular was investigated due to the poor iron binding properties of *Exalg* compared to *Exkite* (see Chapter 5).



Scheme 23 Synthesis of *Exalg* with varying equivalences of ligand **33**.

4.2 Infrared Spectroscopy

Infrared (IR) spectroscopy is used in the qualitative characterisation of organic molecules and polymers to determine distinctive functional groups or bonds within the molecule by studying fundamental vibrations of covalent bonds.¹¹³ The IR spectrum of sodium alginate alone shows a broad –OH peak at 3255 cm⁻¹, and a carbonyl peak corresponding to the carboxylic acid salt at 1594 cm⁻¹. The ligand **33** also shows –OH absorption at 3200 cm⁻¹, –CH absorption at 3000 cm⁻¹

and carbonyl peak from the amide at 1645 cm^{-1} . After ligand incorporation, *Exalg* has distinctive peaks at 3295 cm^{-1} and 3000 cm^{-1} corresponding to -OH and -CH absorption, and a strong carbonyl amide absorption at 1636 cm^{-1} resulting from C=O vibration. Furthermore, the fingerprint region of *Exalg* is also very similar to that of ligand **33** which is also indicative of ligand incorporation (Figure 26).



Figure 26 IR spectra of alginate, ligand **33** and *Exalg*.

Similarly, chitosan alone exhibits -OH/-NH and -CH absorption at 3353 cm^{-1} and 3000 cm^{-1} respectively, and amine N-H bend absorption at 1652 cm^{-1} . Deferasirox **6** shows broad -OH absorption at 3000 cm^{-1} which is overlapped with the C-H peak at 2980 cm^{-1} , and a carbonyl C=O peak at 1683 cm^{-1} which is at a lowered frequency of absorption due to conjugation of the carbonyl with the aromatic ring. After ligand addition, *Exkite* also shows -OH absorption and overlapped -CH absorptions at 3379 cm^{-1} and 2985 cm^{-1} . The carbonyl absorption at 1623 cm^{-1} , shifted

approximately 60 cm^{-1} from the carbonyl of deferasirox **6**, indicates amide formation and the fingerprint region also resembles that of the ligand **6** (Figure 27).

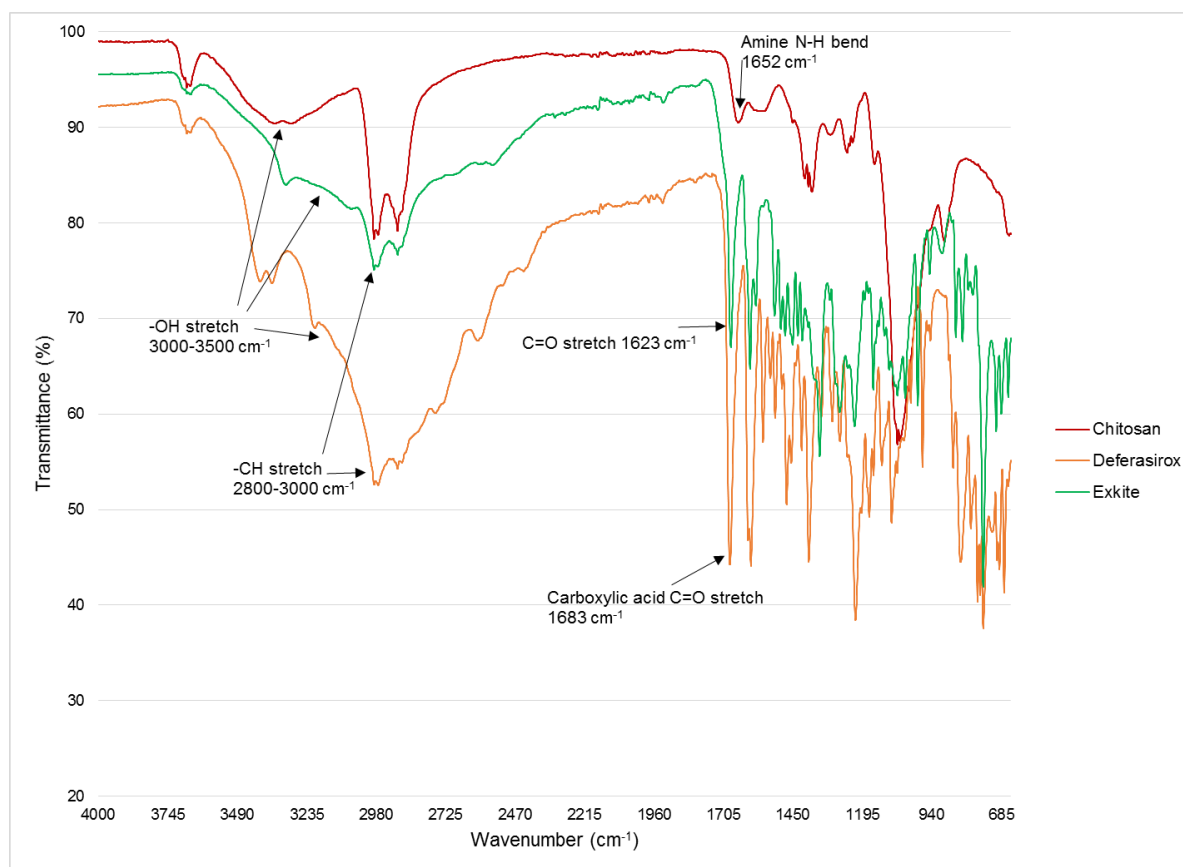


Figure 27 IR spectra of chitosan, deferasirox **6**, and *Exkite*.

4.3 Nuclear Magnetic Resonance Spectroscopy

Nuclear magnetic resonance (NMR) spectroscopy is universally utilised for the elucidation of structures of organic compounds as it allows the detection of atomic nuclei and the relative chemical environment that they are in.¹¹⁴ A large range of solvents were investigated for NMR spectroscopic studies and it was found that *Exalg* is soluble in d_6 -DMSO and *Exkite* is soluble in d-TFA. The analysis of ^1H NMR spectra of *Exkite* (Figure 28) and *Exalg* (Figure 29) show clear aromatic protons that can be integrated to correspond to the twelve aromatic protons of deferasirox ligand **6** and modified ligand **33**. There are also broad undefined peaks at 2.00 - 5.50 ppm from the aliphatic protons of chitosan and alginate polymer backbones.

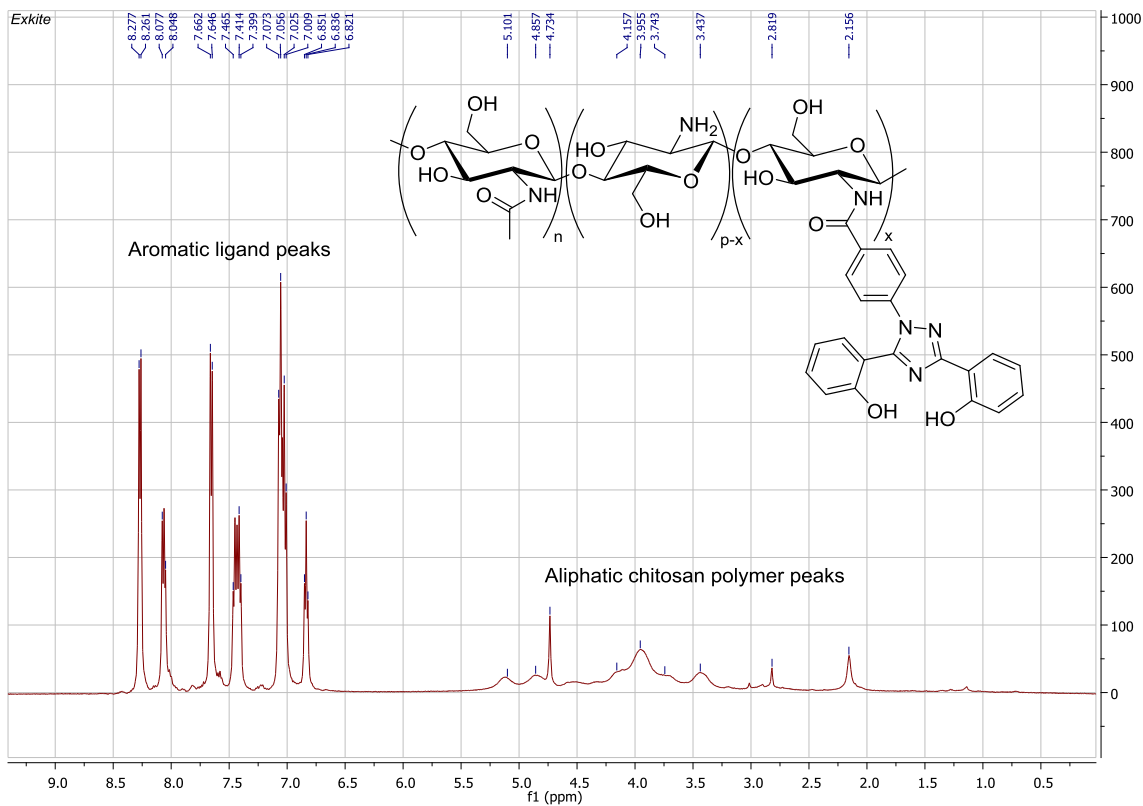


Figure 28 ^1H NMR spectrum of *Exkite* in d-TFA (residual signal at 11.50 ppm not shown).

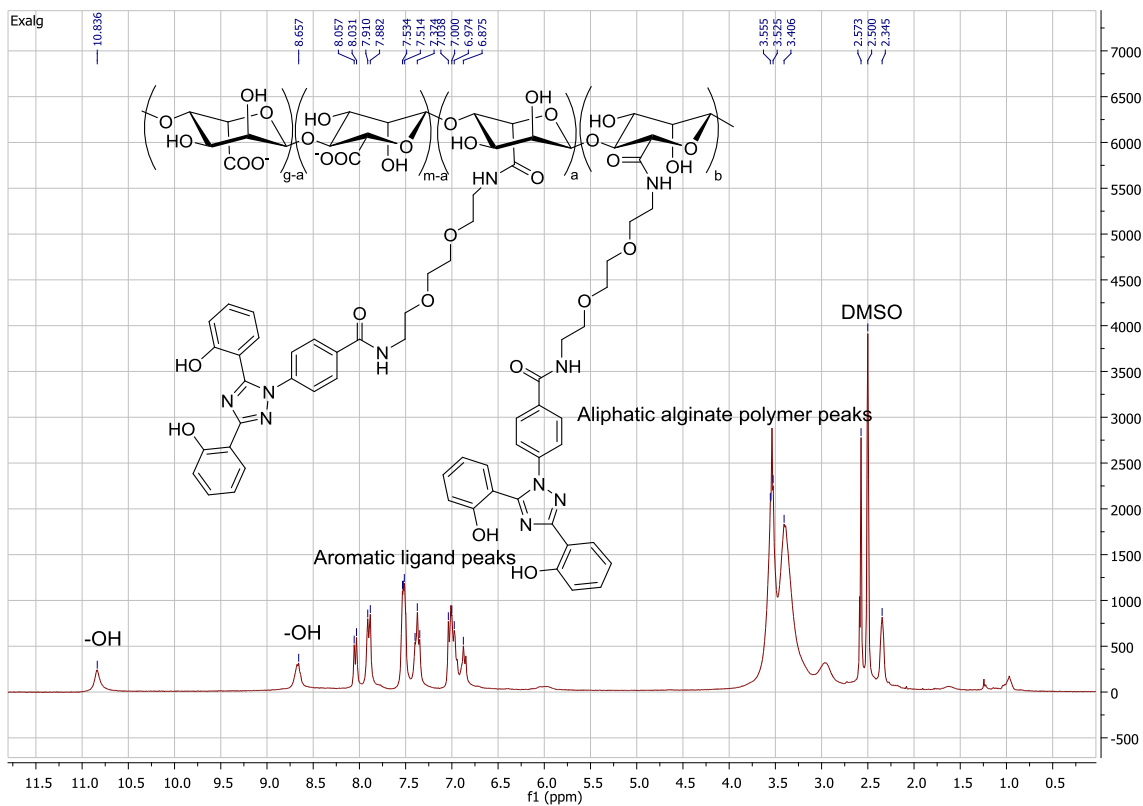


Figure 29 ^1H NMR spectrum of *Exalg* in d₆-DMSO.

Quantitative information was also extracted from the ^1H NMR spectra to determine the percentage of ligand incorporation into the polymer backbones by integrating the relative aromatic and aliphatic regions. The ligand is the source of aromatic protons so comparison of this integral to that of aliphatic protons from the polymer backbone enabled the calculation of percentage incorporation of polymers (Table 3).

Table 3 Percentage incorporation of polymers as calculated by proton NMR spectra integrations.

Entry	Compound	Ligand equiv	% Incorporation by inspection of ^1H NMR spectra
1	<i>Exkite</i>	1.00	37
2	<i>Exalg_{0.25}</i>	0.25	25
3	<i>Exalg_{0.50}</i>	0.50	27
4	<i>Exalg_{0.75}</i>	0.75	19
5	<i>Exalg_{1.00}</i>	1.00	26
6	<i>Exalg_{1.25}</i>	1.25	20

The percentage incorporation was calculated to be 37% for *Exkite* and 19-27% for *Exalg* series, with the highest incorporation estimated for *Exalg_{0.50}* and the lowest modification for *Exalg_{0.75}*. However, the main limitation of this method is that due to the hygroscopic nature of DMSO, in d_6 -DMSO the residual ^1H NMR signal for H_2O occurs at 3.30 ppm which is in the aliphatic range that was integrated. This signal could not be distinguished from those resulting from alginate due to the broad peaks obtained, and so was included in the aliphatic integrations which may contribute towards overestimation of the aliphatic integration, so will give a lower percentage modification than in actuality. The residual solvent effects can be overcome by using solid state NMR spectroscopy, which is widely applied in polymer chemistry to negate the poor solubility of some polymers in deuterated solvents,¹¹⁵ and for the determination of ^{13}C NMR spectroscopy which typically requires a greater concentration of compound in solution state NMR.¹¹⁶ Alternatively, the

polymers can be subject to acid hydrolysis and the resulting monomers can be analysed by solution state NMR spectroscopy which will allow more detailed characterisation and quantification,¹¹⁴ however oligomers of differing sizes may broaden the spectra.

4.3.1 Diffusion NMR Spectroscopy

Diffusion NMR experiments were conducted and data fitted by Catherine Smith with assistance from Daniel Payne and advice from Dr Melanie Britton. This experiment was done at the recommendation of PhD examiners to improve understanding of conjugation between the polymer and ligand. As these experiments were done post viva voce, the original materials used in the majority of the thesis were unavailable and so these experiments were conducted on different batches of material. Therefore, batch-to-batch variation must be taken into consideration and caution exercised in the interpretation of these results in the context of the remainder of the results presented in this thesis.

Self-diffusion is the random translational motion of molecules driven by internal thermal energy.¹¹⁷

This is dependent on physical parameters in solution state such as size and shape of molecules, temperature and viscosity. The Stokes-Einstein equation can be used to describe the self-diffusion coefficient in which the shape of the molecule is assumed to be spherical (Equation 1).¹¹⁸

$$D = \frac{kT}{6\pi\eta r_s}$$

Equation 1 The Stokes-Einstein equation in which D is the self-diffusion coefficient, k is the Boltzmann constant, T is temperature, η is viscosity of the liquid, and r_s is the hydrodynamic radius of the molecule

Translational diffusion of molecules can be measured by pulsed field gradient NMR spectroscopy, in which a magnetic field gradient is applied to the sample in combination with radio-frequency pulses as used in routine NMR.¹¹⁹ The magnetic gradient pulse is used to phase shift the magnetisation and after a period of time, a second gradient pulse is used to refocus the signal. This refocusing is only achieved for nuclei that have not moved significantly up or down the NMR tube, therefore diffusion reduces the intensity of the resulting signal. By repeating the pulse sequence and incrementing the gradient strength whilst keeping all other NMR parameters constant, the diffusion coefficient of the sample can be calculated from the signal decay with respect to the gradient strength.¹²⁰ The utilisation of diffusion NMR spectroscopy is widespread as it is non-invasive and can be performed on dilute solutions so is particularly suited to studying molecular

dynamics in biological systems.^{121, 122} It is also applied for the study of host and guest interactions in supramolecular chemistry. In the uncomplexed state the host and guest will have different diffusion coefficients depending on their individual size and shape. However, in a complex the host and guest will have the same diffusion coefficient as if they are tightly bound, they will diffuse as a single entity.¹²³ Thus, diffusion NMR can also be used to measure the association of complexes in self-assembly systems.¹²⁴ Furthermore, diffusion NMR may aid the characterisation of dendrimers in which the self-diffusion coefficient can be used to calculate the effective radii of spherical dendrimers *via* the Stokes-Einstein equation.¹²⁵ Similarly, modification of polymers can be monitored by diffusion NMR as the change in molecular size will affect the self-diffusion coefficient so can shed light on key structural properties.^{126, 127}

Diffusion NMR was employed on *Exkite* and *Exalg* to determine the effective association of ligands **6** and **33** on chitosan and alginate polymers respectively. A pulsed gradient stimulated echo (PGSTE) experiment was performed and the signal loss with increasing gradient strength was fitted to the Stejskal-Tanner equation (Equation 2).¹²⁸ Where a monoexponential fit was poor, a biexponential fit was performed, producing two diffusion coefficients.¹²⁹ The biexponential fit is used when two entities within the sample have overlapping NMR signals and this fitting of data allows the determination of both diffusion coefficients that correspond to the two entities within that integration range.¹³⁰

$$\frac{S(\mathbf{G})}{S(0)} = \exp(-(\gamma\delta\mathbf{G})^2 D \left(\Delta - \frac{\delta}{3}\right))$$

Equation 2 The Stejskal-Tanner equation where $\frac{S(\mathbf{G})}{S(0)}$ is the signal decay, γ is the gyromagnetic ratio and D is the self-diffusion coefficient.

The diffusion coefficient of the ligand and polymer were calculated separately from the respective integrated range in ¹H NMR spectra of *Exkite* and *Exalg*. The values obtained for the polymer were compared to the ligand to determine whether the ligand was associated with the polymer.

Table 4 The self-diffusion coefficients for *Exalg* NMR sample calculated by monoexponential and biexponential fits resulting in two values; the best fit for each integrated value is shown in blue.

Entry	Integral range/ ppm	Integral assignment	D/ 10 ⁻¹⁰ m ² s ⁻¹		
			Mono	Bi (1)	Bi (2)
1	2.58 – 3.55	<i>Exalg</i> polymer	1.68	4.61	1.12
2	6.56 – 8.20	<i>Exalg</i> ligand	1.07		
3	2.50	d ₆ -DMSO	3.16	5.10	1.70
4	3.30	Water	4.47	6.27	1.02

Analysis of the *Exalg* sample shows that the best fit value of the self-diffusion coefficient for *Exalg* polymer integral is 1.12 x 10⁻¹⁰ m² s⁻¹ which is comparable to that obtained for *Exalg* ligand integral at 1.07 x 10⁻¹⁰ m² s⁻¹ (Table 4). This strongly suggests that the ligand and polymer are associated covalently as the similarity in their self-diffusion coefficients is indicative of both components moving together. This is similar to the approach used in determining host/guest complexation as similar diffusion coefficients obtained from the integrals of host and guest in a sample is indicative of association.¹³¹ The values obtained for DMSO and water are larger as smaller molecules are likely to be moving faster in solution.¹³² As the self-diffusion coefficient for *Exalg* ligand is also smaller, this also suggests that the ligand is part of the larger entity of the polymer.

Table 5 The self-diffusion coefficients for *Exkite* NMR sample calculated by monoexponential and biexponential fits resulting in two values; the best fit for each integrated value is shown in blue. Samples made up in d-TFA were spiked with d₆-DMSO for reference.

Entry	Integral range/ ppm	Integral assignment	D/ 10 ⁻¹⁰ m ² s ⁻¹		
			Mono	Bi (1)	Bi (2)
1	2.70 – 5.30	<i>Exkite</i> polymer	1.14	4.01	0.70
2	6.80 – 8.40	<i>Exkite</i> ligand	2.16		
3	2.50	d ₆ -DMSO	3.12	4.22	1.05
4	11.50	d-TFA	6.13		

However, the self-diffusion coefficient calculated for *Exkite* polymer integral is $0.70 \times 10^{-10} \text{ m}^2 \text{ s}^{-1}$ which is significantly smaller than that calculated for *Exkite* ligand integral at $2.16 \times 10^{-10} \text{ m}^2 \text{ s}^{-1}$ (Table 5). This suggests that the chitosan polymer and ligand are not associated in solution in this particular sample tested. This may be due to a poor attachment of ligand **6** to chitosan during the synthesis resulting in a mixture of chitosan and ligand rather than modification of the polymer itself. Alternatively, the NMR sample was dissolved in d-TFA due to the poor solubility of the sample, however the strongly acidic nature of the solvent may have hydrolysed the amide conjugation between the ligand and polymer. This result is reflective of one NMR sample prepared in d-TFA; more can be learnt about the polymer-ligand conjugation if other solvent systems are attempted on multiple batches of *Exkite*. However, it is not surprising that there is batch to batch variation as this is a well-known and documented phenomena of conjugated polymer synthesis.^{133, 134} The diffusion NMR data suggests that the ligand is present in the batch of *Exkite* material tested but is not covalently attached to chitosan. Therefore, it is plausible that that chitosan and ligand **6** are interacting electrostatically in a salt form of *Exkite* (Figure 30) by the protonation of the amine group of chitosan and deprotonation of the carboxylic acid of ligand **6**.

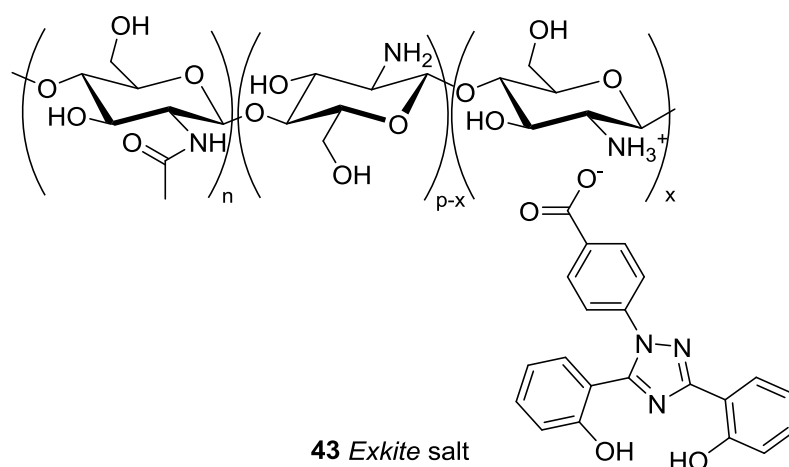


Figure 30 Salt form of *Exkite*

Indeed, drugs which employ supramolecular interactions in which reversible, non-covalent bonds are exploited are emerging to be of importance for controlled drug delivery: block co-polymer

micelles,¹³⁵ vesicles¹³⁶ and self-assembled nanoparticles¹³⁷ can be used to encapsulate hydrophobic or hydrophilic drugs to enhance solubility and deliver at sites of use as supramolecular functional material aggregates. In addition, salt formation is a common and effective method of improving drug solubility and dissolution rates across membranes.¹³⁸ Therefore, as the electrostatic salt interaction is likely to withstand the low pH of the stomach,¹³⁹ the salt form of *Exkite* may offer an alternate mode of delivery of the iron chelator to the colon which can be compared to the covalent binding of ligand to alginate in *Exalg*.

4.4 Ultraviolet-visible Spectroscopy

Ultraviolet-visible (UV-vis) spectroscopy measures the electronic transitions in a molecule between the ground state and excited state (HOMO-LUMO gap) and can be used in the characterisation of analytes, as specific electronic transitions in different molecules can give absorbance at specific wavelengths.¹⁴⁰

Alginate has a distinctive absorption at 265 nm, likely arising from the π to π^* transition of the carbonyl from the carboxylic acid. Aromatic organic molecules with a high degree of conjugation can also show π to π^* transitions such as in ligand **33** which shows peaks at 245 nm and 300 nm. After modification, *Exalg* also shows similar peaks at 247 nm and 302 nm indicative of ligand incorporation (Figure 31).

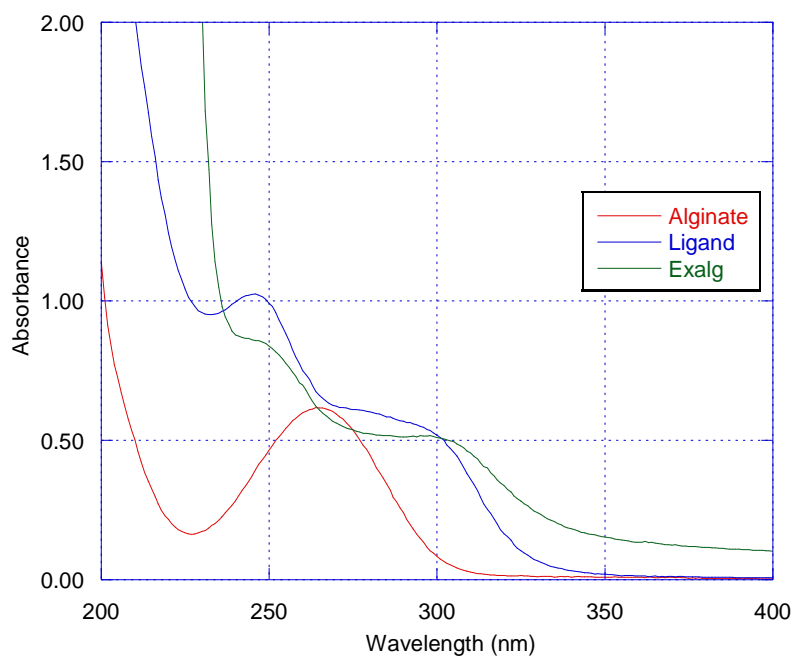


Figure 31 UV-vis spectra of ligand 33 (0.015 mM in water) with absorbance at 245 nm and 300 nm, alginate (0.10% w/v in water) with absorbance at 265 nm and *Exalg* (0.01% w/v dissolved in 1% v/v DMSO in water) with absorbance at 247 nm and 302 nm.

Chitosan itself does not have a distinguishing absorbance at a specific wavelength, however deferasirox ligand **6** absorbs at 245 nm and 315 nm. *Exkite* also shows similar peaks at 248 and 305 nm corresponding to the ligand (Figure 32).

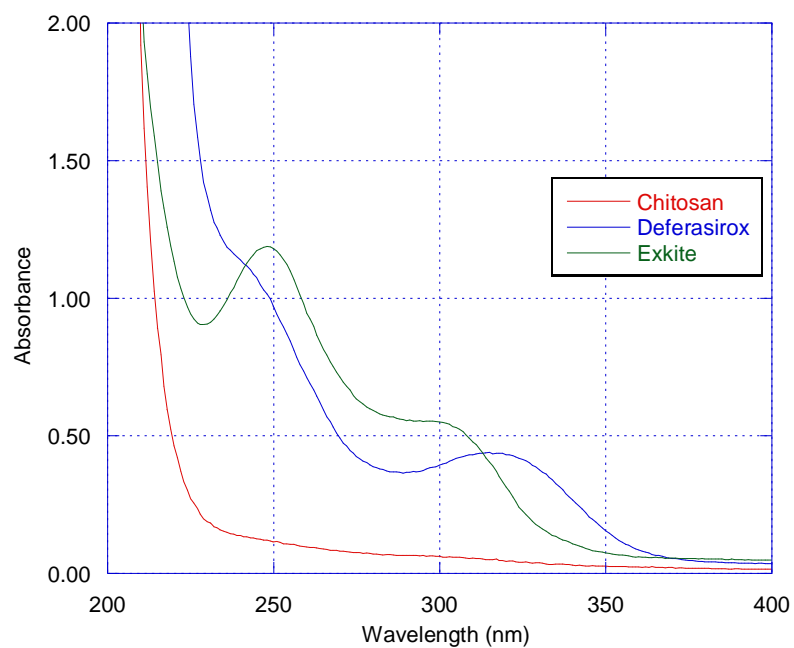


Figure 32 UV-vis spectra of chitosan (0.15% w/v dissolved in 1% v/v acetic acid in water) showing no obvious absorbance, deferasirox ligand **6** (0.04 mM in 0.1 M NaOH solution) with absorbance at 245 nm and 315 nm, and *Exkite* (0.10% w/v in 1M HCl solution) with absorbance at 248 nm and 305 nm.

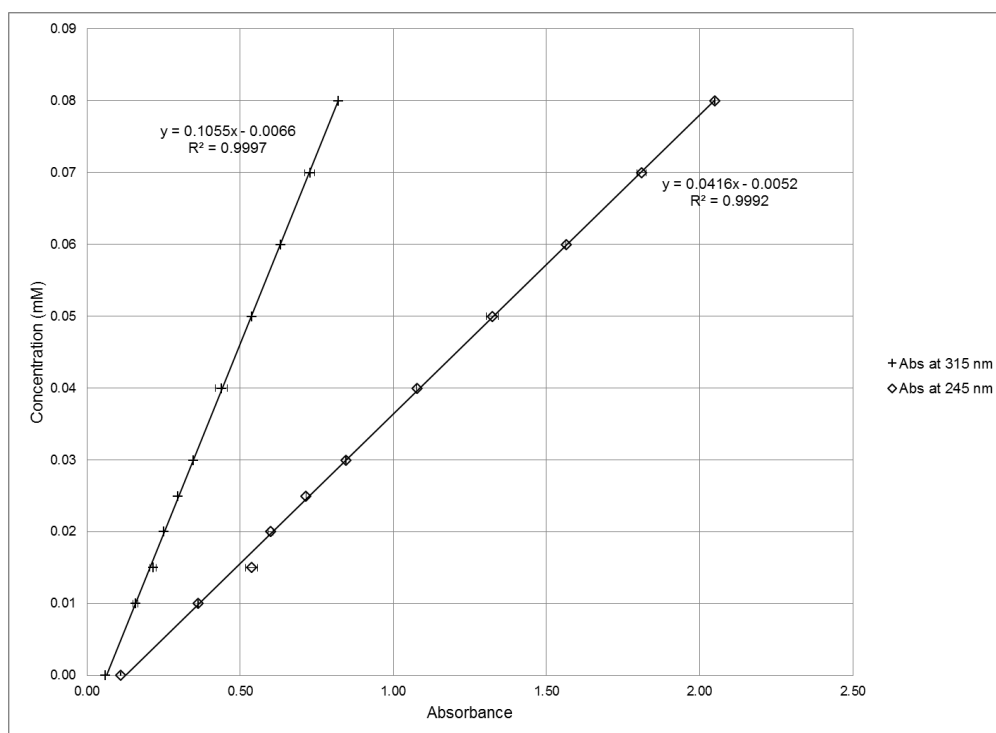
4.4.1 Phenol/Sulphuric acid assay (PSAA)

Measurements of UV-vis spectroscopy can be used quantitatively as the Beer-Lambert law (Equation 3) states that the absorbance (A) is directly proportional to the concentration (c) of the analyte in solution and the path length (l).¹⁴¹ Thus, if the path length (l) and molar extinction coefficient (ϵ) are known it is possible to calculate the concentration of the analyte from the observed absorbance.

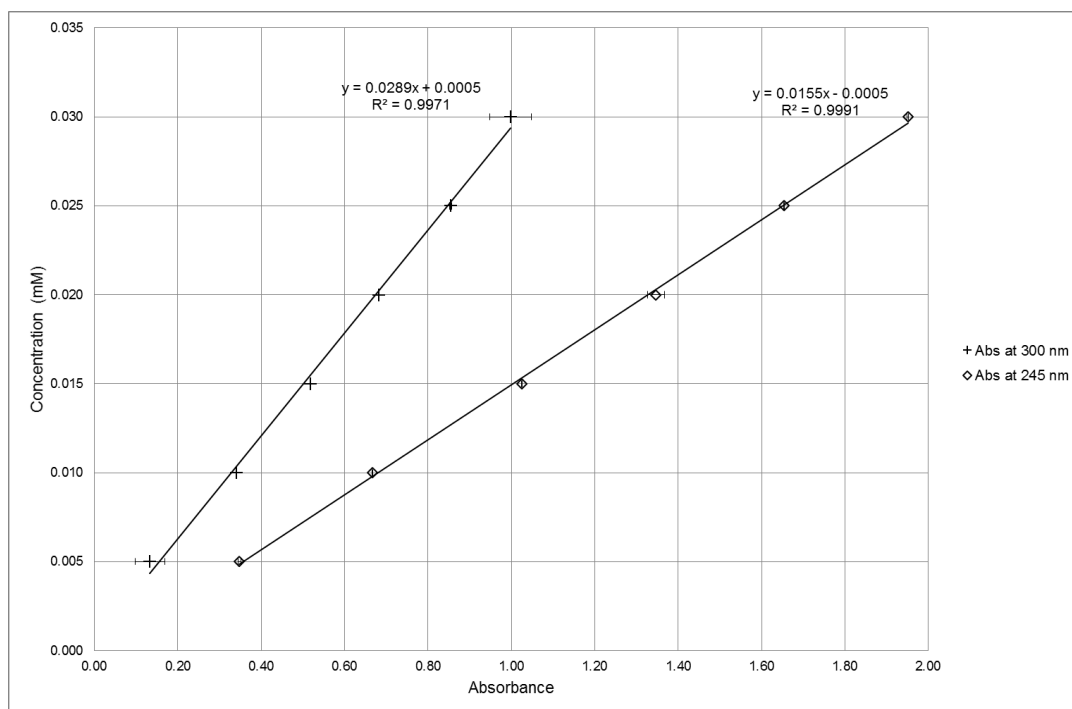
$$A = \epsilon cl$$

Equation 3 The Beer-Lambert law

It is possible to construct calibration curves to calculate the molar extinction coefficient, ϵ for the ligands by measuring absorbance at specific wavelengths at different concentrations of the ligands. Therefore, calibration curves for deferasirox **6** (Graph 1) and ligand **33** (Graph 2) were plotted by measuring the absorbance at λ_{\max} for known concentrations of the ligands.

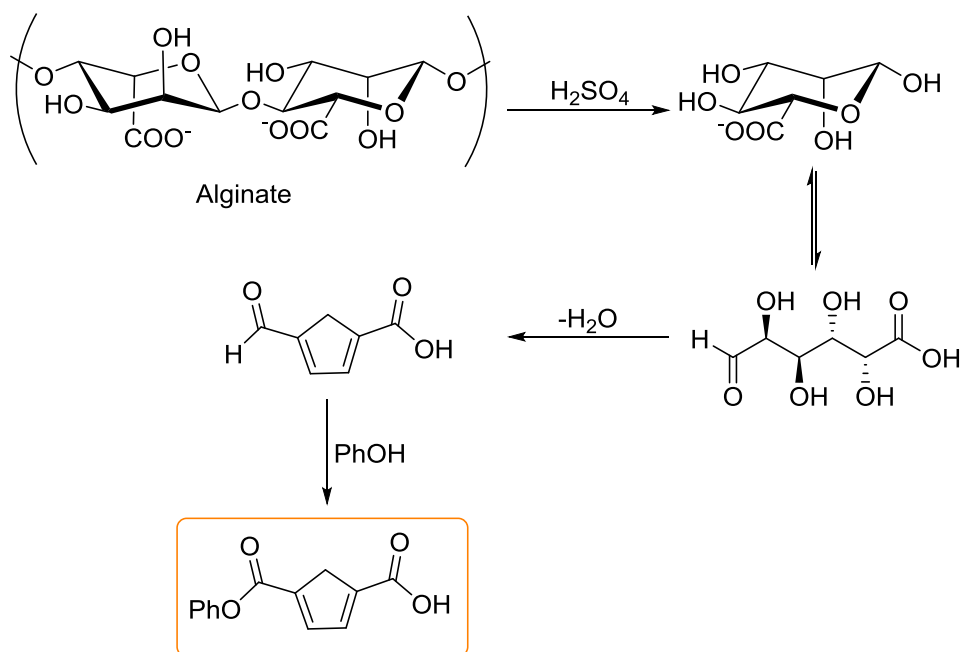


Graph 1 Calibration curve constructed for deferasirox ligand **6** (in 0.1M NaOH) by measuring absorbance at λ_{\max} 315 nm and 245 nm with increasing ligand concentration. All measurements were taken in triplicate, expressed as mean \pm SEM.



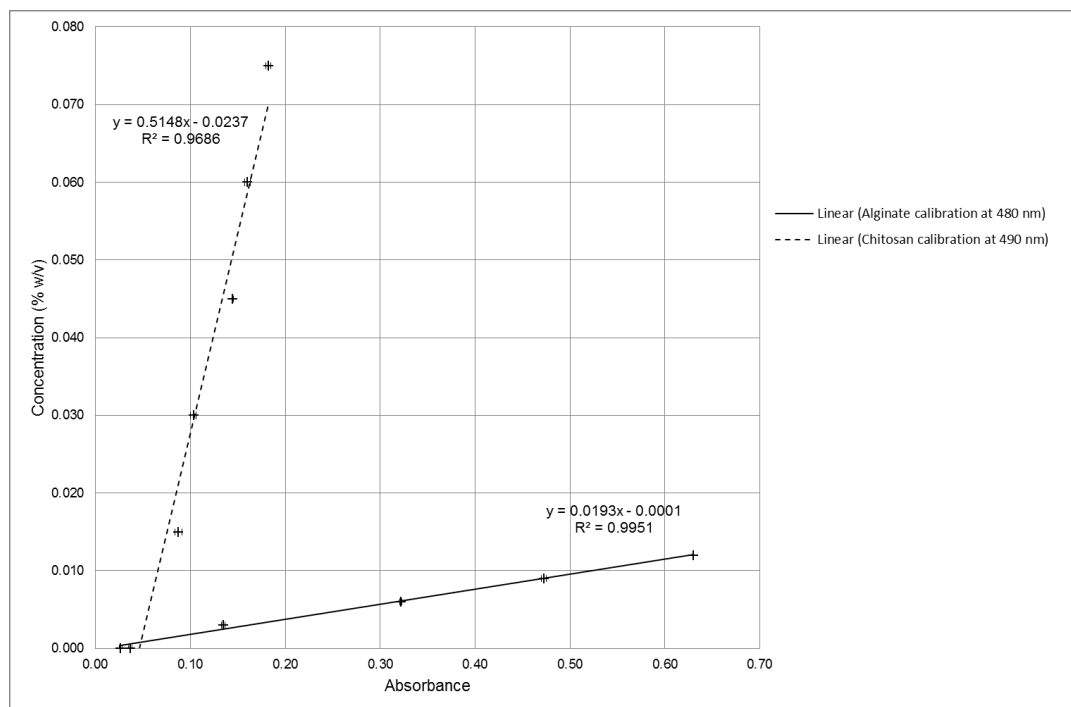
Graph 2 Calibration curve constructed for ligand 33 (in water) by measuring absorbance at λ_{\max} 300 nm and 245 nm with increasing ligand concentration. All measurements were taken in triplicate, expressed as mean \pm SEM.

The calibration curves were used to compare the absorbance observed for *Exkite* or *Exalg* at the same wavelengths in order to determine the concentration of the ligand in the modified polymers. However, in order to determine the percentage modification of the polymers, the concentration of the polysaccharides also need to be known. Although it is possible to construct a similar calibration curve for alginate due to its absorbance at 265 nm, this absorbance is not observed in *Exalg* as it is superimposed by the ligand peaks. Also, chitosan itself does not show any absorbance in the UV-vis spectra so this cannot be quantified using this method. Therefore, phenol/sulphuric acid assay (PSAA) was used for the quantitative determination of polysaccharides. Concentrated sulphuric acid hydrolyses polysaccharides into monosaccharides, which condense to form a furfural product. This further reacts with phenol to produce an orange/yellow compound (Scheme 24).¹⁴² The colour produced is stable and gives a definite absorption in the UV-vis spectrum, and the intensity of the colour produced at a constant phenol concentration is directly proportional to the amount of sugar or polysaccharide in solution.



Scheme 24 Alginate treated with sulphuric acid and phenol produces a coloured furfural product, which can be used to measure carbohydrate concentration by UV-vis spectroscopy.

A calibration curve was constructed for alginate and chitosan in which known concentrations of polymer were treated with sulphuric acid and phenol, and then a UV-vis spectrum was taken to plot concentration vs. absorbance at λ_{max} 480 nm for alginate and 490 nm for chitosan (Graph 3).



Graph 3 Calibration curve obtained for alginate at 480 nm and chitosan at 490 nm after treatment with phenol and sulphuric acid. Measurements were taken in triplicate and expressed as mean \pm SEM.

A solution of *Exalg* was treated in the same way and the absorbance of the resulting peak at 480 nm (Figure 33) was compared to the calibration curve to calculate the concentration of alginate in solution. Unfortunately, when *Exkite* underwent the phenol and sulphuric acid treatment, an appreciable peak at 480 nm was not observed. This may be due to the fact that the poor solubility of *Exkite* meant that this was dissolved in dilute hydrochloric acid solution, and the acidic solution may have interfered with the assay.

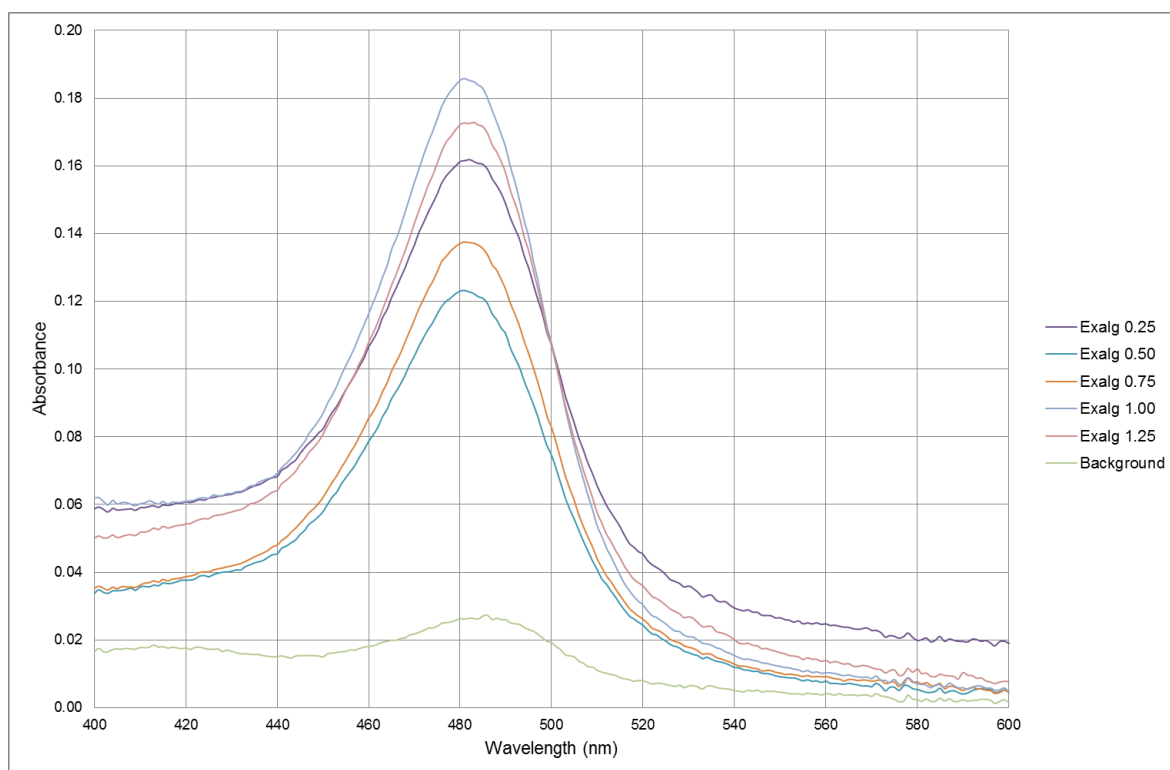


Figure 33 UV-Vis spectra of *Exalg* (in 1% DMSO in water) after phenol and sulphuric acid treatment, with background reading of 1% DMSO in water solution treated with phenol and sulphuric acid.

The calculated concentration of the ligand to polysaccharide ratio was compared for *Exalg* (Scheme 23) to give the relative percentage modification. This gives values between 15 - 27% molar modifications for *Exalg*_{0.25} - *Exalg*_{1.25}, reflecting possible error and variability in the synthesis and PSAA treatment (Table 6). The results suggest that the maximum modification is 27% for *Exalg*_{0.50}, which indicates that there is a limiting factor to the ligand incorporation in *Exalg*.

Table 6 The calculated molar percentage modifications by PSAA for *Exalg* series showing highest modification for *Exalg*_{0.50}.

Entry	Compound	Ligand equiv	% molar modification by PSAA
1	<i>Exalg</i> _{0.25}	0.25	21
2	<i>Exalg</i> _{0.50}	0.50	27
3	<i>Exalg</i> _{0.75}	0.75	23
4	<i>Exalg</i> _{1.00}	1.00	15
5	<i>Exalg</i> _{1.25}	1.25	16

4.5 X-Ray Photoelectron Spectroscopy

X-Ray photoelectron spectroscopy (XPS) gives qualitative and quantitative information about surface elemental composition of the tested material. This technique is based on the photoelectric effect, which is the process of using photons to remove electrons from bulk material (Figure 34).

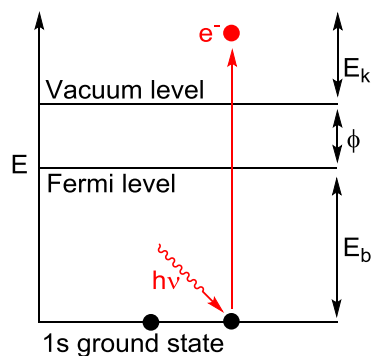


Figure 34 The photoemission process used in XPS.

When photons are directed at the surface of a material, the electrons can become excited from the ground state and can eventually escape into the vacuum by overcoming the work function (ϕ) of the material. The kinetic energy (E_k) of the escaped electrons are measured which can be used to calculate the binding energy (E_b) since the energy of the photons ($h\nu$) are also known (Equation 4).¹⁴³ The work function is the energy required to remove an electron from the excited state to the vacuum immediately outside the solid surface, and this is usually a fixed characteristic of the surface material.

$$E_b = h\nu - E_k - \phi$$

Equation 4 Binding energy E_b is calculated by subtracting kinetic energy E_k and work function ϕ from the energy of the photon $h\nu$, where h is Planck's constant and ν is frequency of photons.

Electrons are emitted with specific kinetic energy so that the calculated binding energies can be used to specifically identify the elemental composition of a sample, as emission lines are well tabulated for most elements. The normalised area under an elemental peak can be used to quantify elemental composition. Furthermore, qualitative data about the chemical state, hybridisation and chemical environment can also be elucidated by relative structure and shift of the elemental peaks.¹⁴⁴

This is a non-destructive technique from which a large amount of information can be gleaned, however it typically requires ultra-high vacuum and the detection limits mean that elements with a low mass such as hydrogen and helium cannot be detected. Also, since the instrument only measures the energy of the photoemitted electrons that reach the detector, this is suited to measuring the surface chemistry of a material. Electrons from deeper below the sample surface must travel through the sample to escape and can undergo inelastic collisions, recombination, and be trapped in an excited state which reduce the number of photoelectrons that reach the surface.¹⁴³

Measurements using XPS were obtained for all polymer samples and the high resolution spectra for carbon, nitrogen and oxygen are shown for *Exkite* and *Exalg0.50* (Figure 35 and Figure 36). The peaks obtained were compared to literature values to assign relative shifts to different chemical environments. The integrated area under the peaks were used to calculate elemental ratios and the subsequent modifications of the polymers.

The C 1s spectrum of alginate (Figure 35a) can be deconvoluted into three peaks corresponding to three carbon environments in the compound; $\underline{\text{C}}=\text{O}$ peak at 288.6 eV due to the carboxylic acid moiety, $\underline{\text{C}}-\text{O}$ peak at 286.9 eV and $\underline{\text{C}}-\text{OH}$ peak at 285.1 eV.¹⁴⁵

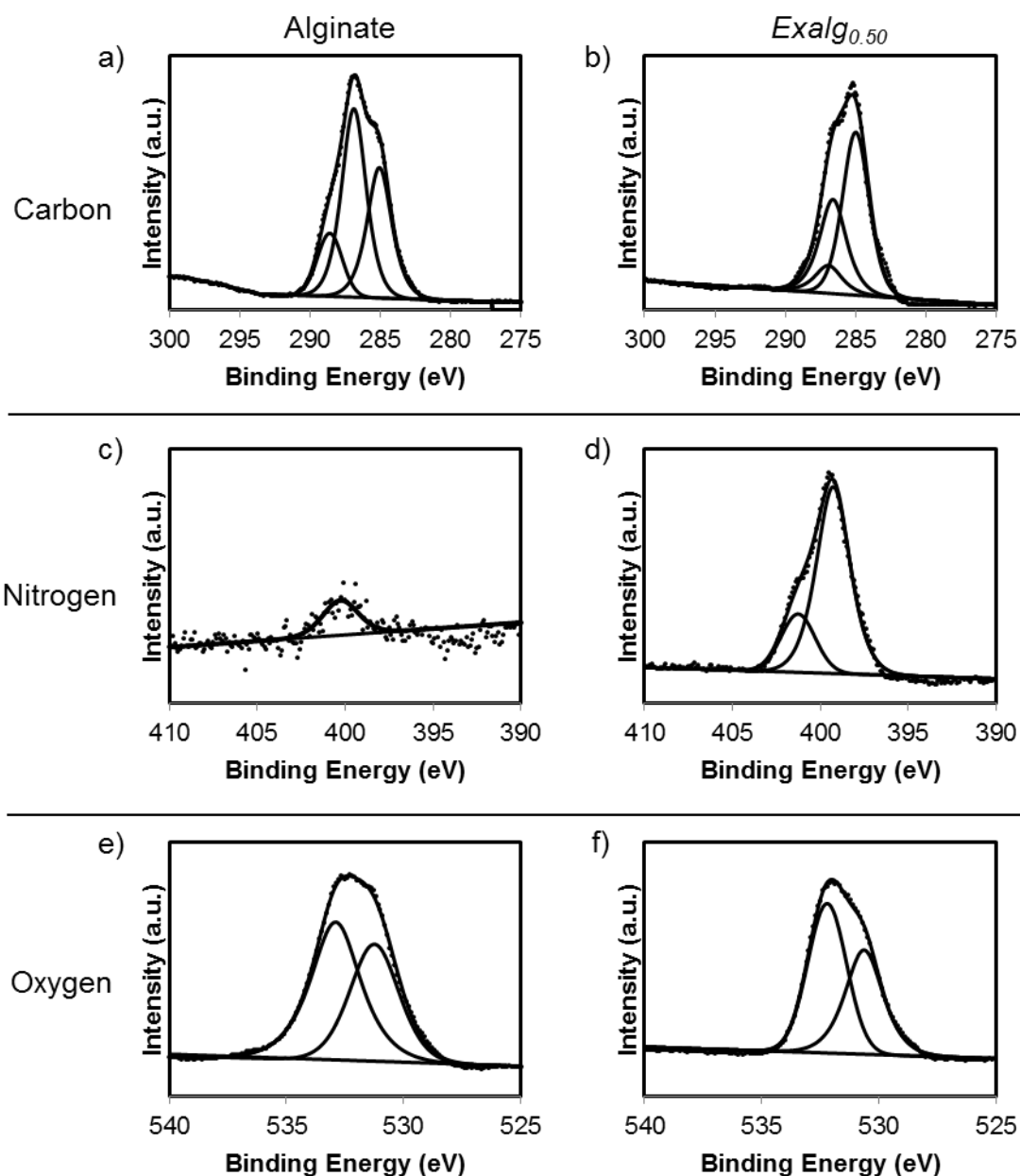


Figure 35 XPS spectra of: a) alginate C 1s, b) *Exalg*_{0.50} C 1s both show three deconvoluted peaks for different carbon environments; c) alginate N 1s shows negligible nitrogen composition, d) *Exalg*_{0.50} N 1s shows peaks from triazole and amide nitrogen; e) alginate O 1s, f) *Exalg*_{0.50} O 1s both show carbonyl and alcohol oxygen species.

Similarly, *Exalg*_{0.50} (Figure 35b) displays three peaks in the carbon region resulting from five carbon species. The peak at 287.0 eV is due to $\underline{\text{C}}=\text{O}$ of amide, peak at 286.6 eV is due to $\underline{\text{C}}-\text{N}$ and $\underline{\text{C}}-\text{O}$ species, and the peak at 285.0 eV is due to the remaining $\underline{\text{C}}-\text{OH}$ and C-C species.¹⁴⁵ The nitrogen composition of alginate is negligible (Figure 35c), however *Exalg*_{0.50} shows N 1s peak at 399.4 eV resulting from $\underline{\text{N}}-\text{C}$ of the triazole ring of the ligand¹⁴⁶, and a peak at 401.6 eV due to the

amide nitrogen (Figure 35d).¹⁴⁷ The O 1s spectra for both alginate (Figure 35e) and *Exalg*_{0.50} (Figure 35f) show deconvoluted oxygen peaks at 531.3 eV and 530.6 eV respectively resulting from C=O of amide, and peaks at 532.9 eV and 532.2 eV respectively due to C-O and C-OH species.¹⁴⁵

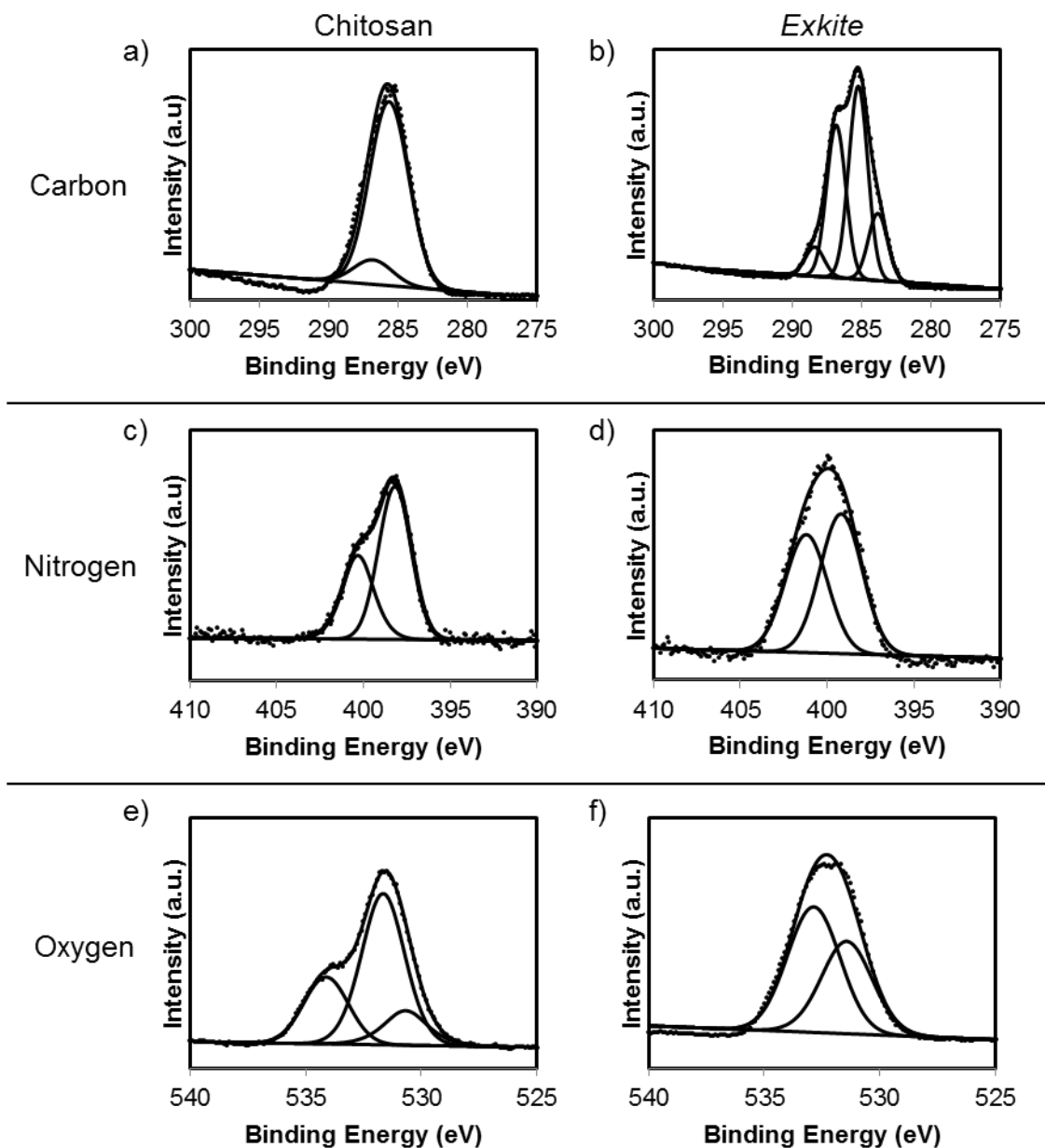


Figure 36 XPS spectra of: a) chitosan C 1s, b) *Exkite* C 1s both show peaks from multiple carbon environments; c) chitosan N 1s shows peaks from amide and amine nitrogen, d) *Exkite* N 1s shows peaks from triazole and amide nitrogen; e) chitosan O 1s, f) *Exkite* O 1s both show peaks from carbonyl and alcohol oxygen environments.

The C 1s spectrum of chitosan (Figure 36a) consists of a peak at 287.0 eV resulting from $\underline{\text{C}}=\text{O}$ of the *N*-acylated glucosamine unit, and a peak at 285.7 eV which is attributed to the accumulation of $\underline{\text{C}}-\text{N}$, $\underline{\text{C}}-\text{O}$ and $\underline{\text{C}}-\text{OH}$ species. However, the C 1s spectrum of *Exkite* (Figure 36b) can be deconvoluted into four peaks; the peak at 288.4 eV corresponds to $\underline{\text{C}}=\text{O}$ carbonyl, the peak at 286.9 eV is due to $\underline{\text{C}}-\text{N}$ environment, the peak at 285.3 eV can be accredited to C-C and $\underline{\text{C}}-\text{O}$ species, and the final peak at 284.0 eV is a result of $\underline{\text{C}}-\text{OH}$ species.¹⁴⁵ Chitosan shows two peaks in the resolved N 1s spectrum (Figure 36c) due to amide nitrogen at 400.3 eV and amine nitrogen at 398.2 eV.¹⁴⁴ *Exkite* also shows two peaks in the N 1s spectrum (Figure 36d); the peak at 401.2 eV is due to amide nitrogen and peak at 399.2 eV can be recognised as C- $\underline{\text{N}}$ environment of the ligand.¹⁴⁷ The O 1s spectrum of chitosan (Figure 36e) is shown to consist of three peaks corresponding to three oxygen environments; $\text{C}=\underline{\text{O}}$ of acylated amide group at 530.6 eV, the peak at 531.7 eV is due to C- $\underline{\text{O}}\text{H}$ species and the peak at 534.1 eV is a result of C- $\underline{\text{O}}$ species.¹⁴⁴ Similarly, *Exkite* (Figure 36f) shows a peak at 531.5 eV resulting from $\text{C}=\underline{\text{O}}$ amide which is higher in intensity than in chitosan due to ligand incorporation, and a peak at 532.8 eV which is combination of C- $\underline{\text{O}}\text{H}$ and C- $\underline{\text{O}}$ environments.¹⁴⁵

The normalised area under the peak for each element was determined and used to calculate the graft ratio for the polymer material believed to be conjugated to the ligand, which is the ratio of modified monomer units compared to the total number of monomer units (Equation 5).

$$\text{Graft ratio} = \frac{y}{x + y}$$

Equation 5 General equation for graft ratio where *y* is the number of modified monomer units and *x* is the number of unmodified monomer units.

A method described by Wang *et al.*⁹⁴ was adopted for the derivation of graft ratio for *Exalg* and *Exkite*, using N/C ratio as determined by XPS analysis. In the graft ratio of *Exalg* (Equation 6), 6

and 27 are the number of carbon atoms in an alginate monomer unit and the ligand respectively, and 5 is the number of nitrogen atoms from the ligand.

$$\text{Graft ratio Exalg} = \frac{6^{\frac{N}{C}}}{5 - 27^{\frac{N}{C}}}$$

Equation 6 Graft ratio of Exalg based on N/C ratio

Similarly, in the graft ratio of Exkite (Equation 7), 6 and 21 are the number of carbon atoms in a chitosan monomer unit and the ligand respectively, and 4 is the number of nitrogen atoms in a modified monomer unit.

$$\text{Graft ratio Exkite} = \frac{6^{\frac{N}{C}}}{4 - 21^{\frac{N}{C}}}$$

Equation 7 Graft ratio of Exkite based on N/C ratio

The calculated N/C ratios from XPS analysis were used to determine the graft ratio for the modified polymers (Table 7).

Table 7 The N/C ratio and graft ratio of polymers as calculated by XPS analysis.

Entry	Compound	Ligand equiv	N (Area)	C (Area)	N/C	Graft ratio (%)
1	Chitosan	-	0.01	0.07	-	-
2	Exkite	1.00	0.03	0.28	0.12	46
3	Alginate	-	0.00	0.16	-	-
4	Exalg _{0.25}	0.25	0.03	0.27	0.13	48
5	Exalg _{0.50}	0.50	0.04	0.32	0.14	66
6	Exalg _{0.75}	0.75	0.03	0.21	0.14	62
7	Exalg _{1.00}	1.00	0.04	0.29	0.13	53
8	Exalg _{1.25}	1.25	0.04	0.28	0.14	67

This shows that *Exkite* is 46% modified with ligand, whilst *Exalg* modification ranges from 48% for *Exalg_{0.25}* to 67% for *Exalg_{1.25}*. Although theoretically it is not possible to obtain a graft ratio of more than 25% for *Exalg_{0.25}* and 50% for *Exalg_{0.50}*, this may be an artefact of alginate activated by NHS/EDAC.HCl as one equivalent of these reagents were used in all cases, thus increasing nitrogen content due to the activated species. However, as previously there is no significant increase in graft ratio with increasing ligand equivalence of *Exalg*.

4.6 Summary

Analysis by IR spectroscopy shows amide carbonyl peaks for the modified polymers, ¹H NMR spectroscopy displays peaks corresponding to the polymer and ligand, and UV-vis spectroscopy revealed specific absorbance indicative of ligand incorporation for both polymers. Although the absolute values calculated for percentage incorporation from each method differed, with the exception of XPS the average incorporation calculated for *Exalg* is 20%. Analysis by all methods suggest that there is a limiting factor in the incorporation of ligand with alginate, as increasing ligand equivalence did not greatly affect polymer modification. This may be related to the number of carboxylic acid sites of alginate that were activated by NHS/EDAC.HCl coupling agents, or the number of active sites that were accessible to the ligand, as well as any tertiary structure features of alginate which may have affected incorporation.¹⁴⁸ Additionally, the average percentage ligand incorporation calculated for *Exkite* is 40% when one equivalence of ligand was used.

The synthesis of *Exkite* and *Exalg* were repeated and the characterisation results were compared. The IR spectra show similar absorbance at 3295 cm⁻¹ and 3000 cm⁻¹ for *Exalg 2* corresponding to –OH and –CH absorption, and a carbonyl amide absorption at 1636 cm⁻¹ resulting from C=O vibration (Figure 37). Although *Exkite 2* also shows –OH absorption and overlapped –CH absorptions at 3380 cm⁻¹ and 2985 cm⁻¹, the carbonyl absorption is slightly higher at 1680 cm⁻¹ which may be due to the free ligand **6** in the salt form of *Exkite*.

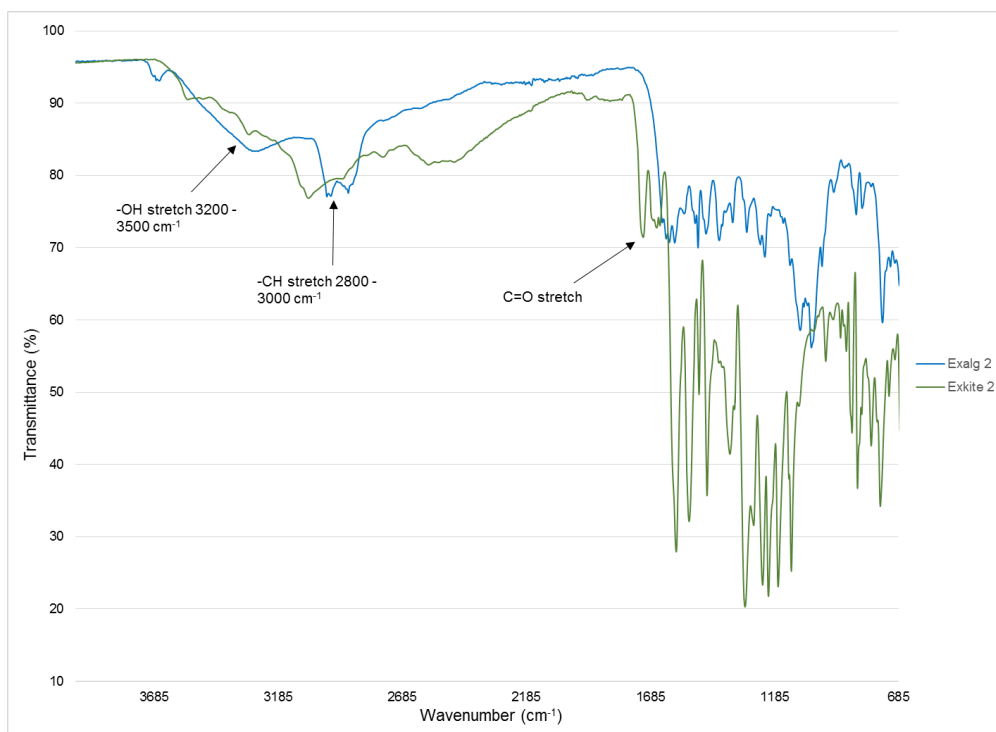


Figure 37 UV-vis spectra of *Exalg 2* and *Exkite 2*.

Nevertheless, the ^1H NMR spectra are similar to previous, showing aliphatic polymer peaks and aromatic ligand peaks for both *Exalg 2* (Figure 38) and *Exkite 2* (Figure 39).

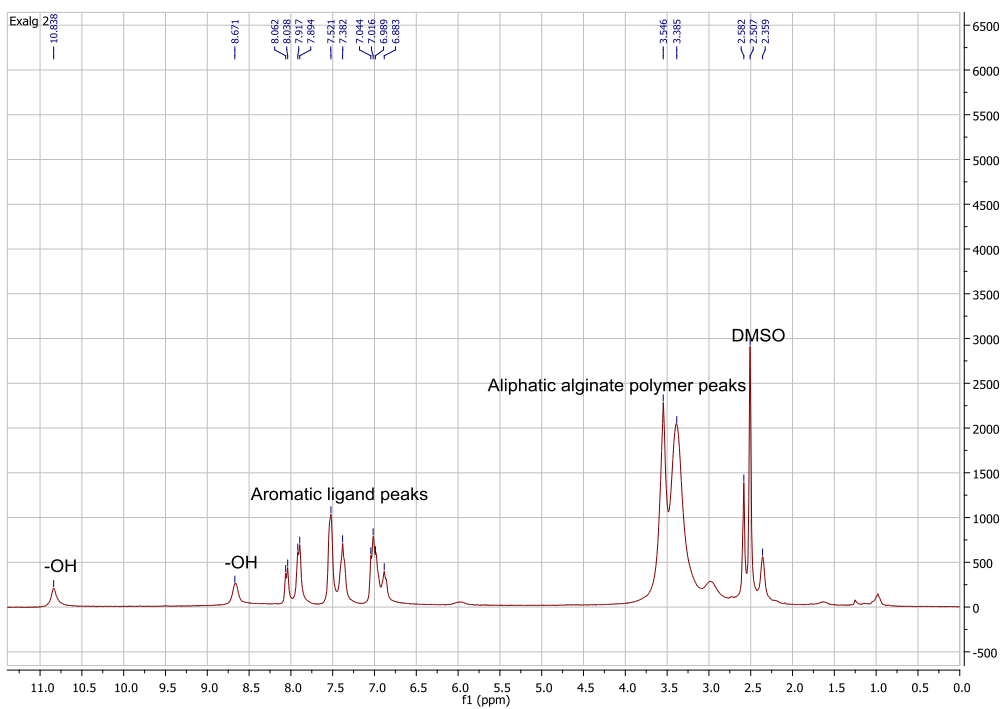


Figure 38 ^1H NMR spectra of *Exalg 2* in $\text{d}_6\text{-DMSO}$.

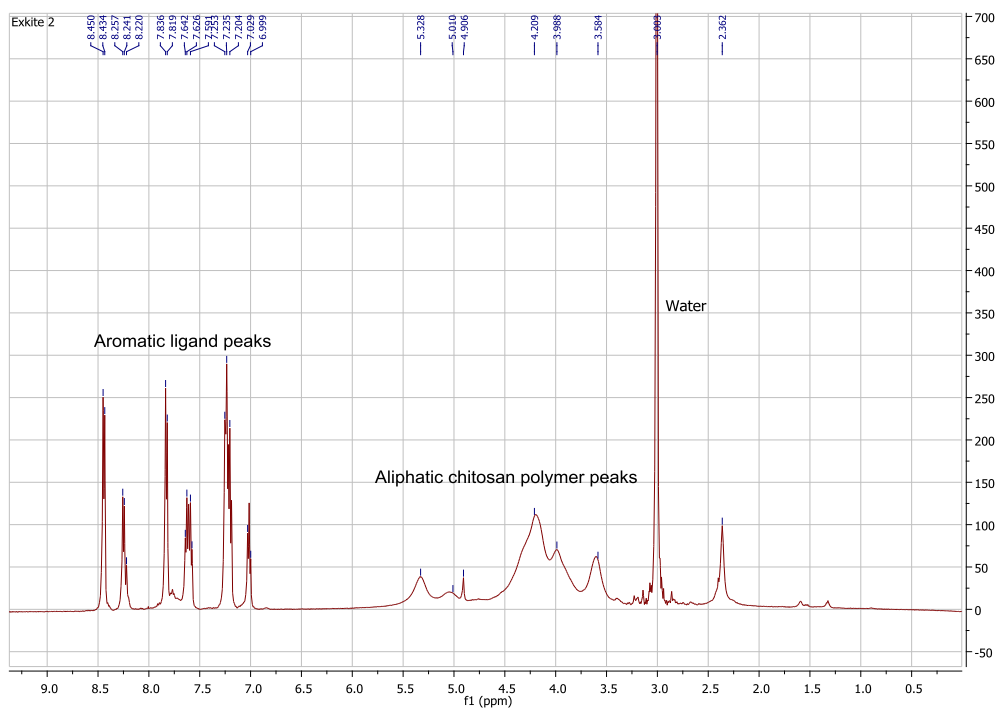


Figure 39 ^1H NMR spectra of *Exkite 2* in d-TFA.

The UV-vis spectra also exhibit similar absorbance at 247 nm and 302 nm for *Exalg 2*, and 248 nm and 305 nm for *Exkite 2* indicative of ligand incorporation (Figure 40).

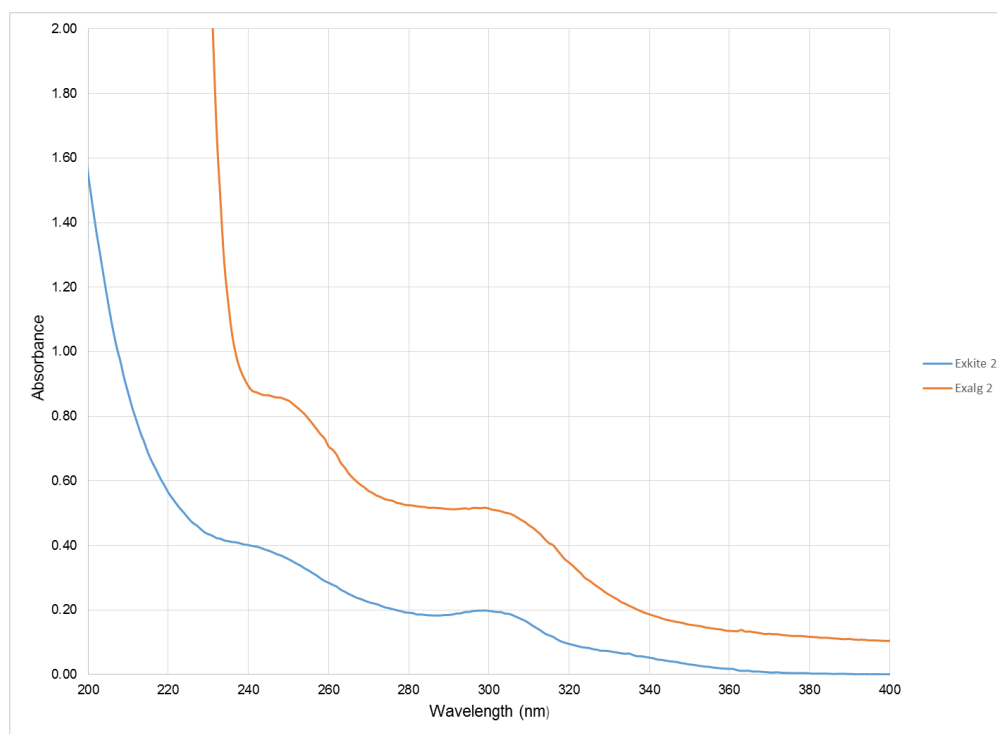


Figure 40 UV-vis spectra of *Exkite 2* (0.10% w/v in 1M HCl solution) and *Exalg 2* (0.01% w/v dissolved in 1% v/v DMSO in water).

Matrix-assisted laser desorption/ionization (MALDI) mass spectrometry was also attempted but was unsuccessful in determining a change in molecular weight upon modification of the polymers due to the large polydispersity of the polymers. A range of molecular weights were observed for polymers before and after modification. Attempts to employ elemental analysis was also unsuccessful as comparison of theoretical C/N ratio to actual ratio obtained from elemental analysis was difficult due to the relatively small change in the theoretical C/N ratio of *Exalg* and *Exkite* with increasing modification.

Diffusion NMR spectroscopy conducted as an addendum to the data shows that the ligand is covalently attached to alginate polymer in *Exalg* due to the similar self-diffusion coefficients obtained for ligand and polymer. However, the differing self-diffusion coefficients obtained for ligand and polymer in *Exkite* suggests that this sample is a mixture of chitosan and ligand **6** perhaps in a salt form. This is representative for the sample tested and hence the results must be interpreted with caution; more can be learnt about the synthesis if this is repeated on multiple batches of *Exkite*.

5 Iron binding studies

5.1 Background

Characterisation of the modified polymers demonstrated ligand attachment in *Exalg* by diffusion NMR spectroscopy and the presence of the ligand in *Exkite* in which ligand conjugation was more difficult to discern, and is likely to be present as *Exkite* salt according to diffusion NMR studies conducted after the data in this chapter was obtained (Chapter 4). The magnitude of iron binding of *Exalg* and *Exkite* were investigated in comparison to the native polymers to assess the change in iron binding properties upon addition of an iron chelator. This was principally assessed by two methods. Firstly, iron binding was probed by UV-vis spectroscopy in which polymer solutions were titrated with iron solutions to monitor a change or shift in absorbance in the UV-vis profile, which may be attributed to the formation of an iron complex species. Secondly, iron binding was assessed by dialysis which involves suspending the polymer solution in a semi-permeable membrane, placed in an iron solution for a period of time, after which the concentration of iron in polymer solution is measured to obtain the degree of iron uptake.

5.2 Titrations by UV-vis spectroscopy

Iron binding was studied by UV-vis spectroscopy by titrating a known quantity of iron solution into a solution of polymer to monitor a change in absorbance.¹⁴⁹ Initially, iron chloride solution (10 mM $\text{FeCl}_3 \cdot 6\text{H}_2\text{O}$) was titrated into water alone, which shows an increase in absorbance at 290 nm due to the interaction of iron with water to form of $[\text{Fe}(\text{H}_2\text{O})_6]^{3+}$ complex (Figure 41).¹⁵⁰ Crystal field theory (CFT) states that this is due to an attraction between positively charged metal cation and electron rich ligand.¹⁵¹ However, as the ligand approaches the cation the electrons of the ligand and those in the *d* orbitals of the metal closest to the ligand repel causing a splitting of five degenerate *d* orbitals of Fe (III) to form a triply degenerate t_{2g} and doubly degenerate e_g sets of

orbitals in an octahedral field with an energy difference of Δ_{oct} .¹⁵² The t_{2g} set consists of d_{xy} , d_{xz} and d_{yz} orbitals as their lobes do not point directly at the ligands so are lower in energy. The e_g set consists of $d_{x^2-y^2}$ and d_z^2 which have lobes pointing directly at the ligands so experience the greatest repulsion and are higher in energy.¹⁵³ The absorption of energy from visible light allows an electronic transition to occur between the lower lying t_{2g} set and e_g set of crystal field orbitals giving rise to an absorption band in the UV-vis spectrum.¹⁵⁴

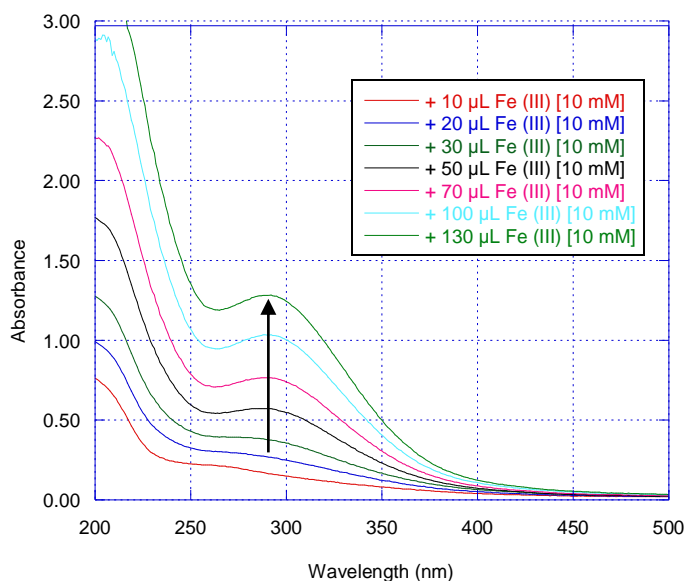


Figure 41 UV-vis spectra of 10 mM $\text{FeCl}_3 \cdot 6\text{H}_2\text{O}$ titrations into water.

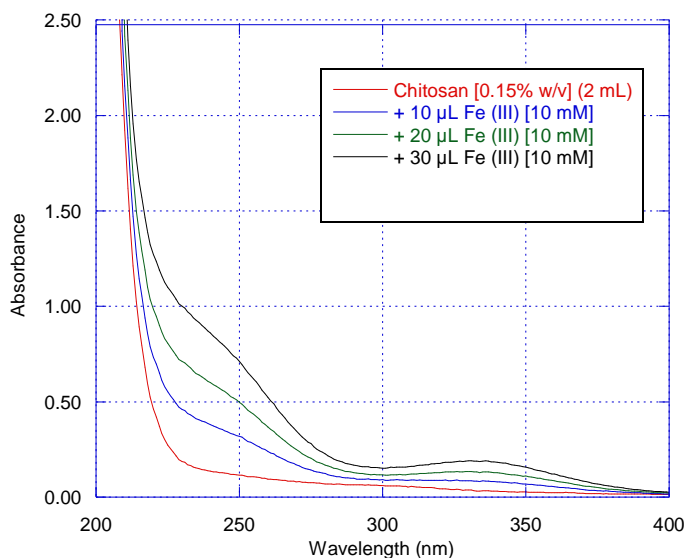


Figure 42 UV-Vis spectra of 10 mM $\text{FeCl}_3 \cdot 6\text{H}_2\text{O}$ titrations into chitosan (0.15% w/v dissolved in 1% v/v acetic acid in water) does not indicate any binding.

Iron binding of chitosan was probed by titrating iron chloride solution (10 mM $\text{FeCl}_3 \cdot 6\text{H}_2\text{O}$) into chitosan solution (Figure 42). Although there seems to be the emergence of a peak at 330 nm, this is not significant suggesting poor iron binding by chitosan.

Additionally, iron chloride solution (10 mM $\text{FeCl}_3 \cdot 6\text{H}_2\text{O}$) was titrated into *Exkite* solution (Figure 43), and a shift in absorbance was observed from 305 nm when there is no Fe (III) present, to 322 nm suggesting the formation of an iron complex. This is likely due to be from a charge transfer within the complex which occurs when there is an electronic transition between a metal based orbital and a ligand based orbital. As the ligand has vacant low lying π^* orbitals, the observed transition may be from the occupied metal t_{2g} orbital to the ligand π^* orbital.¹⁵⁵ Further titrations increased the absorbance at 322 nm due to increasing amounts of the iron complex species being formed (Figure 44).

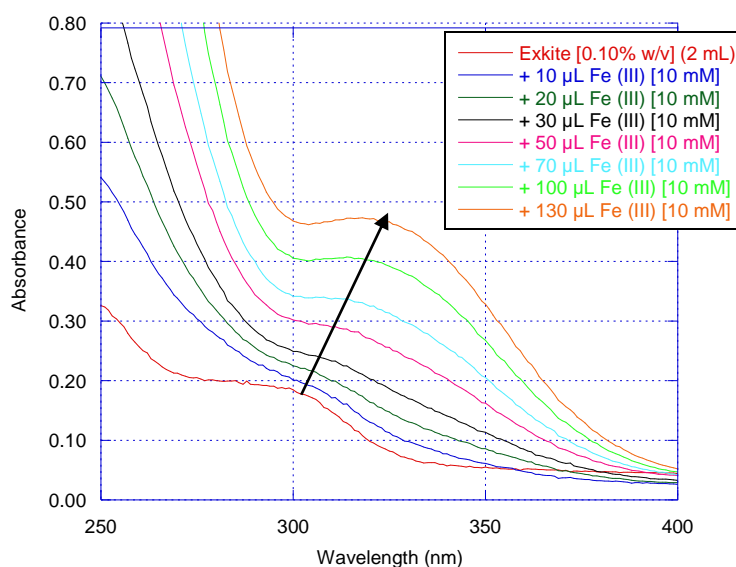


Figure 43 UV-vis spectra of 10 mM $\text{FeCl}_3 \cdot 6\text{H}_2\text{O}$ titrations into *Exkite* (0.10% w/v in 1M HCl solution) showing a shift in absorbance.

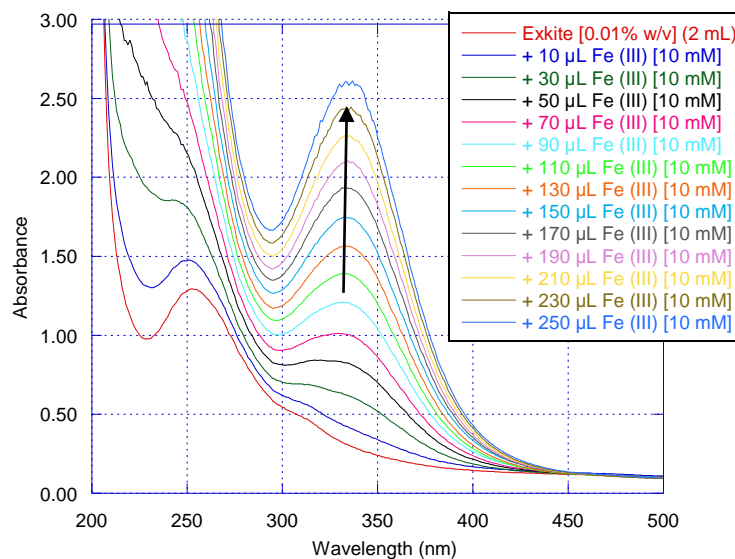


Figure 44 UV-vis spectra of 10 mM FeCl₃·6H₂O titrations into *Exkite* (0.10% w/v in 1M HCl solution) showing an increase in absorbance at high iron concentrations.

In order to obtain a binding curve from this UV-vis data, it was necessary to know where the absorbance is at a maximum for each concentration of Fe (III) that was used in the titrations; i.e. at the stationary point where $dy/dx = 0$. Therefore, the position of maximum absorbance for each concentration of Fe (III) titration into *Exkite* was taken and a subsequent plot of the shift in wavelength, $\Delta\lambda$ vs. final Fe (III) concentration for each titration enabled the plotting of a binding curve (Figure 45).

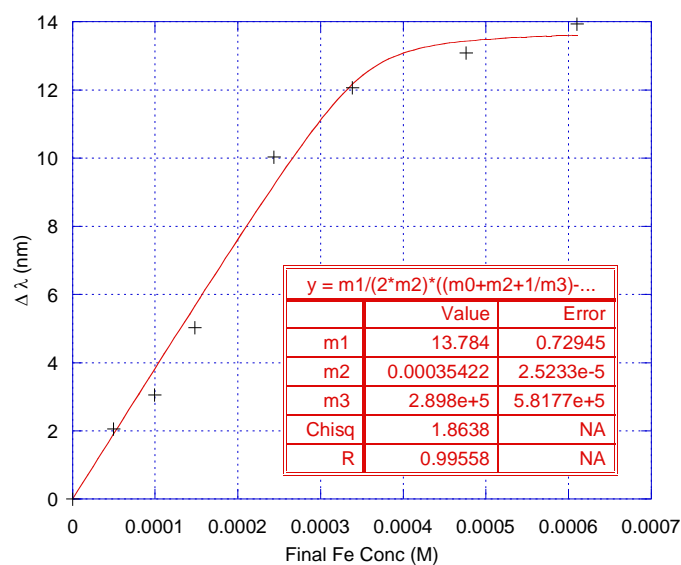


Figure 45 Attempted fitting of binding curve for iron titrations into *Exkite* by measuring shift in λ .

Unfortunately, as the saturation point of binding was not reached, this resulted in a poor fit of the binding curve with an approximate binding constant of the order 10^5 . An attempt to titrate higher concentrations of Fe (III) to obtain saturation resulted in precipitation of the iron complex which caused light scattering and interfered with the measurement of the UV-vis spectra. In addition, iron hydroxide complexes are known to undergo hydrolysis in solution to give insoluble complexes which precipitate out of solution.¹⁵⁶ Similar titrations using iron sulphate solution (10 mM $\text{FeSO}_4 \cdot 7\text{H}_2\text{O}$) to assess Fe (II) binding of *Exkite* was unsuccessful as there was no observed shift or increase in absorbance. This may be due to weak electronic transitions within the complex which cannot be observed by UV-vis spectroscopy.

Iron titrations into alginate solution using iron chloride solution (10 mM $\text{FeCl}_3 \cdot 6\text{H}_2\text{O}$) was also performed, which showed an increase in absorbance at 265 nm indicative of interaction of alginate with iron, however the increase in absorbance is not consistent with increase in iron concentration possibly due to the gelling of alginate in the presence of a cation which was visually observed in the cuvette upon addition of iron (Figure 46).^{85, 157}

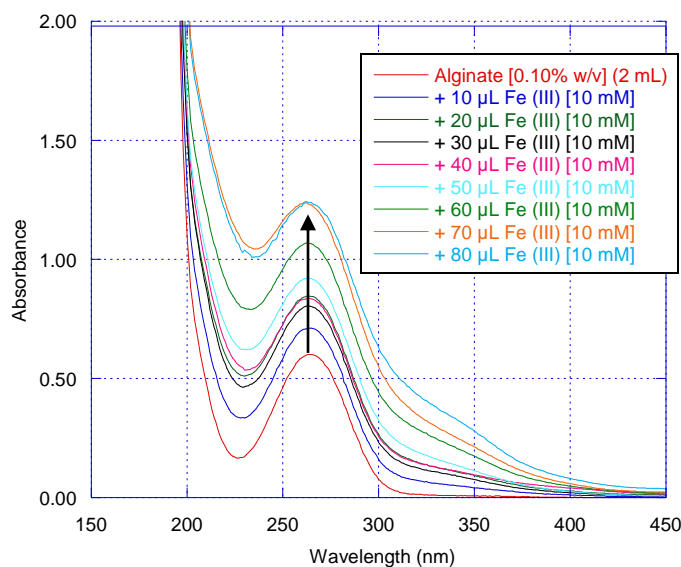


Figure 46 UV-Vis spectra of 10 mM $\text{FeCl}_3 \cdot 6\text{H}_2\text{O}$ titrations into alginate (0.10% w/v in water) shows increase in absorbance at 265 nm.

Iron titration into *Exalg*_{1.00} solution also showed a shift in the peak at 302 nm to 310 nm in the presence of Fe (III) which suggests the formation of an iron complex, and further titrations increased the absorbance at 310 nm (Figure 47).

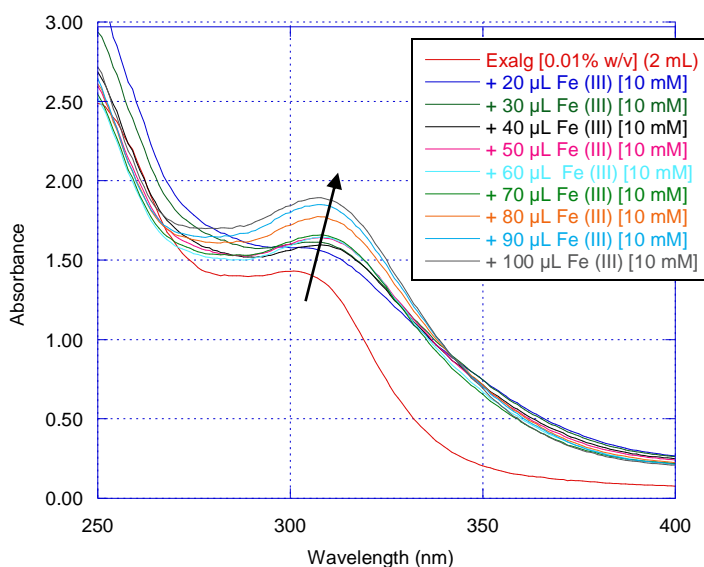


Figure 47 UV-Vis spectra of 10 mM $\text{FeCl}_3 \cdot 6\text{H}_2\text{O}$ titrations into *Exalg*_{1.00} (0.01% w/v dissolved in 1% v/v DMSO in water) showing shift in absorbance upon iron titrations.

However, as with alginate the increase in absorption at 310 nm does not increase directly in response to iron concentration.

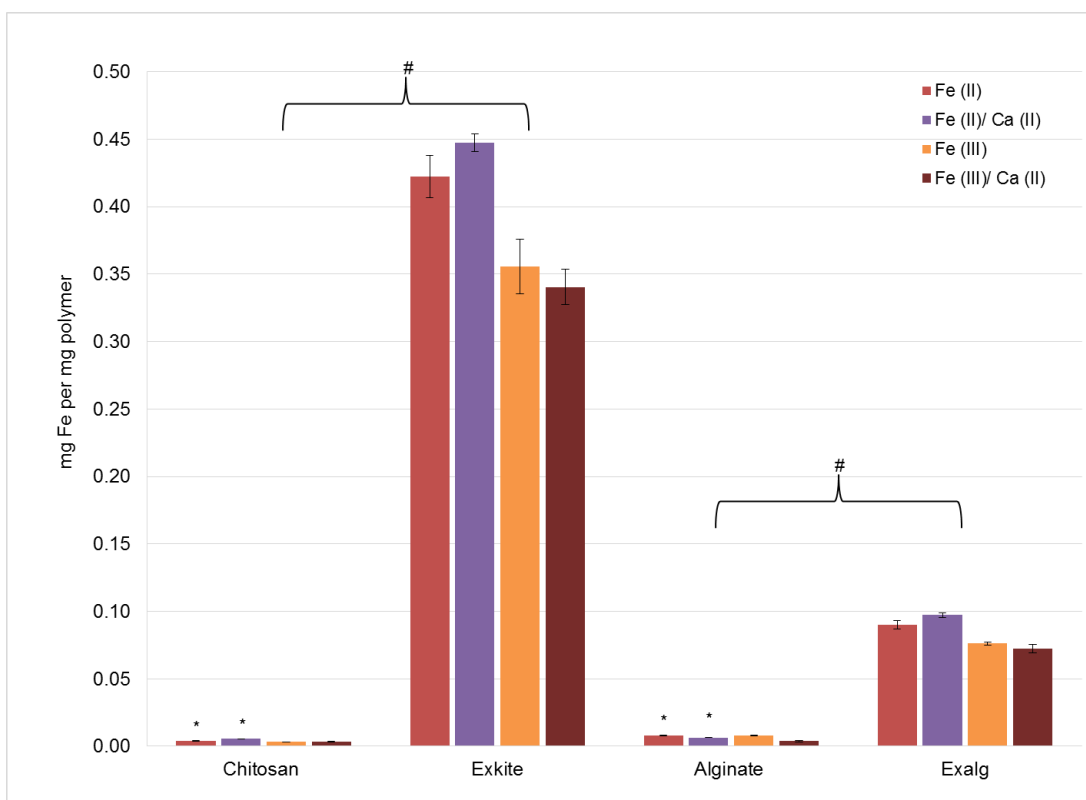
5.3 Dialysis methods

The extent of iron binding can also be measured by dialysis, which involves the suspension of polymer solutions of known concentration in semi-permeable cellulose membrane, submerged in a supernatant at physiological concentrations of iron in the colon derived from an approximate dietary intake of 5 mg of elemental iron.¹⁵⁸ Whilst the polymers are too large in size to escape the dialysis tubing, iron can move freely through the tubing to allow iron binding by polymers, and at the end of the experiment the concentration of iron within the polymer solutions can be measured by ferrozine assay or atomic absorption spectroscopy, which is a quantitative method of calculating the iron binding properties of polymers. Ferrous (0.20 mM $\text{FeSO}_4 \cdot 7\text{H}_2\text{O}$) and ferric (0.20 mM

$\text{FeCl}_3 \cdot 6\text{H}_2\text{O}$) binding of the polymers was investigated in the presence and absence of calcium ($2.00 \text{ mM CaCl}_2 \cdot 2\text{H}_2\text{O}$) at physiologically relevant concentrations. Calcium is known to be present in the human lumen,¹⁵⁹ and alginate is recognised for binding calcium with good affinity forming egg box structures (Section 1.8.1). Therefore it is informative to understand if modification with an iron chelator altered this intrinsic calcium binding property as polymers need to be selective in iron binding in the presence of other cations. Potential calcium binding by *Exalg* modified from alginate may be problematic if this is significant as it will result in the removal of physiologically relevant non-target cation.

Initial dialysis experiments were conducted in dilute acidic media in order to better solvate iron complexes and to prevent the precipitation of iron oxides during the experiment.¹⁶⁰ Polymer solutions of chitosan, *Exkite*, alginate and *Exalg1.00*, which was chosen arbitrarily for comparison, were suspended in dialysis tubing and immersed in ferrous and ferric iron in the presence and absence of calcium for two hours with gentle agitation. Iron concentration was measured by flame atomic absorption spectroscopy (AAS), which utilises the principle that electrons can be promoted to an excited state by absorbing a defined quantity of energy, and the wavelength at which this occurs is specific to an electronic transition within an element.¹⁶¹ Therefore, the absorbance at a particular wavelength can be used to quantify elemental composition, which requires construction of a calibration curve to establish the relation between observed absorbance and iron concentration and hence relies on the Beer-Lambert law (Equation 3). The observed iron concentrations were used to calculate mg iron per mg polymer (Graph 4). This experiment shows a statistically significant increase ($p < 0.006$) in iron binding of *Exkite* compared to chitosan. Both ferrous and ferric binding has improved over 100 fold suggesting no selectivity between ferric and ferrous iron, and the presence of calcium does not have an effect. Iron binding of *Exalg1.00* has also improved

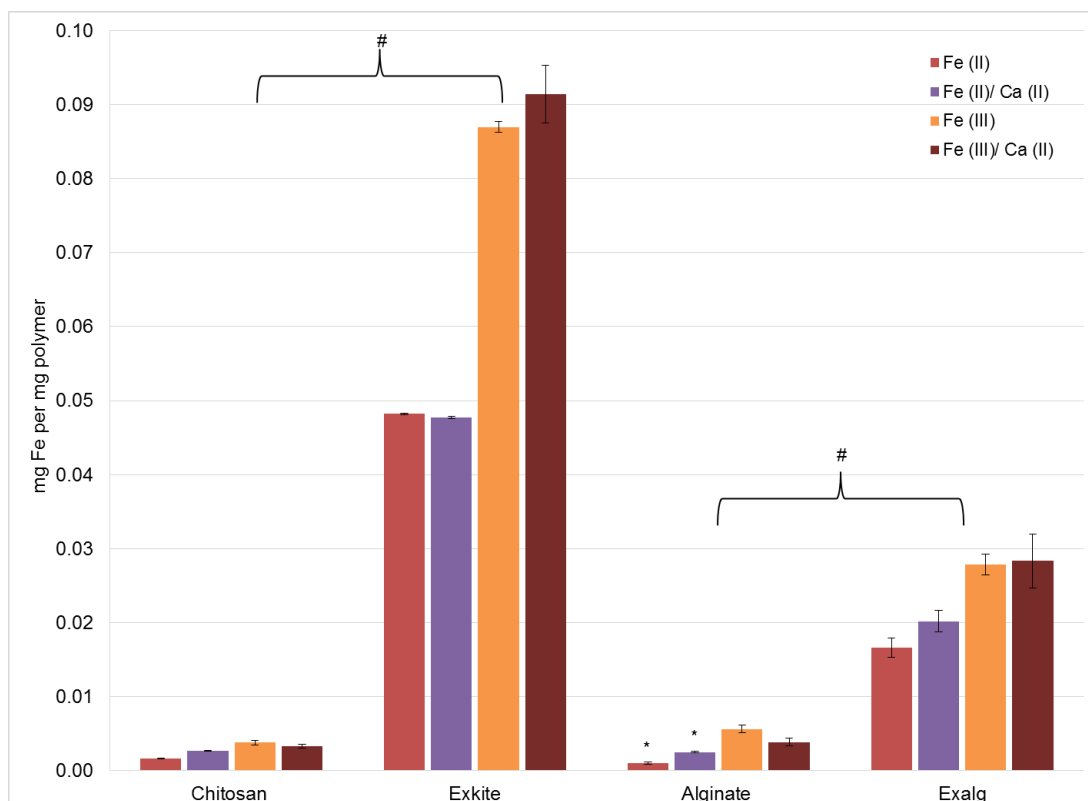
compared to alginate alone ($p < 0.002$), however there is only a tenfold increase in ferrous and ferric binding in the presence and absence of calcium.



Graph 4 Iron binding of polymers by dialysis in acidic media for two hours determined by AAS. Experiments were performed in triplicate, data is presented as mean \pm SEM, * and # denote statistically significant difference calculated by Student's *t*-test ($p < 0.05$).

The dialysis experiment in acidic media was repeated in which the polymer solutions in dialysis tubing were immersed in iron solutions for two hours followed by immersion in water for two hours. The subsequent washing step was conducted in order to determine the effective leaching of bound iron and any apparent selectivity between ferric and ferrous iron during this process, iron concentration was determined by AAS. Although there is still an increase in iron content of *Exkite* relative to chitosan ($p < 0.004$), and *Exalg_{1.00}* relative to alginate ($p < 0.04$), overall there is a decrease in total iron concentrations observed after washing due to leaching of iron (Graph 5). This is evident for *Exkite* in which ferrous iron concentration decreased from 0.422 ± 0.016 mg to 0.048 ± 0.0001 mg Fe per mg polymer after the washing step. However, there is greater retention of Fe (III) in *Exkite* which may be due to greater selectivity of the ligand towards ferric iron than ferrous

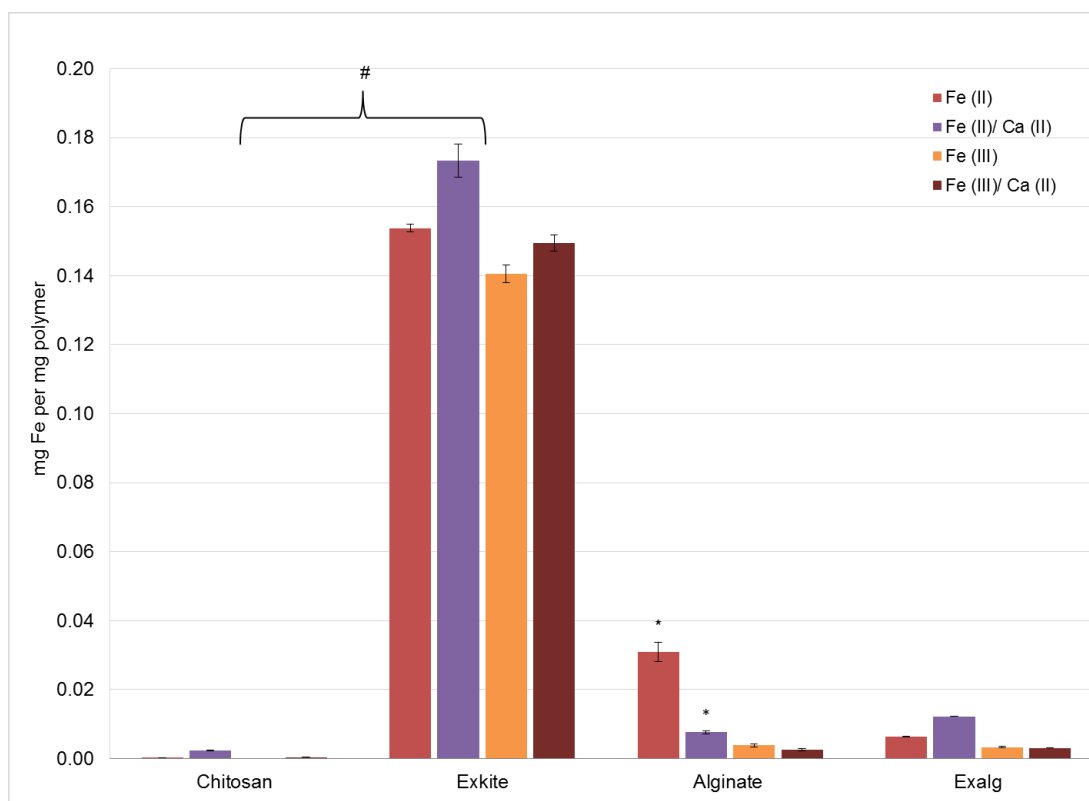
iron, which is unaltered in the presence of calcium. There is also a decrease in ferrous iron concentration of *Exalg1.00* from 0.090 ± 0.003 mg to 0.017 ± 0.001 mg Fe per mg polymer after washing and a slight selectivity for ferric over ferrous iron is also observed. Despite conducting the washing step, *Exkite* whether present as conjugated polymer or salt, is still superior at iron binding relative to *Exalg1.00*.



Graph 5 Iron binding of polymers after dialysis for two hours in acidic media followed by washing for two hours determined by AAS. Experiments were performed in triplicate, data is presented as mean \pm SEM, * and # denote statistically significant difference calculated by Student's *t*-test ($p < 0.05$).

As former dialysis experiments had been conducted in dilute acidic media, it was proposed that this may affect the actual iron binding of the polymers as formation of the iron complex requires deprotonation of the phenolic oxygen of deferasirox ligand moiety. Hereafter further dialysis studies were done without acid in the supernatant in which polymer solutions were suspended in iron solutions for two hours with no further washing step, and iron concentration determined by AAS (Graph 6). In this instance, there is still a great increase in ferric and ferrous iron binding between chitosan and *Exkite* of over 100 fold ($p < 0.0001$) and calcium did not have an effect on

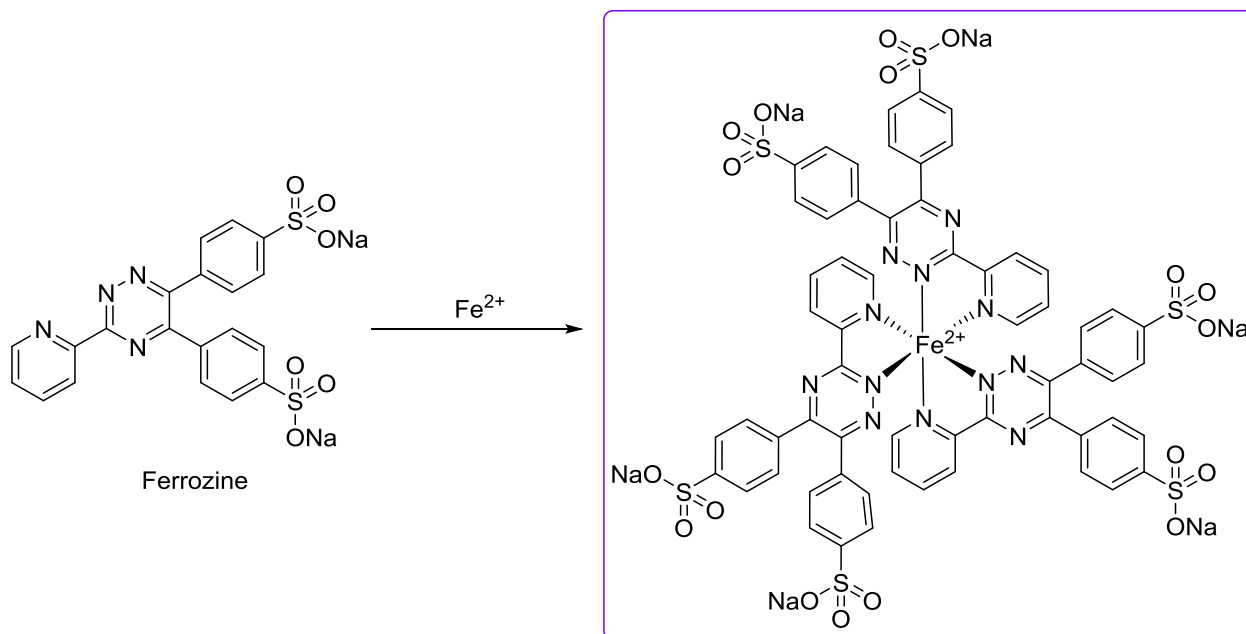
iron binding. However, alginate now shows good ferrous iron chelation which decreased in the presence of calcium ($p = 0.004$) due to competitive binding and affinity to form egg box structures, however ferric binding of alginate was poor. This correlates with reported pH dependency of calcium binding to alginate as the carboxyl groups of alginate are required to be deprotonated for effective cation binding, therefore calcium binding is improved at higher pH.¹⁶² Effective steady state binding of calcium by alginate was shown to be achieved above pH 6, which is consistent with a reported pKa for alginate of 3.4 – 4.4.⁸⁰ Furthermore, the iron binding of *Exalg1.00* not only seemed to be low but worse than that of alginate. This could be an artefact of incomplete combustion or may be due to the formation of metal oxides¹⁶³ which reduces the sensitivity during AAS measurements giving an erroneous value that is lower than in reality.



Graph 6 Iron binding of polymers after dialysis without acid in supernatant for two hours determined by AAS. Experiments were performed in triplicate, data is presented as mean \pm SEM, * and # denote statistically significant difference calculated by Student's *t*-test ($p < 0.05$).

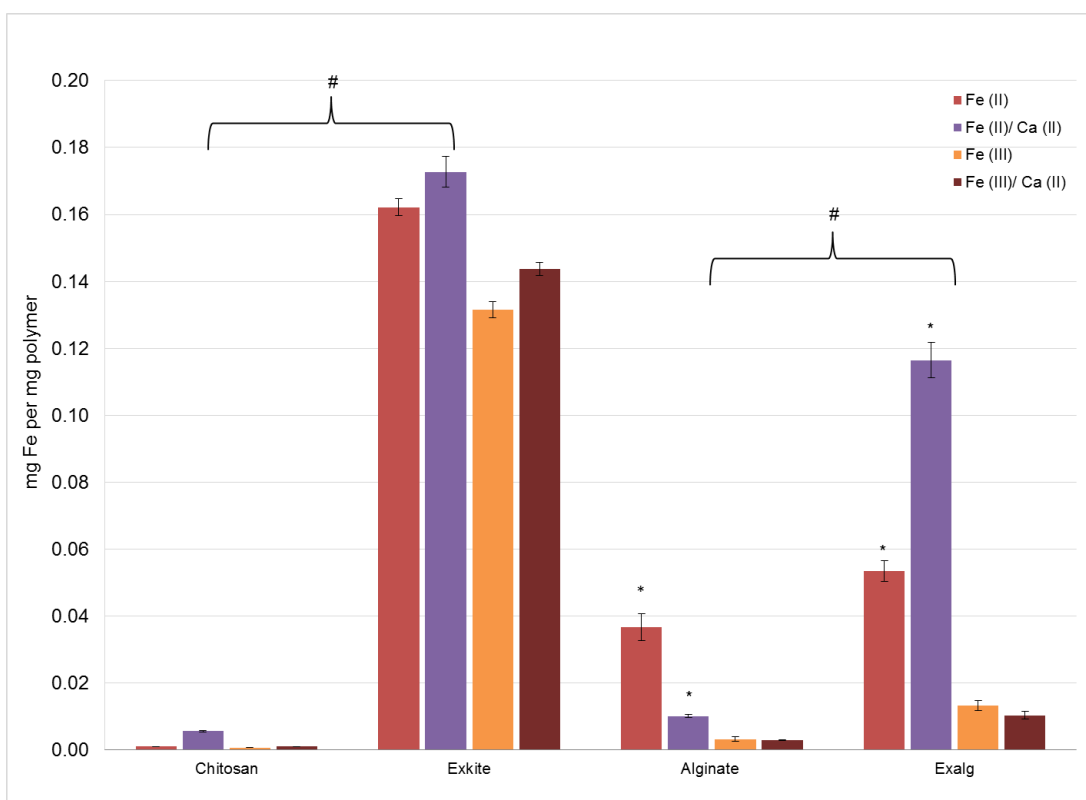
An alternate method of measuring iron concentration was sought: the ferrozine assay is a colorimetric assay¹⁶⁴ in which the ferrozine molecule turns from colourless to purple upon binding

of iron so that the intensity of colour produced is directly proportional to the amount of iron in solution (Scheme 25).¹⁶⁵ This works well for ferrous iron but can also be applied for the detection of ferric iron if a reducing agent such as sodium ascorbate is used.¹⁶⁶



Scheme 25 The ferrozine molecule which forms a purple coloured stable tris-iron complex utilised for the colorimetric determination of iron.

Dialysis of polymers in iron solutions was conducted for two hours and subsequent iron concentration was measured by the ferrozine assay. As the ferrozine molecule is an iron chelator in itself with a ferrous iron binding constant¹⁶⁷ of $3.65 \times 10^{15} \text{ M}^{-3}$, competitive binding is envisaged with the modified polymers in this assay. Therefore, hydrochloric acid and sodium ascorbate were added to samples to perturb iron binding with the ligand moiety and to retain iron in the reduced ferrous form to allow detection by ferrozine. The calibration samples were also prepared in the same way in order account for any effects from the addition of hydrochloric acid to the assay. The results of the ferrozine assay (Graph 7) show similar results as previously for chitosan and *Exkite* in that there is a marked increase in ferrous and ferric iron binding of *Exkite* relative to chitosan ($p < 0.001$). Alginate also shows similar iron content to that observed by AAS, however *Exalg1.00* now displays improved iron binding relative to alginate that is statistically significant ($p < 0.03$).

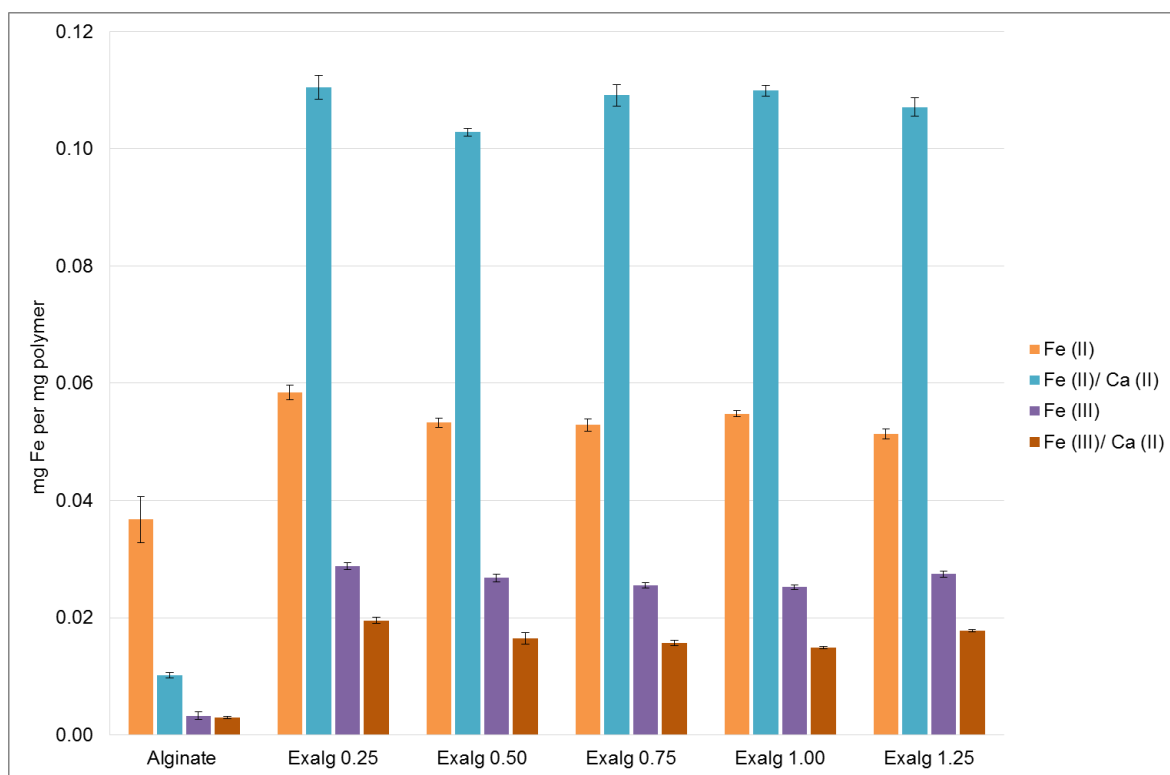


Graph 7 Iron binding of polymers after dialysis without acid in supernatant for two hours determined by ferrozine assay. Experiments were performed in triplicate, data is presented as mean \pm SEM, * and # denote statistically significant difference calculated by Student's *t*-test ($p < 0.05$).

The deferasirox ligand binds calcium poorly, with an approximate Ca (II) binding constant⁵⁸ of the order 10^5 . However, calcium is known to encourage gelling in alginate polymers which has been exploited previously to entrap cells for cell transplantation in which cells are mixed with an alginate/calcium solution.¹⁶⁸ Therefore, whilst ferrous binding of alginate decreases in the presence of calcium due to competitive binding and the formation of egg-box structures, the increase in ferrous binding of *Exalg*_{1.00} in the presence of calcium may be due to gelling effects trapping iron in the polymer matrix rather than chelation of iron itself. Moreover, the ferric binding of alginate and *Exalg*_{1.00} is low which may be attributed to tertiary structure polymer effects as alginate is known to dimerise¹⁶⁹ in the presence of cations contributing to the formation of egg-box structures. The cavities formed upon dimerization are ideally occupied by Ca (II) ions with an effective ionic radii of 100 pm.¹⁷⁰ The Fe (II) ions are sufficiently similar in size at 78 pm to occupy the cavities of alginate, hence good ferrous iron binding is observed for alginate and *Exalg*. However, Fe (III)

has an effective ionic radii of 64 pm¹⁷⁰ which may be too small to occupy the dimeric cavities, hence poor ferric iron binding is observed for alginate and *Exalg*. In addition, the poor ferric iron binding may be attributed to the formation of iron oxides during the process of dialysis in the absence of acid in solution, which precipitated¹⁶⁰ out and therefore become unavailable for iron binding.

Due to the poor iron binding of *Exalg*_{1.00} compared to *Exkite*, a series of *Exalg* polymers were synthesised by varying the ligand equivalence in the synthesis (Scheme 23) to determine whether the iron binding properties could be improved by altering the amount of ligand on the polymer. Iron binding studies of these polymers by dialysis and measurement of iron concentration by the ferrozine assay shows that iron binding is consistently similar throughout polymers *Exalg*_{0.25} - *Exalg*_{1.25} (Graph 8).



Graph 8 Iron binding by dialysis for two hours determined by ferrozine assay of *Exalg*_{0.25}- *Exalg*_{1.25}. Experiments were performed in triplicate, data is presented as mean \pm SEM, * and # denote statistically significant difference calculated by Student's *t*-test ($p < 0.05$).

Although iron binding of *Exalg* has improved moderately compared to alginate ($p < 0.03$), there is no variation in iron binding with increasing equivalence of ligand which correlates with the consistent ligand loading observed for these polymers, and supports the hypothesis that there is a limiting factor to the incorporation of ligand. Overall, the iron binding of the *Exalg* series is still low compared to *Exkite*, which is a result of low and consistent modification of the alginate polymer throughout the *Exalg* series so that there is only a small amount of attached ligands available for chelation. In addition, a modified version of deferasirox ligand was utilised for coupling onto alginate which may have affected its intrinsic iron binding properties compared to deferasirox alone which was used for coupling to chitosan.

5.4 Summary

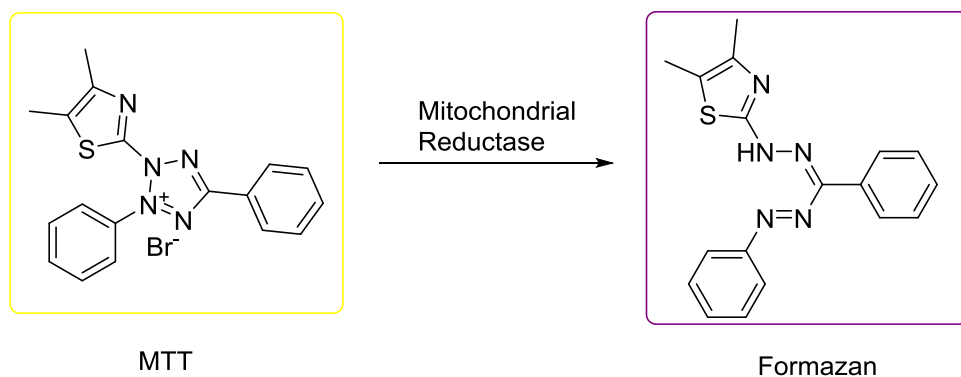
Assessment of iron binding by UV-vis spectroscopy titrations showed a shift in absorbance for *Exkite* indicative of the formation of an iron complex. Although a shift in absorbance was also observed for *Exalg1.00*, this was not consistent with increasing iron concentration due gelling effects of alginate. Dialysis experiments showed *Exkite* to be superior at iron binding with an improvement of over 100 fold for both ferrous and ferric iron with and without calcium by AAS and ferrozine assay. However, *Exalg* showed comparatively poor iron binding which is similar throughout *Exalg0.25* – *Exalg1.25* polymers with only a tenfold increase in ferrous binding in the presence of calcium which is more likely due to entrapment of iron through gelling rather than iron chelation.

6 Cellular studies

6.1 Background

Iron binding studies by UV-vis spectroscopy and dialysis exhibited *Exkite*, whether present as conjugated polymer or salt, to be superior at iron chelation compared to *Exalg* and native polymers chitosan and alginate (Chapter 5). This was further probed by investigating *in vitro* iron binding properties of all polymers to assess intracellular iron binding activity. Cellular studies were conducted on RKO cells which is a poorly differentiated human colon carcinoma cell line.¹⁷¹

In order to determine the appropriate concentration of compounds to use in the iron assessments, a MTT (3-(4,5-dimethylthiazol-2-yl)-2,5-diphenyl tetrazolium bromide) assay was initially performed to assess cellular viability. This is a colorimetric assay in which MTT, a yellow tetrazole is reduced to purple formazan crystals in metabolically active cells by the action of mitochondrial reductase (Scheme 26).¹⁷² Upon application of different concentrations of a compound to cells followed by a MTT assay, a dose response curve can be constructed as the intensity of the purple colour corresponds to proportion of living cells, expressed as cellular viability normalised relative to the control.



Scheme 26 The reduction of yellow MTT to purple formazan by living cells quantified by the MTT assay to assess cellular viability.

Once the appropriate concentration of polymers to use was established by the MTT assay, intracellular iron binding was probed by stimulating RKO cells with iron in the presence and

absence of polymers to determine iron uptake. Ferritin was used as an internal biomarker as this is the ubiquitous intracellular iron storage protein of 450 kDa consisting of 24 subunits composed of light and heavy chain units with an apparent molecular weight of 19 kDa and 21 kDa respectively.¹⁷³ Due to the toxic nature of free iron, ferritin serves to store excess iron in a non-toxic form with each complex capable of storing up 4500 ferric iron ions.¹⁷⁴ Serum ferritin concentrations correlate well with total body iron stores so are used clinically to assess iron stores for the diagnosis of iron deficiency or overload disorders.¹⁷⁵

Ferrous iron was used to stimulate cells as iron uptake by intestinal cells occurs through the action of divalent metal transporter 1 (DMT1) which transports ferrous iron into the enterocytes. Ferrous iron is also more soluble than ferric iron which can form iron oxides and precipitate out of solution. Moreover, sodium ascorbate functions both as a reducing agent to inhibit the oxidation of ferrous iron to ferric iron¹⁷⁶ and also acts as a weak chelator forming an iron-ascorbate complex which also increases solubility of iron to enhance cellular iron uptake.¹⁷⁷ Indeed, dietary ascorbate is known to increase iron absorption in the lumen and is often clinically co-administered with oral iron supplementation in individuals with iron deficiency diseases.¹⁷⁸

After a period of incubation of RKO cells at the desired experimental conditions, ferritin expression was measured by gel electrophoresis (western blot) in which proteins are separated according to their size and specific antibodies are applied to identify proteins, which can be semi-quantified by densitometry. Ferritin enzyme-linked immunosorbent assay (ELISA) was also used to quantify ferritin expression which is a colorimetric assay that uses ferritin specific antibodies to identify the protein. Finally, total intracellular iron was measured by the ferrozine assay which takes into account iron from ferritin, the labile iron pool and that being utilised in other functions of the cell.

6.2 MTT assay

Dose response curves shown in this chapter were plotted by Haobo Ge using Logistic Fit on Origin software.

Cellular viability of RKO cells in the presence of polymers was assessed by MTT assay. Due to the lack of differentiation in iron binding by dialysis observed for *Exalg*_{0.25} – *Exalg*_{1.25}, *Exalg*_{0.50} was arbitrarily chosen for further investigation by cellular studies and is henceforth referred to as *Exalg*. Cells were cultured with varying concentrations of chitosan, *Exkite*, alginate and *Exalg* for 24 hours, followed by the addition of MTT for the determination of cellular viability.

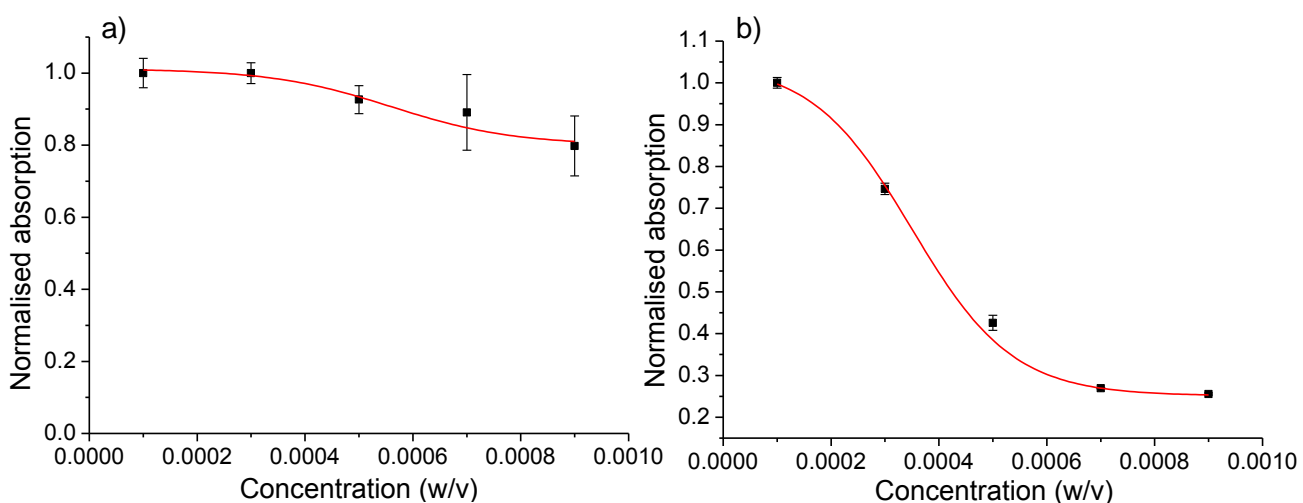


Figure 48 Dose response curve from MTT assay for a) chitosan and b) *Exkite* showing decreasing cellular viability of RKO cells with increasing *Exkite* concentration (% w/v is expressed as numerical decimal). Experiments were done in triplicate, data is presented as mean \pm SEM. Student's *t*-test to assess statistical significance for *Exkite* relative to control is $p < 0.002$, change in viability of cells treated with chitosan not statistically significant.

The cellular viability of cells treated with chitosan and *Exkite* was compared as fold change relative to control normalised to one, which had no compound treatment so was taken to have optimum cellular viability. The dose response curve (Figure 48) shows that chitosan has little effect on RKO cells as there is no statistical effect on viability. However, *Exkite* shows decreasing viability with increasing concentration, with viability only a fifth of that compared to control at 0.09% w/v *Exkite* ($p = 0.016$). The concentrations 0.03% w/v and 0.05% w/v *Exkite* were taken forward into subsequent experiments as the cellular viability of *Exkite* at these concentrations shows that the

application of *Exkite* is having some cytotoxic effects on cells which may be due to intracellular iron chelation, but there are enough cells viable in order to study this effect further.

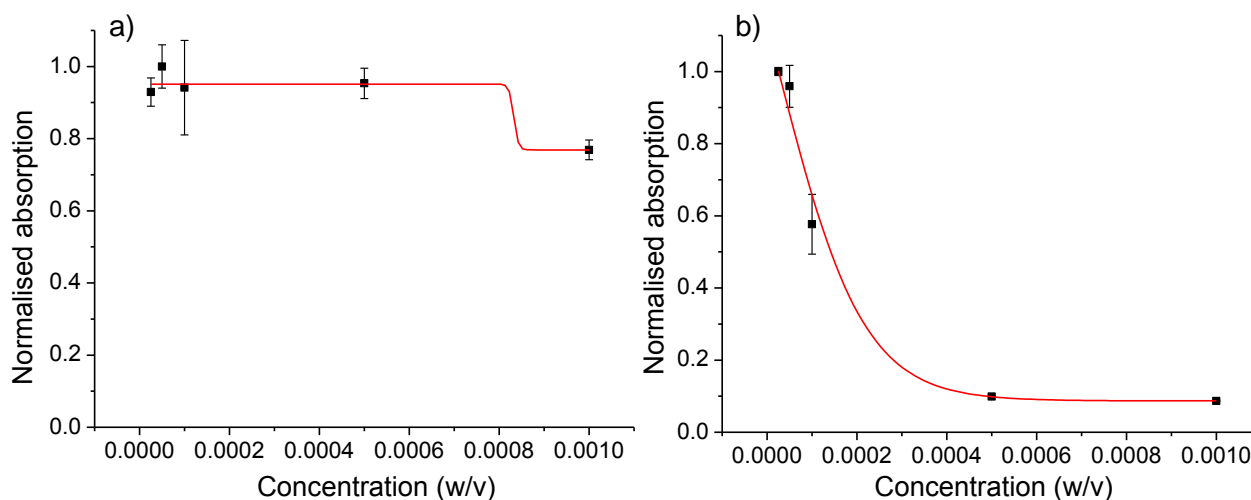


Figure 49 Dose response curve from MTT assay for a) alginate and b) *Exalg* showing decreasing cellular viability of RKO cells with increasing *Exalg* concentration (% w/v is expressed as numerical decimal). Experiments were done in triplicate, data is presented as mean \pm SEM. Student's *t*-test to assess statistical significance for *Exalg* relative to control is $p < 0.05$, change in viability of cells treated with alginate not statistically significant.

The dose response curve for alginate and *Exalg* (Figure 49) shows that cellular viability is not statistically altered when cells were challenged with alginate. Conversely, viability is greatly reduced with increasing concentrations of *Exalg* on RKO cells, with viability reaching a tenth of that observed for control at 0.10% w/v *Exalg* ($p = 0.001$). Due to the significant drop in viability at higher concentrations, the concentrations of *Exalg* chosen for subsequent experiments were 0.005% and 0.01% w/v. Although different experimental concentrations were chosen for alginate based and chitosan based polymers, this was determined by the toxicity of these polymers on RKO cells and the effective amount of viable cells that will be available for further experiments probing iron chelation. As *Exalg* seems to be more toxic towards RKO cells than *Exkite*, lower experimental concentrations of *Exalg* were chosen for subsequent experiments than *Exkite* as deemed fit by the MTT assay. The consequent purpose is to study intracellular iron chelation by these polymers which may contribute towards their toxic effects, whilst having enough viable cells for further assays.

6.3 Ferritin western blot

To ascertain whether the polymers are able to chelate iron *in vitro*, RKO cells were cultured in the presence and absence of aqueous iron sulphate (100 μM), sodium ascorbate (10 μM) and the appropriate concentration of polymer solution. Chitosan and *Exkite* were applied at 0.03% and 0.05% w/v, whilst alginate and *Exalg* were applied at 0.005% and 0.01% w/v in cell culture media. Positive control was conducted in aqueous iron sulphate with sodium ascorbate in cell culture media, and negative control was treated with cell culture media alone.

After incubation for 24 hours, the cell samples were lysed and analysed by western blot. This separates cellular proteins according to size, and the protein of interest is probed by antibodies. The blot produces an image of the proteins in which darker bands represent higher concentration of protein which can be analysed semi-quantitatively by densitometry.

The western blot (Figure 50a) shows bands for ferritin at ~ 20 kDa and β -actin which is a highly conserved protein involved in cell structure and integrity with a molecular weight of 42 kDa. This is used in western blotting as an internal control to ensure equal amounts of protein overall is loaded onto the gel for electrophoresis.¹⁷⁹ Since β -actin bands for all samples are equivalent, any differences in the concentration of ferritin observed is due to differences in cellular ferritin expression as a result of experimental conditions.

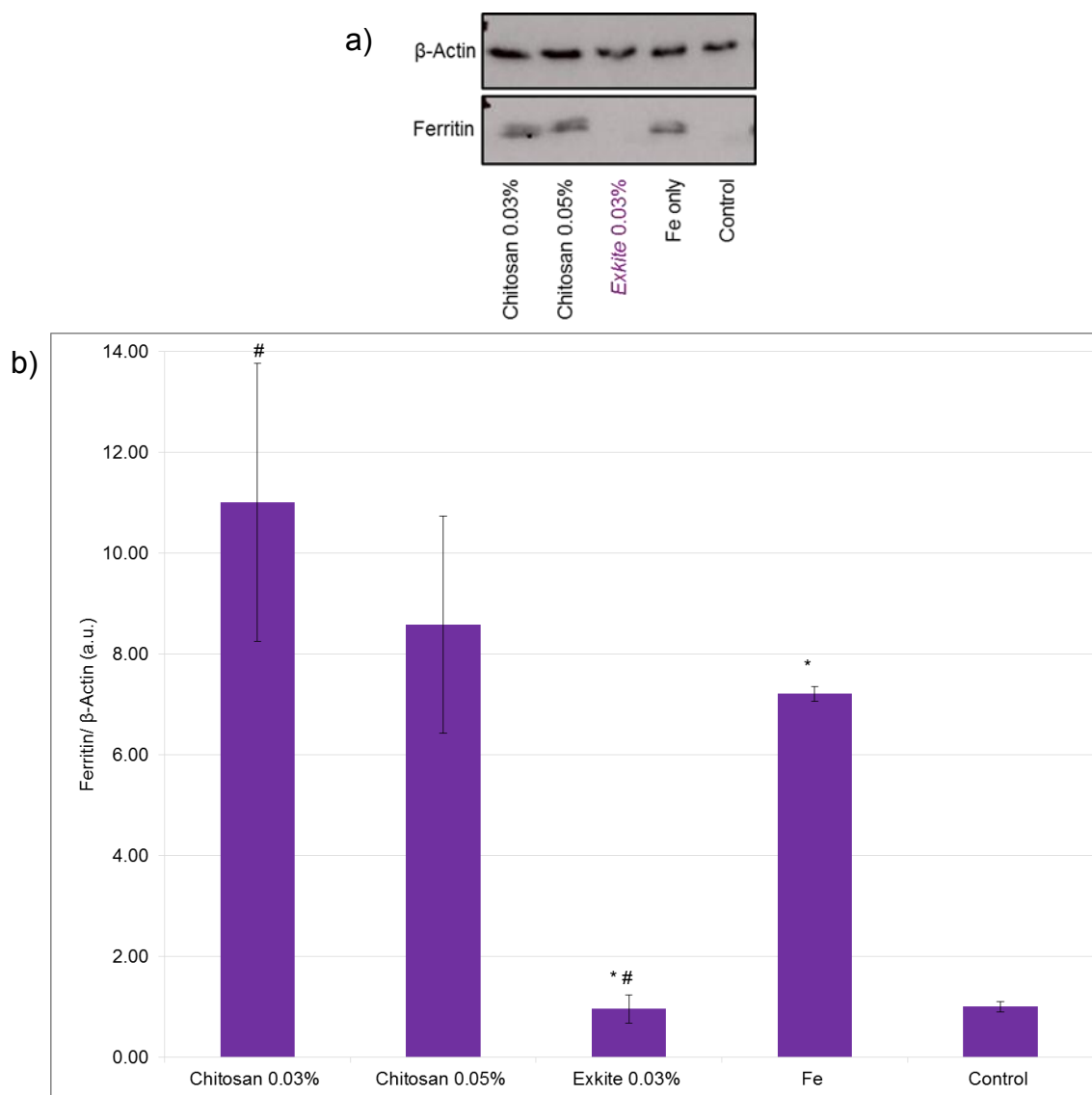


Figure 50 a) Ferritin western blot for cells cultured with iron in the presence of chitosan and *Exkite*, b) densitometric analysis of ferritin western blot as a ratio of ferritin to β -actin, expressed relative to control normalised to one. Experiments were done three times in triplicate for each concentration, data is presented as mean \pm SEM, * and # represent statistical significance by Student's *t*-test ($p < 0.05$).

Stimulation of cells with iron elicits a seven fold increase in ferritin expression relative to negative control which had no iron treatment (Figure 50b). There is no statistically significant difference in the iron mediated ferritin induction in cells treated with chitosan 0.03% and 0.05% w/v suggesting that chitosan is poor at iron chelation as iron is available for intracellular uptake. However, ferritin protein expression is statistically repressed in cells co-cultured with iron and *Exkite* 0.03% w/v by an eighth or more compared to equivalent concentration of chitosan ($p = 0.04$) and iron only positive control ($p = 0.009$). Chelation of iron by *Exkite* is preventing iron uptake by cells,

inhibiting ferritin expression. Cell lysates treated with *Exkite* 0.05% w/v did not contain enough protein for western blot analysis due to poor cellular viability.

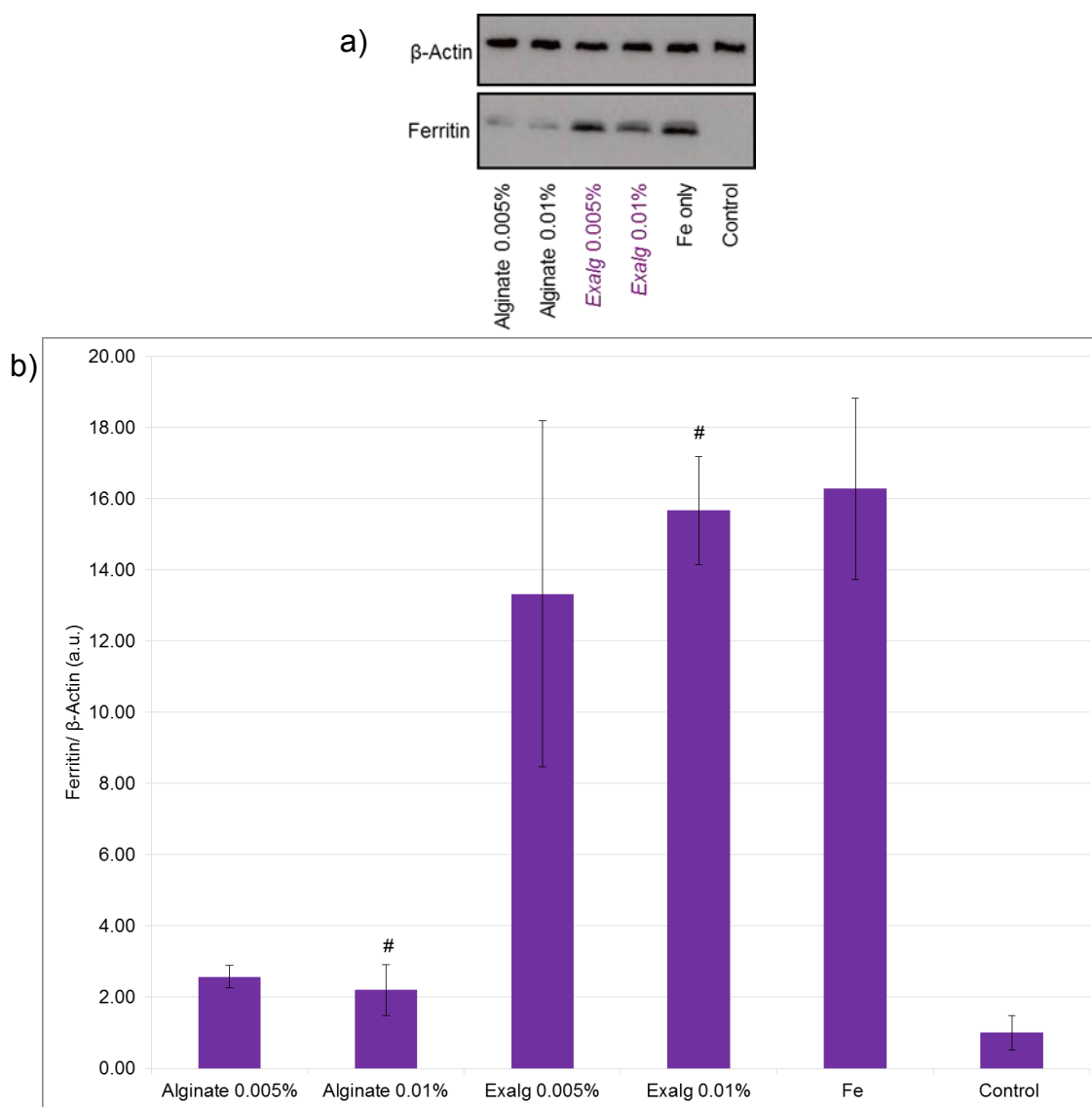


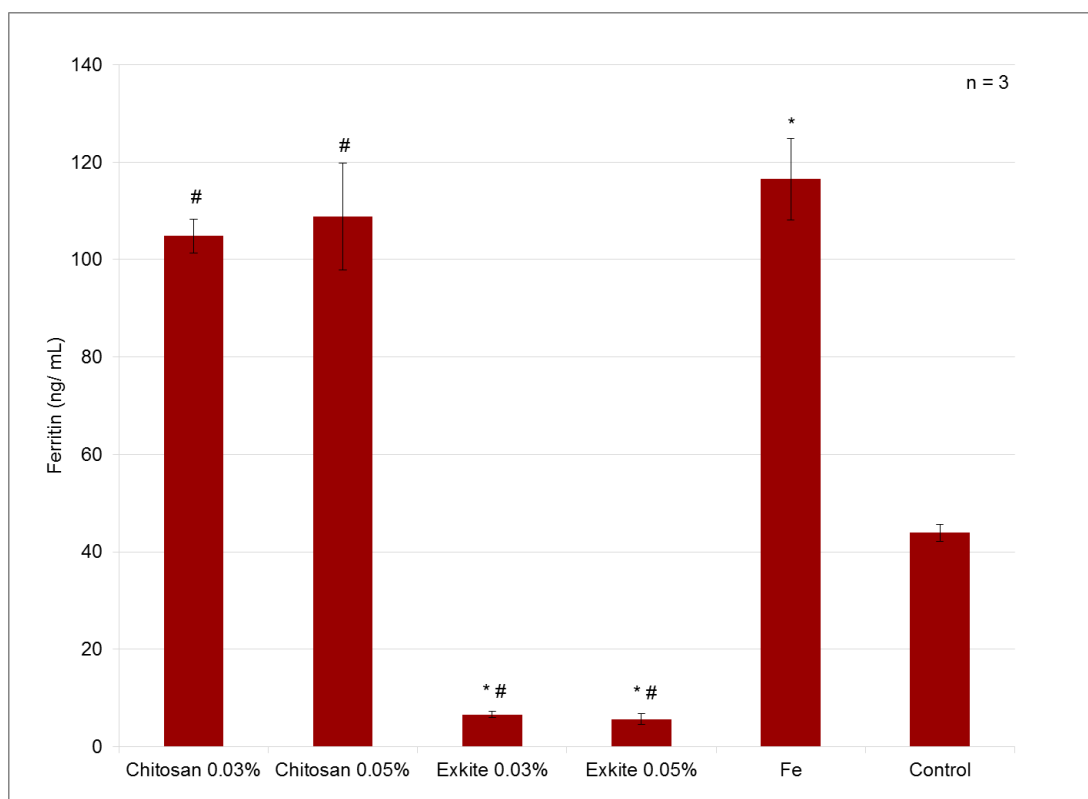
Figure 51 a) Ferritin western blot for cells cultured with iron in the presence of alginate and *Exalg*, b) densitometric analysis of ferritin western blot as a ratio of ferritin to β -actin, expressed relative to control normalised to one. Experiments were done three times in triplicate for each concentration, data is presented as mean \pm SEM, # represent statistical significance by Student's *t*-test ($p < 0.05$).

Co-stimulation of RKO cells with iron and *Exalg* does not elicit a significant difference to iron mediated ferritin expression as this is similar to that observed for iron only positive control, suggesting that *Exalg* is poor at iron binding (Figure 51a). Cells challenged with iron and alginate show a suppression in ferritin protein expression compared to iron only positive control and cells treated with equivalent concentration of *Exalg*. In particular, the difference is statistically

significant for cells treated with alginate 0.01% compared to *Exalg* 0.01% w/v ($p = 0.005$) (Figure 51b). Alginate displays inherent *in vitro* iron binding potential that is superior to that of *Exalg* despite modification of this polymer with an iron chelator. The superior iron chelation by alginate may be attributed to its greater solubility in aqueous media enabling it to chelate iron better out of solution. In addition, there is emerging interest in the use of alginate in colorectal cancer therapy¹⁸⁰ which may be effective due to its intracellular iron chelation properties.

6.4 Ferritin ELISA

Ferritin ELISA was used to support results of western blot by the colorimetric detection of ferritin in cell lysates by antibodies for quantitative analysis. Lysates prepared in an analogous manner to that described for western blots were also analysed by ferritin ELISA.

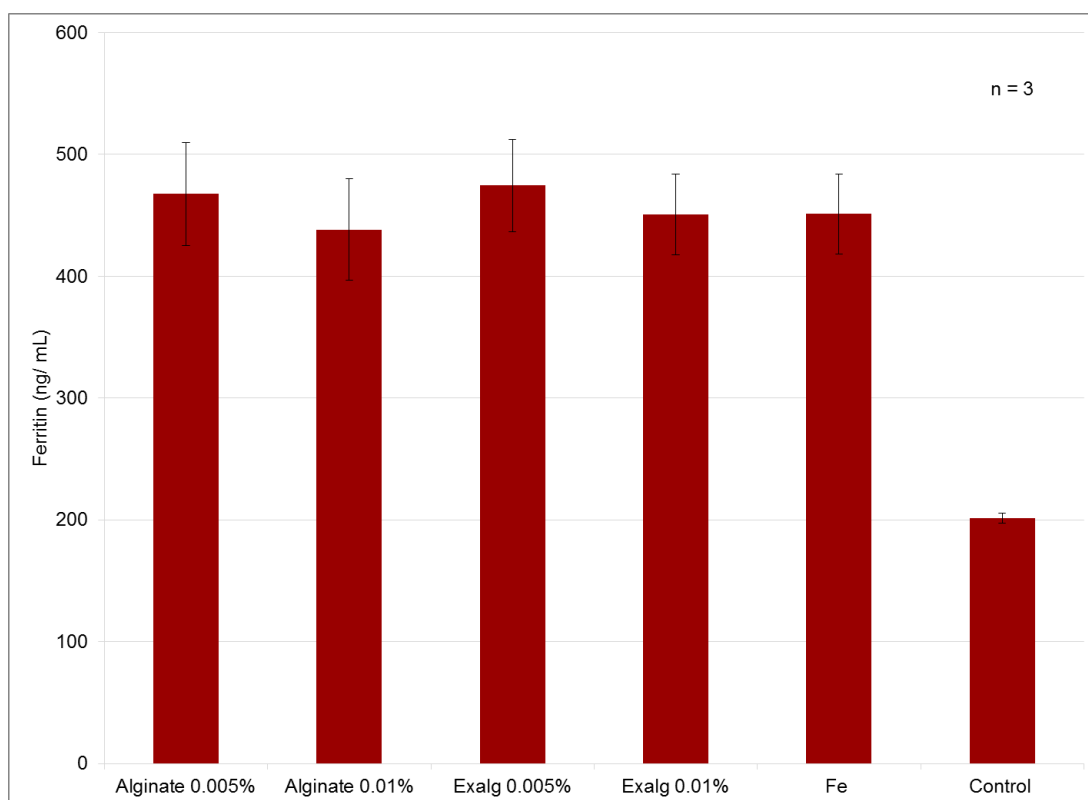


Graph 9 Ferritin ELISA of cells stimulated with iron in the presence of chitosan and *Exkite*. Experiments were done three times in triplicate for each concentration, data is presented as mean \pm SEM, * and # represent statistical significance by Student's *t*-test ($p < 0.05$).

The ferritin ELISA for cells challenged with iron (Graph 9) displays increased ferritin expression compared to negative control. The ferritin expression of RKO cells treated with iron and chitosan is unaltered compared to iron only positive control. The iron mediated ferritin expression is greatly suppressed when cells were stimulated with iron and *Exkite*, which is a statistically significant reduction for cells treated with *Exkite* 0.03% and 0.05% w/v compared to treatment with chitosan at equivalent concentrations ($p < 0.0002$), and also with respect to iron only control ($p < 0.0001$).

Furthermore, due to the heightened sensitivity of this assay, it can be observed that ferritin concentration of cell lysates treated with *Exkite* 0.03% and 0.05% w/v is 6.59 and 5.64 ng/mL respectively which is lower than that of negative control at 43.95 ng/mL which had no iron treatment. This suggests that not only is the iron chelation of the polymer preventing iron from entering cells, it is also chelating existing iron that is already within cells perhaps by entering cells or by being immobilised on the surface of cells. Modulation of intracellular iron in MCF-7 and MDA-MB-231 breast cancer cells by DFO were indeed shown to disrupt a range of cell signalling pathways, activate apoptosis (programmed cell death), and enhance the sensitivity of the breast cancer cells to chemotherapeutics doxorubicin and cisplatin.¹⁸¹ Therefore, the chelation of intracellular iron in RKO cells is especially beneficial as it offers multiple mechanisms in which to retard or impede cancer cell growth.

The ferritin ELISA of cells co-stimulated with iron in the presence of alginate and *Exalg* (Graph 10) shows no significant effect on the iron mediated ferritin expression which is consistent with iron only control. This is indicative of poor iron chelation by these polymers as iron is freely available for uptake.



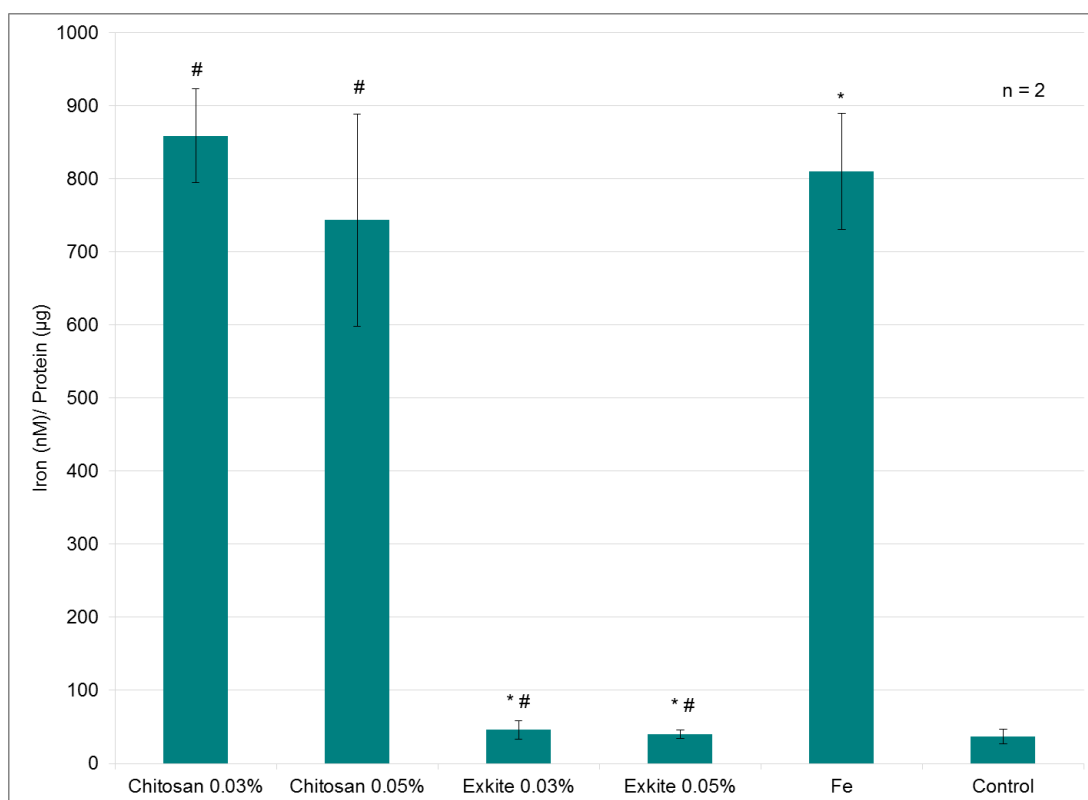
Graph 10 Ferritin expression by ELISA for RKO cells co-cultured with iron in the presence of alginate and *Exalg*. Experiments were done three times in triplicate for each concentration, data is presented as mean \pm SEM, * and # represent statistical significance by Student's *t*-test ($p < 0.05$).

However, it is of note that the western blot showed that ferritin expression was suppressed when cells were treated with iron and alginate. Although immunoassays are designed to be specific for the protein of interest by using protein specific antibodies, variation has been observed in practice due to interference which may result in a false-positive or false-negative result. This may arise from cross-reactivity of the detecting antibody with other proteins or endogenous substances in the sample with chemical differences but structural similarities, effects of buffer in the matrix and sample storage.¹⁸² In addition, proteins such as ferritin which are known to be present at a wide range of concentrations in cells are more susceptible to erroneous results in a one-step immunoassays such as the ELISA in which antigen, antibody and marker incubate simultaneously.¹⁸³ This may be the cause of the differences observed between ferritin Western blot and ELISA as different antibodies were also used in the methods.

6.5 Intracellular iron by ferrozine assay

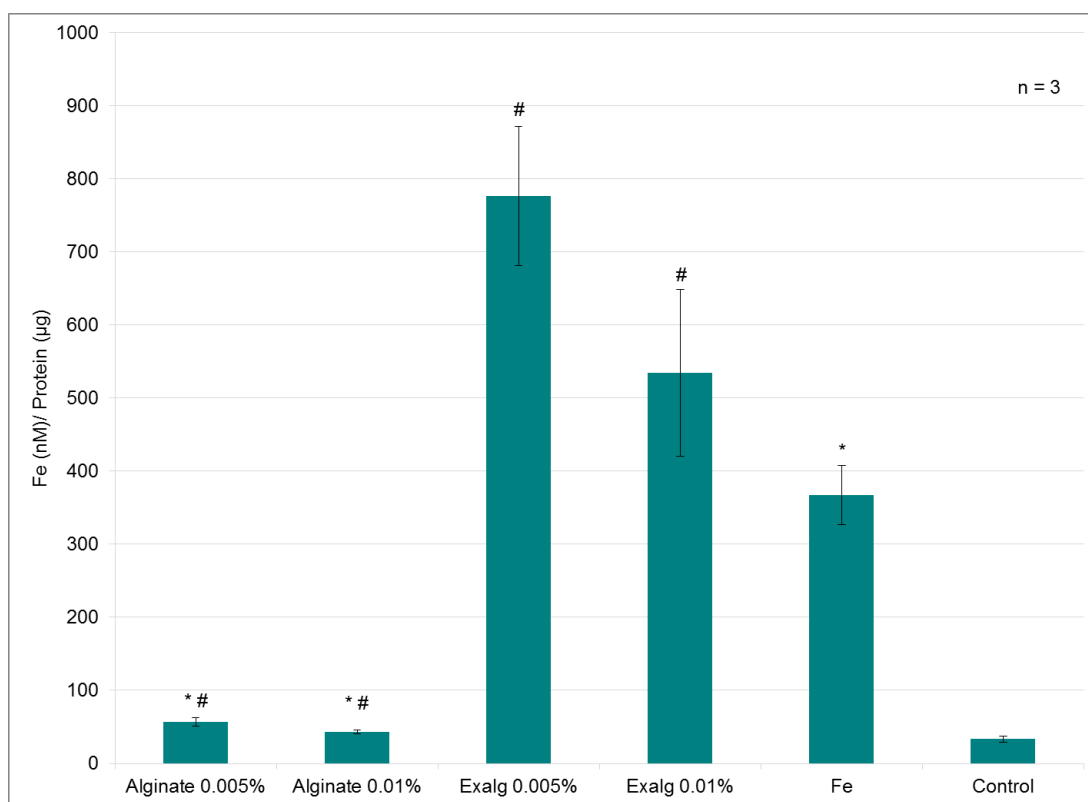
Total intracellular iron was also measured by ferrozine assay following a period of cell culture at the chosen experimental conditions. Prior to stimulation in iron and polymer solutions, cells were serum starved by incubation in foetal calf serum (FCS) free media for one hour, which contains essential growth factors and nutrients required for cellular viability and proliferation.¹⁸⁴ This was followed by stimulation for one hour at enhanced conditions using aqueous iron sulphate (100 μ M), sodium ascorbate (500 μ M) and predetermined concentrations of polymer solutions: chitosan and *Exkite* at 0.03% and 0.05% w/v, alginate and *Exalg* at 0.005% and 0.01% w/v. The serum starvation followed by stimulation is to maximise iron loading of the cells for heightened iron detection. Positive control was conducted in aqueous iron sulphate solution with sodium ascorbate in cell culture media, and negative control was treated with cell culture media alone. The cells were subsequently washed thoroughly with PBS, lysed and analysed by the ferrozine assay to measure total intracellular composition of elemental iron. This is a colorimetric assay in which the construction of calibration curves allows quantification of iron concentration expressed relative to protein concentration of cell lysates.¹⁸⁵

Following a period of cell culture, total intracellular iron has increased from 37 nM/ μ g protein in the negative control to 810 nM/ μ g protein in the positive iron only control (Graph 11) in accordance with greater iron uptake in an iron rich environment. Intracellular iron levels are not statistically different to cells co-stimulated with iron and chitosan 0.03% and 0.05% w/v. However total intracellular iron composition has statistically reduced upon co-stimulation with iron and *Exkite* 0.03% and 0.05% w/v compared to co-stimulation with iron and chitosan ($p < 0.004$), and also with respect to iron only control ($p < 0.0001$). This is in agreement with results obtained for ferritin expression by western blot and ELISA indicative of intracellular iron binding by *Exkite*.



Graph 11 Ferrozine assay of RKO cells treated with iron in the presence *Exkite* and chitosan. Experiments were done twice in triplicate for each concentration, data is presented as mean \pm SEM, * and # represent statistical significance by Student's *t*-test ($p < 0.05$).

Cells challenged with iron and *Exalg* do not exhibit a statistically significant difference in intracellular iron accumulation compared to iron only control (Graph 12). Conversely, cells challenged with iron and alginate show a marked decrease in intracellular iron from 367 nM/ μ g protein in iron only positive control to 56 nM/ μ g protein in cells treated with iron and alginate 0.005% w/v, and 43 ng/ μ g protein in cells treated with iron and alginate 0.01% w/v. This is a statistically significant reduction compared to *Exalg* at similar concentrations of treatment and iron only control ($p < 0.0001$). This is in accordance with results from western blot ferritin analysis suggesting that alginate itself is superior at *in vitro* iron binding relative to *Exalg*.



Graph 12 Ferrozine assay for RKO cells treated with iron, alginate and *Exalg*. Experiments were done three times in triplicate for each concentration, data is presented as mean \pm SEM, * and # represent statistical significance by Student's *t*-test ($p < 0.05$).

6.6 Probing intracellular *Exkite* activity

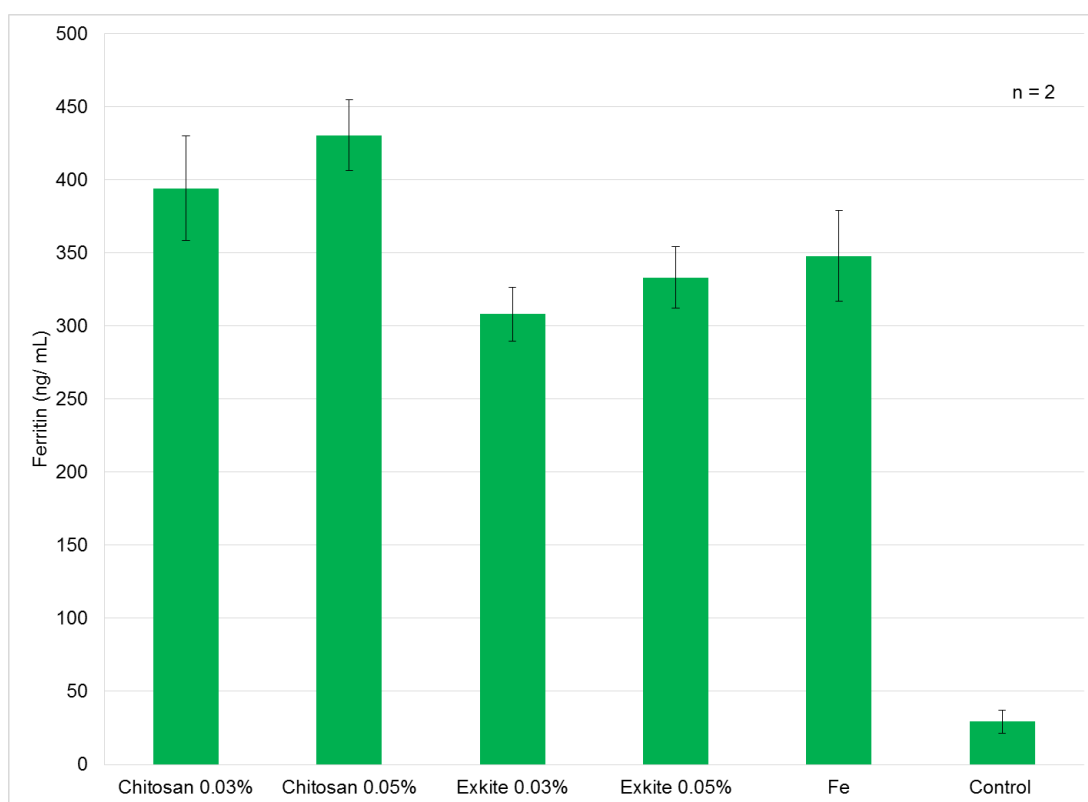
The iron assessments show that *Exkite* is able to chelate iron in an intracellular setting, preventing the uptake of iron to give reduced ferritin levels and overall iron status compared to cells treated with chitosan or iron only positive control. The ferritin ELISA in particular showed that *Exkite* was able to decrease iron induced ferritin expression to such an extent that it was lower than that of negative control with no iron treatment, suggesting scavenging of the existing iron within cells. This is possible if the chelator is able to enter cells, if *Exkite* is present in the salt form as indicated by diffusion NMR studies on a subsequent batch. Chitosan is known to enhance absorption of polar molecules and peptide drugs across mucosal epithelia when protonated. The proposed mechanism of action suggest that chitosan is able to do this by bioadhesion and transient widening of tight junctions in the membrane.¹⁸⁶ Additionally, highly quaternised *N*-trimethyl chitosan was shown to greatly enhance absorption of mannitol across intestinal epithelial Caco-2 cells.¹⁸⁷ Hence, the

superior iron chelation observed for cells treated with *Exkite* may arise from the salt form of *Exkite*, in which the protonated chitosan enhances the absorption of the anionic iron chelator across the RKO cell membrane.

Therefore, investigations were conducted into the extent of ligand immobilisation within cells. Cell lysates were prepared for assessment by ferritin ELISA by sequential addition of aqueous iron solution and then polymer solution to cells. Firstly, aqueous iron sulphate (100 μM) with sodium ascorbate (10 μM) was added to RKO cells and incubated for 24 hours to allow prolonged iron uptake and ferritin expression. Subsequently, the iron solutions were removed, cells were washed with PBS and incubated with chitosan and *Exkite* 0.03% and 0.05% w/v solutions for 24 hours. The sequential addition of iron solutions followed by polymer solutions to the cells allows assessment of the capability of polymers to scavenge iron from within cells after iron uptake as opposed to iron chelation in an iron rich cellular environment. Cell lysates were prepared as previously and analysed by ferritin ELISA.

The incubation of RKO cells with iron followed by chitosan and *Exkite* exhibit iron mediated ferritin expression that is comparable to that of iron only control at 348 ng/mL (Graph 13). In this instance, the addition of chitosan and *Exkite* after iron uptake does not dampen ferritin expression suggesting poor iron scavenging ability of these polymers once iron is bound in the ferritin complex. This is not entirely surprising as iron is known to be bound strongly by ferritin so removal of ferritin bound iron is a competitive process. However, siderophores have evolved to scavenge iron from cells of microorganisms and hence catechols, which are the predominant iron binding sub-unit of many siderophores, have been shown to release iron from ferritin by direct chelation.¹⁸⁸ In addition, naturally occurring dithiols DL-dihydrolipoate and DL-dihydrolipoamide have also been shown to remove ferritin bound iron when applied in excess,¹⁸⁹ which was found to be

dependent upon the pH and the reduction of ferric iron to the ferrous form.¹⁹⁰ Although the removal of ferritin bound iron was not observed in this case, it is possible by some small molecule chelators.



Graph 13 Sequential addition of iron followed by polymer solution to RKO cells. Experiments were done twice in triplicate for each concentration, data is presented as mean \pm SEM, * and # represent statistical significance by Student's *t*-test ($p < 0.05$).

6.7 Summary

The cellular viability of RKO cells when incubated with the polymers was assessed by MTT assay which showed that alginate and chitosan are not particularly toxic towards RKO cells, however *Exkite* and *Exalg* exhibit decreasing cellular viability with increasing concentration of incubation. The concentrations of polymers chosen for further iron assays were 0.03% and 0.05% w/v for chitosan and *Exkite*, 0.005% and 0.01% w/v for alginate and *Exalg*.

Stimulation of RKO cells with *Exalg* in the presence of iron does not affect ferritin expression or total intracellular iron concentration, which indicates that this is particularly poor at iron chelation *in vitro*. However, cells incubated with iron and alginate show suppression in ferritin expression

by western blot and reduction in total intracellular iron by ferrozine assay. Alginate is known to accommodate cations and is water soluble compared to the poor solubility of *Exalg* which may have contributed to the greater *in vitro* chelation activity observed. Previous dialysis experiments of *Exalg* showed that this polymer is capable of binding iron better than alginate, hence *in vitro* iron binding potential may be improved upon enhanced solubility of the polymer in conditions required for cellular analysis.

Treatment of RKO cells with iron and chitosan does not inhibit cellular iron uptake owing to the poor solubility and chelation properties of chitosan. Incubation of cells with iron and *Exkite* shows significant reduction in ferritin protein expression by ferritin western blot and ELISA, and total intracellular iron is also reduced by the ferrozine assay. This is in accordance with the superior iron chelation properties of *Exkite* observed in UV-vis spectroscopy and dialysis studies.

The reduction in ferritin expression when cells were stimulated with iron and *Exkite* was so great that it was comparable or lower than that of negative control with no iron treatment indicative of iron chelation within cells. This suggests that *Exkite* may be present in the salt form, consistent with NMR diffusion studies, in which protonated chitosan enhances the uptake of the iron chelator which inhibits intracellular iron uptake and ferritin expression. This was probed by stimulating cells sequentially by iron then *Exkite*, which showed good iron uptake and ferritin expression by cells but *Exkite* was unable to enter cells to scavenge iron out of the ferritin complex.

7 Mouse model studies

The mouse experiments described in this chapter were conducted by Sorina Radulescu and Victoria Stavrou. This involved gavage of mice, monitoring of health, euthanasia and dissection. All mice experiments were conducted in accordance with Home Office project license 70/8198 under protocol 19b5 and 40/3613 under protocol 19b3. The preparation of microscope slides and H&E staining were provided by The Department of Cellular Pathology, Queen Elizabeth Hospital. Immunohistochemistry and scoring of slides were done by myself with assistance from Victoria Stavrou.

7.1 Background

The iron binding data by dialysis showed that *Exkite* material obtained as described was superior for the chelation of iron over *Exalg* (Chapter 5). Cellular studies using RKO colorectal cancer cells also showed that *Exkite* was able to chelate iron in an intracellular setting when cells were stimulated with iron in the presence of *Exkite*, inhibiting cellular iron uptake to reduce ferritin expression and total intracellular iron (Chapter 6). Although it is not conclusive whether the ligand is covalently attached to chitosan or whether *Exkite* exists in the salt form as a supramolecular aggregate, the overwhelming positive evidence towards the superior iron chelation properties of the *Exkite* material warranted further investigation. Furthermore, due to the prevalence of supramolecular drug carriers and the intestinal absorption enhancing properties of protonated chitosan,¹⁹¹ *Exkite* salt is potentially a better therapeutic compared to the conjugated counterpart. Therefore, regardless of whether the ligand is covalently or non-covalently attached to chitosan, the positive results of *Exkite* were followed into mouse model studies.

In vivo activity of *Exkite* was probed by using mouse models of colorectal cancer that have similar genetic mutations to that found commonly in human colorectal cancer (CRC). The aim of this is to probe *in vivo* safety and tolerability of *Exkite*, and whether *Exkite* can extend the survival of mice predisposed to developing intestinal tumours as well as analysis of histological changes to intestinal epithelium of mice given *Exkite*.

The tumour suppressor gene adenomatous polyposis coli (*Apc*) is essential for maintaining cellular homeostasis but is found to be mutated or inactive in 80% of CRC cases, which is regarded as a

key early event in the initiation of CRC.¹⁹² A germline heterozygous Apc mutation followed by a somatic mutation in the wild type Apc allele results in familial adenomatous polyposis (FAP) which gives rise to the development of numerous colonic polyps, which if left unchecked can go on to become cancerous. Sporadic CRC occurs with homozygous Apc mutations acquired during the lifetime of an individual.¹⁹³ Many mouse models have been developed with mice carrying heterozygous Apc mutation, however homozygous mutations in mice leads to embryonic lethality.¹⁹² Therefore, cre-lox recombination technology is used to perform insertions or deletions at specific points of DNA in a particular cell type, which can be triggered by an external stimulus.¹⁹⁴ This allows targeted DNA modification of particular cells in an organism and is achieved by the Cre recombinase enzyme which recombines a pair of target (lox) sequences in the DNA. The lox sequence can be appropriately placed to allow for specific gene activation or repression. When a lox sequence is placed either side of a target gene, this is called a floxed gene.¹⁹⁵ Therefore, homozygous inactivation of floxed genes can be induced in adult mice to mimic genetic aberrations of human diseases.¹⁹⁶ As such, Apc Hom (Cre⁺ Apc^{ff}) mice is a transgenic inducible model of sporadic CRC with homozygous Apc inactivation in the intestinal epithelium.¹⁹⁷ This results in multiple intestinal tumours as Apc is well conserved between humans and rodents, however Apc inactivation in mice leads to tumour formation predominantly in the small intestine as opposed to the large intestine in humans.¹⁹⁸

Similarly, phosphatase and tensin homolog (Pten) is also a tumour suppressor gene often found mutated in many sporadic cancers including CRC. Germline mutations in Pten gives rise to multiple hamartoma syndromes such as Cowden's disease with individuals having an increased risk of cancer, especially cancer of the gastrointestinal tract. Apc Hom Pten Hom (Cre⁺ Apc^{ff} Pten^{ff}) mice is also a transgenic inducible model with homozygous inactivation of Apc and Pten,

which gives rise to aggressive tumorigenesis of the small intestine due to the inactivation of both tumour suppressor genes.¹⁹⁹

The intestinal epithelium is ordered into crypts and villi in which cells produced in the crypts migrate up the villi until cell death or are shed into the gut lumen. Cell renewal is usually a tightly regulated process however, inactivation of tumour suppressor genes *Apc* and *Pten* results in uncontrolled mitosis (cell division) and reduced apoptosis (programmed cell death) of stem cells in intestinal crypts. This gives rise to enlarged crypts compared to wild type mice and the subsequent development of intestinal tumours (Figure 52).²⁰⁰

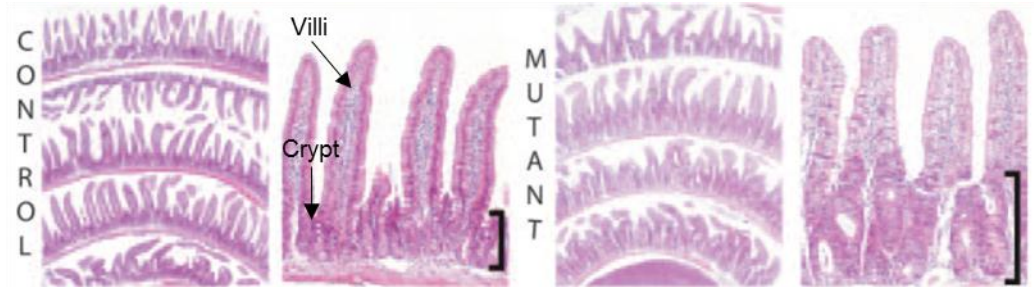


Figure 52 Hematoxylin and Eosin (H&E) stained intestinal sections of control mouse (*Vil-CreER^{T2} Apc^{fl/+}*) and mutant mouse containing homozygous *Apc* inactivation along crypt-villus axis (*Vil-CreER^{T2} Apc^{fl/fl}*) shows enlarged crypts compared to control mouse due to intense cellular proliferation from loss of *Apc*. (Copyright *The Company of Biologists* Publisher 2005).

Apc Hom and *Apc* Hom *Pten* Hom mice were gavaged (Licence 40/3613 under protocol 19b3) with *Exkite* to study survival. As *Exkite* was administered as a suspension in water, this was compared to mice that were given water alone as the vehicle. Mice were euthanized when they showed symptoms of being sick such as weight loss, pale feet and hunched posture. The small intestine was dissected, preserved in paraffin block, and was submitted to histological staining to assess for mitosis and apoptosis to give an indication of tumour proliferation or suppression upon treatment.

7.2 Exkite safety and tolerability in mice

Initial mice experiments were conducted with wild type mice to assess tolerability of *Exkite* and to find an appropriate dose to use for further *in vivo* experiments. Wild type mice were given daily 200 μ L gavages of *Exkite* for five days at varying concentrations: 0.01%, 0.10%, 0.25%, 0.50% and 1% w/v limited by the viscosity of the solution with 1% w/v being the highest concentration of *Exkite* that was able to be taken up by a gavage syringe. After five days, none of the mice showed any adverse symptoms such as weight loss or hunched posture so further mice experiments were conducted with 1% w/v *Exkite*.

Wild type mice were also used to assess *in vivo* metabolism of *Exkite*, in particular to assess the possibility of absorption of non-conjugated ligand from *Exkite* salt into the blood stream which may cause anaemia by chelation of systemic iron.

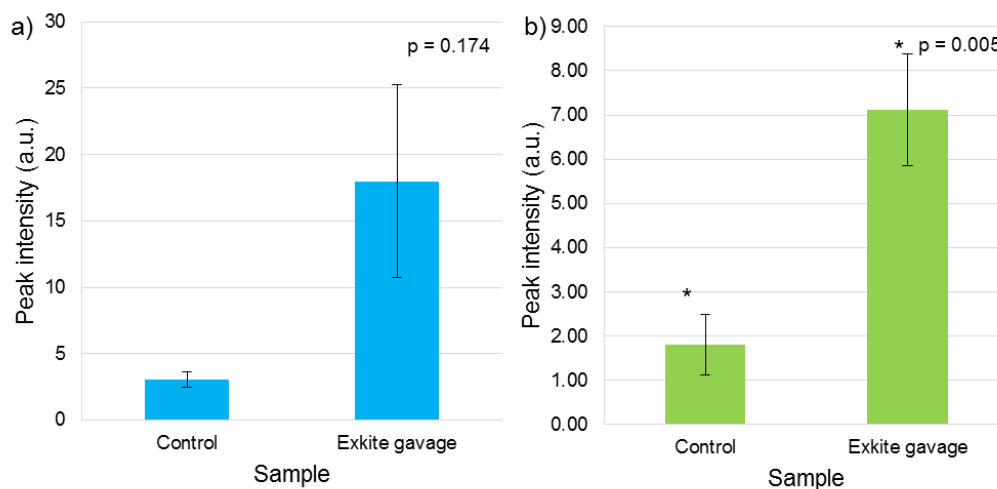


Figure 53 Analysis by MALDI spectrometry for presence of deferasirox at 374.11 Da, a) blood plasma of wild type mice gavaged *Exkite* or water control and b) intestinal crypts extracted from wild type mice gavaged *Exkite* or water control. Experiments were done with n = 3 mice, data is presented as mean \pm SEM, * represent statistical significance by Student's *t*-test (p < 0.05).

Wild type mice were administered 200 μ L of 1% w/v *Exkite* or water as control and were euthanized one hour after treatment. Blood plasma and intestinal crypts were collected and analysed by MALDI spectrometry for the presence of deferasirox or any of its known metabolites.⁵⁹ Analysis of blood plasma shows that there is an observable difference but this is not statistically

significant between mice gavaged with *Exkite* or water at 374.11 Da corresponding to the mass of deferasirox (Figure 53a, $p = 0.174$).

However, analysis of intestinal crypt cells shows a three-fold increase in intensity at 374.11 Da for mice given *Exkite* relative to control (Figure 53b, $p = 0.005$), and although this is noticeable it is not substantial. This may be from free ligand in *Exkite* salt or from ligand detachment, but the relatively small amount found suggest that this will not pose a serious risk to chelation of systemic iron. Other metabolites of deferasirox as proposed by Bruin *et al.* in rats were not observed. This includes glucuronidation at the carboxylate group and at phenolic hydroxy groups, as well as hydroxylations catalysed by cytochrome P450 (Figure 54).⁵⁹

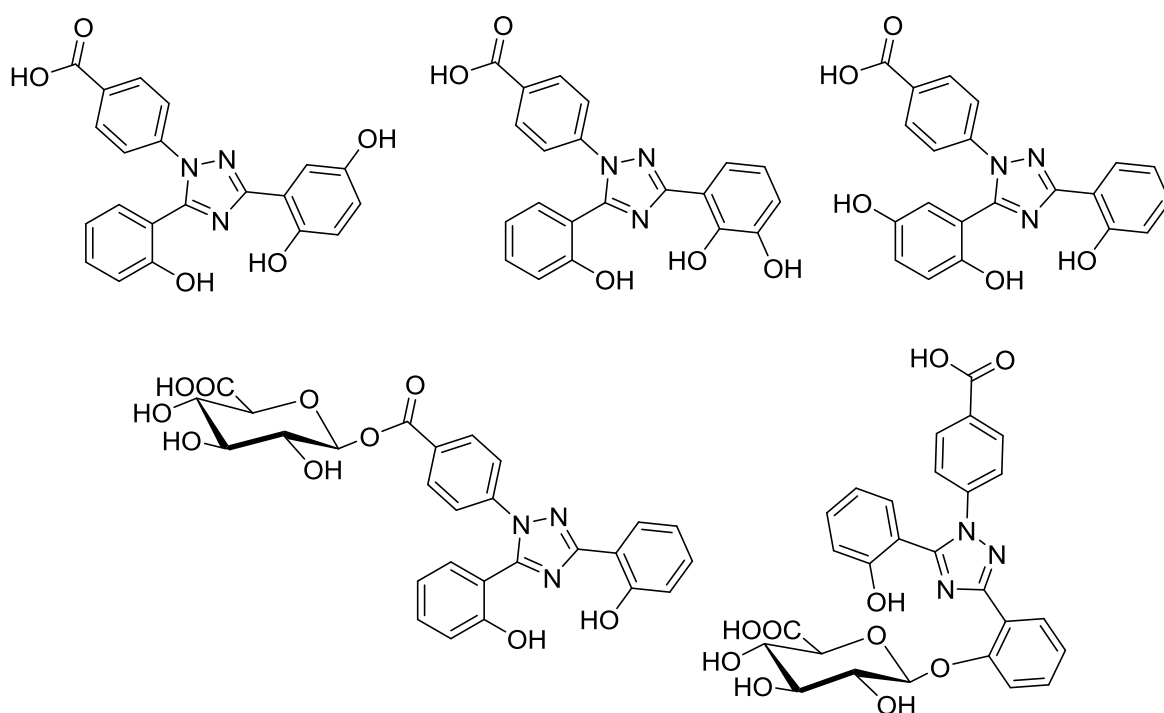


Figure 54 Major metabolites of deferasirox detected in plasma, urine, bile, and faeces of rats.

7.3 Mouse survival

Apc Hom and Apc Hom Pten Hom mice were utilised as models of sporadic CRC which were all placed on a control diet. After induction of tumorigenesis by tamoxifen injection at 6 weeks of age,

the mice were subject to a dose of 200 μ L of 1% w/v *Exkite* or 200 μ L of water as the vehicle control, administered by oral gavage on alternate days until they became sick.

Previous studies by Radulescu *et al.* using an *Apc* hom mouse model ($Lgr5creER^{T2+}Apc^{f/f}$) showed increased survival of mice that were fed an iron deficient diet compared to a control diet with median survival of 89 days and 61 days respectively ($p = 0.001$).²⁶ This was attributed to attenuated tumorigenesis with the iron deficient diet. Therefore, it would be expected that significant chelation of dietary iron by *Exkite* would increase survival of mice by a similar process.

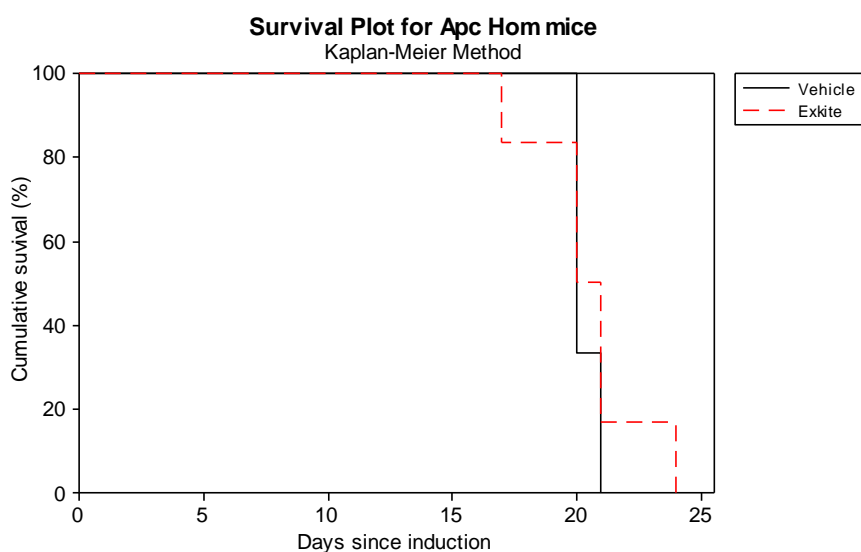


Figure 55 *Apc* Hom mice administered *Exkite* ($n = 6$) or vehicle ($n = 3$), survival plot shows no difference in survival for mice given *Exkite* or vehicle.

The survival plot (Figure 55) shows that there is no difference in the survival of *Apc* Hom mice that were given *Exkite* compared to the vehicle comprising equivalent volume of water, with a median survival of 20 days since induction for both mice subject to *Exkite* and vehicle control.

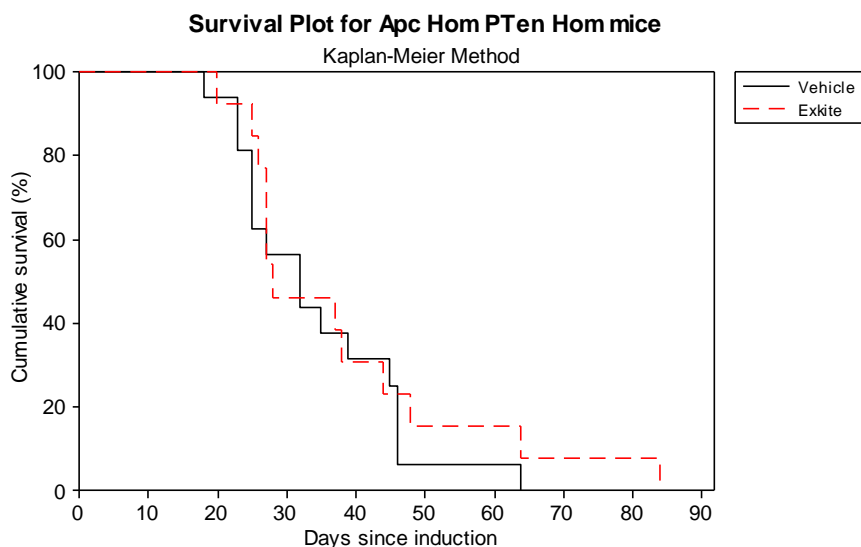


Figure 56 Apc Hom Pten Hom mice administered *Exkite* (n = 13) or vehicle (n = 16), Survival plot shows no difference in survival for mice given *Exkite* or vehicle.

There is no apparent change in the survival of Apc Hom Pten Hom mice that were given *Exkite* with a median of 28 days compared to the vehicle control mice with a median of 32 days (Figure 56, $p = 0.55$). This suggests that chelation of dietary iron by *Exkite* is not profound enough to prolong survival of mice in both models used.

7.4 Histology

At the end of the survival study, histological sections of the small intestine of the mice were taken. These slides were then stained by hematoxylin and eosin (H&E) which is a non-specific stain to show cellular morphology from which mitotic and apoptotic cells can be identified.²⁰¹

Slides were also stained by immunohistochemistry in which phosphohistone (PHT) was utilised as a marker for mitosis as histone is specifically phosphorylated in the mitotic cycle during chromatin condensation.²⁰² Caspase 3 is a serine protease that induces apoptosis, such that activation of this protease is an unambiguous indicator of this cell suicide mechanism.²⁰³ The use of specific antibodies for the detection of phosphohistone and caspase 3 results in positive staining of mitotic and apoptotic cells. The extent of mitosis or apoptosis was assessed by scoring 25 continuous crypts

by counting positively stained cells and the total number of cell in the crypt. This is expressed as an index which is the average percentage of cells in mitosis or apoptosis relative to the total number of cells per crypt.

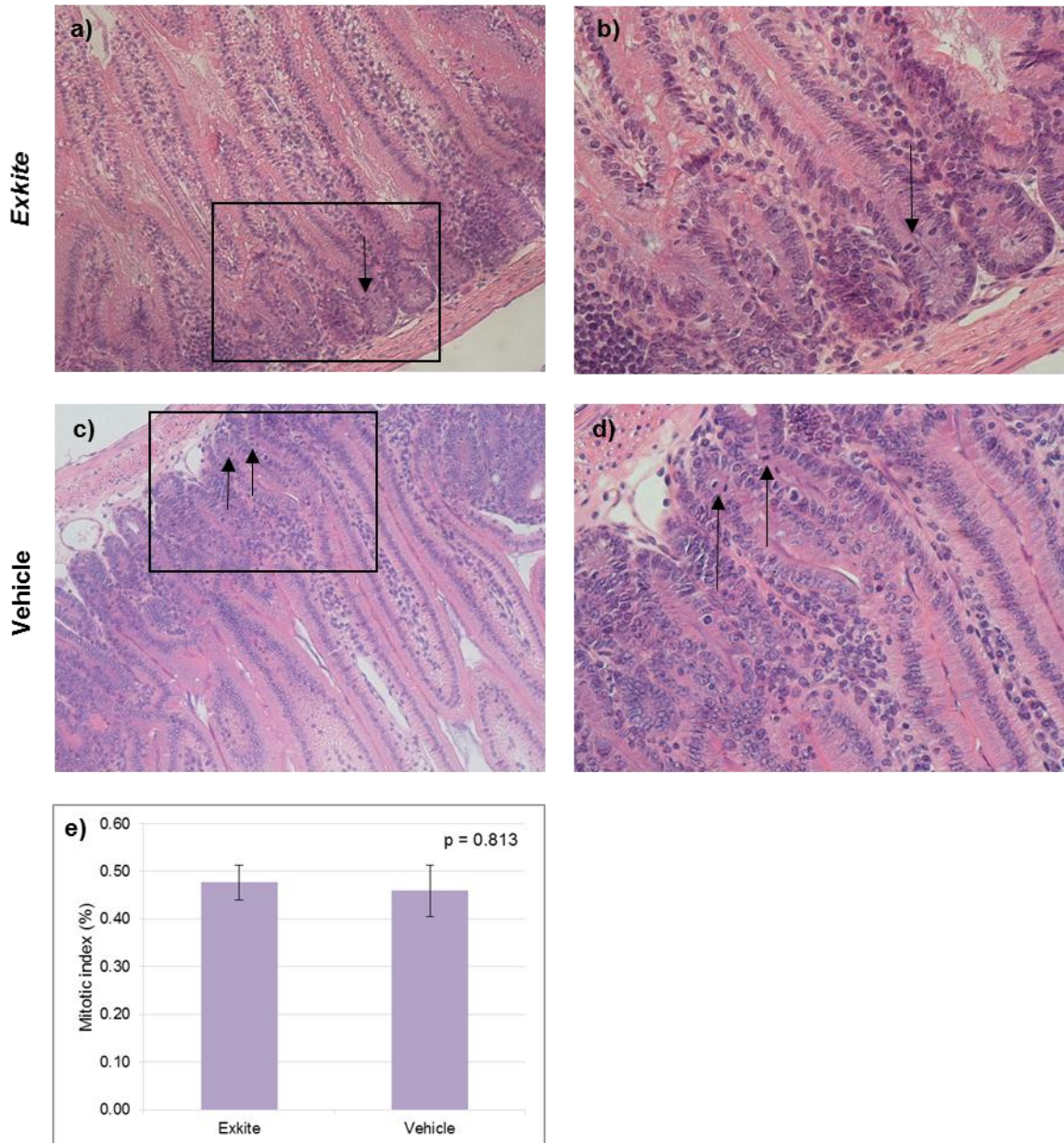


Figure 57 Representative images of intestinal tissue sections from Apc Hom mice stained by H&E, arrows indicate mitotic cells in crypts: a) H&E section of mouse treated with *Exkite* (magnification x 20), b) Enlarged magnification (x 40) H&E section of mouse treated with *Exkite*, c) H&E section of mouse treated with vehicle (magnification x 20), d) Enlarged magnification (x 40) H&E section of mouse treated with vehicle, e) Mitotic index from H&E stain shows no difference between treatments. Data is presented as mean \pm SEM, * represent statistical significance by Student's *t*-test ($p < 0.05$).

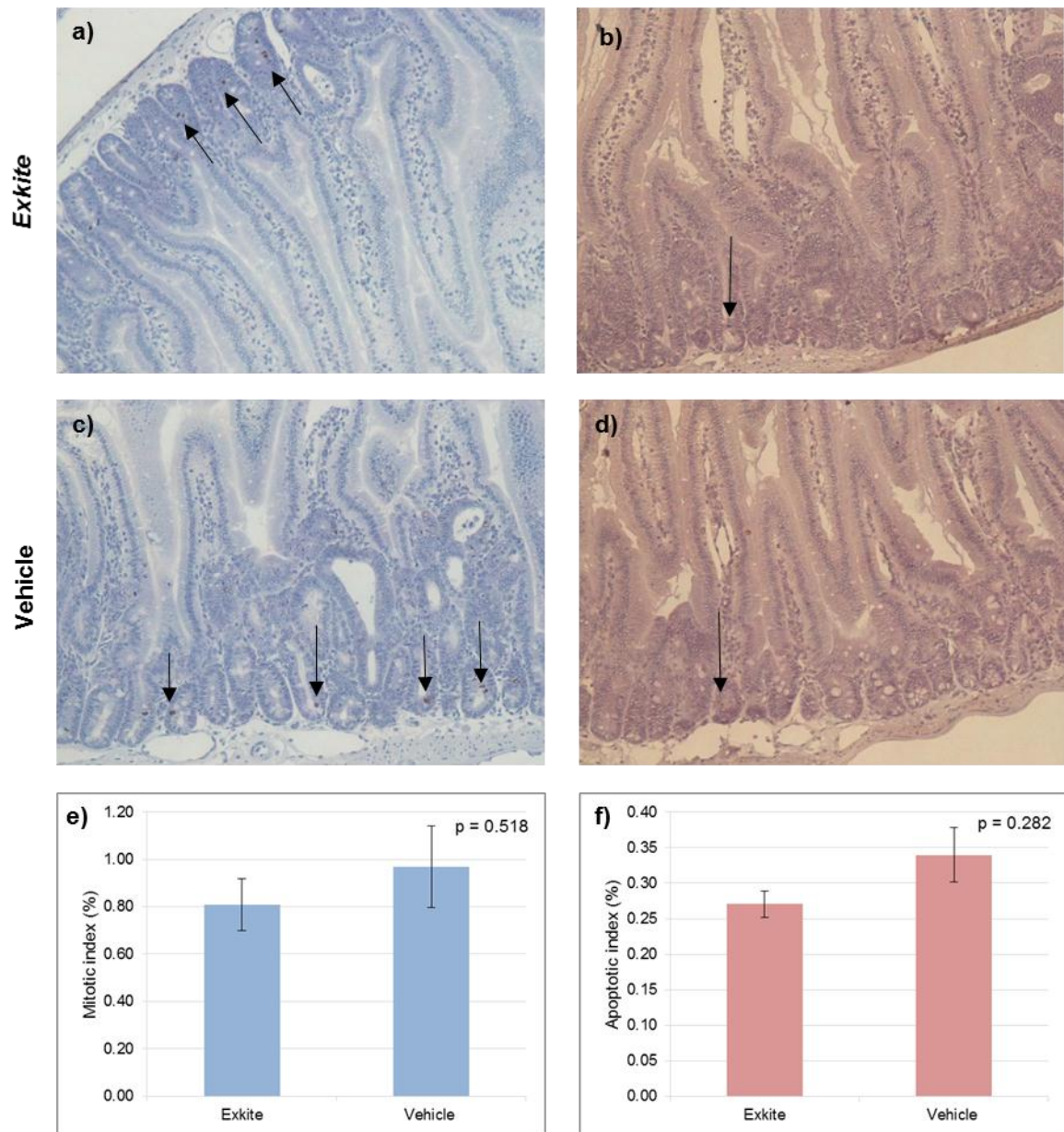


Figure 58 Representative images of intestinal tissue sections from Apc Hom mice for PHT and caspase 3 stains, arrows indicate mitotic or apoptotic cells in crypts, magnification x 20 for all: a) PHT section of mouse treated with *Exkite*, b) Caspase 3 section of mouse treated with *Exkite*, c) PHT section of mouse treated with vehicle, d) Caspase 3 section of mouse treated with vehicle, e) Mitotic index from PHT stain shows no difference between treatments, f) Apoptotic index from caspase 3 stain shows no difference between treatments. Data is presented as mean \pm SEM, * represent statistical significance by Student's *t*-test ($p < 0.05$).

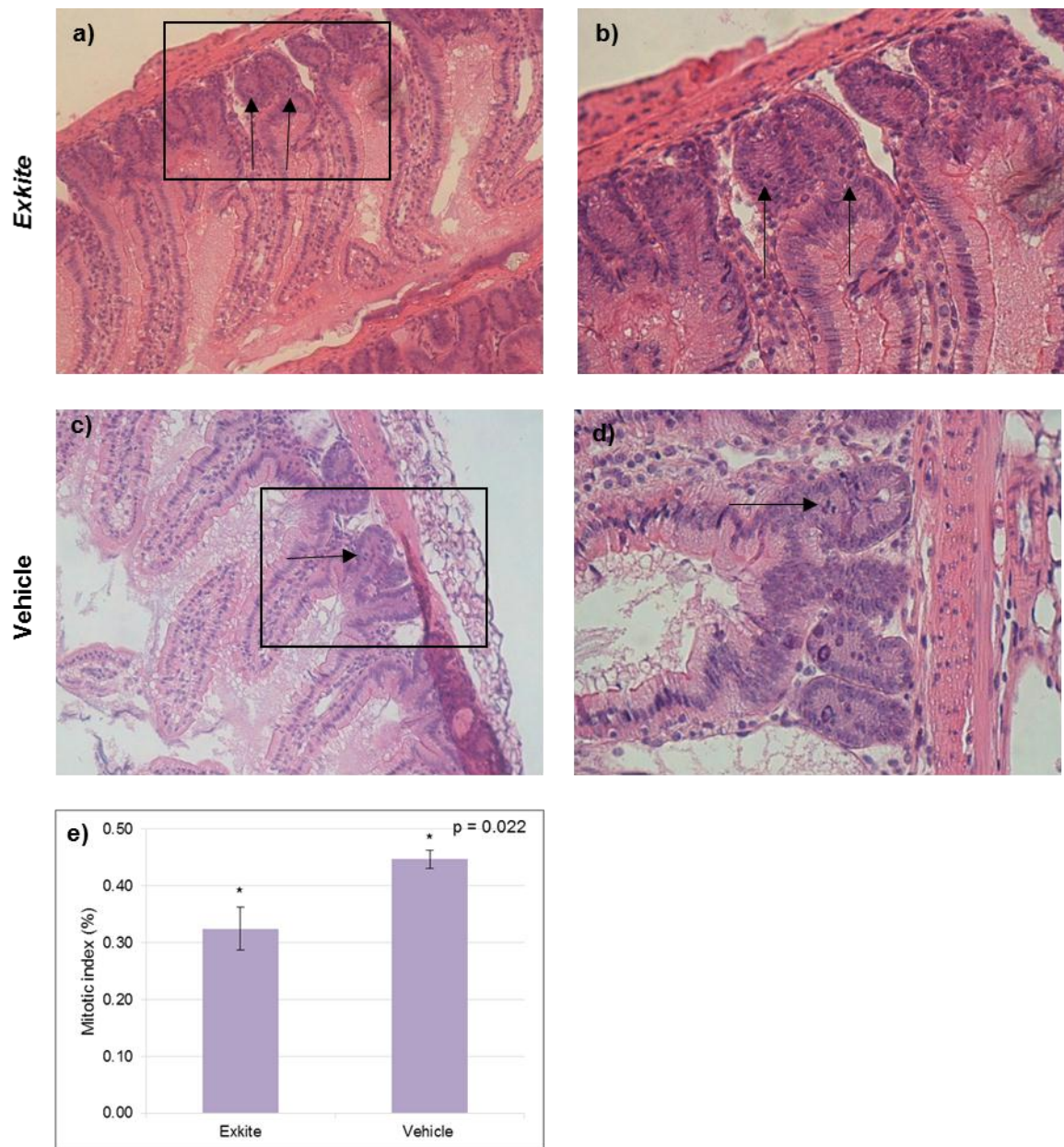


Figure 59 Representative images of intestinal tissue sections from *Apc Hom Pten Hom* mice stained by H&E, arrows indicate mitotic cells in crypts: a) H&E section of mouse treated with *Exkite* (magnification x 20), b) Enlarged magnification (x 40) H&E section of mouse treated with *Exkite*, c) H&E section of mouse treated with vehicle (magnification x 20), d) Enlarged magnification (x 40) H&E section of mouse treated with vehicle, e) Mitotic index from H&E stain shows statistically significant decrease in mitosis of mice treated with *Exkite* relative to vehicle. Data is presented as mean \pm SEM, * represent statistical significance by Student's *t*-test ($p < 0.05$).

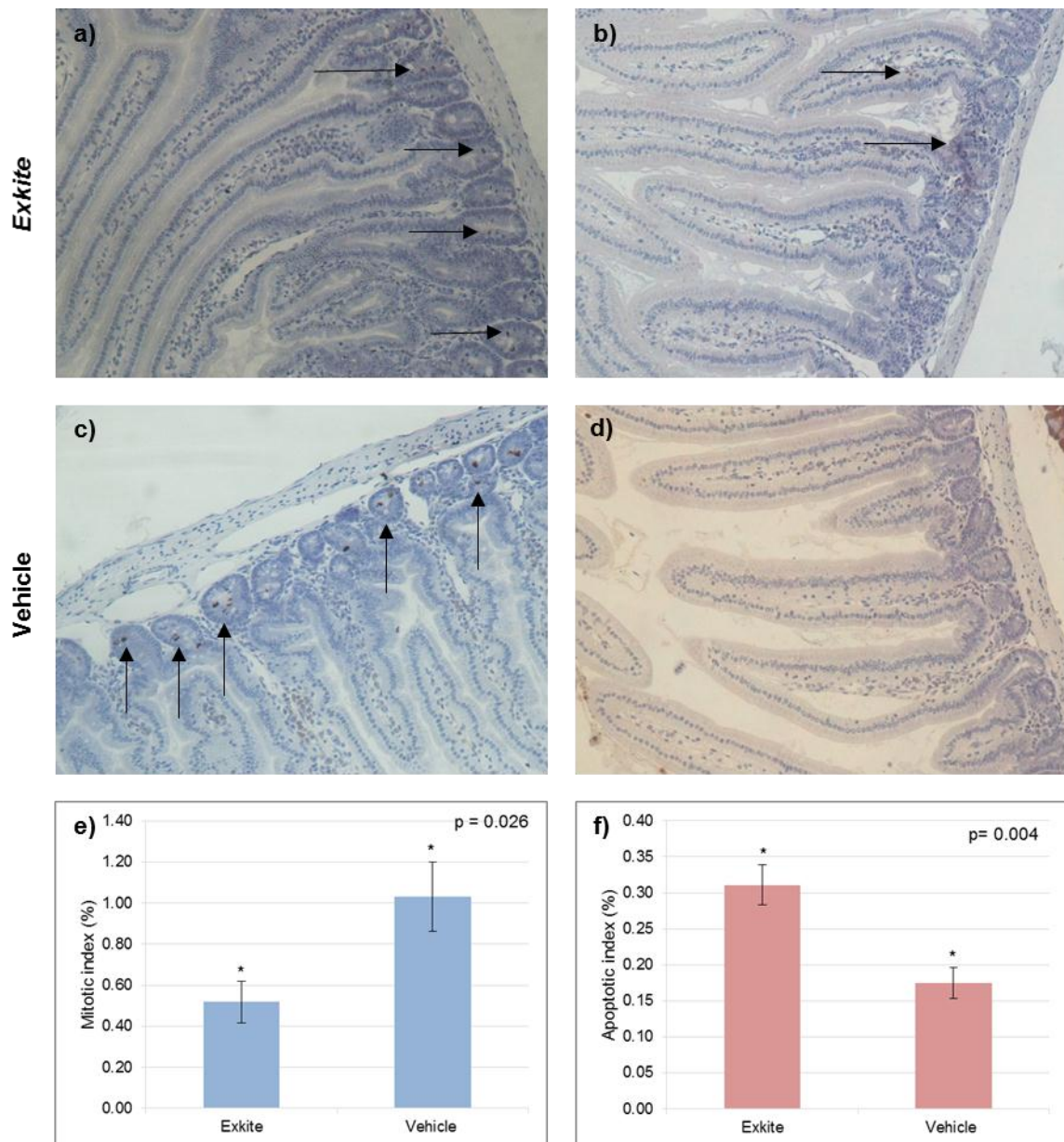


Figure 60 Representative images of intestinal tissue sections from *Apc Hom Pten Hom* mice for PHT and caspase 3 stains, arrows indicate mitotic or apoptotic cells in crypts, magnification x 20 for all: a) PHT section of mouse treated with *Exkite*, b) Caspase 3 section of mouse treated with *Exkite*, c) PHT section of mouse treated with vehicle, d) Caspase 3 section of mouse treated with vehicle, e) Mitotic index from PHT stain shows reduction in mitosis for mice treated with *Exkite* relative to vehicle, f) Apoptotic index from caspase 3 stain shows increase in apoptosis for mice treated with *Exkite* relative to vehicle. Data is presented as mean \pm SEM, * represent statistical significance by Student's *t*-test ($p < 0.05$)

Scoring slides for *Apc Hom* mice revealed that there is no appreciable difference in mitotic index between mice that were administered *Exkite* or vehicle water control, by H&E staining (Figure 57e, $p = 0.813$) or PHT expression (Figure 58e, $p = 0.518$). Likewise, there is no difference in the apoptotic index between the two treatments as calculated from caspase 3 immunostained tissue sections (Figure 58f, $p = 0.282$).

However, Apc Hom Pten Hom mice showed statistically significant reduction in mitosis in mice treated with *Exkite* compared to vehicle alone by both H&E staining (Figure 59e, $p = 0.022$) and PHT immunostained sections (Figure 60e, $p = 0.026$). This is complimented by an increase in apoptosis by amplified caspase 3 expression in mice treated with *Exkite* relative to vehicle (Figure 60f, $p = 0.004$). In this mouse model, the inactivation of tumour suppressor genes Apc and Pten results in intense cellular proliferation of intestinal crypts leading to enlarged crypts and tumorigenesis. Therefore, the observation that *Exkite* reduces cellular proliferation by mitosis whilst simultaneously increasing cell death by apoptosis indicates an attenuation of tumorigenesis. This result is supported by previous studies in which scoring intestinal crypts of AHC⁺Apc^{f/f} mice that were fed an iron deficient diet showed a decrease in mitotic index and increase in apoptotic index ($p = 0.015$), and associated decrease in tumour burden compared to mice on a control diet, whereas mice fed an iron rich diet showed the opposite trend.²⁶ This was attributed to iron levels directly affecting intestinal crypt cells to survive and proliferate. Furthermore, deferasirox induces early apoptosis by increasing expression of caspase 3 in human malignant lymphoma cells²⁰⁴ and myeloid leukemia cells²⁰⁵ by chelation of iron inhibiting cellular proliferation. Hence, it is likely that the reduced mitotic index and increased apoptotic index of mice treated with *Exkite* in this model is a result of iron chelation *in vivo*, as it is well known that iron is essential for cellular division.

7.5 Summary

Safety and tolerability of *Exkite* towards mice was assessed by subjecting wild type mice to daily gavage of varying concentrations of *Exkite* for five days from which the optimal dose was deemed to be 200 μ L of 1% w/v *Exkite*. Subsequently, wild type mice administered *Exkite* indicated minute amounts of free deferasirox ligand in intestinal crypt cells which may be ligand from *Exkite* salt as determined by diffusion NMR or ligand cleavage from decomposition of ligand conjugated *Exkite*.

Nevertheless, administering *Exkite* to CRC mouse models did not extend survival in either Apc Hom or Apc Hom Pten Hom mice. Histological analysis of intestinal tissue for Apc Hom mice did not show any difference in apoptotic or mitotic index in mice treated with *Exkite* compared to water vehicle control. However, Apc Hom Pten Hom mice treated with *Exkite* showed reduced mitosis and increased apoptosis of intestinal crypt cells compared to control. Although this did not translate into increased survival of mice treated with *Exkite*, this suggests *in vivo* activity of *Exkite* material by iron chelation to diminish tumorigenesis by preventing uncontrolled cellular proliferation.

8 Conclusion and Future work

8.1 Conclusion

The ligand deferasirox was identified as an appropriate iron chelator for investigation in this project owing to its safety and tolerability profile, and its superior iron binding properties relative to other chelators. This was synthesised in two steps from commercially available starting materials, and various modifications were attempted which demonstrated the chemical versatility of this ligand, and allowed the accumulation of a library of deferasirox related ligands. In particular, modifications to deferasirox were focused upon incorporating suitable functionalities for attaching onto non-absorbable backbones alginate and chitosan. These biopolymers were chosen for their non-toxicity and are already used in the food industry so are safe for oral consumption. Carbodiimide chemistry was utilised to attempt to attach deferasirox **6** to chitosan to yield *Exkite 43*, and modified ligand **33** was attached to alginate to yield *Exalg 42*. In addition, the ligand loading of *Exalg* was probed by reacting alginate with varying amount of ligand **33** to yield *Exalg_{0.25} – Exalg_{1.25}*.

Characterisation of polymers by IR, NMR and UV-vis spectroscopy confirmed ligand incorporation of polymers. Attempts to quantify ligand incorporation of *Exkite* by ¹H NMR spectroscopy and XPS indicated modification of 40%. Quantification of modification of *Exalg_{0.25} – Exalg_{1.25}* polymers by ¹H NMR spectroscopy and phenol/sulphuric acid assay suggest modification of 20% for all *Exalg* polymers. Analysis by XPS suggest higher modification on account of observed nitrogen composition but this may be an artefact of activated NHS/EDAC.HCl species as opposed to the ligand. Modification of all *Exalg* polymers was similar despite varying ligand equivalence in the synthesis. This suggests a restrictive factor to ligand incorporation which may arise from steric bulk or tertiary structure effects as incorporation of some ligands onto

alginate may prevent the approach of other ligand molecules due to steric hindrance on the polymer. This may also be related to the extent of activation of carboxylic acid sites by coupling agents. Further probing by diffusion NMR spectroscopy confirmed that the modified ligand **33** was indeed attached to alginate in *Exalg* owing to similar self-diffusion coefficients between the polymer and the ligand. However, significantly different self-diffusion coefficients were observed between the ligand and polymer in *Exkite* which suggests that the ligand is not associated with the polymer. This can be attributed to *Exkite* salt in which the electrostatic interactions between protonated chitosan and deprotonated ligand **6** give rise to a supramolecular aggregate, and may indicate batch to batch variation in the synthesis of *Exkite*.

Iron binding upon ligand incorporation of modified polymers was probed by the titration of iron solution into polymer solutions to measure a change in absorbance by UV-vis spectroscopy. Titrations into *Exkite* and *Exalg* revealed a shift in absorbance indicative of iron complex formation. Iron binding was also investigated by dialysis methods, and iron concentrations measured by AAS and ferrozine assay. *Exkite* elicited 100-fold increase in ferrous and ferric iron binding in the presence and absence of calcium relative to native polymer chitosan. *Exalg* only presented a moderate increase in iron binding; ferrous binding is greater in the presence of calcium, possibly due to gelling in the presence of Ca^+ to form egg box structures and trapping of iron. Iron binding of *Exalg*_{0.25} – *Exalg*_{1.25} was consistent due to similar modification of all *Exalg* polymers.

In vitro cellular studies were conducted using RKO colorectal cancer cells. Incubation of cells with iron and *Exkite* elicited a suppression in iron induced ferritin expression by western blot and ELISA. *Exkite* was shown to prevent the uptake of ambient iron as total intracellular iron was also reduced by ferrozine assay relative to iron only control and cells treated with iron and chitosan. However, stimulation of cells with iron and *Exalg* failed to have an effect on ferritin expression or total intracellular iron concentration, indicating poor *in vitro* iron chelation of *Exalg*. Surprisingly, cells

stimulated with iron and alginate itself suppressed iron mediated ferritin expression by western blot, and total intracellular iron is reduced by ferrozine assay compared to iron only control. The greater aqueous solubility of alginate may have contributed to the superior *in vitro* iron chelation observed.

In vivo chelation properties of *Exkite* was probed by using mouse models of CRC in which uncontrolled growth of intestinal crypt cells leads to the formation of intestinal tumours. Although Apc Hom mice that were administered *Exkite* did not display any positive effects, Apc Hom Pten Hom mice that were administered *Exkite* showed reduced mitotic index and increased apoptotic index of intestinal crypt cells relative to vehicle control. Despite the fact that this did not extend to an increase in mouse survival, the anti-neoplastic effects observed demonstrate *in vivo* activity of *Exkite*, and contribute to the growing evidence that in the background of CRC, iron chelation in the intestine has the potential to suppress carcinogenesis.

8.2 Future work

The modified polymers *Exkite* and *Exalg* investigated in this project represent the first generation of non-absorbable iron chelators which allowed the development of synthesis, characterisation and iron binding testing methods. Although the ligand conjugation of *Exkite* is not conclusive, the delivery of *Exkite* in the salt form requires further investigation. The development of the polymer Chemistry is on-going in the Fossey group in collaboration with the Fernandez-Trillo group. It was established that iron chelation properties of polymers can be improved by incorporation of a ligand, and these can be applied for effective iron chelation in an *in vitro* and *in vivo* setting. However, there were some important factors that became apparent during the course of this project which need to be taken into account if non-absorbable iron chelators are to be progressed into a clinical setting.

The physical properties of modified polymers such as solubility are important as this can directly influence iron binding. The *in vitro* and *in vivo* iron binding of *Exkite* and *Exalg* may be improved by increasing the aqueous solubility of the polymers so that it is more readily available to chelate iron out of solution. This will also enable easier characterisation by the use of traditional polymer characterisation techniques such as gel permeation chromatography and rheology. In addition, the precipitation of iron-polymer complex during UV-vis spectroscopy titrations meant that an accurate binding constant could not be elucidated from a binding curve. Increasing the solubility of modified polymers will allow better quantification of iron binding as isothermal titration calorimetry (ITC) can be used to calculate binding constants.

The aqueous solubility of *Exkite* and *Exalg* can be improved by the incorporation of water soluble polyethylene glycol (PEG) groups to offset the hydrophobic nature of the deferasirox ligand moiety. Alternatively, the ligand loading can be limited to be low by using stoichiometric control with respect to ligand to polymer ratio in the synthesis so that the aqueous solubility of the polymer backbone is retained. Despite the use of water soluble ligand **33** in reaction with alginate, the product *Exalg* was still poorly water soluble. Therefore, other ligands may be investigated for attachment onto a non-absorbable backbone. In particular, desferrioxamine (DFO) is water soluble and contains a free amine that is not utilised in iron binding, which can be used to react with alginate (Scheme 27).

DFO-polymer conjugates have been previously synthesised and applied to improve the vascular retention and toxicity of the ligand when administered intravenously. It is possible to investigate these polymers such as starch-DFO⁷⁰ **7** and PEG-DFO⁷¹ **8** conjugates in the context of CRC. Their iron binding properties can be determined by application to RKO cancer cells and CRC mouse models to determine whether they are non-absorbable when administered orally.

Surprisingly alginate performed well in intracellular iron binding experiments, and further investigations into the use of alginate alone in CRC therapy is on-going. Different types of alginate from different sources, the effects of molecular weight and M/G ratio upon iron binding are all being considered. Alginate therapy offers a non-toxic and practical alternative to synthetic chelators for CRC therapy, however the potential drawback is that alginate has a higher affinity towards calcium than iron. The removal of a non-target cation such as calcium may cause a deficiency of a physiologically important metal leading to complications. In addition, calcium has been shown to have protective properties in the context of CRC in epidemiological studies so removal of this metal should be avoided.²⁰⁶

The mode of delivery of an active agent is also an important consideration. Delivery of *Exkite* material in the salt form may increase the intracellular uptake of the iron chelator due to the intestinal absorption enhancing properties of chitosan.¹⁹¹ Matrix metalloproteinases (MMPs), which are known to be overexpressed in cancer cells, are zinc dependant endopeptidases²⁰⁷ which are capable of degrading extracellular matrix (ECM) proteins²⁰⁸ so are capable of cleaving peptide bonds of conjugated ligands. Additionally, oral administration of the active agent means that it has to withstand drastic pH changes in the GI tract from pH 1.0 - 3.0 in the stomach to pH 6.0 - 7.0 in the large intestine.²⁰⁹ Essential nutritional iron is absorbed in the small intestine so it is also vital that chelation of dietary iron does not happen too early in the GI tract. One method to overcome these problems is to encapsulate the active compound for controlled release in the large intestine. This could be in a pH responsive coating^{210, 211} or degradation of the capsule by gut microbiota for site specific release.²¹² Larger beads or microparticles that are large enough not to be absorbed in the GI tract can also be used instead of a non-absorbable backbone, to have chelators adsorbed onto the surface.

The current course of treatment for CRC is surgery and chemotherapy alone. Assuming that the correct drug delivery method for the iron binding active is found, this should offer a safer and less expensive adjuvant therapy to the clinical management of the disease with a view of prolonging life and improving survival of CRC patients.

9 Experimental

9.1 General Chemical Experimental

Proton nuclear magnetic resonance (^1H NMR) spectra were recorded on a Bruker AVIII 300 (300 MHz) spectrometer. All spectra were obtained at 22 °C and reported relative to residual solvent peaks in CDCl_3 (δ_{H} 7.26 ppm), d_6 -DMSO (δ_{H} 2.50 ppm), CD_3OD (δ_{H} 3.31), D_2O (δ_{H} 4.79) or d-TFA (δ_{H} 11.3 ppm).²¹³ All coupling constants are expressed as J , data is reported as follows: chemical shift (multiplicity, number of protons, coupling constants, assignment). Chemical shift is quoted to the nearest 0.01 ppm, and coupling constants to the nearest 0.1 Hz. Multiplicity is reported according to the following convention: s = singlet, d = doublet, t = triplet, q = quartet, dd = doublet of doublets, m = multiplet. All spectra were processed with MestReNova (version 6.0.2-5475).

Carbon nuclear magnetic resonance (^{13}C [^1H] NMR) spectra were recorded on a Bruker AVIII 400 (101 MHz) spectrometer which was proton decoupled. Chemical shifts are quoted to the nearest 0.1 ppm relative to residual solvent peaks in CDCl_3 (δ_{C} 77.2 ppm), d_6 -DMSO (δ_{C} 39.5 ppm) or CD_3OD (δ_{C} 49.0 ppm).²¹³

Diffusion NMR experiments were performed on a Bruker DMX300 spectrometer equipped with a 7 T superconducting magnet, operating at a proton resonance frequency of 300.13 MHz. Diffusion coefficients were measured using the ^1H NMR pulsed gradient stimulated echo (PGSTE) experiment at 293 ± 0.3 K. An observation time of $\Delta = 100$ ms was used and the gradient strength was varied over 32 gradient steps with $G_{\text{max}} = 1 \text{ T m}^{-1}$. A repetition time of 2 s was used and δ was kept constant at 2 ms. The signal loss with increasing gradient strength was fitted to the Stejskal-Tanner equation (Equation 8).

$$\frac{S(\mathbf{G})}{S(0)} = \exp(-(\gamma\delta\mathbf{G})^2 D \left(\Delta - \frac{\delta}{3}\right))$$

Equation 8 Stejskal-Tanner equation

Where $\frac{S(\mathbf{G})}{S(0)}$ is the signal decal, γ is the gyromagnetic ratio and D is the self-diffusion coefficient.

Where a monoexponential fit was poor, a biexponential fit was performed, producing two diffusion coefficients. The data were fitted to the minimum number of components necessary.

Flash column chromatography was conducted using silica gel 60F under positive pressure. TLC visualisation was with UV (254 nm), KMnO₄ or Ninhydrin on F₂₅₄ plates.

Mass spectra were recorded with electrospray MS Waters LCT Time of Flight mass spectrometer and with synapt G2-HDMS mass spectrometer in both positive and negative mode.

Melting points were conducted in triplicate and reported as the average and expressed as a range using Melting Point apparatus Stuart Scientific SMP10.

All IR spectra were recorded on a Perkin Elmer Spectrum 100 FT-IR spectrometer with Universal Attenuated Total Reflection Sampling Accessory as an average (10 scans) with the background (10 scans) subtracted.

UV-vis spectra were recorded on a Varian Cary50 spectrophotometer at 22 °C in water using 2.00 mL sample solution in a quartz cuvette with a path length of 1.00 cm.

Elemental analysis was conducted at Warwick Analytical Service on a CE 440 Elemental Analyser.

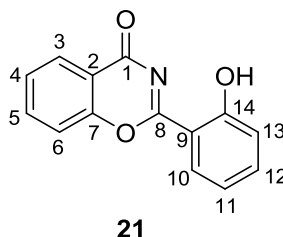
XPS measurements were obtained at Leeds Nanoscience and Nanotechnology Research Equipment Facility (LENRF) with support from EPSRC for funding towards travel and subsistence to take samples to the facility. XPS measurements were performed using a VG Escalab 250 XPS with monochromated aluminium K-alpha X-ray source. The spot size was 500 μm with a power of 150 W. Detailed spectra of individual peaks were taken at energy of 20 eV with a step size of 0.1 eV.

Binding energy was calibrated by setting the carbon 1s peak to 285 eV. Detailed spectra had a Shirley or linear background fitted to them and peaks were fitted using mixed Gaussian-Lorentzian fits (using CASAXPS).

All purchased chemicals were used as received from Sigma Aldrich.

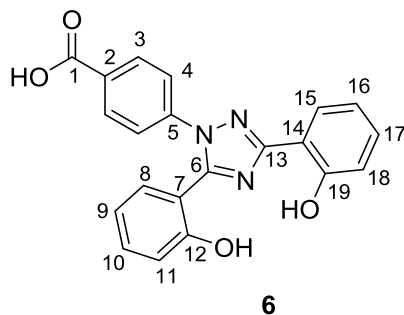
9.2 Compounds synthesised

9.2.1 2-(2-hydroxyphenyl)-4H-benzo[e][1,3]oxazin-4-one



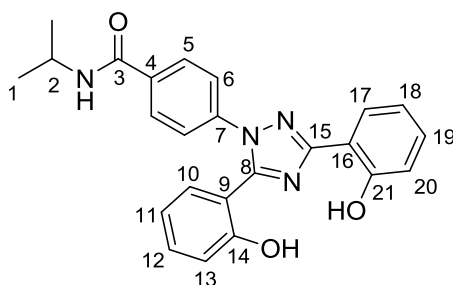
Salicylic acid **19** (6.04 g, 43.75 mmol), salicylamide **20** (5.00 g, 36.46 mmol) and pyridine (0.37 mL, 4.63 mmol) were heated at reflux in xylene (18.00 mL) for 15 minutes. Thionyl chloride (5.83 mL, 80.21 mmol) was added with vigorous stirring over a period of 4 hours, with further stirring for 16 hours at room temperature. Xylene was removed by concentration *in vacuo*, and resulting solid residue was suspended in ethanol (15.00 mL) and acetic acid (0.36 mL). The mixture was heated to reflux and cooled to room temperature. The solid precipitate was isolated and dried to yield **21** (6.59 g, 27.54 mmol, 76%) as yellow solid. R_f 0.37 (3:1 hexane/ ethyl acetate). $^1\text{H NMR}$ (300 MHz, d_6 -DMSO) δ_{H} 12.94 (s, 1H, OH), 8.21 (dd, 1H, $J = 8.4, 1.6$ Hz, H₃), 8.07 (dd, 1H, $J = 7.8, 1.6$ Hz, H₁₀), 7.95 (ddd, 1H, $J = 8.7, 7.4, 1.6$ Hz, H₅), 7.80 (d, 1H, $J = 8.7$ Hz, H₆), 7.69 – 7.55 (m, 2H, H₁₂, H₁₃), 7.16 – 7.03 (m, 2H, H₄, H₁₁). $^{13}\text{C NMR}$ (100 MHz, d_6 -DMSO) δ_{C} 164.8 (C₁), 163.4 (C₁₄), 161.8 (C₇), 153.8 (C₈), 136.7, 136.0, 129.0, 127.2, 126.7, 119.5, 117.9, 117.8, 117.4 (C₂), 111.4 (C₉). $\text{MS } m/z$ 262.1 [M+Na⁺]. IR 1690 (C=O), 1604 (C=N), 1540 (C=C), 1464 (C=C), 1445 (C=C), 1352 (C=C) cm^{-1} . **Melting point range** 198 - 201 °C.

9.2.2 4-(3,5-bis(2-hydroxyphenyl)-1H-1,2,4-triazol-1-yl)benzoic acid



4-Hydrazino-benzoic acid (1.40 g, 9.19 mmol), and triethylamine (1.28 mL, 9.19 mmol) were added to ethanol (40.00 mL) and refluxed for 15 minutes until all components were dissolved. To the clear solution was added **21** (1.40 g, 9.19 mmol) which was further refluxed for 2 hours. After cooling to room temperature, water (5.00 mL) was added until perturbation was observed. The mixture was concentrated to 50% of total volume under reduced pressure, and aqueous 6 M HCl (31.00 mL) was added. The resulting precipitate was isolated and dried to yield **6** (3.12 g, 8.36 mmol, 99%) as dark yellow solid. R_f 0.27 (5% MeOH, 2% NEt₃ in CHCl₃). ¹H NMR (300 MHz, d₆-DMSO) δ_H 13.20 (s, broad, 1H, OH), 10.82 (s, 1H, OH), 10.07 (s, 1H, OH), 8.06 (dd, 1H, J = 7.8, 1.6 Hz, H₈), 7.99 (d, 2H, J = 8.7 Hz, 2H₃), 7.61 – 7.53 (m, 3H, 2H₄, H₁₅), 7.46 – 7.34 (m, 2H, H₁₀, H₁₇), 7.08 – 6.95 (m, 3H, H₉, H₁₆, H₁₁), 6.87 (d, 1H, J = 8.2 Hz, H₁₈). ¹³C NMR (100 MHz, d₆-DMSO) δ_C 166.4 (C₁), 159.9 (C₁₃), 156.4 (C₁₂), 155.2 (C₁₉), 152.0 (C₆), 141.2 (C₅), 132.5, 131.4, 131.0, 130.5, 130.2 (C₂), 126.7, 123.2, 119.6, 119.4, 117.0, 116.2, 114.4 (C₇), 113.6 (C₁₄). MS m/z 372.3 [M⁺]. IR 2971 (O-H), 1683 (C=O), 1616 (C=N), 1603 (C=C), 1560 (C=C), 1532 (C=C), 1515 (C=C), 1490 (C-C), 1473 (C-C) cm⁻¹. Melting point range 257- 260 °C.

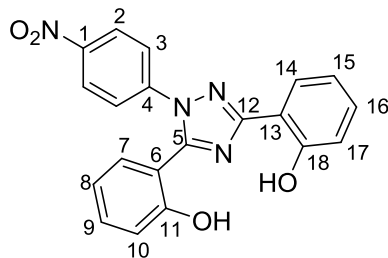
9.2.3 4-(3,5-bis(2-hydroxyphenyl)-1H-1,2,4-triazol-1-yl)-N-isopropylbenzamide



29a

To a solution of **6** (0.100 g, 0.268 mmol) in DCM (40.00 mL) was added NHS (0.037 g, 0.322 mmol) and DCC (0.066 g, 0.322 mmol), and solution was refluxed for 30 minutes. Isopropylamine (0.032 g, 0.536 mmol) was added and solution was further refluxed for 3 hours. The medium was concentrated *in vacuo* and resulting residue was purified by flash column chromatography (1:1 hexane: ethyl acetate), to yield **29a** as white crystalline powder (0.093 g, 0.224 mmol, 83%). **R_f** 0.50 (1:1 hexane: ethyl acetate). **¹H NMR** (300 MHz, CDCl₃) δ_H 11.40 (s, 1H, OH), 9.59 (s, 1H, OH), 8.14 (dd, 1H, *J* = 7.8, 1.6 Hz, H₁₀), 7.95 (d, 2H, *J* = 8.6 Hz, 2H₅), 7.60 (d, 2H, *J* = 8.6 Hz, 2H₆), 7.44 – 7.30 (m, 2H, H₁₁, H₁₈), 7.14 (dd, 1H, *J* = 8.4, 1.0 Hz, H₁₇), 7.11 – 7.01 (m, 2H, H₁₂, H₁₃), 6.93 (dd, 1H, *J* = 8.0, 1.5 Hz, H₂₀), 6.71 – 6.62 (m, 1H, H₁₉), 4.34 (m, 1H, H₂), 4.01, (d broad, 1H, *J* = 7.9 Hz, NH), 1.32 (d, 6H, *J* = 6.5 Hz, 6H₁). **¹³C NMR** (100 MHz, CDCl₃) δ_C 165.1 (C₃), 159.6 (C₁₅), 158.1 (C₁₄), 156.5 (C₂₁), 152.2 (C₈), 140.3 (C₄), 136.6, 133.0, 131.9, 128.6, 127.7, 127.5, 126.3, 119.9, 119.1, 118.4, 117.2, 113.2, 109.9, 42.4 (C₂), 22.8 (C₁). **MS**: *m/z* 437.3 [M + Na⁺]. **IR** 3304 (O-H), 1621 (C=O), 1587 (C=N), 1543 (C=C), 1505 (C-C), 1472 (C-C), 1493 (C-C) cm⁻¹. **Melting point range**: 210 - 212 °C.

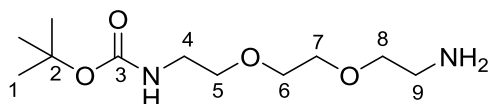
9.2.4 2,2'-(1-(4-nitrophenyl)-1H-1,2,4-triazole-3,5-diyl)diphenol



27

To a solution of **21** (1.000 g, 4.180 mmol) in methanol (20.00 mL) was added 4-nitrophenylhydrazine (0.700 g, 4.600 mmol), which was refluxed for 2.5 hours. Upon cooling, the product precipitates as dark yellow solid which was collected and washed with methanol to yield **27** (0.778 g, 2.080 mmol, 50%). *R_f* 0.38 (3:1 hexane: ethyl acetate). **¹H NMR** (300 MHz, d₆-DMSO) δ_H 10.70 (s, 1H, OH), 10.11 (s, 1H, OH), 8.34 (d, 2H, *J* = 9.1 Hz, H₂), 8.06 (dd, 1H, *J* = 7.8, 1.5 Hz, H₇), 7.73 (d, 2H, *J* = 9.1 Hz, H₃), 7.62 (dd, 1H, *J* = 7.8, 1.5 Hz, H₁₄), 7.47- 7.35 (m, 2H, H₉, H₁₆), 7.09 – 6.97 (m, 3H, H₈, H₁₅, H₁₀), 6.88 (d, 1H, *J* = 8.0 Hz, H₁₇). **¹³C NMR** (100 MHz, d₆-DMSO) δ_C 160.2 (C₁₂), 156.3 (C₁₁), 155.0 (C₁₈), 152.4 (C₁), 148.1 (C₅), 142.8 (C₄), 132.8, 131.6, 131.1, 126.9, 124.7, 124.1, 119.7, 119.6, 117.1, 116.2, 114.2, 113.5. **MS** *m/z* 373.2 [M - H⁺]. **IR** 3010 (O-H), 1652 (C=N), 1593 (N-O), 1482 (N-O), 1328 (C=C), 1306 (C=C), 1273 (C-C), 1254 (C-O), 1112 (C-N) cm⁻¹. **Melting point range** 179 – 181 °C.

9.2.5 Tert-butyl (2-(2-(2-aminoethoxy)ethoxy)ethyl)carbamate

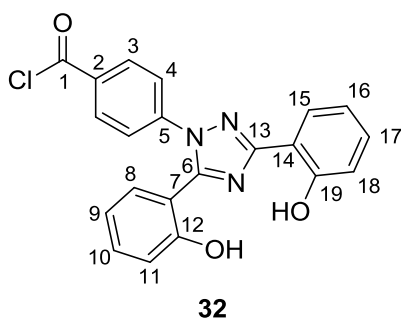


31

Boc anhydride (1.000 g, 1.053 mL, 4.582 mmol) in DCM (5.00 mL) was added portion wise over 2 hours at room temperature to 2,2 (ethylenedioxy) bis(ethylamine) (4.074 g, 4.01 mL, 27.489 mmol) in DCM (10.00 mL). This was further stirred at room temperature for 5 hours and solvent was removed. Water (30.00 mL) was added to the residue and extracted with DCM (6 x 20.00 mL),

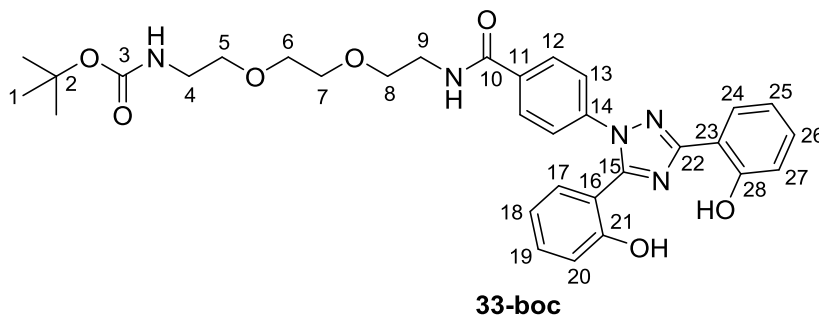
the combined organic extracts were dried (MgSO₄) and concentrated *in vacuo* to yield **31** as pale yellow oil (0.982 g, 3.957 mmol, 86 %). **¹H NMR** (300 MHz, CDCl₃) δ_H 5.66 (s, 1H, NH), 3.59 – 3.50 (m, 4H, 2H₅, 2H₈), 3.50 – 3.40 (m, 4H, 2H₆, 2H₇), 3.27– 3.17 (m, 2H, 2H₉), 2.79 (t, *J* = 5.2 Hz, 2H, 2H₄), 1.48 (s, 2H, 2NH), 1.36 (s, 9H, 9H₁). **¹³C NMR** (100 MHz, CDCl₃) δ_C 154.0 (C₃), 78.5 (C₂), 73.2, 69.9, 41.5 (C₄), 40.1 (C₉), 28.2 (C₁). **MS** *m/z* 249.1 [M + H⁺], 271.1 [M + Na⁺]. **IR**: 3364 (N-H), 2975 (N-H), 2868 (C-H), 1696 (C=O), 1516 (C-C), 1454 (C-C), 1365 (C-O) cm⁻¹.

9.2.6 4-(3,5-bis(2-hydroxyphenyl)-1H-1,2,4-triazol-1-yl)benzoyl chloride



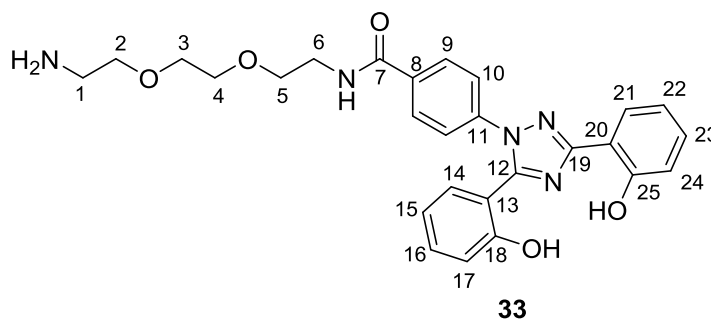
Thionyl chloride (0.20 mL, 2.687 mmol) was added to **6** (0.100 g, 0.268 mmol) in DCM (20.00 mL), and solution refluxed for 22 hours. The residue was concentrated *in vacuo* to yield **32** as dark brown solid (0.104 g, 0.268 mmol, 99%). **R_f** 0.20 (5% MeOH, 1% NEt₃ in CHCl₃). **¹H NMR** (300 MHz, d₆-DMSO) δ_H 8.04 (dd, 1H, *J* = 7.8, 1.6 Hz, H₈), 7.99 (d, 2H, *J* = 8.7 Hz, 2H₃), 7.60 – 7.51 (m, 3H, *J* = 8.7 Hz, 2H₄, H₁₅), 7.45 – 7.32 (m, 2H, H₁₀, H₁₇), 7.07 – 6.94 (m, 3H, H₉, H₁₁, H₁₆), 6.90 (d, *J* = 8.2 Hz, 1H, H₁₈). **¹³C NMR** (100 MHz, d₆-DMSO) δ_C 166.4 (C₁), 159.6 (C₁₃), 156.3 (C₁₂), 155.3 (C₁₉), 152.0 (C₆), 141.1 (C₅), 132.6 (C₂), 131.6, 131.1, 130.6, 130.3, 126.9, 123.4, 119.7, 119.4, 117.1, 116.2, 114.4 (C₇), 113.6 (C₁₄). **MS** *m/z* 414.8 [M + Na⁺]. **IR** 2954 (O-H), 1777 (C=O), 1737 (C=N), 1613 (C=C), 1598 (C=C), 1534 (C-C), 1460 (C-C) cm⁻¹. **Melting point range** 213 – 216 °C.

9.2.7 Tert-butyl-(2-(2-(2-(4-(3,5-bis(2-hydroxyphenyl)-1H-1,2,4-triazol-1-yl)benzamido)ethoxy)ethoxy)ethyl)carbamate



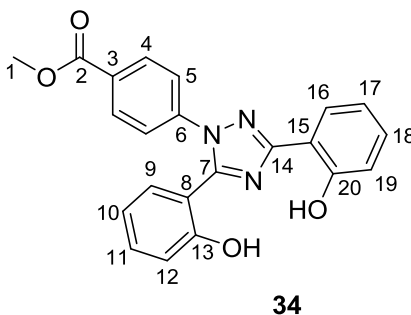
Compound **32** (0.090 g, 0.230 mmol) was added to **31** (0.077 g, 0.310 mmol) in DCM (20.00 mL), followed by triethylamine (0.032 mL, 0.230 mmol). The reaction mixture was stirred for 18 hours at room temperature, quenched by the addition of saturated NaHCO₃ solution (20.00 mL) and extracted with DCM (3 x 20.00 mL). The combined organic extracts were dried (MgSO₄), concentrated and purified by silica plug (5% MeOH, 1% NEt₃ in CHCl₃) to yield boc protected **33-boc** as pale yellow solid (0.100 g, 0.166 mmol, 72%). **R_f** 0.29 (5% MeOH, 1% NEt₃ in CHCl₃). **¹H NMR** (300 MHz, CDCl₃) δ_H 9.68 (s, 1H, OH), 8.59 (s, 1H, OH), 8.06 (dd, 1H, *J* = 7.8, 1.6 Hz, H₁₇), 7.91 (d, 2H, *J* = 7.5 Hz, 2H₁₂), 7.51 (d, 2H, *J* = 7.5 Hz, 2H₁₃), 7.37 – 7.22 (m, 2H, H₁₈, H₂₃), 7.11 – 6.82 (m, 4H, H₁₉, H₂₀, H₂₅, H₂₇), 6.63 (m, 1H, H₂₆), 4.94 (s, 1H, H₂), 3.75 – 3.41 (m, 10H, 2H₇, 2H₆, 2H₅, 2H₄, 2H₈), 3.29 – 3.14 (m, 2H, 2H₄), 2.80 (s, 1H, NH), 1.33 (s, 9H, 9H₁). **¹³C NMR** (100 MHz, CDCl₃) δ_C 166.6 (C₁₀), 166.2 (C₃), 157.7 (C₂₈), 152.1 (C₂₁), 140.5 (C₂₂), 135.8 (C₁₅), 132.9 (C₁₁), 133.8 (C₁₄), 129.3, 128.7, 128.0, 127.6, 125.8, 119.9, 119.2, 118.2, 117.2 (C₁₆), 113.3 (C₂₃), 77.4 (C₂), 70.2 (C₆), 69.7 (C₇), 46.0 (C₅), 40.3 (C₈), 40.0 (C₉), 28.4 (C₄), 9.7 (C₁). **MS** *m/z* 604.3 [M + H⁺], 626.3 [M + Na⁺]. **IR** 3312 (O-H), 2975 (N-H), 2930 (C-H), 1688 (C=O), 1611 (C=C), 1505 (C=C), 1461 (C-C), 1364 (C-O) cm⁻¹. **Melting point range:** 40 – 43 °C.

9.2.8 N-(2-(2-(2-aminoethoxy)ethoxy)ethyl)-4-(3,5-bis(2-hydroxyphenyl)-1H-1,2,4-triazol-1-yl)benzamide



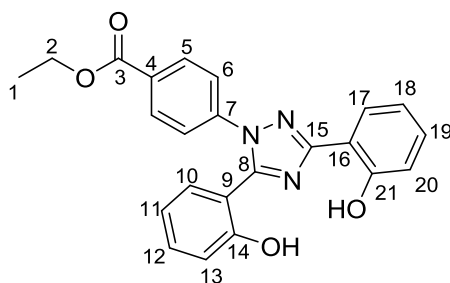
A solution of TFA (2.00 mL) was added to **33-boc** (0.052 g, 0.086 mmol) in DCM (2.00 mL) and stirred at room temperature for 4 hours. Saturated NaHCO₃ solution (20.00 mL) was added and subsequently extracted with DCM (3 x 10 mL), dried (MgSO₄) and concentrated *in vacuo* to yield **33** as yellow solid (0.041 g, 0.081 mmol, 96%). **¹H NMR** (300 MHz, CDCl₃) δ_H 8.13 (dd, 1H, *J* = 7.8, 1.6 Hz, H₁₄), 7.95 (d, 2H, *J* = 7.5 Hz, 2H₉), 7.52 (d, 2H, *J* = 7.5 Hz, 2H₁₀), 7.41 – 7.27 (m, 2H, H₂₁, H₁₅), 7.21 (dd, 1H, *J* = 7.9, 1.5 Hz, H₁₇), 7.13 – 6.96 (m, 2H, H₁₆, H₂₃), 6.92 (d, 1H, *J* = 8.2 Hz, H₂₄), 6.78 (t, 1H, *J* = 7.6 Hz, H₂₂), 3.82 – 3.54 (m, 10H, 2H₂, 2H₆, 2H₅, 2H₄, 2H₃), 3.47 (t, 2H, *J* = 4.6 Hz, 2H₁), 2.75 (s, 2H, NH). **¹³C NMR** (100 MHz, CDCl₃) δ_C 166.5 (C₇), 160.1 (C₁₉), 157.0 (C₁₈), 156.7 (C₂₅), 152.2 (C₁₂), 140.8 (C₈), 135.2, 132.8, 131.6, 129.0, 128.5, 127.4, 125.0, 119.8, 119.3, 117.7, 117.2, 113.5, 112.1 (C₂), 71.6 (C₃), 69.9 (C₄), 69.3 (C₅), 40.9 (C₁), 39.8 (C₆). **MS** *m/z* 504.2 [M + H⁺], 526.1 [M + Na⁺]. **IR** 3053 (O-H), 2869 (N-H), 1644 (C=O), 1624 (C=C), 1586 (C=C), 1461 (C-C), 1247 (C-O) cm⁻¹. **Melting point range** 100 – 104 °C.

9.2.9 Methyl 4-(3,5-bis(2-hydroxyphenyl)-1H-1,2,4-triazol-1-yl)benzoate



Compound **6** (0.055 g, 0.015 mmol) was added to methanol (2.00 mL) and sulphuric acid (12 M, 0.01 mL), and refluxed for 18 hours. Solvent was removed *in vacuo* to yield **34** as dark brown solid (0.060 g, 0.015 mmol, 99%). *R_f* 0.30 (2:1 hexane: ethyl acetate). **¹H NMR** (300 MHz, CD₃OD) δ_H 8.09 (d, 2H, *J* = 8.8 Hz, 2H₄), 7.99 (dd, 1H, *J* = 7.9, 1.6 Hz, H₉), 7.66 (d, 2H, *J* = 8.8 Hz, 2H₅), 7.54 – 7.41 (m, 3H, H₁₆, H₁₈, H₁₁), 7.08 (dd, 1H, *J* = 8.3, 0.6 Hz, H₁₂), 7.05 – 6.92 (m, 3H, H₁₀, H₁₉, H₁₇), 3.87 (s, 3H, H₁). **¹³C NMR** (100 MHz, CD₃OD) δ_C 167.0 (C₂), 157.8 (C₁₄), 157.6 (C₁₃) 153.7 (C₂₀), 151.2 (C₇), 141.2 (C₆), 136.6 (C₃), 135.3, 133.3, 132.2, 131.9, 130.4, 126.1, 121.5, 121.3, 117.8, 111.5 (C₁₅), 108.7 (C₈), 53.19 (C₁). **MS** *m/z* 388.1 [M + H⁺]. **IR** 3213 (O-H), 1718 (C=O), 1607 (C=N), 1545 (C=C), 1521 (C=C), 1478 (C-C), 1428 (C-C) cm⁻¹. **Melting point range:** 147 – 150 °C.

9.2.10 Ethyl 4-(3,5-bis(2-hydroxyphenyl)-1H-1,2,4-triazol-1-yl)benzoate

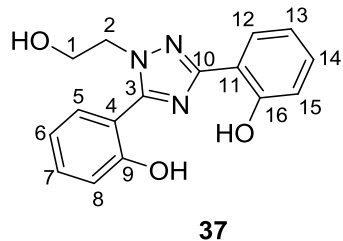


35

Compound **6** (0.100 g, 0.268 mmol) was added to ethanol (4.00 mL) and sulphuric acid (12 M, 0.01 mL), and refluxed for 23 hours. Solvent was removed *in vacuo* to yield **35** as dark brown solid (0.105 g, 0.267 mmol, 99%). *R_f* 0.41 (2:1 hexane: ethyl acetate). **¹H NMR** (300 MHz, CD₃OD) δ_H 8.14 (d, 2H, *J* = 8.7 Hz, 2H₅), 8.05 (dd, 1H, *J* = 7.9, 1.6 Hz, H₁₀), 7.71 (d, 2H, *J* = 8.7 Hz, 2H₆), 7.60 – 7.46 (m, 3H, H₁₂, H₁₉, H₁₇), 7.17 – 6.96 (m, 4H, H₁₁, H₁₃, H₂₀, H₁₈), 4.39 (q, 2H, *J* = 7.1 Hz, 2H₂), 1.39 (t, 3H, *J* = 7.1 Hz, 3H₁). **¹³C NMR** (100 MHz, CD₃OD) δ_C 166.5 (C₃), 157.8 (C₁₅), 157.6 (C₁₄), 153.7 (C₂₁), 151.2 (C₈), 141.2 (C₇), 136.6 (C₄), 135.9, 135.3, 133.7, 132.2, 131.8, 130.4, 126.0, 121.5, 121.3, 117.7, 111.5 (C₉), 108.8 (C₁₆), 62.8 (C₂), 14.6 (C₁). **IR** 3105 (O-H), 1707

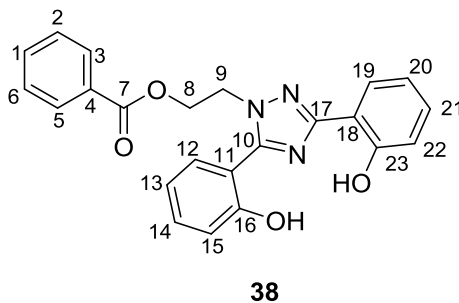
(C=O), 1613 (C=N), 1558 (C=C), 1535 (C=C), 1485 (C=C) cm^{-1} . **Melting point range** 156 – 158 $^{\circ}\text{C}$.

9.2.11 2,2'-(1-(2-hydroxyethyl)-1H-1,2,4-triazole-3,5-diyl)diphenol



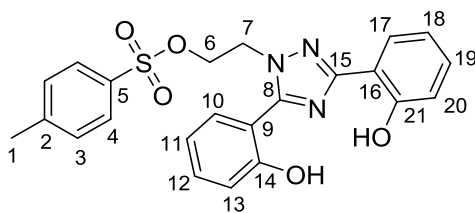
2-Hydroxyethylhydrazine **36** (0.55 mL, 8.360 mmol) was added to **21** (1.000 g, 4.180 mmol) in methanol (30.00 mL) and solution was refluxed for 2 hours. Upon cooling, water (10.00 mL) was added to precipitate product which was collected, washed with water (10.00 mL) and dried to yield **37** as white crystalline solid (0.527 g, 1.770 mmol, 43%). **R_f** 0.26 (2:1 hexane: ethyl acetate). **¹H NMR** (300 MHz, CD₃OD) δ_{H} 8.03 (dd, 1H, $J = 7.8, 1.6$ Hz, H₅), 7.50 (dd, 1H, $J = 7.8, 1.6$ Hz, H₁₂), 7.46- 7.37 (m, 1H, H₇), 7.33- 7.25 (m, 1H, H₁₄), 7.08- 6.89 (m, 4H, H₆, H₈, H₁₅, H₁₃), 4.29 (t, 2H, $J = 5.6$ Hz, 2H₂), 3.94 (t, 2H, $J = 5.6$ Hz, 2H₁), 3.35 (s, 1H, OH). **¹³C NMR** (100 MHz, CD₃OD) δ_{C} 161.5 (C₁₀), 157.9 (C₉), 156.8 (C₁₆), 154.8 (C₃), 133.5, 132.5, 132.0, 127.9, 120.9, 120.6, 117.9, 117.3, 115.7, 61.1 (C₁), 52.9 (C₂). **MS** m/z 298.3 [M + H⁺]. **IR** 3163 (O-H), 2974 (C-H), 1617 (C=N), 1596 (C=C), 1585 (C=C), 1452 (C-C) cm^{-1} . **Melting point range:** 150 – 152 $^{\circ}\text{C}$.

9.2.12 2-(3,5-bis(2-hydroxyphenyl)-1H-1,2,4-triazol-1-yl)ethyl benzoate



Benzoic acid (0.020 g, 0.168 mmol) was dissolved in DCM (20 mL), DCC (0.041 g, 0.202 mmol) and DMAP (0.007 g, 0.057 mmol) were added and solution was stirred at room temperature for 30 minutes, **37** (0.050 g, 0.168 mmol) was added and solution was further stirred for 18 hours. The medium was concentrated *in vacuo* and purified by flash column chromatography (2:1 hexane: ethyl acetate) to yield **38** as a white solid (0.012 g, 0.030 mmol, 18%). R_f 0.3 (2:1 hexane: ethyl acetate). $^1\text{H NMR}$ (300 MHz, CDCl_3) δ_{H} 10.65 (s, 1H, OH), 9.66 (s, 1H, OH), 8.01 (dd, 1H, $J = 7.8, 1.6$ Hz, H_{12}), 7.77 (dd, 2H, $J = 8.4, 1.3$ Hz, H_3, H_5), 7.65 (dd, 1H, $J = 7.9, 1.5$ Hz, H_{19}), 7.52 – 7.40 (m, 1H, H_1), 7.37 – 7.24 (m, 4H, $\text{H}_2, \text{H}_6, \text{H}_{14}, \text{H}_{21}$), 7.08 – 6.85 (m, 4H, $\text{H}_{13}, \text{H}_{15}, \text{H}_{22}, \text{H}_{20}$), 4.86 – 4.74 (m, 4H, 2 $\text{H}_8, 2\text{H}_9$). $^{13}\text{C NMR}$ (100 MHz, CDCl_3) δ_{C} 166.1 (C_7), 159.5 (C_{17}), 157.4 (C_{16}), 156.5 (C_{23}), 153.1 (C_{10}), 133.4, 132.8, 131.6, 129.7, 129.0, 128.4, 127.5, 126.9, 119.8, 119.7, 118.4, 117.1, 113.5, 110.7, 62.4 (C_8), 49.5 (C_9). $\text{MS } m/z$ 401.2 [$\text{M} + \text{H}^+$]. IR 3209 (O-H), 1711 (C=O), 1624 (C=N), 1584 (C=C), 1512 (C=C), 1496 (C-C), 1473 (C-C), 1464 (C-N), 1453 (C-O) cm^{-1} . **Melting point range** 132 – 135 °C.

9.2.13 2-(3,5-bis(2-hydroxyphenyl)-1H-1,2,4-triazol-1-yl)ethyl-4-methyl benzenesulfonate

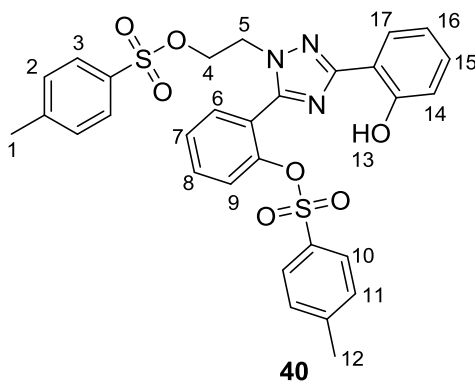


39

Compound **37** (0.150 g, 0.505 mmol) was added to tosyl chloride (0.115 g, 0.605 mmol) and triethylamine (0.102 g, 0.141 mL, 1.010 mmol) in DCM (30.00 mL), and stirred at room temperature for 70 hours. The reaction mixture was washed with water (3 x 20.00 mL), dried (MgSO_4) and concentrated *in vacuo*. The resulting residue was purified by flash column chromatography (1:5 hexane: ethyl acetate) to yield **39** as white crystalline solid (0.093 g, 0.206

mmol, 20%). **R_f** 0.25 (1:5 hexane: ethyl acetate). **¹H NMR** (300 MHz, CDCl₃) δ_H 7.87 (dd, 1H, *J* = 7.8, 1.6 Hz, H₂₀), 7.63 – 7.50 (m, 2H, H₁₂, H₁₃), 7.44 (dd, 1H, *J* = 7.7, 1.2 Hz, H₁₀), 7.41 – 7.35 (m, 1H, H₁₁), 7.25 (ddd, 1H, *J* = 8.7, 7.3, 1.6 Hz, H₁₈), 7.21 – 7.15 (m, 2H, 2H₄), 6.96 – 6.89 (m, 1H, H₁₇), 6.89 – 6.82 (m, 3H, H₁₉, 2H₃), 4.16 – 4.08 (m, 2H, 2H₇), 4.02 – 3.94 (m, 2H, 2H₆), 1.91 (s, 3H, 3H₁). **¹³C NMR** (100 MHz, CDCl₃) δ_C 160.6 (C₂₁), 156.8 (C₁₅), 149.9 (C₈), 146.4 (C₁₄), 146.3 (C₂), 132.5 (C₁₂), 131.8 (C₁₀), 131.3 (C₁₈), 130.8 (C₅), 129.9 (C₃), 127.8 (C₁₁), 127.5 (C₄), 126.4 (C₂₀), 124.8 (C₁₃), 121.0 (C₉), 119.4 (C₁₉), 117.3 (C₁₇), 113.2 (C₁₆), 60.9 (C₆), 51.6 (C₇), 21.1 (C₁). **MS** *m/z* 474.2 [M + Na⁺]. **IR** 3541 (O-H), 3084 (C-H), 1616 (C=N), 1582 (C=C), 1524 (C=C), 1458 (C-C), 1361 (S=O) cm⁻¹. **Melting point range** 124 – 126 °C.

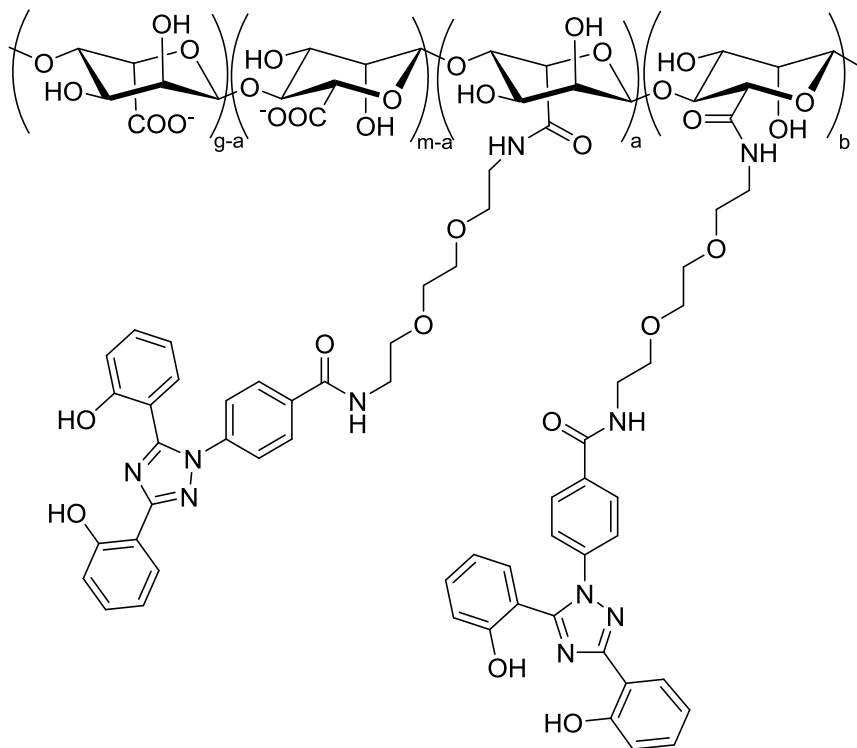
9.2.14 2-(3-(2-hydroxyphenyl)-1-(2-(tosyloxy)ethyl)-1H-1,2,4-triazol-5-yl)phenyl-4-methylbenzenesulfonate



Compound **37** (0.150 g, 0.505 mmol) was added to tosyl chloride (0.115 g, 0.605 mmol) and triethylamine (0.102 g, 0.141 mL, 1.010 mmol) in DCM (30.00 mL), and stirred at room temperature for 70 hours. The reaction mixture was washed with water (3 x 20.00 mL), dried (MgSO₄) and concentrated *in vacuo*. The resulting residue was purified by flash column chromatography (1:5 hexane: ethyl acetate) to yield **40** as yellow oil (0.082 g, 0.135 mmol, 12%). **R_f** 0.46 (1:5 hexane: ethyl acetate). **¹H NMR** (300 MHz, CDCl₃) δ_H 7.76 (dd, 1H, *J* = 7.8, 1.6 Hz, H₂₅), 7.70 – 7.62 (m, 1H, H₁₂), 7.58 (d, 1H, *J* = 8.0 Hz, H₁₃), 7.54 – 7.42 (m, 4H, H₁₀, H₁₁, 2H₄), 7.37 – 7.29 (m, 1H, H₂₃), 7.19 (d, 2H, *J* = 8.0 Hz, 2H₁₆), 7.07 (d, 2H, *J* = 8.0 Hz, 2H₃), 7.01 (dd,

^1H , $J = 8.3, 0.9$ Hz, H_{22}), 6.98 – 6.91 (m, 1H, H_{24}), 6.88 (d, 2H, $J = 8.0$ Hz, 2H_{17}), 4.40 (t, 2H $J = 4.8$ Hz, 2H_6), 4.29 (t, 2H, $J = 4.8$ Hz, 2H_7), 2.13 (s, 3H, 3H_1), 1.96 (s, 3H, 3H_{19}). ^{13}C NMR (100 MHz, CDCl_3) δ_{C} 160.7 (C_{26}), 156.6 (C_{20}), 150.4 (C_8), 146.2 (C_{14}), 146.2 (C_{18}), 145.3 (C_2), 132.6 (C_{12}), 131.8 (C_{10}), 131.7 (C_5), 131.2 (C_{23}), 130.8 (C_{15}), 129.9 (C_{17}), 129.7 (C_3), 128.0 (C_{11}), 127.5 (C_{16}), 127.4 (C_4), 126.5 (C_{25}), 124.6 (C_{13}), 120.7 (C_9), 119.3 (C_{24}), 117.3 (C_{22}), 113.5 (C_{21}), 66.8 (C_6), 48.2 (C_7), 21.2 (C_{19}), 21.1 (C_1). MS m/z 628.2 [$\text{M} + \text{Na}^+$]. IR 3064 (O-H), 1776 (C=N), 1737 (C=C), 1613 (C=C), 1596 (C=C), 1461 (C-C), 1355 (S=O) cm^{-1} .

9.2.15 Alginate-deferasirox conjugate Exalg



42 Exalg

A solution of sodium alginate LFR5/60 (FMC Biopolymer, 0.250 g, 1.262 mmol), EDAC.HCl (0.242 g, 1.262 mmol), and NHS (0.145 g, 1.262 mmol) in MES buffer (30.00 mL, 0.1 M, pH 6) was prepared. To this was added **33** (Table 8) dissolved in MES buffer (10.00 mL, 0.10 M, pH 6) and the reaction mixture was stirred at room temperature for 16 h. The precipitate was isolated, washed with water (3 x 10.00 mL) and dried to yield **42 Exalg** as off-white solid. ^1H NMR (300

MHz, d₆-DMSO) δ_{H} 10.84 (s, 1H), 8.63 (s, 1H), 8.20 – 7.70 (m, 4H), 7.70 – 7.17 (m, 4H), 7.17 – 6.54 (m, 4H), 4.00 – 2.25 (m, xH). **IR** 3295 (O-H), 3000 (C-H), 1636 (C=O), 1628 (C=C), 1608 (C=C), 1586 (C=C), 1505 (C-C), 1461 (C-C), 1090 (C-O), 1028 (C-N) cm⁻¹. **UV/vis** (H₂O, 25 °C): λ_{max} = 247, 302 nm.

Table 8 Details of ligand equivalence, amount used and mass of isolated product.

Entry	Eq 33	mmol 33	Mass 33 (g)	Product	Mass product isolated (g)	% yield by mass	Aliphatic proton integrations (¹ H NMR spec, m)
1	0.25	0.315	0.159	<i>Exalg</i> _{0.25}	0.107	13	30
2	0.50	0.631	0.318	<i>Exalg</i> _{0.50}	0.309	37	38
3	0.75	0.946	0.476	<i>Exalg</i> _{0.75}	0.531	64	48
4	1.00	1.262	0.635	<i>Exalg</i> _{1.00}	0.785	94	39
5	1.25	1.578	0.794	<i>Exalg</i> _{1.25}	0.961	115	40

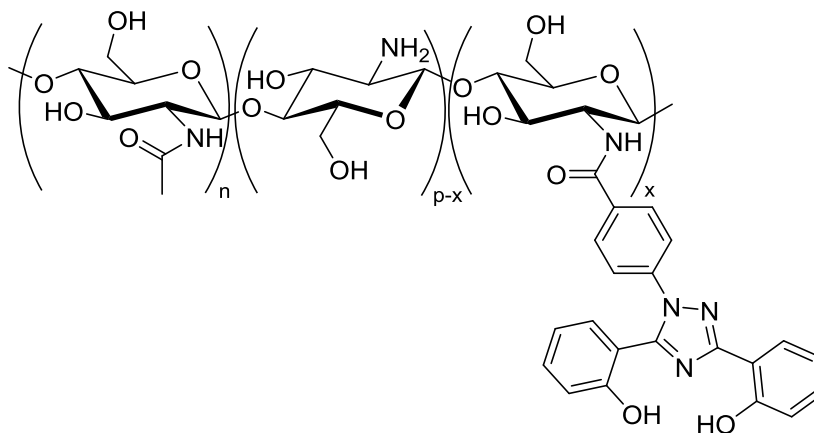
Percentage ligand incorporation by ¹H NMR spectroscopy was calculated by equating 12 aromatic protons (8.70 – 6.00 ppm) to one ligand equivalent. The number of x aliphatic protons (4.00 – 2.25 ppm) was subtracted twelve aliphatic protons corresponding to the linker to give the number of protons that are from the alginate alone. This was divided by 7 protons per alginate monomer unit to get the number of alginate monomer equivalents. One ligand equivalent was divided by the number of alginate monomer equivalents and expressed as a percentage.

Elemental analysis (Nitrogen/Carbon/Hydrogen) calculated for 100% modification N 10.58: C 59.09: H 5.33, found (Table 9).

Table 9 Results of elemental analysis of alginate polymers

Compound	C (% w/w)	H (% w/w)	N (% w/w)
Alginate	30.62	4.09	0.00
<i>Exalg</i> _{0.25}	52.86	5.53	9.79
<i>Exalg</i> _{0.50}	51.78	5.76	9.74
<i>Exalg</i> _{0.75}	51.78	5.64	9.88
<i>Exalg</i> _{1.00}	51.82	5.67	9.87
<i>Exalg</i> _{1.25}	52.89	5.60	10.04

9.2.16 Chitosan-deferasirox conjugate **Exkite**



A solution of EDAC. HCl (0.062 g, 0.322 mmol) and NHS (0.038 g, 0.322 mmol) in deionised water (50.00 mL) was added to **6** (0.100 g, 0.269 mmol) dissolved in a few drops of DMSO. Chitosan was then added (0.044 g, 0.268 mmol of monomer units) and solution stirred at rt for 17.5 h. Reaction solution was transferred to semi-permeable cellulose membrane (14 kDa molecular weight cut off, 76 mm flat width, Sigma Aldrich D9402) and dialysed in deionised water for three days, with the water changed twice daily. Water was removed *in vacuo* to yield **43 Exkite** as pale

brown film (0.109 g, 90%). $^1\text{H NMR}$ (300 MHz, d-TFA) δ_{H} 8.50 – 8.27 (m, 2H), 8.18 – 8.05 (m, 1H), 7.70 – 7.60 (m, 2H), 7.30 – 7.48 (m, 2H), 7.09 – 6.92 (m, 4H), 6.82 – 6.91 (m, 1H), 5.30 – 2.50 (m, 9H). **IR**: 3379 (O-H), 2985 (N-H), 1623 (C=O), 1591 (C=C), 1506 (C=C), 1493 (C-C), 1472 (C-C), 1462 (C-C), 1369 (C-O) cm^{-1} . **UV/vis** (H_2O , 25 °C): λ_{max} = 248, 305 nm.

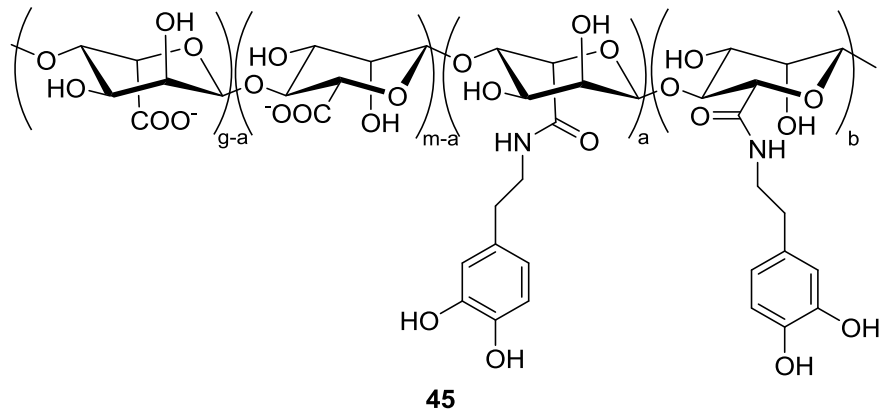
Percentage ligand incorporation by $^1\text{H NMR}$ spectroscopy was calculated by equating 12 aromatic protons (8.50 – 6.00 ppm) to one ligand equivalent. The number of aliphatic protons (5.30 – 2.50 ppm) was divided by 7 protons per chitosan monomer unit to get the number of chitosan monomer equivalents. One ligand equivalent was divided by the number of chitosan monomer equivalents and expressed as a percentage.

Elemental analysis (Nitrogen/Carbon/Hydrogen) calculated for 100% modification N 10.85: C 62.79: H 4.68, found (Table 10).

Table 10 Elemental analysis results for chitosan polymers

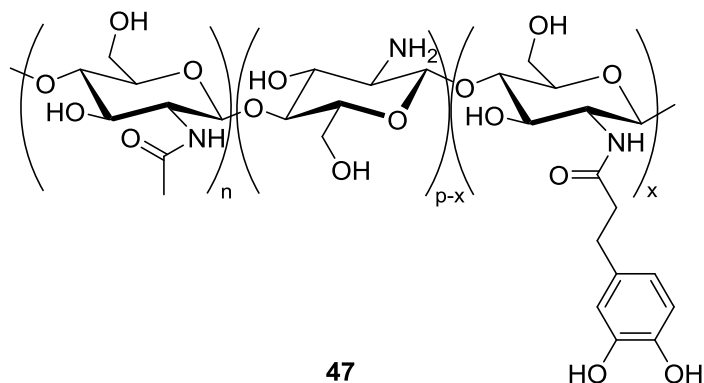
Compound	C (% w/w)	H (% w/w)	N (% w/w)
Chitosan	42.31	6.53	7.46
<i>Exkite</i>	55.34	4.77	9.31

9.2.17 Alginate-catechol conjugate



A solution of sodium alginate LFR5/60 (0.176 g, 1.000 mmol), dopamine hydrochloride (0.190 g, 1.000 mmol), EDC.HCl (0.192 g, 1.000 mmol) and NHS (0.116 g, 1.000 mmol) in MES buffer solution (50.00 mL, 0.1 M, ph 6) was stirred at rt for 16 h. The reaction mixture was dialysed through a semi-permeable cellulose membrane (14 kDa molecular weight cut off, 76 mm flat width, Sigma Aldrich D9402) in aqueous media, the media was changed twice a day for three days. Compound **45** was obtained as white solid by freeze drying (0.125 g, 49%). **IR** 3252 (O-H), 1732 (C=O), 1673 (C=C), 1610 (C=C), 1520 (C=C), 1406 (C-C), 1092 (C-C), 1031 (C-O) cm^{-1} . **Elemental Analysis** (Nitrogen/Carbon/Hydrogen) calculated for 100% modification N 4.5: C 54.02: H 5.50, found: N 5.28: C 38.99: H 6.01.

9.2.18 Chitosan-catechol conjugate



A solution of hydrocaffeic acid (0.500 g, 2.745 mmol), EDAC.HCl (0.631 g, 3.294 mmol) and NHS (0.379 g, 3.294 mmol) was prepared in water: ethanol mixture (1:1 15.00 mL: 15.00 mL). To this was added a solution of chitosan (0.445 g, 2.745 mmol) in acidic aqueous media (60.00 mL water acidified by HCl to pH 5), and the resulting reaction mixture was stirred at room temperature for 16 h. Reaction solution was transferred to semi-permeable cellulose membrane (14 kDa molecular weight cut off, 76 mm flat width, Sigma Aldrich D9402) and dialysed in acidic aqueous media (pH 5) for three days, with the aqueous media changed regularly. The dialysed solution was freeze dried to yield **47** as a brown solid (0.784 g, 70%). **IR**: 3347 (O-H), 1631 (C=O), 1527 (C=C),

1441 (C-C), 1069 (C-O) cm^{-1} . **Elemental Analysis** (Nitrogen/Carbon/Hydrogen) calculated for 100% modification N 4.31: C 55.38: H 5.89, found: N 5.50: C 38.06: H 6.21.

9.3 Phenol/Sulphuric acid assay

9.3.1 Ligand concentration

Deferasirox ligand **6** was dissolved in 0.1 M NaOH solution and UV-vis spectroscopy readings were taken at varying concentrations using Varian Cary50 spectrophotometer at 22 °C. A calibration curve was constructed by plotting absorbance vs. concentration at 245 and 315 nm.

Modified ligand **33** was dissolved in water and UV-vis spectroscopy readings were taken at varying concentrations using Varian Cary50 spectrophotometer at 22 °C. A calibration curve was constructed by plotting absorbance vs. concentration at 245 and 300 nm.

Exalg solutions were made by dissolving polymers in DMSO and diluting in water (0.010 g polymer/2.00 mL DMSO diluted up to 140.00 mL in water), and *Exkite* solutions were dissolved in 1M HCl (0.010 g polymer/150.00 mL 1M HCl). These polymer solutions were used for further iron binding studies. UV-vis spectra of polymers were taken and absorbance at 245 and 315 nm for *Exkite*, 245 and 300 nm for *Exalg* were compared to ligand calibration curves to determine amount of ligand in polymer.

9.3.2 Polymer concentration

Alginate solutions were made in water and chitosan solutions were made in 1% v/v acetic acid at varying concentrations. *Exkite* and *Exalg* solutions were used as prepared above. Polymer solution (2.00 mL) was decanted into a glass vial and 80% w/w phenol solution (0.05 mL) was added and solutions mixed by shaking. Concentrated sulphuric acid (5.00 mL) was added rapidly and solution was allowed to stand at room temperature for 10 minutes, then mixed by shaking. The solutions

were placed in a water bath at 30 °C for 20 minutes and readings were taken by UV-vis spectroscopy.¹⁴² Calibration curves for alginate were constructed by plotting absorbance vs. concentration at 480 nm and for chitosan at 490 nm. *Exkite* and *Exalg* were treated in the same way; chitosan concentration in *Exkite* was determined by comparing absorbance at 490 nm to chitosan calibration curves, and alginate concentration in *Exalg* was determined by comparing absorbance at 480 nm to calibration curves.

9.3.3 Percentage modification

The percentage modification of polymers was calculated by comparison of the ligand concentration to polymer concentration as determined by phenol/sulphuric acid assay and UV-vis spectroscopy in the same volume of polymer (2.00 mL/cuvette). All readings were taken in triplicate, and background readings of solutions that polymers were dissolved in were also obtained to ensure no background interference.

9.4 UV-Vis spectroscopy iron titration experiments

Polymer solutions 0.15% w/v chitosan, 0.10% w/v *Exkite*, 0.10% w/v alginate, 0.01% w/v *Exalg* were titrated with sequential addition of 10 µL iron chloride solution (10 mM FeCl₃.6H₂O) into 2.00 mL polymer solution in quartz cuvette. The solution was mixed between each addition and UV-vis spectra recorded. A gradual shift or increase in absorbance at λ_{\max} was taken to indicate iron chelation by polymers.

9.5 Iron binding by polymer dialysis

9.5.1 Dialysis experiments

Polymer solutions 0.10% w/v chitosan, 0.10% w/v alginate, 0.007% w/v *Exalg* (0.010 g polymer/ 2.00 mL DMSO diluted up to 140.00 mL in water), and 0.007% w/v *Exkite* (0.010 g polymer/

150.00 mL 1M HCl), were sealed (3 x 10.00 mL) into a dialysis membrane (14 kDa molecular weight cut off, 76 mm flat width, Sigma Aldrich D9402). Polymer solutions in dialysis membrane were incubated in ferrous iron (0.20 mM FeSO₄·7H₂O, 750.00 mL), ferrous iron with calcium (0.20 mM FeSO₄·7H₂O, 2.00 mM CaCl₂·2H₂O, 750.00 mL), ferric iron (0.20 mM FeCl₃·6H₂O, 750.00 mL), and ferric iron with calcium (0.20 mM FeCl₃·6H₂O, 2.00 mM CaCl₂·2H₂O, 750.00 mL) for 2 hours with agitation. Dialysis in acidic supernatant required addition of concentrated hydrochloric acid (12 M HCl, 0.75 mL in 750.00 mL). When washing step was conducted, the sealed dialysis membrane was washed in deionised water (750.00 mL) for 2 hours. All experiments were performed in triplicate.

9.5.2 Ferrozine assay of polymers

Ferrozine stock solution was prepared by adding sodium ascorbate (0.911 g), ferrozine (0.089 g), and sodium acetate (13.776 g) to deionised water (152.50 mL). After dialysis, each polymer sample (200 µL) was mixed with ferrozine stock (600 µL) and concentrated hydrochloric acid (12 M HCl, 50 µL). Calibration curve for iron was constructed by preparing varying concentrations of ferrous iron solutions in 0.1% v/v HCl at 0.75 mM, 0.50 mM, 0.25 mM, 0.125 mM and 0.10 mM that were also treated in the same way. All samples were plated out in triplicate (3 x 200 µL) into a flat-bottomed clear 96 well plate and absorbance read at 550 nm on Victor 2 Wallac 1420 microplate reader. Iron binding of polymers was determined by comparison to calibration curve.

9.5.3 Atomic absorption spectroscopy

Dialysed samples (10.00 mL) were concentrated *in vacuo* and re-dissolved in nitric acid (16 M HNO₃, 0.50 mL) and hydrochloric acid (3 M HCl, 9.50 mL). Samples were heated to 80 °C and sonicated for 2 – 4 hours. Calibration standards were prepared by serial dilutions of 1000 ppm iron in 1 M nitric acid (Fischer J803005) at 0.5 ppm, 1 ppm, 5 ppm, 10 ppm, 15 ppm and 20 ppm. Iron

content of samples were analysed by Perkin Elmer Instruments Analyst 300 atomic absorption spectrophotometer, equipped with iron specific hollow cathode lamp with maximum current of 10 mA. The samples were atomised using an acetylene-air flame. Iron binding of polymers was determined by comparison to calibration curve.

9.6 Cell culture

Human colorectal carcinoma RKO cells obtained from ATCC were stored in liquid nitrogen and thawed for use. The cells were cultured in Dulbecco's Modified Eagle's Medium (DMEM, Sigma Aldrich) supplemented with 10% v/v foetal calf serum (FCS, Gibco Life Technologies), 100 units/mL penicillin and 0.1 mg/mL streptomycin. Cells were incubated at 37 °C and 5% CO₂.

Cells were routinely maintained as adherent monolayers, and were passaged at 80% confluence by aspirating the culture medium, washing with sterile phosphate buffered saline (PBS) and incubating with Trypsin (TrypLE™ Express (1x), Gibco Life Technologies, 5.00 mL for 5 minutes) until cells had detached. Culture media (5.00 mL) was added and then centrifuged at 1500 rpm for 5 minutes. The cell pellet was re-suspended in culture media and reseeded into tissue culture flasks and cultured in the standard manner. All cell culture procedures were performed in a laminar flow tissue culture cabinet using aseptic technique.

9.7 MTT cell viability assay

RKO cells (1×10^5 cells/mL) were seeded into 6-well plates (Corning) at 2.00 mL/well. After cells were allowed to adhere for 24 hours, the medium was replaced with stimulation medium and further incubated for 24 hours. This consisted of varying concentrations of chitosan, *Exkite*, alginate or *Exalg* diluted from 1% w/v stock solutions into modified DMEM (10% FCS, 100 units/mL penicillin and 0.1 mg/mL streptomycin). Experiments were done in triplicate for each concentration and control was conducted in cell culture media alone. MTT [3-(4,5-dimethylthiazol-2-yl)-2,5-

diphenyltetrazolium bromide] (Sigma-Aldrich) was dissolved into sterile PBS (0.005 g/mL) and further filtered sterilised to remove any insoluble particles. MTT solution (100 μ L) was added to each well and incubated for 3 hours. The media was aspirated and replaced with DMSO (1.00 mL/well) to dissolve accumulated formazan crystals. After 10 - 15 minutes at room temperature, DMSO solution from each well of 6-well plate was transferred in triplicate to 96-well plate (100 μ L x 3 from each well). Plates were read at 490 nm on Victor 2 Wallac 1420 microplate reader. The resulting optical densities were used to calculate viability as fold change with respect to control.

9.8 Western blot

9.8.1 Sample preparation

RKO cells (1×10^5 cells/mL) were seeded into 6-well plates at 2.00 mL/well and allowed to adhere for 24 hours. Iron stock solution was made by dissolving iron sulphate (10 mM $\text{FeSO}_4 \cdot 7\text{H}_2\text{O}$, 0.1112 g) and sodium ascorbate (1 mM, 0.008 g) into deionised water (40.00 mL), which was further filtered sterilised to remove any insoluble particles. The stock solution was added to modified DMEM (100 μ L/10.00 mL DMEM) to give final concentrations of 100 μ M iron sulphate and 10 μ M sodium ascorbate. Polymer solutions were added to iron loaded modified DMEM, diluted from 1% stock solutions to achieve final concentrations of 0.03% w/v *Exkite* and Chitosan (0.30 mL polymer stock/10.00 mL DMEM), 0.05% w/v *Exkite* and Chitosan (0.50 mL polymer stock/10.00 mL DMEM), 0.005% w/v alginate and *Exalg* (0.05 mL polymer stock/10.00 mL DMEM), 0.01% alginate and *Exalg* (0.10 mL polymer stock/10.00 mL DMEM).

The media was aspirated and replaced with stimulation medium containing iron sulphate (100 μ M), sodium ascorbate (10 μ M) and the appropriate concentration of polymer in DMEM (2.00 mL/well) and further incubated for 24 hours. Experiments were done in triplicate for each polymer

concentration, positive control was conducted in iron loaded modified DMEM (100 μ M FeSO₄·7H₂O, 10 μ M sodium ascorbate), negative control was conducted in modified DMEM alone.

At the end of the incubation period, the media was removed and cells washed with ice cold PBS buffer (3 x 1.00 mL/well), and lysed with radioimmunoprecipitation assay (RIPA) buffer (100 μ L/well) whilst being kept on ice. RIPA buffer contains 1% v/v NP40 detergent, 0.5% w/v sodium deoxycholate, 0.1% w/v sodium dodecyl sulphate (SDS) and a mixture of proprietary protease inhibitors (1 protease inhibitor tablet (Roche) dissolved per 50.00 mL RIPA buffer).

Cell lysates were subject to probe sonication (10 seconds, Soniprep 150 MSE Sonyo). The amount of protein in each sample was quantified using Pierce™ BCA Protein Assay Kit, according to manufacturer's instructions using 96-well plate done in triplicate for each sample (3 x 10 μ L). The plate was read at 550 nm using Victor 2 Wallac 1420 microplate reader. Standard calibration curves were constructed for the determination of protein content. The volume of cell lysate containing 20 μ g of protein was calculated and this volume was added to 5 μ L of 5x SDS sample loading buffer (0.0625 M Tris HCl pH 6.7, 10% v/v glycerol, 2% w/v SDS, 1% v/v β -mercaptoethanol and 0.001% w/v bromophenol blue). Samples were then heated to 100 °C for 5 minutes and centrifuged briefly to bring samples to bottom of tubes.

9.8.2 SDS-Polyacrylamide gel electrophoresis (SDS-PAGE)

Stacking and resolving gels for SDS-PAGE were prepared according to recipe (Table 11). A BioRad Protean–II mini-gel apparatus was used, and resolving gel was poured between two glass plates. Isopropanol was added to the top to form a thin layer to ensure uniformity of resolving gel. After leaving gel to set (5 - 10 minutes), isopropanol was poured out and stacking gel applied to the top of resolving gel with immediate insertion of miniprep combs (1.5 mm combs for 10 lanes). After stacking gel was set (5 - 10 minutes), combs were removed and wells equilibrated with

electrophoresis running buffer (0.192 M glycine, 0.01% w/v SDS, 25 mM Tris HCl pH 8.3). One well per gel was loaded with an aliquot of pre-stained protein ladder (5 μ L, Thermo Scientific 26619). The remaining wells were loaded with prepared cell lysates at the predetermined volume containing 20 μ g protein. Electrophoresis was conducted at 100 V (15 minutes), and then increased to 180 V (45 minutes) until the dye front reached the bottom of the gel.

Table 11 Composition of SDS-PAGE stacking and resolving gels, sufficient for the preparation of two gels.

Reagent	Resolving gel (12.5%)	Stacking gel
$^d\text{H}_2\text{O}$	1.90 mL	3.70 mL
Buffer	10.00 mL (0.2% w/v SDS, 0.75 M Tris HCl, pH 8.8)	5.00 ml (0.2% w/v SDS, 0.25 M Tris HCl, pH 6.8)
Acrylamide	8.10 mL	1.30 mL
Ammonium persulphate	30 mg	30 mg
TEMED (add last for gelling)	60 μ L	60 μ L

9.8.3 Transfer of gels

Proteins separated by SDS-PAGE were transferred directly onto Hybond hydrophobic polyvinylidene difluoride membranes (GE Healthcare, RPN2020F). Membranes were cut to size and activated by soaking in methanol (30 seconds) and placed in transfer buffer (48 mM Tris HCl, 39 mM glycine, 20% v/v methanol, 0.0375% w/v SDS). The gels were removed from resolving apparatus, stacking gel at top and dark bands at the bottom were disposed. Gels were placed on top of the membrane and inserted into transfer cartridges ensuring that this was placed in between sponges and filter paper soaked in transfer buffer. The transfer tank was filled with transfer buffer and an ice pack to offer constant cooling, and was run at 100 V for 70 minutes.

9.8.4 Blocking membranes

Membranes were removed from transfer tanks and blocked by placing in 5% w/v milk solution, prepared from skimmed milk powder dissolved in tris-buffered saline tween (TBST) (10 mM Tris-Cl pH 8.0, 150 mM NaCl, 0.05% tween-20). Membranes were incubated for 1 hour at room temperature on a plate shaker.

9.8.5 Primary antibody

Blocking milk was removed and membranes were cut into two sections along 35 kDa line by using the pre-stained protein ladder as a guide. The top sections of the membranes were incubated with anti- β -actin primary antibody (Abcam, ab8226), and bottom sections were incubated with anti-ferritin primary antibody (Abcam, ab69090). Both antibodies were diluted at ratio 1:5000 in 5% w/v skimmed milk powder in TBST, which was added to membranes and incubated at 4 °C overnight on plate shaker.

9.8.6 Secondary antibody

Primary antibody was removed followed by a brief wash of membranes with TBST. Membranes were further washed with TBST (3 x 10 minutes) accompanied by agitation on plate shaker. Secondary peroxidase conjugated antibodies were prepared by diluting antibodies 1: 10,000 in 5% w/v skimmed milk powder in TBST; anti-mouse antibody used for β -actin and anti-rabbit antibody used for ferritin (Abcam). This was applied to membranes and incubated for 1 hour at room temperature on plate shaker. Secondary antibodies were removed and membranes washed by TBST (3 x 10 minutes).

9.8.7 Developing blots

Membranes were placed in a plastic bag sealed on three sides and enhanced chemiluminescence (ECL) reagent was added (5.00 mL/membrane, GE Healthcare, RPN2106 prepared according to

manufacturer's instructions.) The bag was sealed and exposed to ECL reagent (5 minutes), after which the bag was unsealed, ECL reagent removed and placed in an imaging cassette. The blots were developed in a darkroom using Amersham Hyprfilm™ (GE Healthcare, 28-9068-46) on a Xograph X2 automatic developer.

Blots were scanned and densitometry was analysed using ImageJ software and Microsoft Excel, in which ferritin bands were normalised relative to β -actin bands.

9.9 Ferritin ELISA

Cell lysates prepared for western blots were also used for analysis by ferritin ELISA. After lysis of cells in RIPA buffer, samples were stored at -20 °C until use and were subsequently thawed on ice. Ferritin ELISA was conducted using a Spectro ferritin ELISA kit (Ramco Laboratories Inc, S-22) according to manufacturer's instructions, using the pre-coated 96-well plate provided. Absorbance of samples were read at 490 nm and 595 nm on Victor 2 Wallac 1420 microplate reader. Results were processed using Microsoft Excel by construction of calibration curves as instructed in the kit.

9.10 Intracellular ferrozine assay

9.10.1 Sample preparation

RKO cells (3×10^5 cells/mL) were seeded into 6-well plates at 2.00 mL/well and allowed to adhere for 24 hours. Iron stock solution was made by dissolving iron sulphate (10 mM $\text{FeSO}_4 \cdot 7\text{H}_2\text{O}$, 0.1112 g) and sodium ascorbate (50 mM, 0.396 g) into deionised water (40.00 mL), which was further filtered sterilised to remove any insoluble particles. Serum-free DMEM was prepared (100 units/mL penicillin and 0.1 mg/ mL streptomycin only). The stock solution was added to serum-free DMEM (100 μL /10.00 mL DMEM) to give final concentrations of 100 μM iron sulphate and 500 μM sodium ascorbate. Polymer solutions were added to iron loaded serum-free DMEM,

diluted from 1% stock solutions to achieve final concentrations of 0.03% w/v *Exkite* and Chitosan (0.30 mL polymer stock/10.00 mL DMEM), 0.05% w/v *Exkite* and Chitosan (0.50 mL polymer stock/10.00 mL DMEM), 0.005% w/v alginate and *Exalg* (0.05 mL polymer stock/10.00 mL DMEM), 0.01% alginate and *Exalg* (0.10 mL polymer stock/10.00 mL DMEM).

The media was aspirated and replaced with serum-free DMEM and incubated for 1 hour to serum starve cells. Serum-free media was removed and replaced with stimulation medium containing iron sulphate (100 μ M), sodium ascorbate (500 μ M) and the appropriate concentration of polymer in serum-free DMEM (2.00 mL per well) and further incubated for 1 hour. Experiments were done in triplicate for each polymer concentration, positive control was conducted in iron loaded serum-free DMEM (100 μ M $\text{FeSO}_4 \cdot 7\text{H}_2\text{O}$, 500 μ M sodium ascorbate), negative control was conducted in serum-free DMEM alone.

At the end of the incubation period, the media was removed and cells washed with ice cold PBS buffer (3 x 1.00 mL/well), and lysed with HEPES saline buffer (10 mM 4-(2-hydroxyethyl)-1-piperazineethanesulfonic acid (HEPES) in 0.9% w/v sodium chloride at pH 7.4, 150 μ L/well) whilst being kept on ice.

9.10.2 Protein assay

The amount of protein in each sample was quantified using PierceTM BCA Protein Assay Kit, according to manufacturer's instructions, using 96-well plate done in triplicate for each sample (3 x 10 μ L). The plate was read at 550 nm using Victor 2 Wallac 1420 microplate reader. Standard calibration curves were constructed for the determination of protein content.

9.10.3 Ferrozine assay

Cell lysate (90 μ L) was added to TCA solution (200 μ L, 20% w/v trichloroacetic acid (TCA) in 4% w/v sodium pyrophosphate) and heated to 100 $^{\circ}$ C for 10 minutes. The tubes were centrifuged

to bring solutions to the bottom. Ferrozine stock solution was prepared by adding sodium ascorbate (0.911 g), ferrozine (0.089 g), and sodium acetate (13.776 g) to deionised water (122.00 mL). The cell lysate and TCA solution (200 μ L) was added to ferrozine stock solution (600 μ L) and thoroughly mixed. This solution was plated out in triplicate in a flat bottomed clear 96-well plate (3 x 200 μ L). Calibration solutions were made using iron sulphate in 0.1% v/v HCl at 0.75 mM, 0.50 mM, 0.25 mM, 0.125 mM, 0.10 mM and were mixed (200 μ L) with ferrozine stock solution (600 μ L) and plated out in triplicate. The plate was read at 550 nm using Victor 2 Wallac 1420 microplate reader. Standard calibration curves were constructed for the determination of iron content, which was normalised to protein content in each sample.

9.11 Preloading cells with iron

In order to determine *in vitro* *Exkite* activity and possible ligand cleavage, RKO cells were preloaded with iron, then treated with polymers. RKO cells (2×10^5 cells/mL) were seeded into 6-well plates (2.00 mL/well) and allowed to adhere for 24 hours. Iron stock solution was made by dissolving iron sulphate (10 mM $\text{FeSO}_4 \cdot 7\text{H}_2\text{O}$, 0.1112 g) and sodium ascorbate (1 mM, 0.008 g) into deionised water (40.00 mL), which was further filtered sterilised to remove any insoluble particles. The stock solution was added to modified DMEM (100 μ L/ 10.00 mL DMEM) to give final concentrations of 100 μ M iron sulphate and 10 μ M sodium ascorbate. The media was aspirated and replaced with iron loaded modified DMEM (2.00 mL/well), and further incubated for 24 hours.

Polymer solutions were added to modified DMEM, diluted from 1% stock solutions to achieve final concentrations of 0.03% w/v *Exkite* and chitosan (0.30 mL polymer stock/10.00 mL DMEM), 0.05% w/v *Exkite* and chitosan (0.50 mL polymer stock/10.00 mL DMEM). Iron loaded media was aspirated and cells were washed with PBS (3 x 1.00 mL/well). Stimulation medium containing polymer solutions was added (2.00 mL/well) and incubated for 24 hours. Experiments were done

in triplicate for each polymer concentration, positive control was conducted in iron loaded modified DMEM (100 μ M FeSO₄·7H₂O, 10 μ M sodium ascorbate), negative control was conducted in modified DMEM alone. The media was removed and cells washed with ice cold PBS buffer (3 x 1.00 mL/well), and lysed with RIPA buffer (100 μ L/well) whilst being kept on ice.

Samples were analysed by ferritin ELISA which was conducted using a Spectro ferritin ELISA kit (Ramco Laboratories Inc, S-22) according to manufacturer's instructions, using the pre-coated 96-well plate provided. Absorbance of samples were read at 490 nm and 595 nm on Victor 2 Wallac 1420 microplate reader. Results were processed using Microsoft Excel by construction of calibration curves as instructed in the kit.

9.12 Murine studies

Wild type mice have no genetic modifications. Mice used in experiments were at least 6 weeks of age weighing a minimum of 20.00 g.

Apc Hom (Cre⁺ Apc^{f/f}) mice is a transgenic inducible model of sporadic CRC with homozygous Apc inactivation in the intestinal epithelium. Mice were induced at 6 weeks of age after they weighed a minimum of 20.00 g by tamoxifen (Sigma Aldrich) injection of 4 x 3.00 mg given on consecutive days.

Apc Hom Pten Hom (Cre⁺ Apc^{f/f} Pten^{f/f}) mice is a transgenic inducible model with homozygous inactivation of Apc and Pten. Mice were induced at 6 weeks of age after they weighed a minimum of 20.00 g by tamoxifen (Sigma Aldrich) injection of 1 x 3.00 mg.

All mouse experiments were performed according to UK Home Office Guidelines and approved by University of Birmingham Ethics Committee in accordance with project licence 70/8198 under protocol 19b 5 and 40/3613 under protocol 19b3.

9.13 *Exkite* activity in mice

9.13.1 Exkite safety and tolerability

Wild type mice (n = 1 per dose) were given daily 200 μ L gavages of *Exkite* for five days at varying concentrations: 0.01%, 0.10%, 0.25%, 0.50% and 1% w/v, using gavage needle and luer lock 1.00 mL syringe. After the allotted treatment period the mice were culled under humane conditions.

9.13.2 Deferasirox detection in blood plasma

Wild type mice (n = 3) were administered a single dose of 200 μ L 1% w/v *Exkite* by oral gavage, control mice (n = 3) were subject to 200 μ L water using gavage needle and luer lock 1.00 mL syringe. After one hour, the mice were culled under humane conditions. Blood samples were obtained by direct cardiac puncture and aliquoted into Capiject® blood tubes. The blood was allowed to clot and centrifuged at 5000 rpm for 10 minutes after which the serum was aspirated. Blood serum was diluted in water (1:2 ratio) and analysed by MALDI spectroscopy by plating sample (2 μ L) with α -cyano-4-hydroxycinnamic acid (CHCA) matrix (1 μ L), analysed on Bruker Ultraflextreme MALDI spectrometer.

9.13.3 Deferasirox detection in crypt cells

Wild type mice (n = 3) were administered a single dose of 200 μ L 1% w/v *Exkite* by oral gavage, control mice (n = 3) were subject to 200 μ L water using gavage needle and luer lock 1.00 mL syringe. After one hour, the mice were culled under humane conditions.

The small intestine was dissected and placed in cold PBS (10.00 mL), and cut into small pieces. The intestine was repeatedly agitated and washed with cold PBS (10 x 10.00 mL) and supernatant discarded until supernatant was clear. After the final wash, cold PBS (25.00 mL) was added with EDTA (100 μ L) and incubated on ice for 30 minutes. The EDTA supernatant was discarded, and

intestines were washed gently with PBS (10.00 mL). The intestines were mechanically agitated by hard pipetting of cold PBS (10.00 mL) and the supernatant was decanted to obtain the first fraction of crypt cells. This was repeated three more times to obtain four crypt fractions. The fractions were checked under the microscope and crypt enriched fractions were combined, and made up to 50.00 mL by the addition of Advanced DMEM/F12 (ADF). The solution was centrifuged at 1200 rpm for 5 minutes to obtain a cell pellet. The supernatant was discarded and pellet was re-suspended in Advanced DMEM/F12 (10.00 mL) and passed through a 70 μ m cell strainer, which was washed with additional DMEM (5.00 mL). This was centrifuged at 600 rpm for 2 minutes, supernatant discarded and pellet re-suspended. This process was repeated two more times and supernatant was discarded. To the cell pellet, PBS (1.00 mL) was added, cells re-suspended and centrifuged at 1300 rpm for 5 minutes. The PBS supernatant was discarded and ethanol (100 μ L) added and thoroughly mixed. This was centrifuged at 1300 rpm for 5 minutes and ethanol supernatant was aspirated and allowed to air dry. Samples were re-dissolved in ethanol (10 μ L) and deionised water (10 μ L) and thoroughly mixed.

Samples were analysed by MALDI spectrometry by plating sample (2 μ L) with α -cyano-4-hydroxycinnamic acid (CHCA) matrix (1 μ L), analysed on Bruker Ultraflex extreme MALDI spectrometer.

9.14 Mouse survival studies

Mouse survival studies were conducted with Apc Hom (Cre⁺ Apc^{ff}) mice and Apc Hom Pten Hom (Cre⁺ Apc^{ff} Pten^{ff}) which were used immediately following induction by tamoxifen injection. The mice were administered 200 μ L of 1% w/v *Exkite* (n = 6 Apc Hom, n = 13 Apc Hom Pten Hom) or 200 μ L of water as the vehicle control (n = 3 Apc Hom, n = 16 Apc Hom Pten Hom), administered by oral gavage using gavage needle and luer lock 1.00 mL syringe on alternate days (Mon/ Wed/ Fri) until they became sick. Mice were presumed sick when they showed symptoms

of weight loss (< 20% pre-experimental weight), hunched posture, pale feet, pinched face, piloerection, lack of movement and isolation in cage. All mice were culled under humane conditions, small intestines were dissected and fixed in 10% v/v neutral buffered formalin and embedded in paraffin.

9.15 Immunohistochemistry

9.15.1 De-wax and rehydrate slides

Archived small intestine tissue from mouse survival studies were sectioned at 5 µm intervals and applied to SuperFrost glass. Slides were washed in xylene for 2 minutes for removal of excess paraffin wax, and hydrated by sequential submersion in 100% ethanol followed by 80% v/v ethanol.

9.15.2 Antigen retrieval

A solution of citric acid (10.50 g) in deionised water (0.50 L) was made, and a solution of sodium citrate (29.40 g) in deionised water (1.00 L) was made. Citric acid solution (27.00 mL) was added to sodium citrate solution (123.00 mL) and total volume was made up to 1.50 L by the addition of deionised water. This solution was added to a pressure cooker and slides were submerged, pressure cooker was heated in a microwave for 20 minutes until pressure was optimised for 10 – 15 seconds and allowed to cool.

9.15.3 Prevention of endogenous staining/Blocking

Slides were blotted dry and outlined by a hydrophobic delineating pen (Dako). A solution of 3% w/v hydrogen peroxide was added to cover surface of slides (100 – 200 µL) for 10 minutes. Slides were washed in PBS (3 x 1.00 mL/slide) and incubated for 30 minutes with 1% w/v albumin in PBS.

9.15.4 Primary antibody

Anti-caspase 3 antibody (R&D Systems, AF 835) was diluted into 1% w/v albumin at 1:800 ratio, and anti-phosphohistone antibody (R&D Systems) was diluted into 1% w/v albumin at 1:500 ratio. The slides were tapped dry and antibodies applied to ensure surface coverage (100 – 200 μ L) and incubated overnight at 4 °C. Slides were then washed in PBS (3 x 1.00 mL/slide).

9.15.5 Secondary antibody

Secondary antibody was applied (Dual – link Dako kit HRP Yellow) at 2-3 drops per slide for both caspase 3 and phosphohistone slides and incubated at room temperature for 30 minutes. Slides were tapped dry and washed in PBS (3 x 5 minutes).

9.15.6 Visualisation of positivity

A visualisation kit (DAB) was used according to the manufacturer's instructions. The premixed solution was added to each slide (200 μ L) and incubated for 30 seconds – 5 minutes until positive brown staining was observed, and washed thoroughly in water. Slides were counterstained in haematoxylin for 20 seconds and washed sequentially in water twice, Scott's Tap water (Sigma Aldrich), then water again. Slides were dehydrated by washing in 80% w/v ethanol, then 100% ethanol and finally in xylene. Slides were mounted by the application of a cover slip using DPX Mountant (Sigma Aldrich).

9.15.7 Scoring of slides

H&E sections were stained by a service provided by The Department of Cellular Pathology, Queen Elizabeth Hospital.

The slides were scored by counting 25 continuous crypts for positive staining per mouse, with 6 mice taken per group. Slides stained by H&E were scored for mitosis by identification of cells undergoing division. The extent of mitosis is expressed as mitotic index, which is the percentage

of cells in mitosis relative to total number of cells per crypt. The extent of apoptosis is expressed as apoptotic index, which is the percentage of cells in apoptosis relative to total number of cells per crypt.

Images were visualised using a Nikon Eclipse E600 microscope and digital image captured using a Nikon DXM1200F camera, with the use of Nikon ACT-1 2.62 software for image acquisition.

9.16 Statistical analysis

Data was analysed using Microsoft Excel Professional 2010. Data is expressed as an average of triplicate readings in most cases \pm the standard error in the mean (SEM). Statistical significance was determined by Student's paired *t*-test where significance was accepted when $p < 0.05$.

10 References

1. J. W. Morgan and E. Anders, *Proc. Natl. Acad. Sci.*, 1980, **77**, 6973-6977.
2. M. W. Hentze, M. U. Muckenthaler and N. C. Andrews, *Cell*, 2004, **117**, 285-297.
3. N. T. V. Le and D. R. Richardson, *Biochim. Biophys. Acta*, 2002, **1603**, 31-46.
4. N. Maio and T. A. Rouault, *Biochim. Biophys. Acta*, 2014, In press.
5. D. S. Kalinowski and D. R. Richardson, *Pharmacol. Rev.*, 2005, **57**, 547-583.
6. D. N. Seril, J. Liao, C. S. Yang and G. Y. Yang, *Dig. Dis. Sci.*, 2005, **50**, 696-707.
7. A. C. G. Chua, B. Klopčič, I. C. Lawrance, J. K. Olynyk and D. Trinder, *World J. Gastroenterol.*, 2010, **16**, 663-672.
8. I. Cavill, M. Auerbach, G. R. Bailie, P. Barrett-Lee, Y. Beguin, P. Kaltwasser, T. Littlewood, I. C. Macdougall and K. Wilson, *Curr. Med. Res. Opin.*, 2006, **22**, 731-737.
9. S. L. Schrier, F. Centis, M. Verneris, L. Ma and E. Angelucci, *Redox Rep.*, 2003, **8**, 241-245.
10. M.-C. Corti, M. Gaziano and C. H. Hennekens, *Ann. Epidemiol.*, 1997, **7**, 62-68.
11. X. Huang, *Mutat. Res. Fundam. Mol. Mech. Mutagen.*, 2003, **533**, 153-171.
12. I. Kato, A. M. Dnistrian, M. Schwartz, P. Toniolo, K. Koenig, R. E. Shore, A. Zeleniuch-Jacquotte, A. Akhmedkhanov and E. Riboli, *Int. J. Cancer*, 1999, **80**, 693-698.
13. D.-H. Lee, K. E. Anderson, L. J. Harnack, A. R. Folsom and D. R. Jacobs, *J. Natl. Cancer Inst.*, 2004, **96**, 403-407.
14. *UK Pat.*, PCT/GB2010/001987, 2011.
15. R. L. Nelson, *Nutr. Rev.*, 2001, **59**, 140-148.
16. R. L. Nelson, F. G. Davis, V. Persky and E. Becker, *Cancer*, 1995, **76**, 875-879.
17. J. Ferlay, I. Soerjomataram, M. Ervik, R. Dikshit, S. Eser, C. Mathers, M. Rebelo, D. Parkin, D. Forman and F. Bray, in *Globocan, Cancer Incidence and Mortality Worldwide*, <http://globocan.iarc.fr>, 2008.
18. A. G. Mainous, J. M. Gill and C. J. Everett, *Ann. Fam. Med.*, 2005, **3**, 131-137.
19. S. V. Torti and F. M. Torti, *Nat. Rev. Cancer*, 2013, **13**, 342-355.
20. E. Nemeth and T. Ganz, *Annu. Rev. Nutr.*, 2006, **26**, 323-342.
21. D. R. Richardson, D. S. Kalinowski, S. Lau, P. J. Jansson and D. B. Lovejoy, *Biochim. Biophys. Acta*, 2009, **1790**, 702-717.
22. G. Weiss and L. T. Goodnough, *N. Engl. J. Med.*, 2005, **352**, 1011-1023.

23. J. Boulton, K. Roberts, M. J. Brookes, S. Hughes, J. P. Bury, S. S. Cross, G. J. Anderson, R. Spychal, T. Iqbal and C. Tselepis, *Clin. Cancer Res.*, 2008, **14**, 379-387.
24. Y. Mori, H. Nagase, H. Ando, A. Horii, S. Ichii, S. Nakatsuru, T. Aoki, Y. Miki, T. Mori and Y. Nakamura, *Hum. Mol. Genet.*, 1992, **1**, 229-233.
25. M. J. Brookes, J. Boulton, K. Roberts, B. T. Cooper, N. A. Hotchin, G. Matthews, T. Iqbal and C. Tselepis, *Oncogene*, 2008, **27**, 966-975.
26. S. Radulescu, Matthew J. Brookes, P. Salgueiro, Rachel A. Ridgway, E. McGhee, K. Anderson, Samuel J. Ford, Daniel H. Stones, Tariq H. Iqbal, C. Tselepis and Owen J. Sansom, *Cell Rep.*, 2012, **2**, 270-282.
27. A. D. Millar, D. S. Rampton and D. R. Blake, *Aliment. Pharmacol. Ther.*, 2000, **14**, 1163-1168.
28. T. Werner, S. J. Wagner, I. Martinez, J. Walter, J. S. Chang, T. Clavel, S. Kisling, K. Schuemann and D. Haller, *Gut*, 2011, **60**, 325-333.
29. C. Ratledge and L. G. Dover, *Annu. Rev. Microbiol.*, 2000, **54**, 881-941.
30. J. M. McCord, *Clinical Biochemistry*, 1993, **26**, 351-357.
31. N. F. Olivieri and G. M. Brittenham, *Blood*, 1997, **89**, 739-761.
32. L. E. Scott and C. Orvig, *Chem. Rev.*, 2009, **109**, 4885-4910.
33. R. C. Hider, S. Roy, Y. M. Ma, X. Le Kong and J. Preston, *Metallomics*, 2011, **3**, 239-249.
34. Z. D. Liu and R. C. Hider, *Coord. Chem. Rev.*, 2002, **232**, 151-171.
35. Z. Li, H. Tanaka, F. Galiano and J. Glass, *J. Exp. Clin. Cancer Res.*, 2011, **30**, 34-44.
36. A. S. Vinogradov, A. B. Preobrajenski, S. A. Krasnikov, T. Chasse, R. Szargan, A. Knop-Gericke, R. Schlogl and P. Bressler, *Surf. Rev. Lett.*, 2002, **09**, 359-364.
37. P. C. Junk, *J. Coord. Chem.*, 2005, **58**, 355-361.
38. D. S. Kalinowski and D. R. Richardson, *Chem. Res. Toxicol.*, 2007, **20**, 715-720.
39. S. Decurtins, F. Felix, J. Ferguson, H. U. Guedel and A. Ludi, *J. Am. Chem. Soc.*, 1980, **102**, 4102-4106.
40. Z. D. Liu and R. C. Hider, *Med. Res. Rev.*, 2002, **22**, 26-64.
41. D. C. Harris and P. Aisen, *Biochim. Biophys. Acta*, 1973, **329**, 156-158.
42. B. Halliwell, *Free Radic. Biol. Med.*, 1989, **7**, 645-651.
43. S. Singh, H. Khodr, M. I. Taylor and R. C. Hider, in *Free Radicals and Oxidative Stress: Environment, Drugs and Food Additives*, eds. C. RiceEvans, B. Halliwell and G. G. Lunt, Portland Press Ltd, London, 1995, pp. 127-137.
44. K. N. Raymond, E. A. Dertz and S. S. Kim, *Proc. Natl. Acad. Sci.*, 2003, **100**, 3584-3588.

45. R. J. Bergeron, *Chem. Rev.*, 1984, **84**, 587-602.
46. A. Avdeef, S. R. Sofen, T. L. Bregante and K. N. Raymond, *J. Am. Chem. Soc.*, 1978, **100**, 5362-5370.
47. C. J. Carrano and K. N. Raymond, *J. Am. Chem. Soc.*, 1979, **101**, 5401-5404.
48. M. J. Pippard, S. T. Callender and D. J. Weatherall, *Clin. Sci. Mol. Med.*, 1978, **54**, 99-106.
49. M. J. Pippard, M. J. Jackson, K. Hoffman, M. Petrou and C. B. Modell, *Scand. J. Haematol.*, 1986, **36**, 466-472.
50. M. Sillanpää and M.-L. Sihvonen, *Talanta*, 1997, **44**, 1487-1497.
51. Z. Chang, in *Pharmaceutical Sciences Encyclopedia*, John Wiley & Sons, Inc., 2010.
52. G. Banfi, L. Salvagno Gian and G. Lippi, *Clin. Chem. Lab. Med.*, 2007, **45**, 565-576.
53. K. Dominguez and W. S. Ward, *Syst. Biol. Reprod. Med.*, 2009, **55**, 193-199.
54. P. S. Dobbin, R. C. Hider, A. D. Hall, P. D. Taylor, P. Sarpong, J. B. Porter, G. Y. Xiao and D. Vanderhelm, *J. Med. Chem.*, 1993, **36**, 2448-2458.
55. A. Piga, S. Roggero, I. Salussolia, D. Massano, M. Serra and F. Longo, *Ann. NY Acad. Sci.*, 2010, **1202**, 75-78.
56. J. L. Stumpf, *Am. J. Health Syst. Pharm.*, 2007, **64**, 606-616.
57. S. Steinhauser, U. Heinz, M. Bartholoma, T. Weyhermuller, H. Nick and K. Hegetschweiler, *Eur. J. Inorg. Chem.*, 2004, 4177-4192.
58. U. Heinz, K. Hegetschweiler, P. Acklin, B. Faller, R. Lattmann and H. P. Schnebli, *Angew. Chem., Int. Ed.*, 1999, **38**, 2568-2570.
59. G. J. M. Bruin, T. Faller, H. Wiegand, A. Schweitzer, H. Nick, J. Schneider, K.-O. Boernsen and F. Waldmeier, *Drug Metab. Dispos.*, 2008, **36**, 2523-2538.
60. G. Kamalinia, F. Khodagholi, F. Atyabi, M. Amini, F. Shaerzadeh, M. Sharifzadeh and R. Dinarvand, *Mol. Pharm.*, 2013.
61. M. R. Bedford, S. J. Ford, R. D. Horniblow, T. H. Iqbal and C. Tselepis, *J. Clin. Pharmacol.*, 2013, **53**, 885-891.
62. S. J. Ford, P. Obeidy, D. B. Lovejoy, M. Bedford, L. Nichols, C. Chadwick, O. Tucker, G. Y. L. Lui, D. S. Kalinowski, P. J. Jansson, T. H. Iqbal, D. Alderson, D. R. Richardson and C. Tselepis, *Br. J. Pharmacol.*, 2013, **168**, 1316-1328.
63. G. Y. L. Lui, P. Obeidy, S. J. Ford, C. Tselepis, D. M. Sharp, P. J. Jansson, D. S. Kalinowski, Z. Kovacevic, D. B. Lovejoy and D. R. Richardson, *Mol. Pharmacol.*, 2013, **83**, 179-190.
64. M. Mocioi, A. M. Albu, C. Mateescu, G. Voicu, E. Rusen, B. Marculescu and L. Mutihac, *J. Appl. Polym. Sci.*, 2007, **103**, 1397-1405.

65. A. Warshawsky, *Angew. Chem., Int. Ed.*, 1982, **109**, 171-196.
66. C. G. Rampley and K. L. Ogden, *Environ. Sci. Technol.*, 1998, **32**, 987-993.
67. T. Zhou, G. Winkelmann, Z.-Y. Dai and R. C. Hider, *J. Pharm. Pharmacol.*, 2011, **63**, 893-903.
68. P. E. Hallaway, J. W. Eaton, S. S. Panter and B. E. Hedlund, *Proc. Natl. Acad. Sci.*, 1989, **86**, 10108-10112.
69. J. R. Mahoney, Jr., P. E. Hallaway, B. E. Hedlund and J. W. Eaton, *J. Clin. Invest.*, 1989, **84**, 1362-1366.
70. P. Harmatz, R. W. Grady, P. Dragsten, E. Vichinsky, P. Giardina, J. Madden, M. Jeng, B. Miller, G. Hanson and B. Hedlund, *Br. J. Haematol.*, 2007, **138**, 374-381.
71. N. A. A. Rossi, I. Mustafa, J. K. Jackson, H. M. Burt, S. A. Horte, M. D. Scott and J. N. Kizhakkedathu, *Biomaterials*, 2009, **30**, 638-648.
72. Y. Takagai, A. Takahashi, H. Yamaguchi, T. Kubota and S. Igarashi, *J. Colloid Interface Sci.*, 2007, **313**, 359-362.
73. A. Winston, D. V. Varaprasad, J. J. Metterville and H. Rosenkrantz, *J. Pharmacol. Exp. Ther.*, 1985, **232**, 644-649.
74. Z. Mohammadi, S. X. Xie, A. L. Golub, S. H. Gehrke and C. Berkland, *J. Appl. Polym. Sci.*, 2011, **121**, 1384-1392.
75. T. Zhou, X. Le Kong, Z. D. Liu, D. Y. Liu and R. C. Hider, *Biomacromolecules*, 2008, **9**, 1372-1380.
76. D. Astruc, E. Boisselier and C. Ornelas, *Chem. Rev.*, 2010, **110**, 1857-1959.
77. T. Zhou, R. C. Hider, Z. D. Liu and H. Neubert, *Tetrahedron Lett.*, 2004, **45**, 9393-9396.
78. T. Zhou, Z. D. Liu, H. Neubert, X. Le Kong, Y. M. Ma and R. C. Hider, *Bioorg. Med. Chem. Lett.*, 2005, **15**, 5007-5011.
79. J. Lim, V. J. Venditto and E. E. Simanek, *Bioorg. Med. Chem.*, 2010, **18**, 5749-5753.
80. J. E. Gregor, E. Fenton, G. Brokenshire, P. Van Den Brink and B. O'Sullivan, *Water Res.*, 1996, **30**, 1319-1324.
81. I. Donati, S. Holtan, Y. A. Mørch, M. Borgogna and M. Dentini, *Biomacromolecules*, 2005, **6**, 1031-1040.
82. B. Polyak, S. Geresh and R. S. Marks, *Biomacromolecules*, 2004, **5**, 389-396.
83. Z. Honghe, *Carbohydr. Res.*, 1997, **302**, 97-101.
84. G. T. Grant, E. R. Morris, D. A. Rees, P. J. C. Smith and D. Thom, *FEBS Lett.*, 1973, **32**, 195-198.

85. Z.-Y. Wang, Q.-Z. Zhang, M. Konno and S. Saito, *Biopolymers*, 1993, **33**, 703-711.
86. Z. Y. Wang, J. W. White, M. Konno, S. Saito and T. Nozawa, *Biopolymers*, 1995, **35**, 227-238.
87. K. I. Draget and C. Taylor, *Food Hydrocoll.*, 2011, **25**, 251-256.
88. I. A. Brownlee, *Food Hydrocoll.*, 2011, **25**, 238-250.
89. A. Jimenez-Escrig and F. J. Sanchez-Muniz, *Nutr. Res.*, 2000, **20**, 585-598.
90. R. Horniblow, D. Stones, S. Radulescu, O. Sansom, Z. Pikramenou and C. Tselepis, *Am. J. Hematol.*, 2013, **88**, E182-E182.
91. J. A. Rowley, G. Madlambayan and D. J. Mooney, *Biomaterials*, 1999, **20**, 45-53.
92. P. Eiselt, K. Y. Lee and D. J. Mooney, *Macromolecules*, 1999, **32**, 5561-5566.
93. J. Yang, M. Goto, H. Ise, C. S. Cho and T. Akaike, *Biomaterials*, 2002, **23**, 471-479.
94. X. L. Wang, Z. Y. Jiang, J. F. Shi, Y. P. Liang, C. H. Zhang and H. Wu, *ACS Appl. Mater. Interfaces*, 2012, **4**, 3476-3483.
95. A. Kodyan, E. A. Silva, J. Kim, M. Aizenberg and D. J. Mooney, *ACS Nano*, 2012, **6**, 4796-4805.
96. M. Kumar, *React. Funct. Polym.*, 2000, **46**, 1-27.
97. S. E. Bailey, T. J. Olin, R. M. Bricka and D. D. Adrian, *Water Res.*, 1999, **33**, 2469-2479.
98. E. Guibal, *Sep. Purif. Technol.*, 2004, **38**, 43-74.
99. E. L. McConnell, S. Murdan and A. W. Basit, *J. Pharm. Sci.*, 2008, **97**, 3820-3829.
100. C. L. Vernazza, G. R. Gibson and R. A. Rastall, *Carbohydr. Polym.*, 2005, **60**, 539-545.
101. S. C. Chen, Y. C. Wu, F. L. Mi, Y. H. Lin, L. C. Yu and H. W. Sung, *J. Control. Release*, 2004, **96**, 285-300.
102. A. Islam, T. Yasin, I. Bano and M. Riaz, *J. Appl. Polym. Sci.*, 2012, **124**, 4184-4192.
103. A. Z. Chen, M. Y. Chen, S. B. Wang, X. N. Huang, Y. G. Liu and Z. X. Chen, *J. Appl. Polym. Sci.*, 2012, **124**, 3728-3736.
104. M. R. Gandhi, G. N. Kousalya and S. Meenakshi, *J. Appl. Polym. Sci.*, 2012, **124**, 1858-1865.
105. Q. Song, Z. Zhang, J. Gao and C. Ding, *J. Appl. Polym. Sci.*, 2011, **119**, 3282-3285.
106. R. A. A. Muzzarelli, P. Ilari and M. Petrarulo, *Int. J. Biol. Macromol.*, 1994, **16**, 177-180.
107. M. Morimoto, H. Saimoto, H. Usui, Y. Okamoto, S. Minami and Y. Shigemasa, *Biomacromolecules*, 2001, **2**, 1133-1136.
108. H. Sashiwa, Y. Shigemasa and R. Roy, *Macromolecules*, 2001, **34**, 3905-3909.

109. M. N. V. R. Kumar, R. A. A. Muzzarelli, C. Muzzarelli, H. Sashiwa and A. J. Domb, *Chem. Rev.*, 2004, **104**, 6017-6084.
110. K. Aiedeh and M. O. Taha, *Eur. J. Pharm. Sci.*, 2001, **13**, 159-168.
111. R. Sullivan, J. Peppercorn, K. Sikora, J. Zalcborg, N. J. Meropol, E. Amir, D. Khayat, P. Boyle, P. Autier, I. F. Tannock, T. Fojo, J. Siderov, S. Williamson, S. Camporesi, J. G. McVie, A. D. Purushotham, P. Naredi, A. Eggermont, M. F. Brennan, M. L. Steinberg, M. De Ridder, S. A. McCloskey, D. Verellen, T. Roberts, G. Storme, R. J. Hicks, P. J. Ell, B. R. Hirsch, D. P. Carbone, K. A. Schulman, P. Catchpole, D. Taylor, J. Geissler, N. G. Brinker, D. Meltzer, D. Kerr and M. Aapro, *Lancet Oncol.*, 2011, **12**, 933-980.
112. N. Brosse, M.-F. Pinto and B. Jamart-Grégoire, *J. Chem. Soc., Perkin Trans. 1*, 1998, **22**, 3685-3688.
113. H. Kim and M. Cho, *Chem. Rev.*, 2013, **113**, 5817-5847.
114. A. C. de Souza, T. Rietkerk, C. G. M. Selin and P. P. Lankhorst, *Carbohydr. Polym.*, 2013, **95**, 657-663.
115. J. Clauss, K. Schmidt-Rohr and H. W. Spiess, *Acta Polym.*, 1993, **44**, 1-17.
116. X. H. Tang, S. Y. Tan and Y. T. Wang, *J. Appl. Polym. Sci.*, 2002, **83**, 1886-1891.
117. J. Hrabe, G. Kaur and D. N. Guilfoyle, *J. Med. Phys.*, 2007, **32**, 34-42.
118. C. S. Johnson Jr, *Prog. Nucl. Magn. Reson. Spectrosc.*, 1999, **34**, 203-256.
119. M. M. Britton, *Chem. Soc. Rev.*, 2010, **39**, 4036-4043.
120. K. Nicolay, K. P. J. Braun, R. A. d. Graaf, R. M. Dijkhuizen and M. J. Kruiskamp, *NMR Biomed.*, 2001, **14**, 94-111.
121. T. L. James and G. G. McDonald, *J. Magn. Reson., Ser A* 1973, **11**, 58-61.
122. S. Yao, G. Howlett and R. Norton, *J. Biomol. NMR*, 2000, **16**, 109-119.
123. Y. Cohen, L. Avram and L. Frish, *Angew. Chem., Int. Ed.*, 2005, **44**, 520-554.
124. M. S. Kaucher, Y.-F. Lam, S. Pieraccini, G. Gottarelli and J. T. Davis, *Chem. Eur. J.*, 2005, **11**, 164-173.
125. H. Ihre, A. Hult and E. Söderlind, *J. Am. Chem. Soc.*, 1996, **118**, 6388-6395.
126. Y. Uemura, J. McNulty and P. M. Macdonald, *Macromolecules*, 1995, **28**, 4150-4158.
127. H. Walderhaug, F. K. Hansen, S. Abrahmsen, K. Persson and P. Stilbs, *J. Phys. Chem.*, 1993, **97**, 8336-8342.
128. E. O. Stejskal and J. E. Tanner, *J. Chem. Phys.*, 1965, **42**, 288-292.
129. A. J. Mills, J. Wilkie and M. M. Britton, *J. Phys. Chem. B*, 2014, **118**, 10767-10775.

130. M. Nilsson, M. A. Connell, A. L. Davis and G. A. Morris, *Anal. Chem.*, 2006, **78**, 3040-3045.
131. C. Cabaleiro-Lago, M. Nilsson and O. Söderman, *Langmuir*, 2005, **21**, 11637-11644.
132. A. Macchioni, G. Ciancaleoni, C. Zuccaccia and D. Zuccaccia, *Chem. Soc. Rev.*, 2008, **37**, 479-489.
133. N.-P. Huang, J. Vörös, S. M. De Paul, M. Textor and N. D. Spencer, *Langmuir*, 2002, **18**, 220-230.
134. F. Grenier, B. R. Aïch, Y.-Y. Lai, M. Guérette, A. B. Holmes, Y. Tao, W. W. H. Wong and M. Leclerc, *Chem. Mater.*, 2015, **27**, 2137-2143.
135. R. Haag, *Angew. Chem., Int. Ed.*, 2004, **43**, 278-282.
136. H.-J. Yoon and W.-D. Jang, *J. Mater. Chem.*, 2010, **20**, 211-222.
137. H. Gheybi and M. Adeli, *Polym. Chem.*, 2015, **6**, 2580-2615.
138. A. T. M. Serajuddin, *Adv. Drug Delivery Rev.*, 2007, **59**, 603-616.
139. D. Hörter and J. B. Dressman, *Adv. Drug Delivery Rev.*, 2001, **46**, 75-87.
140. N. D. Lourenço, J. A. Lopes, C. F. Almeida, M. C. Sarraguça and H. M. Pinheiro, *Anal. Bioanal. Chem.*, 2012, **404**, 1211-1237.
141. J. M. Parnis and K. B. Oldham, *J. Photochem. Photobiol. A Chem.*, 2013, **267**, 6-10.
142. M. Dubois, K. A. Gilles, J. K. Hamilton, P. A. Rebers and F. Smith, *Anal. Chem.*, 1956, **28**, 350-356.
143. J. M. Hollander and W. L. Jolly, *Acc. Chem. Res.*, 1970, **3**, 193-200.
144. K. Wang and Q. Liu, *Carbohydr. Res.*, 2014, **386**, 48-56.
145. J. F. Moulder, W. F. Stickle, P. E. Sobol and B. K.D., *Handbook of X-ray Photoelectron Spectroscopy*, Perkin-Elmer USA, 1992.
146. S. Ciampi, M. James, M. H. Choudhury, N. A. Darwish and J. J. Gooding, *Phys. Chem. Chem. Phys.*, 2013, **15**, 9879-9890.
147. N. Maalouli, A. Barras, A. Siriwardena, M. Bouazaoui, R. Boukherroub and S. Szunerits, *Analyst*, 2013, **138**, 805-812.
148. H. K. Reimschuessel, *Environ. Health Perspect.*, 1975, **11**, 9-20.
149. P. J. Charley, B. Sarkar, C. F. Stitt and P. Saltman, *Biochim. Biophys. Acta*, 1963, **69**, 313-321.
150. A. S. Brill and R. J. P. Williams, *Biochem. J.*, 1961, **78**, 246-253.
151. R. C. Johnson, *J. Chem. Educ.*, 1965, **42**, 147.
152. J. N. Demas and B. A. DeGraff, *Anal. Chem.*, 1991, **63**, 829A-837A.

153. R. G. Pearson, *J. Chem. Educ.*, 1961, **38**, 164.
154. F. D'Souza, P. Boulas, A. M. Aukauloo, R. Guillard, M. Kisters, E. Vogel and K. M. Kadish, *J. Phys. Chem.*, 1994, **98**, 11885-11891.
155. A. B. P. Lever, *J. Chem. Educ.*, 1974, **51**, 612.
156. R. M. Cornell, R. Giovanoli and W. Schneider, *J. Chem. Technol. Biotechnol.*, 1989, **46**, 115-134.
157. Z. Y. Wang, Q. Z. Zhang, M. Konno and S. Saito, *Biopolymers*, 1994, **34**, 737-746.
158. E. R. Monsen, L. Hallberg, M. Layrisse, D. M. Hegsted, J. D. Cook, W. Mertz and C. A. Finch, *Am. J. Clin. Nutr.*, 1978, **31**, 134-141.
159. M. J. Ruwart, M. S. Klepper and B. D. Rush, *Prostaglandins Med.*, 1979, **2**, 285-291.
160. K. H. Gayer and L. Woontner, *J. Phys. Chem.*, 1956, **60**, 1569-1571.
161. J. W. Robinson, *Anal. Chem.*, 1960, **32**, 17A-29A.
162. U. Schlemmer, *Food Chem.*, 1989, **32**, 223-234.
163. A. F. Lagalante, *Appl. Spectrosc. Rev.*, 2004, **34**, 173-189.
164. C. R. Gibbs, *Anal. Chem.*, 1976, **48**, 1197-1201.
165. L. L. Stookey, *Anal. Chem.*, 1970, **42**, 779-781.
166. M. M. Gibbs, *Water Res.*, 1979, **13**, 295-297.
167. M. Guo, C. Perez, Y. Wei, E. Rapoza, G. Su, F. Bou-Abdallah and N. D. Chasteen, *Dalton Trans.*, 2007, 4951-4961.
168. O. Smidsrød and G. Skjak-Braek, *Trends Biotechnol.*, 1990, **8**, 71-78.
169. D. A. Rees and E. J. Welsh, *Angew. Chem. Int. Ed.*, 1977, **16**, 214-224.
170. R. D. Shannon, *Acta Crystallogr. Sect. A*, 1976, **32**, 751-767.
171. D. Boyd, G. Florent, P. Kim and M. Brattain, *Cancer Res.*, 1988, **48**, 3112-3116.
172. T. Mosmann, *J. Immunol. Methods*, 1983, **65**, 55-63.
173. E. C. Theil, *Annu. Rev. Biochem.*, 1987, **56**, 289-315.
174. S. C. Andrews, P. M. Harrison, S. J. Yewdall, P. Arosio, S. Levi, W. Bottke, M. von Darl, J.-F. Briat, J.-P. Laulhère and S. Lobreaux, *J. Inorg. Biochem.*, 1992, **47**, 161-174.
175. W. Wang, M. A. Knovich, L. G. Coffman, F. M. Torti and S. V. Torti, *Biochim. Biophys. Acta*, 2010, **1800**, 760-769.
176. C. M. Plug, D. Dekker and A. Bult, *Pharm. Weekbl. Sci.*, 1984, **6**, 245-248.
177. A. E. Thumser, A. A. Rashed, P. A. Sharp and J. K. Lodge, *Food Chem.*, 2010, **123**, 281-285.

178. K. J. H. Wienk, J. J. M. Marx, M. Santos, A. G. Lemmens, E. J. Brink, R. Van Der Meer and A. C. Beynen, *Br. J. Nutr.*, 1997, **77**, 123-131.
179. R. Ghosh, J. E. Gilda and A. V. Gomes, *Expert Rev. Proteomics*, 2014, **11**, 549-560.
180. R. Horniblow, S. Radulescu, M. Schneider, M. Dowle, T. Iqbal, R. Palmer, G. Latunde-Dada, Z. Pikramenou and C. Tselepis, *Eur. J. Cancer*, 2014, **50**, S173-S173.
181. I. P. Pogribny, V. P. Tryndyak, M. Pogribna, S. Shpyleva, G. Surratt, G. Gamboa da Costa and F. A. Beland, *Int. J. Oncol.*, 2013, **42**, 1822-1832.
182. J. Tate and G. Ward, *Clin. Biochem. Rev.*, 2004, **25**, 105-120.
183. C. M. Sturgeon and A. Viljoen, *Ann. Clin. Biochem.*, 2011, **48**, 418-432.
184. A. G. M. Marr, J. A. Owen and G. S. Wilson, *Biochim. Biophys. Acta*, 1962, **63**, 276-285.
185. J. Riemer, H. H. Hoepken, H. Czerwinska, S. R. Robinson and R. Dringen, *Anal. Biochem.*, 2004, **331**, 370-375.
186. M. Thanou, J. C. Verhoef and H. E. Junginger, *Adv. Drug Delivery Rev.*, 2001, **52**, 117-126.
187. A. F. Kotzé, M. M. Thanou, H. L. Lueben, A. G. De Boer, J. C. Verhoef and H. E. Junginger, *J. Pharm. Sci.*, 1999, **88**, 253-257.
188. P. Sanchez, N. Galvez, E. Colacio, E. Minones and J. M. Dominguez-Vera, *Dalton Trans.*, 2005, 811-813.
189. F. Bonomi, A. Cerioli and S. Pagani, *Biochim. Biophys. Acta.*, 1989, **994**, 180-186.
190. F. Bonomi and S. Pagani, *Eur. J. Biochem.*, 1986, **155**, 295-300.
191. M. Thanou, J. C. Verhoef and H. E. Junginger, *Adv. Drug Delivery Rev.*, 2001, **50**, S91-S101.
192. K. Aoki and M. M. Taketo, *J. Cell. Sci.*, 2007, **120**, 3327-3335.
193. N. S. Fearnhead, M. P. Britton and W. F. Bodmer, *Hum. Mol. Genet.*, 2001, **10**, 721-733.
194. M. Lakso, B. Sauer, B. Mosinger, E. J. Lee, R. W. Manning, S. H. Yu, K. L. Mulder and H. Westphal, *Proc. Natl. Acad. Sci.*, 1992, **89**, 6232-6236.
195. D. Metzger and P. Chambon, *Methods*, 2001, **24**, 71-80.
196. H. Shibata, K. Toyama, H. Shioya, M. Ito, M. Hirota, S. Hasegawa, H. Matsumoto, H. Takano, T. Akiyama, K. Toyoshima, R. Kanamaru, Y. Kanegae, I. Saito, Y. Nakamura, K. Shiba and T. Noda, *Science*, 1997, **278**, 120-123.
197. O. J. Sansom, K. R. Reed, A. J. Hayes, H. Ireland, H. Brinkmann, I. P. Newton, E. Battle, P. Simon-Assmann, H. Clevers, I. S. Nathke, A. R. Clarke and D. J. Winton, *Genes Dev.*, 2004, **18**, 1385-1390.

198. M. Zeineldin and K. L. Neufeld, *Cancer Res.*, 2013, **73**, 2389-2399.
199. V. Marsh, D. J. Winton, G. T. Williams, N. Dubois, A. Trumpp, O. J. Sansom and A. R. Clarke, *Nat. Genet.*, 2008, **40**, 1436-1444.
200. P. Andreu, S. Colnot, C. Godard, S. Gad, P. Chafey, M. Niwa-Kawakita, P. Laurent-Puig, A. Kahn, S. Robine, C. Perret and B. Romagnolo, *Development* 2005, **132**, 1443-1451.
201. A. H. Fischer, K. A. Jacobson, J. Rose and R. Zeller, *Cold Spring Harb. Protoc.*, 2008, **5**, 4986-4987.
202. C. Tapia, H. Kutzner, T. Mentzel, S. Savic, D. Baumhoer and K. Glatz, *Am. J. Surg. Pathol.*, 2006, **30**, 83-89.
203. A. M. Gown and M. C. Willingham, *J. Histochem. Cytochem.*, 2002, **50**, 449-454.
204. J. G. Choi, J.-L. Kim, J. Park, S. Lee, S. J. Park, J. S. Kim and C. W. Choi, *Korean J. Hematol.*, 2012, **47**, 194-201.
205. J. L. Kim, H. N. Kang, M. H. Kang, Y. A. Yoo, J. S. Kim and C. W. Choi, *Acta Haematol.*, 2011, **126**, 241-245.
206. M. Huncharek, J. Muscat and B. Kupelnick, *Nutr. Cancer*, 2008, **61**, 47-69.
207. C. Ansari, G. A. Tikhomirov, S. H. Hong, R. A. Falconer, P. M. Loadman, J. H. Gill, R. Castaneda, F. K. Hazard, L. Tong, O. D. Lenkov, D. W. Felsher, J. Rao and H. E. Daldrup-Link, *Small*, 2014, **10**, 566-575.
208. C. Gialeli, A. D. Theocharis and N. K. Karamanos, *FEBS J.*, 2011, **278**, 16-27.
209. D. F. Evans, G. Pye, R. Bramley, A. G. Clark, T. J. Dyson and J. D. Hardcastle, *Gut*, 1988, **29**, 1035-1041.
210. C. Feng, R. Song, G. Sun, M. Kong, Z. Bao, Y. Li, X. Cheng, D. Cha, H. Park and X. Chen, *Biomacromolecules*, 2014, **15**, 985-996.
211. S. K. Bhat, J. Keshavayya, V. H. Kulkarni, V. K. R. Reddy, P. V. Kulkarni and A. R. Kulkarni, *J. Appl. Polym. Sci.*, 2012, **125**, 1736-1744.
212. T. F. Vandamme, A. Lenourry, C. Charrueau and J. C. Chaumeil, *Carbohydr. Polym.*, 2002, **48**, 219-231.
213. H. E. Gottlieb, V. Kotlyar and A. Nudelman, *J. Org. Chem.*, 1997, **62**, 7512-7515.